Proceedings

of the

4th ROCK MECHANICS SYMPOSIUM

held at

Ottawa

March 29-30, 1967

Published by

Mines Branch

DEPARTMENT OF ENERGY, MINES AND RESOURCES

Ottawa, 1967

96038—1½

Available by mail from the Queen's Printer, Ottawa,
and at the following Canadian Government bookshops:

HALIFAX
1735 Barrington Street

MONTREAL
Æterna-Vie Building, 1182 St. Catherine St. West

OTTAWA
Daly Building, Corner Mackenzie and Rideau

TORONTO
221 Yonge Street

WINNIPEG
Mall Center Bldg., 499 Portage Avenue

VANCOUVER
657 Granville Street

or through your bookseller

Price $6.50 Catalogue No. M37-1167

Price subject to change without notice

ROGER DUHAMEL, F.R.S.C.
Queen's Printer and Controller of Stationery
Ottawa, Canada
1968

Foreword

Through the initiative of Professors R.G.K. Morrison, A.V. Corlett and H.R. Rice of McGill, Queen's and Toronto Universities respectively Canadian rock mechanics symposia were initiated and held at those universities in the years 1962, 1963 and 1965. From the beginning, these symposia have been supported by the Mines Branch through the contribution of papers and through the publication of the Proceedings. It is a credit to the organizers of these symposia that they have been well attended and have been the scene of many fruitful discussions.

With the completion of the initially planned three symposia, the Canadian Advisory Committee on Rock Mechanics took the initiative to propose that the 4th Symposium be jointly sponsored by the Canadian Institute of Mining and Metallurgy and the Committee, supported as previously by the Mines Branch. Accordingly, the 4th Canadian Rock Mechanics Symposium was held in conjunction with the Annual General Meeting of the CIMM in March 1967. The symposium was organized by the Committee's subcommittee consisting of Professor A.V. Corlett, Dr. W.R. Horn, Professor A. Bauer and Mr. V. Haw together with the Technical Program Committee of the CIMM.

The theme of the symposium - field studies - was selected to be of greater interest to those who would not be specialists in the field of rock mechanics but who would be interested in attending the symposium while at the Annual General Meeting of the CIMM. In addition, in view of it being Canada's Centennial year together with Canada being hosts of the Expo World's Fair, it was considered appropriate to invite international participation. We were fortunate in having contributions from the United Kingdom, Sweden, U.S.A. and the Republic of South Africa.

Rock mechanics is a difficult scientific area for quick results. At this stage, it requires encouragement, much research and good communications. These symposia contribute to these requirements and are assisting in the progress of the subject from the area of pure science to established engineering. Much credit is due to the many individuals in the universities, in the mining companies, in goverument agencies and in the professional societies for cooperating in advancing the subject through these meetings.

A. Kerr, Technical Program Chairman,
Canadian Institute of Mining
and Metallurgy.

D.F. Coates, Chairman,
Canadian Advisory Committee on Rock Mechanics.

CONTENTS

OPEN PIT DRILLING - FACTORS INFLUENCING DRILLING RATES

A. Bauer and P.N. Calder**

Abstract

An empirical rotary drilling equation, derived from previously published field data, is used to relate the drilling rate to rock strength, pulldown weight, rotary RPM and hole diameter. To account for these empirical results laboratory indentor tests were conducted to study rock failure beneath "button" bit inserts, as used in drilling hard rock.

The results of these tests are described and it is shown how a model based on indentor penetration and sub-surface fracturing can be used to describe and predict drill performance. The model explains the dependence of the drilling rate at a given pulldown weight on rock strength and RPM. Further work is required, however, to describe completely the relationship between pulldown weight and drilling speed.

Introduction

In previous articles (1, 2, 3) it was shown how the uniaxial compressive strength of rock could be used to give a good estimate of rock drillability. Correlations were given for various sizes of rotary, percussive and jet-piercing drills. It was shown how, with improved bit design and larger machines, rotary drills were extending the range of rock types in which they offered the best economics. Today they offer the best economics in most rock types encountered in mining. This has been at the expense of hammer drills and jet-piercing machines, both of which have undergone no major improvement in recent years. This paper deals with the factors affecting rotary drill performance.

*Mining Engineering Department, Queen's University, Kingston, Ontario

Rotary Drilling Equation

Based on curves previously published (1, 2, 3) relating penetration rate in the field to RPM, pulldown weight and rock strength, it is possible to write an empirical equation containing these relevant factors which affect rotary drill performance. This equation is as follows:

$$R = \frac{(61 - 28 \, \text{Log}_{10}Sc) \times W \times RPM}{250 \times \phi} \quad \ldots\ldots 1$$

where

R = penetration rate in ft/hr

Sc = uniaxial compressive rock strength in psi x 10^{-3}

W = pulldown weight of machine in lb x 10^{-3}

ϕ = hole diameter in inches.

Table 1 gives a list of currently available rotary drills with their capacities. These machines are all designed to have an operating maximum of about 90 RPM. Many operators run their machines at lower values however and 60 RPM was typical for hard rock operations until relatively recently.

Figure 1 shows the recommended pulldown weight per inch of bit diameter for bits currently available. The larger the bit the greater the proportion of bearing area, hence the improved weight capacity. This limitation is continually being improved upon with advances in metallurgical and engineering design.

Figure 2 gives the penetration rate versus rock compressive strength for various hole diameters based on Equation 1. In each case the recommended pulldown weight, as in Figure 1, was used along with an RPM of 60. The compressive strength ranges of a few common rocke are also shown in this figure. Nearly all rocks mined fall within a compressive strength range of 5,000 – 50,000 psi. Figure 2 shows that the larger drills can obtain penetration rates of about 25 ft/hr in the hardest of these rocks (50,000 psi, quartz-magnetite, taconite). This would have been unheard of only a few years ago.

Drilling rates for conditions other than those of Figure 1 can readily be calculated using Equation 1, as shown in the following example:

Example:

In a rock with a uniaxial compressive strength of 40,000 psi a 100,000 lb machine is drilling 12-1/4 In. holes. The operator is using a pull-down weight of 50,000 lb and a rotary speed of 45 RPM. What is the penetration rate and how can this be improved upon?

From Equation 1:

$$R = \frac{(61 - 28 \times 1.602) \times 50 \times 45}{250 \times (12\text{-}1/4)}$$

$$\underline{R = 11.8 \text{ ft/hr.}}$$

If the pulldown weight is increased to 90,000 lb then the weight per inch of bit diameter is 7,300 lb which from Figure 1 is satisfactory. This will improve performance. The rotary speed can also be increased to increase the penetration rate, which for 90,000 lb and 90 RPM is:

$$R = \frac{(61 - 28 \times 1.602) \times 90 \times 90}{250 \times 12\text{-}1/4}$$

$$R = \underline{42.6 \text{ ft/hr.}}$$

These penetration rates represent the footage drilled during the time actually spent drilling. Many operators keep track of drilling rates on a shift basis. Normally only 65-70 per cent of the time a drill is manned will be spent drilling. The rest of the time will be spent moving, changing bits, etc. Thus the penetration rates on a shift basis In this example would be, 7.7 and 27.7 ft/hr.

TABLE 1

Capacities of some Typical Rotary Drilling Machines

Type	Machine wt-lb.	Max RPM	Hole Size-in.
30 R	35,000	90	6-3/4
40 R	45,000	90	7-7/8
50 R	60,000	90	9-7/8
60 BH	65,000	90	9-7/8
45 R	75,000	90	9-7/8
60 R	100,000	90	12-1/4
61 R	120,000	90	15

Pulldown Weight

It can be seen from Equation 1 that the penetration rate is directly proportional to the pulldown weight. The maximum pulldown weight a machine can deliver is the weight of the machine itself. Figure 3 shows the weight of machine required to deliver the desired weight per inch of bit for various hole sizes. The largest currently available rotary drill is the 61-R which weighs about 120,000 lb and can be fitted to drill either 12-1/4-in. or 15-in.-diam holes.

With the trend towards greater bench heights, increased burdens and spacings, and larger mining shovels it is apparent that even larger hole sizes will soon be in demand. Considering this and the fact that bit design improvements will allow for greater pulldowns, then if the present trend continues these machines will soon become unwieldy in size if one goes exclusively to increased pulldown weight for increased performance.

Rotary Speed

From Equation 1 the penetration rate is also directly proportional to the RPM. Thus an increase in RPM could be used as a substitute for an increase in machine weight to obtain the same result. Figure 4 shows the RPMs that would be required to maintain a penetration rate of 35 ft/hr in a rock of compressive strength equal to 30,000 psi with increasing hole size. The machine weight is constant at 75,000 lb. For stronger rocks the RPM equivalent would increase.

When operating a machine at a higher RPM it is important that the machine be in good mechanical condition, otherwise vibration problems may be encountered. Tests were conducted in taconite up to 100 RPM without encountering any vibration problem.

From the above considerations, the development of higher speed rotary drills would seem to be a better alternative than the construction of still larger and heavier machines. In addition, the efficiency of present machines could be greatly increased by giving them additional rotary speed capacity. For example, an RPM of 120 would double the penetration rates shown in Figure 2. Running at higher RPMs should have no effect on bit life provided the air system of the machine is sufficient for cooling bearings.

The Mechanics of Rock Failure in Drilling

Drilling is accomplished by the action of a bit against a rock surface. The function of a drill bit is to transmit energy from the machine to the rock in the most efficient manner. Figure 5 shows a typical three cone rotary bit with tungsten carbide inserts. This type of bit is used in hard rock formations ($Sc > 15$), in softer formations steel teeth replace the inserts. Figure 6 shows a percussive bit with tungsten carbide inserts. In order to design a bit that will give optimum results it is necessary to understand the mechanism by which rock fails under the action of these inserts (called indentors). Figure 7 shows the bottom hole pattern created by a 9-7/8-in. tri-cone rotary bit in specularite-magnetite ore. It is apparent that energy is transmitted simply by pushing the bit indentors against the rock and that the rotary action is principally to bring the next indentors around in hard rock. A study of indentor penetration in rock was therefore undertaken to determine the important parameters in drilling.

Indentor Testing Procedure

Tungsten carbide inserts were mounted in steel platens as shown in Figure 8A. The majority of tests were with 9/16-in.-diam hemispherical or 1/2-in.-diam blunt conical (see Figure 22) indentors, which are standard inserts used in various brands of rotary bits. Tests were run with single, and in some instances double and triple hemispherical indentors. A few tests were also run using wedges and streamlined indentors. The tests consist of pressing the indentors normally into flat rock surfaces using a 200,000 lb Riehle Testing Machine equipped with an X-Y recorder to automatically record the force-penetration data. The loading rate was .033 in./min. Faster loading rates, up to 2 in./min were run with no noticeable change in the results. Figure 8B shows some typical craters produced in Queenstown limestone using single hemispherical indentors. Figure 8C shows similar results in Barre granite.

Force Penetration Curves

Figure 9 illustrates the force penetration data for a series of tests in Queenstown limestone. In the QL 7 series a single hemispherical indentor was used, and a single conical indentor was used in the QL 8 and QL 9 series. In these tests penetration was halted at 0.1 in. The hemispherical indentor gave a linear force-penetration curve straight from the origin while the conical indentor gave a gradually increasing slope until a stable value was reached. The peaks and other discontinuities represent relief due to failures in the rock and will be discussed later.

Figure 10 shows examples of the force-penetration plots for a series of tests with a single conical indentor in Queenstown limestone. These tests were conducted to a depth of 0.2 in. Again the tendency for an increasing slope to some fixed value was evident. Figure 11 shows the results using a hemispherical indentor, and as in Figure 9 the slope was linear.

Figure 12 is for single conical indentor tests in New Hampshire pink granite, and Figure 13 is for single conical (BG 1) and single hemispherical (BG 2, BG 3) tests in Barre granite. It can be seen that in this case the slope of the force penetration curve for the hemispherical indentor increased slightly to some value from the origin, in a manner similar to the conical indentor in limestone. This behaviour is typical of harder rocks.

96038—2½

Figure 14 gives the results of tests conducted in specularite-magnetite ore with a single hemispherical indentor. This rock showed no tendency to relieve itself of the load applied. Figure 15 shows the results of similar tests in taconite. These curves do contain discontinuities due to stress relief.

Figure 16 (C2, C4) shows test results obtained using a single hemispherical indentor with an insert spacing of 2 in. It can be seen that the slopes of the force-penetration curves using the double indentor are approximately double the slopes using the single indentor as would be expected.

Figure 17A shows the results of a triple hemispherical indentor test (1-1/2 in. centres) in Queenstown limestone. The slope of the linear portion of the force-penetration curve is approximately three times that of the single indentor case. Figure 17B shows the result produced using a 1/2-in.-diam streamlined (bullet-shaped) indentor in Queenstown limestone. A very large crater was formed in this case at a relative low load. Figure 17C shows the test result using a 3-1/16-in.-long wedge of 60° included angle in specularite-magnetite. Here again the slope increased from the origin to a constant value.

Indentor Crater Characteristics

Figure 18A shows the crater produced in test QL 6-2. The force-penetration curve for this test is included in Figure 11. Notice the peak in the force-penetration curve at a load of 8,000 lb and a depth of .08 in. This corresponds to the formation of the large chips surrounding the crater centre. Figure 18B shows a plan view of the crater following sectioning and chip removal, the scale gives an idea of the crater size.

Figures 18C and D are close-ups of the indentor "seats". The surfaces of these are glassy in appearance and have probably undergone some recrystallization due to intense pressure. Below this glassy surface is a shell of highly compacted material which is bleached in appearance (Figure 18). Extruding from the base of this shell are finger-like wedges of crushed material which work their way into sub-surface cracks caused by the stress field set up around the indentor. These stress fields will he discussed later.

In some tests the blocks split vertically under the indentor instead of forming chips at the upper surface. This problem was eliminated by using larger blocks and, in some cases, by setting the blocks in concrete with reinforcing bars. The mode of failure when these vertical splits formed however was quite interesting and gave additional evidence of the formation of zones of crushed wedging material. Several of these are shown in Figure 19.

Figures 20A and B show sectioned views through indentor seats in limestone, C and D show wedges extending sub-surface cracks in limestone.

In Figure 21 sectioned views of craters in several materials are shown. In each the shell of crushed material has been removed. Sub-surface crack patterns and discolorations due to crushing are evident.

Figure 22 shows bottom, side and top views of two large limestone chips showing their typical shapes. An idealized indentor cratering model, based on the evidence of the previous discussion, is shown in Figure 23.

Rock Penetration Model for Indentors

One important conclusion that can immediately be drawn from the indentor tests is that, for indentor shapes commonly employed in drilling, the force-penetration relation is either linear or becomes linear as penetration proceeds. It is also apparent that indentors "seat" themselves on a shell of highly compacted material as the applied load builds up. The result is that the area of the indentor rock contact also becomes constant as penetration proceeds.

Based on this evidence, the following rock penetration model for indentors is proposed:

$$\frac{dF}{dh} = KA \qquad \ldots\ldots 2$$

where h = depth of penetration

K = rock penetration constant

F = applied force

A = horizontal projection of indentor area at depth h .

Based on Equation 2 the following general relations for various indentor shapes may be derived:

Wedges:

$$A = 2\ L\ h\ \tan\ (\theta/2)$$

where L = length of wedge

θ = included angle of wedge

$$\therefore \quad K = \frac{F}{L \tan\ (\theta/2)\ h^2} \qquad \ldots\ldots 3$$

Hemispheres:

$$A = \pi h (2r - h)$$

for $h \leq r$

r = radius of hemisphere

$$\therefore \quad K = \frac{F}{\pi h^2 (r - \frac{h}{3})} \qquad \text{.....} 4$$

Cones:

Let θ = included angle of cone, then

$$A = \pi (h \tan (\theta/2))^2$$

$$\therefore \quad K = \frac{3F}{\pi h \tan^2 (\theta/2)} \qquad \text{.....} 5$$

Constant Area

For an indentor of constant area:

$$K = \frac{F}{h A} \qquad \text{.....} 6$$

K is therefore simply the slope of the force-penetration curve when it becomes linear, divided by the contact area.

The following conclusion regarding the energy (E) required for indentor penetration may be drawn, (4):

Since $E = \int_o^h F \, dh$

$$E = KA \int_o^h h \, dh$$

$$E = \frac{AKh^2}{2}$$

or: $h \propto E^{1/2}$ 7

Rock Penetration Constant

Table 2 gives the rock penetration constant K , determined for the various rocks tested from the stable slopes of the force-penetration curves. The curved initial portions of the curves can be explained by the dependence of A on h, Equations 3, 4, 5, until a constant-bearing area is built up. Log plots of an area under the force-penetration plots versus penetration are linear with slopes of 1/2 indicating that Equation 7 is obeyed and A is constant essentially since the area under the initial sloping parts is small. The uniaxial compressive strengths of the rocks, determined using a length-to-diameter ratio of 2-1/2 : 1 are also included in Table 2. Figure 24 is a plot of Sc versus K, and shows an excellent linear correlation between the two.

An interesting sidelight is that indentor tests of this type could be used to determine the uniaxial compressive strengths of rocks both in the laboratory and in situ.

TABLE 2

Rock Penetration Constants (K) and Uniaxial Compressive Strengths (Sc) of the Rocks Tested

Rock Type	K - $\frac{\text{lb}}{\text{IN}^3} \times 10^{-6}$	Sc-psi
Marble	4.26	5,520
Queenstown Limestone	9.69	10,900
Barre Granite	13.4	14,300
New Hampshire Pink Granite	18.2	19,100
Specularite-magnetite Ore	22.5	23,500
Taconite Ore	29.0	28,700

Rock Failure Beneath Indentors

The full depth of rock destruction achieved by an indentor is caused by its penetration plus the rock fractured beneath it by the stresses it induces. The linear relationship of K versus Sc having been established, remains to determine the extent of damage due to the stress fields around the indentor. Assuming a homogeneous, isotropic, elastic media, Boussinesq's Equations 5, 6 can be applied, Equations 7, 8, 9.

Figure 25A shows the case of a line load acting normally on the edge of a semi-infinite plate. The stress distribution for this case may be solved using the two dimensional form of Boussinesq's equations. These stresses will be similar to those induced beneath the tip of a wedge-shaped indentor in an elastic situation. Figure 25B shows a point load acting normally on the surface of an elastic half space. The three dimensional form of Boussinesq's equations give the stresses for this case. These may be taken as an approximation of the stresses beneath a hemispherical or conical indentor in rock. Figure 26 shows the stress trajectories for both these cases.

Once the stresses beneath an indentor are determined it is necessary to assume a failure criterion in order to predict failure, Equation 10. At low values of confining pressures the simple Mohr-Coulomb criteria give a good approximation. Referring to Figure 27, failure will occur when the shear stress, τ , equals $C + \sigma \tan \phi$

where C = cohesive strength of material

ϕ = angle of internal friction

σ = normal stress.

Failure occurs at an angle Ψ , as shown, and:

$$\Psi = 45 + \phi/2 \qquad \ldots\ldots 8$$

Also from the geometry:

$$\frac{\sigma_{max} + \sigma_c}{\sigma_{min} + \sigma_c} = \omega \qquad \ldots\ldots 9$$

where

$$\omega = \tan^2 45 + \phi/2 \qquad \ldots\ldots 10$$

and

$$Sc = \frac{2 \sin \phi \ \sigma c}{(1 - \sin \phi)} \qquad \ldots\ldots 11$$

The dotted line in Figure 27 represents a modified failure envelope which has the form of a parabola, Equation 11. This type of failure envelope should be used where confining pressures are involved ($\sigma_{max} > Sc$).

Failure surfaces may be defined as surfaces everywhere tangent to the direction of failure. The direction of failure, Ψ , is given by Equation 8. Thus knowing the principal stress trajectories the failure planes are known. Failure planes for the case of line and point loads take the form of logarithmic spirals, as shown in Figures 26A and B. The shape of these spirals explains the shape of sub-surface crack patterns in indentor testing.

Line Load Case

In this case Boussinesq's equations are:

$$\sigma_r = \frac{2 \ F \ \sin \theta}{\pi r} \qquad \ldots\ldots 12$$

$$\sigma \theta = \tau_{r\theta} = 0 \qquad \ldots\ldots 13$$

The stress distribution is one of simple radial compression. Consider a circle of diameter d drawn with its centre along the axis of loading and tangent to the surface. At any point on the circle, $r = d \sin\theta$, substituting this in Equation 12, gives:

$$\sigma_r = \frac{2F}{\pi d}$$

using Equations 9, 10 and 11:

$$d = \frac{4F}{(1 - \sin\phi)\, Sc} \qquad \ldots\ldots 14$$

This equation defines a cylindrical failure envelope within which failure will have occurred for a given applied load and physical rock properties. Thus the solid portion of the spirals shown in Figure 26 represent the extent of failure for a set of given conditions, the broken spirals show the paths along which failure will proceed as the applied load is increased. It should be noted that an infinite force would be required to extend the failure spirals to the surface.

Point Load Case. The failure envelope in this case is roughly a sphere, symmetric about the axis of loading and tangent to the surface, as shown in Figure 26B.

Along the axis of loading Boussinesq's equations for this case are as follows:

$$\sigma_r = \sigma_{min} = 0$$

$$\sigma_z = \sigma_{max} = \frac{3F}{2\pi d^2} \qquad \ldots\ldots 15$$

Using Equations 9, 10 and 11:

$$d = \left(\frac{3 F \sin\phi}{\pi Sc\, (1 - \sin\phi)\, (\omega - 1)} \right)^{1/2} \qquad \ldots\ldots 16$$

Multiple Loads. It is possible to calculate the total stress field set-up when there is more than one simultaneous contact point. However, indentors that touch simultaneously in present rock bits are too far apart to reinforce one another.

Rotary Drilling Model

Based on the indentor test results and analytic considerations just presented, the following rotary drilling model is proposed.

The penetration achieved by an indentor pushed into a rock surface can be calculated using the rock penetration constant as previously described. In addition, the extent of rock fracture beneath the indentor tip can be estimated using Equation 16. If the spacing between successive points of indentor application is equal to d, the diameter of the spherical failure envelope predicted by Equation 16, the two spheres will touch and thus break a piece out. Ideally then, the amount of penetration caused by this action would be $d/2$. The actual case is more complicated and such things as wedging, discontinuities caused by previous indentations, etc., play a part. As an approximation the penetration caused by this factor will be taken as $K_1 d$ and K_1 will be determined from field data. The total penetration H, is then:

$$H = K_1 \left(\frac{3\ F\ (2 \sin\phi)}{2\ \pi\ (1 - \sin\phi)\ (Sc\ (\omega - 1))} \right)^{1/2} + h \qquad \ldots\ldots 17$$

where

h is the indentor penetration calculated using K and, for a hemispherical indentor, Equation 4.

Assuming an angle of internal friction $\phi = 30°$, which is a good approximation for most rocks, Equation 17 reduces to:

$$H = K \left(\frac{3\ F}{2\ \pi\ \ Sc} \right)^{1/2} + h \qquad \ldots\ldots 18$$

In Figure 28 values calculated using Equation 18 are compared with field data. The field data is from 60-R tests at a pulldown weight of 80,000 lb and an RPM of 60 using 9-7/8-in. bits. In order to use Equation 18 the maximum weight acting on an individual compact must be estimated. Referring to Figure 5 it is evident that between 14 and 18 compacts will touch simultaneously. The maximum weight per indentor is therefore estimated as:

$$F = \frac{80,000}{16} = 5,000 \text{ lb}$$

Using this Figure and K_1, estimated at 0.4, the penetration rate in ft/hr is calculated as follows:

H is calculated using Equation 18. This value represents the thickness of the layer of rock removed from the hole bottom during each rotation of the bit.

$$\therefore \quad \text{ft/hr} = \frac{H \times RPM \times 60}{12}$$

It is seen that the model fits the field data quite well.

1. It is possible to determine a rock penetration constant, K, which varies linearly with the uniaxial compressive strength of the rock. This constant can be used to predict the slopes of indentor force-penetration curves.

2. If sufficient force is applied to an indentor, a chipping process takes place. This can be explained by considering the extent and direction of failure because of the stresses involved, and the effect of wedging caused by crushed material being forced into partially formed failure planes.

3. The force required to cause chipping on the surface of flat undamaged samples is much greater than the force per insert available on present drilling equipment.

4. The total penetration achieved per indentor in rotary drilling is made up of a linear portion because of indentor penetration (< 10 per cent of total), plus a portion caused by stress fracture beneath the indentor tip. Calculations based on these considerations for a given RPM and pulldown weight follow field data quite well.

5. Since most of the hole penetration is achieved by stress fracturing (> 90 per cent), it can be stated from Equation 18 that:

$$R \propto \left(\frac{F}{Sc}\right)^{1/2} \qquad \ldots\ldots 19$$

where R is the penetration rate.

6. The $R \propto \dfrac{1}{Sc^{1/2}}$ relationship is in close agreement with field data, this accounts for the good correlation in Figure 28.

7. The $R \propto F^{1/2}$ relationship is not in agreement with observed results. Equation 1, based on field data, shows that over the range for which results are available, $R \propto F$.

8. Referring back to item 1 in this list, it is possible that for the fractured and irregular conditions which prevail at hole bottom chipping is possible at the loads available. This would account for the observed high penetration rates. Further investigation should be conducted in this area.

9. Indentor tests can be performed on rocks, either in the laboratory or in situ, to give a good estimate of drilling penetration rates and uniaxial compressive strengths.

10. The most promising possibility for a major improvement in drill performance at this time is the use of high rotary speeds in drilling.

Acknowledgments

This paper is extracted from a thesis to be submitted by Peter N. Calder in partial fulfilment of the requirements for the Master of Science Degree at Queen's University. Mr. Calder is the holder of an International Nickel Company of Canada Fellowship, and this is gratefully acknowledged. Thanks are extended to the Bucyrus-Erie Company, Hewitt Equipment Limited, and Mussens of Canada Limited, for their help; to National Research Council for financial support under Grant No. A3405, and to the ore producers who supplied samples.

References

(1) Bauer, A., Carr, N.H., Calder, P.N., Harris, G.R.:
1965: Drilling and Blasting at Smallwood Mine, - Proc. VII Symp Rock Mech., Pennsylvania State Univ., June.

(2) Bauer, A. and Calder, P.N.:
1966: Drilling in open pit iron mines, presented at Am. Mining Congr., Sept. Abstracted in Can. Pit and Quarry, December.

(3) Bauer, A.:
1967: Open pit drilling, presented at A.I.M.E. Meeting, Duluth, Minn., Jan.

(4) Hartman, H.L.:
1959: Basic studies of percussion drilling, Trans. A.I.M.E. (Mining), TP4785A.

(5) Timoshenko, S. and Goodier, J.:
1951: Theory of Elasticity, McGraw-Hill.

(6) Durelli, A.J., Phillips, E.A., Tsao, C.H.:
1958: Introduction to the Theoretical and Experimental Analysis of Stress and Strain, McGraw-Hill.

(7) Tandanand, S. and Hartman, H.L.:
1962: Stress distribution beneath a wedge-shaped drill bit loaded statically, Internat. Symp. Mining Res., Pergamon Press.

(8) Reichmuth, D.R.:
1962: Correlation of Force-Displacement Data, V Symp. Rock Mech., Univ. Minnesota.

(9) Paul, B., Sikarskie, D.L.:
1965: A Preliminary Theory of Static Penetration by a Rigid Wedge into a Brittle Material, - VII Symp. Rock Mech., Pennsylvania State Univ., June.

(10) Clausing, D.P.:
1959: Comparison of Griffith's Theory with Mohr's Failure Theory, Quart. Colorado Sch. Mines, v. 54.

(11) Fairhurst, C.:
1964: On the validity of the Brazilian test for brittle materials, Internat. J. Rock Mech. Mining Sci., v. 1, pp. 535–546, Pergamon Press.

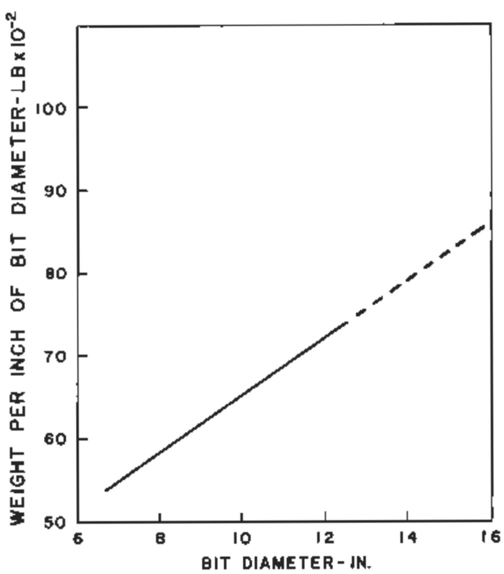

Figure 1. Recommended pulldown weight per inch of bit diameter vs bit diameter.

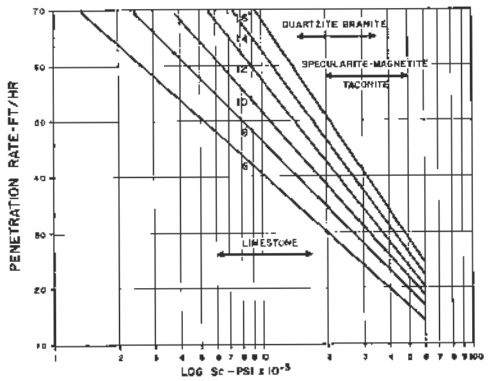

Figure 2.
Penetration rate versus rock compressive strength for various hole diameters at the recommended weight per inch of bit and 60 RPM.

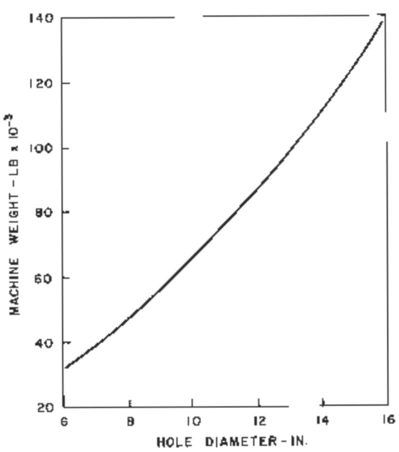

Figure 3. Machine weight required to give desired weight per inch of bit for various hole sizes.

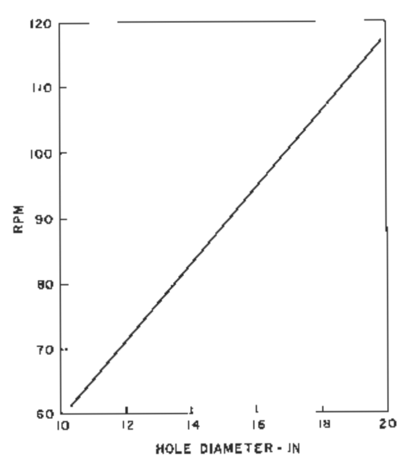

Figure 4. RPM required to maintain a penetration rate of 35 ft/hr with Sc = 30 and a pulldown weight of 75,000 lb.

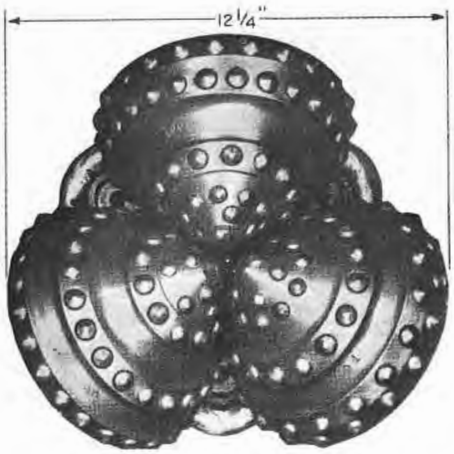

Figure 5. Typical tri-cone rotary bit with tungsten carbide inserts.

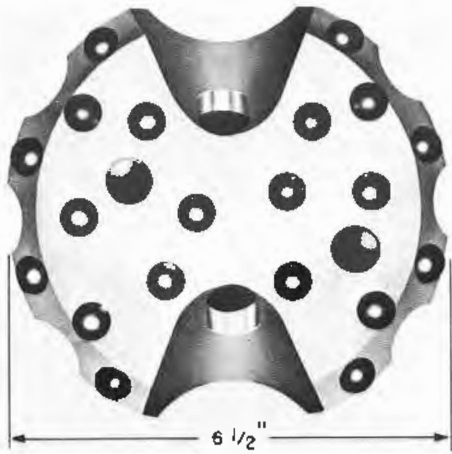

Figure 6. Typical percussive "button" bit.

Figure 7. Right-hand hole pattern produced by a 9-7/8-in. tri-cone rotary bit in specularite-magnetite ore.

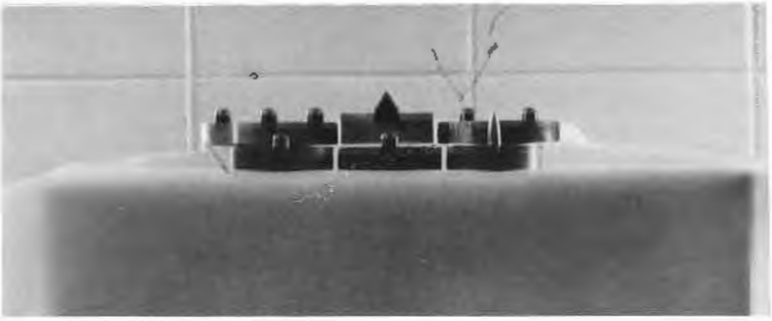

A

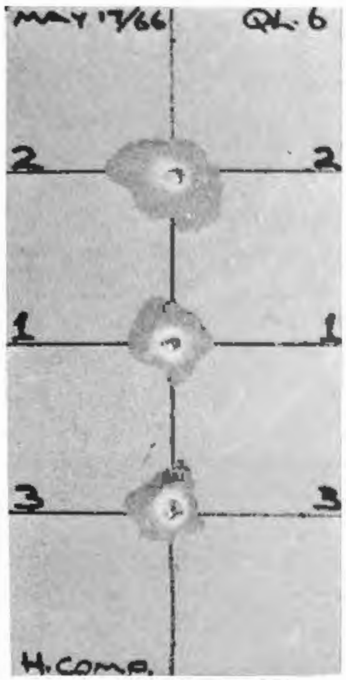

B
3" x 3" GRID

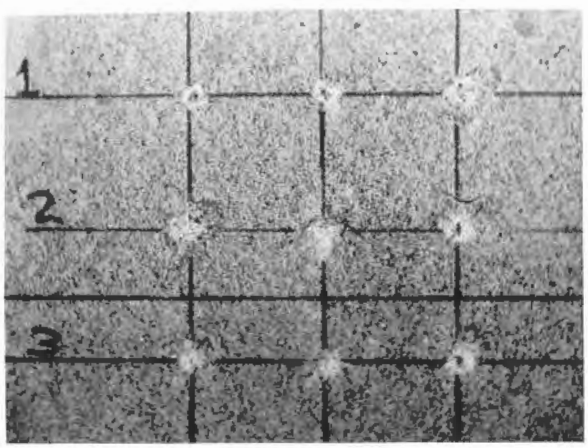

C
3" x 3" GRID

Figure 8. A - Typical indentors used in tests, B - Typical craters produced in limestone (Queenstown) and, C - Granite (Barre) using single hemispherical indentors.

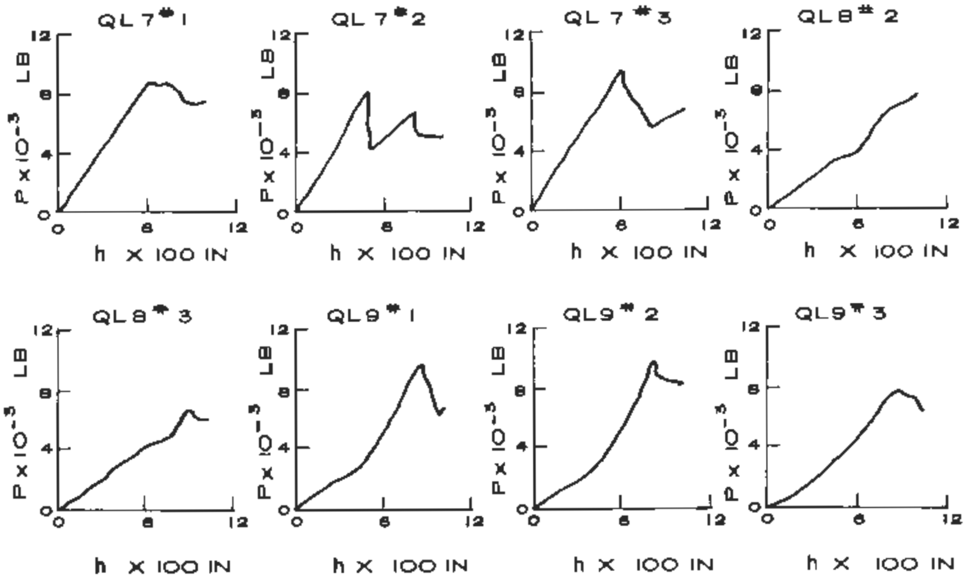

Figure 9. Single indentor tests in Queenstown limestone with hemispherical (QL 7) and conical (QL 8–9) indentors to a depth of 0.1 in.

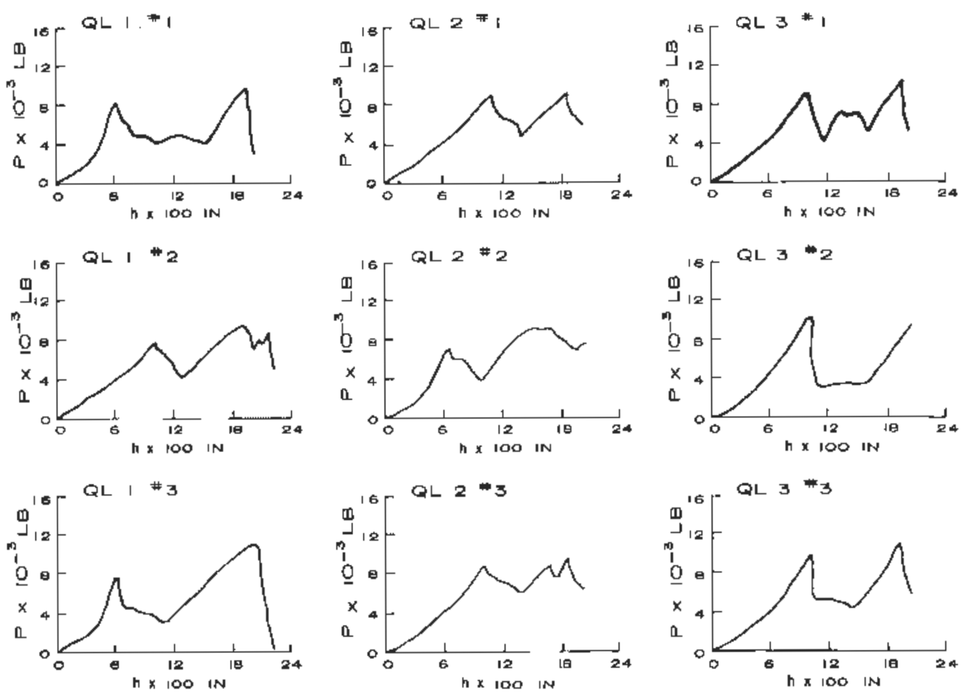

Figure 10. Single conical indentor tests in Queenstown limestone to a depth of 0.2 in.

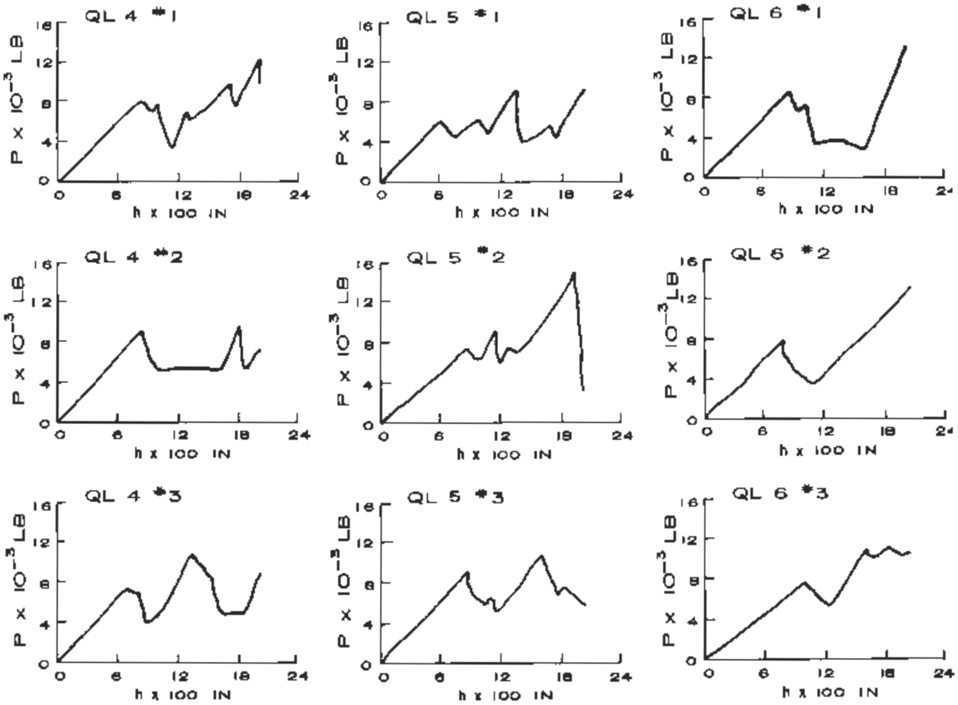

Figure 11. Single hemispherical indentor tests in Queenstown limestone to a depth of 0.2 in.

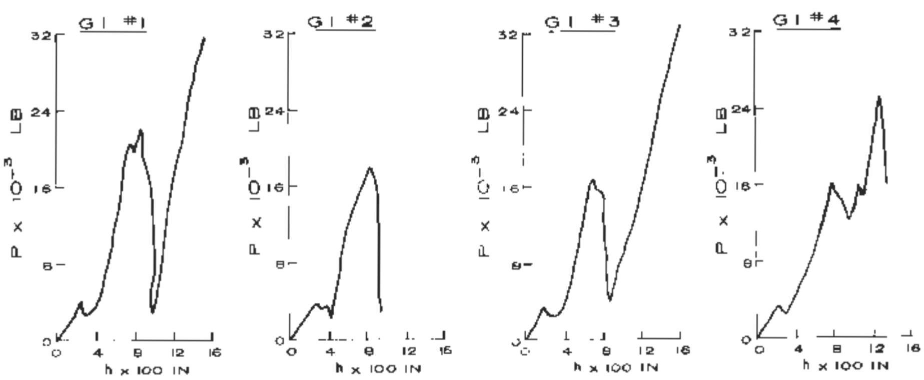

Figure 12. Single conical indentor tests in New Hampshire pink granite.

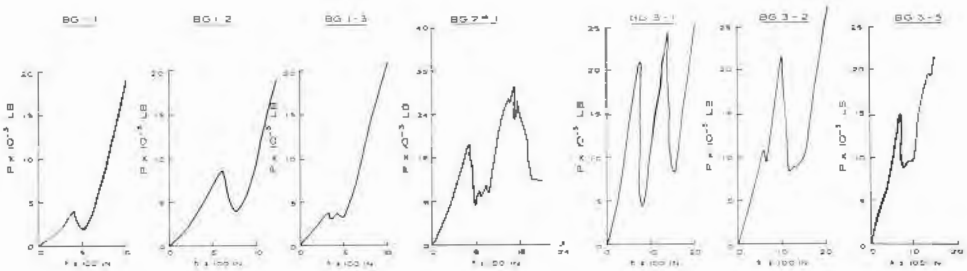

Figure 13. Single conical (BG 1) and hemispherical (BG 2 – BG3) indentor tests in Barre granite.

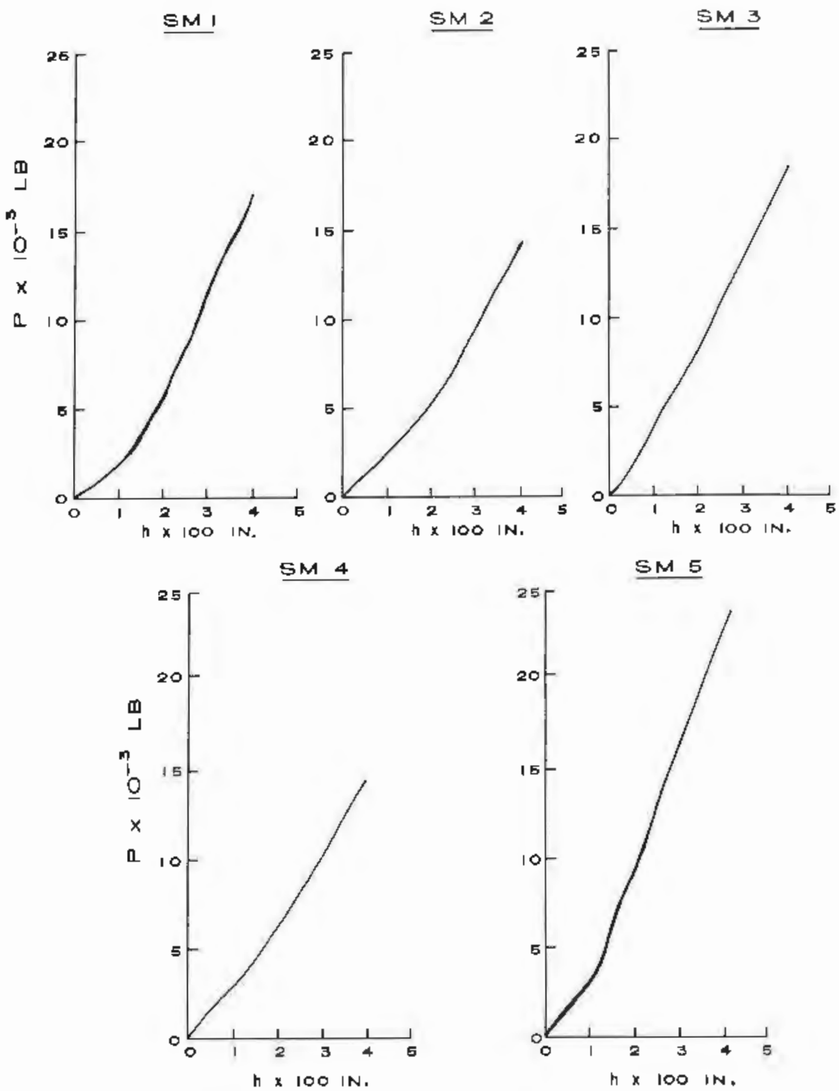

Figure 14. Single hemispherical indentor tests in specularite-magnetite ore.

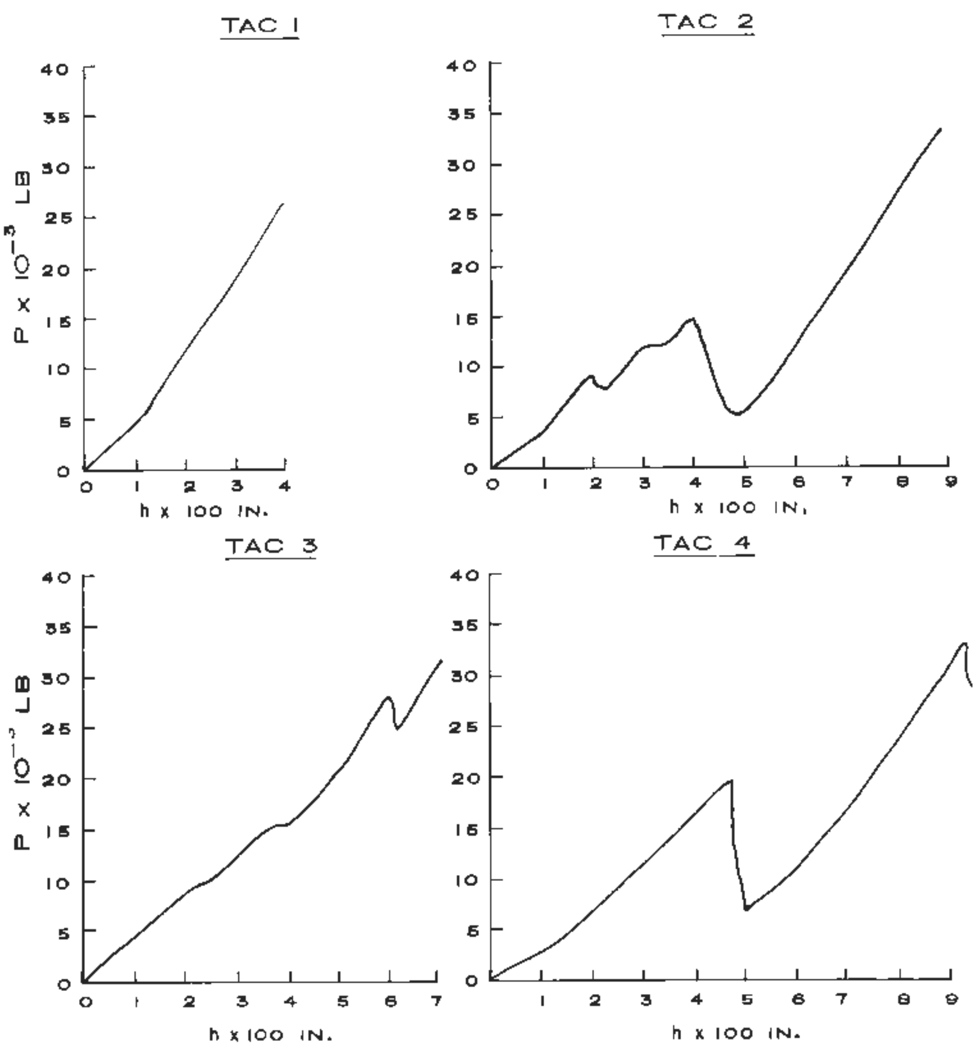

Figure 15. Single hemispherical indentor tests in taconite ore.

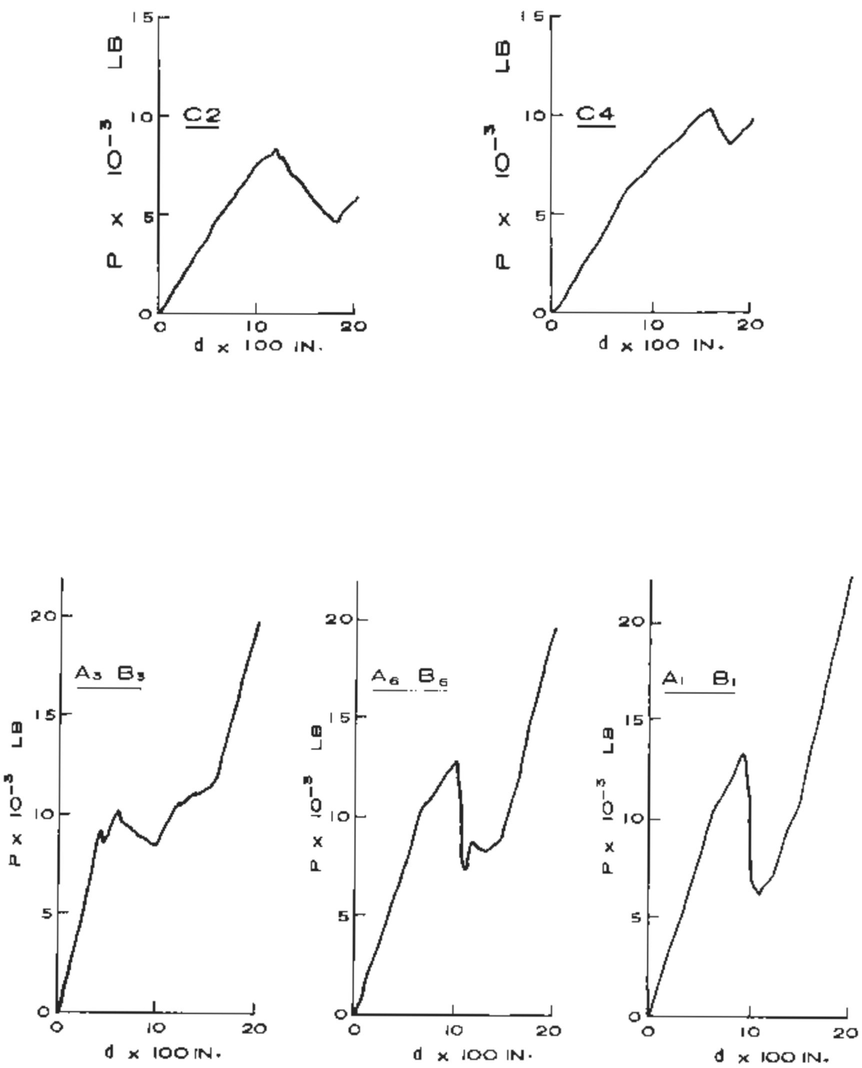

Figure 16. Single (C) and double (A–B) hemispherical indentor test results in marble.

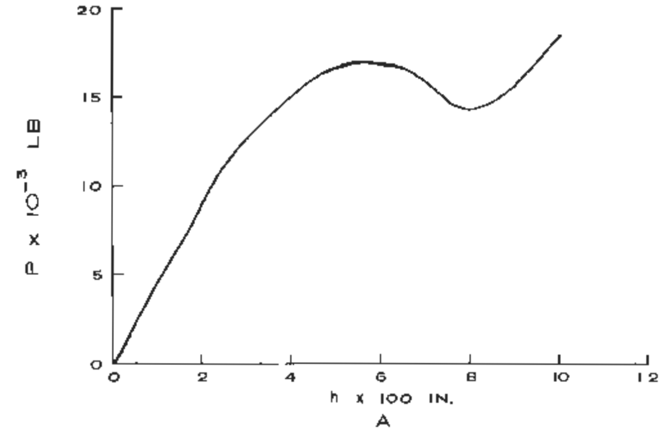

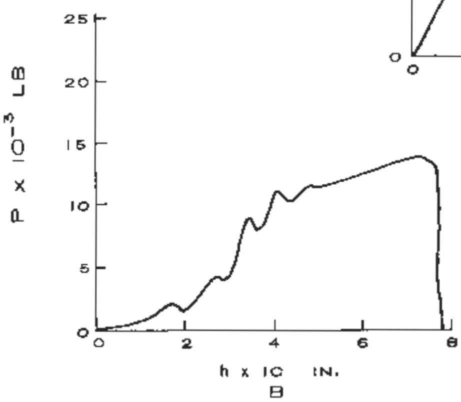

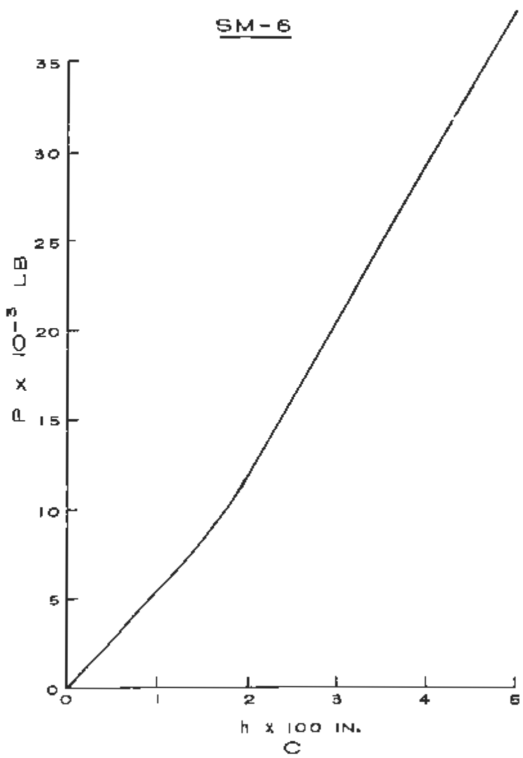

Figure 17. A - Triple hemispherical (1-1/2-in. spacings) indentor test in Queenstown limestone, B - 1/2-in. diameter streamlined indentor test in Queenstown limestone, C - Test with 60° wedge (3-1/16-in.-long) in specularite-magnetite ore.

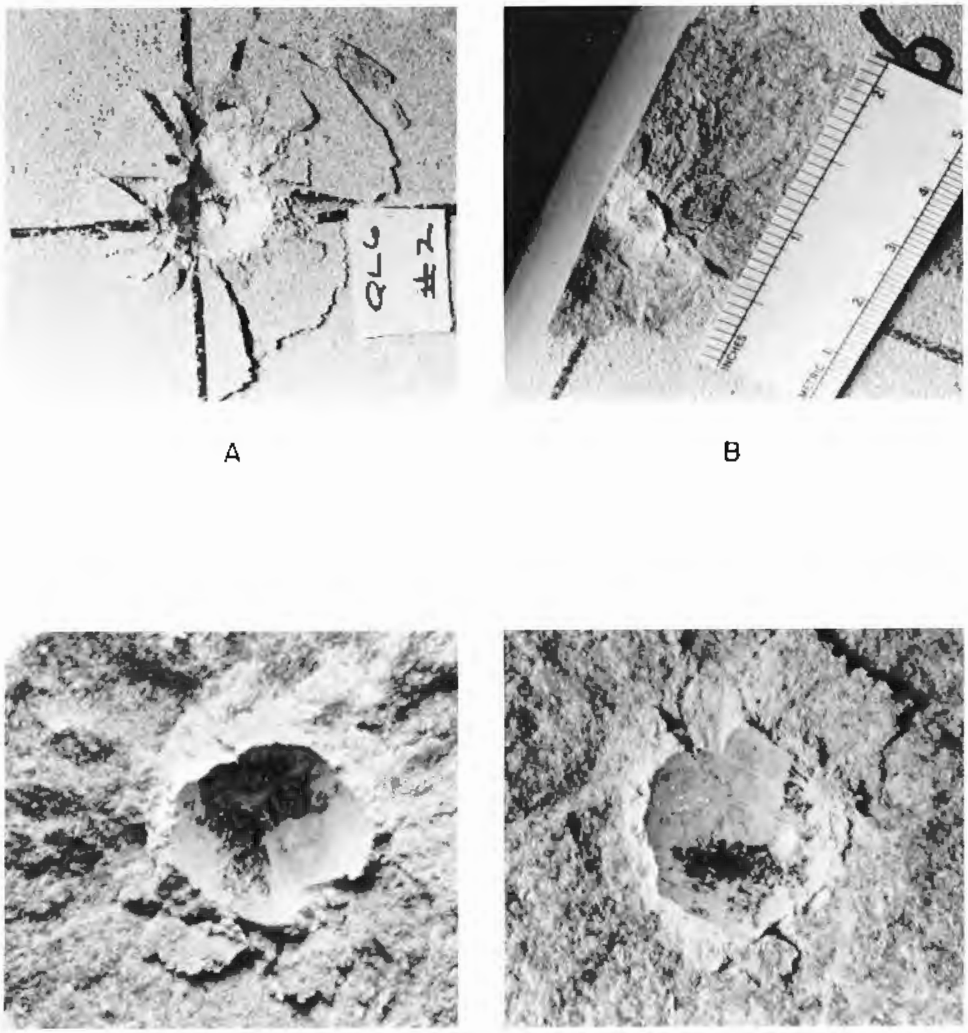

Figure 18. A - Close-up of chips around a typical limestone crater, B - Plan of sectioned sample showing horizontal wedging, (C-D) Close-ups of indentor "seats" in crater showing crushed material and horizontal wedges.

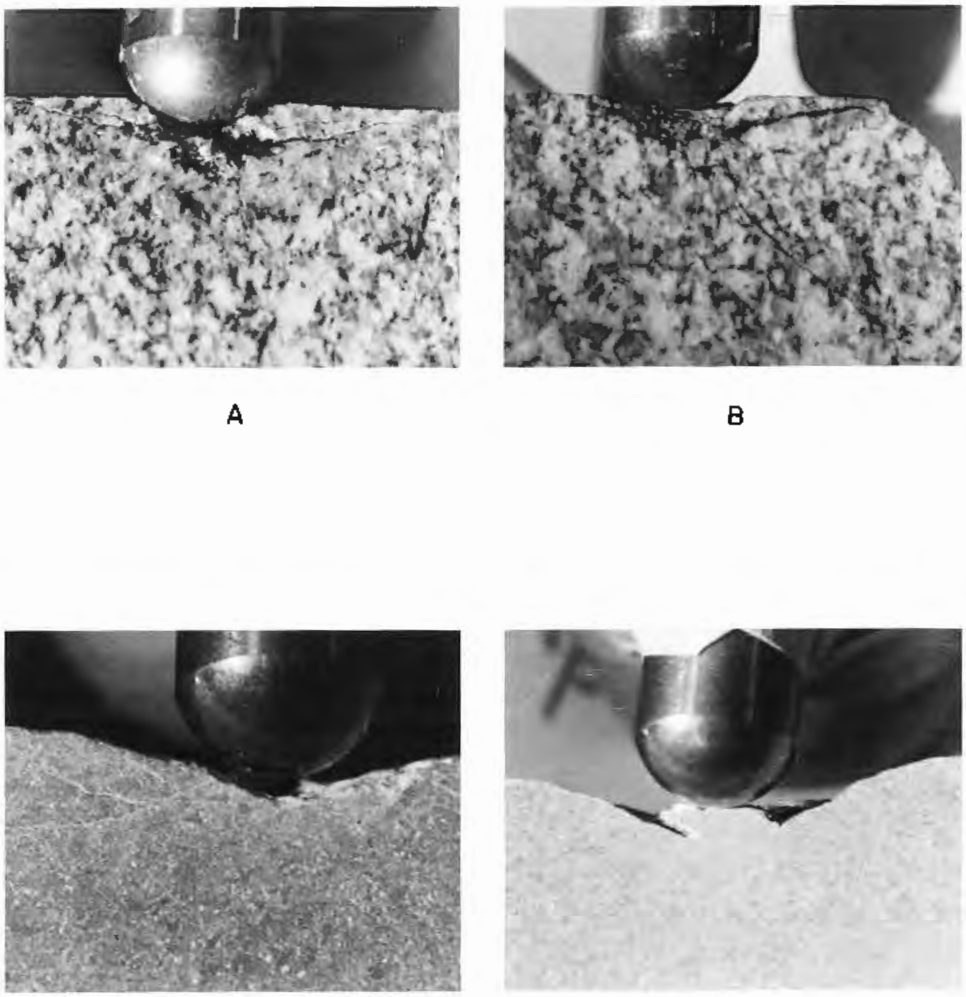

A B

C D

Figure 21. Sectioned views showing sub-surface cracks due to hemispherical indentor loading in Barre granite, (A, B) and Queenstown limestone (C, D).

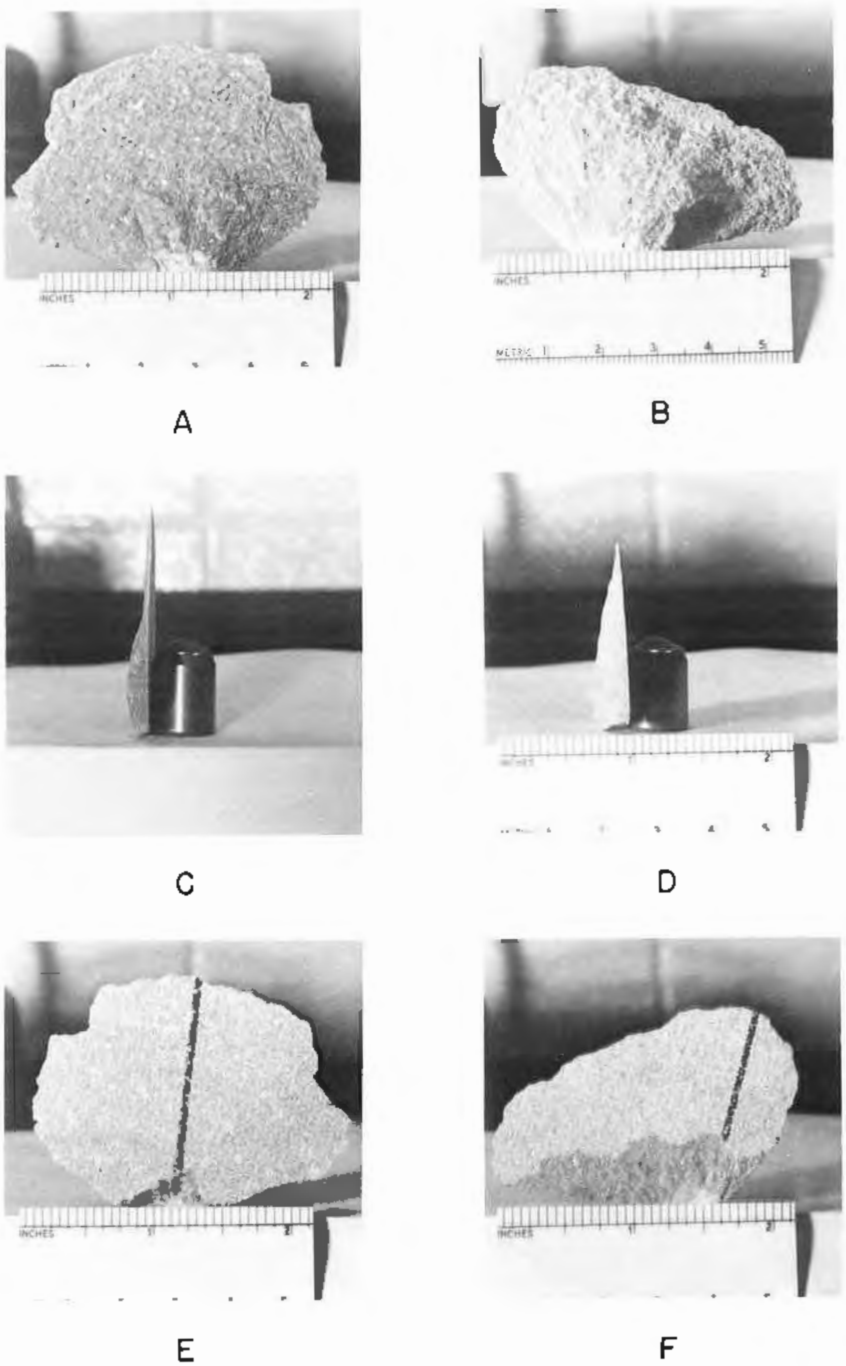

Figure 22. Bottom (A-B), side (C-D) and top (E-F) views of two large chips produced by hemispherical indentor tests in limestone.

96038—3½

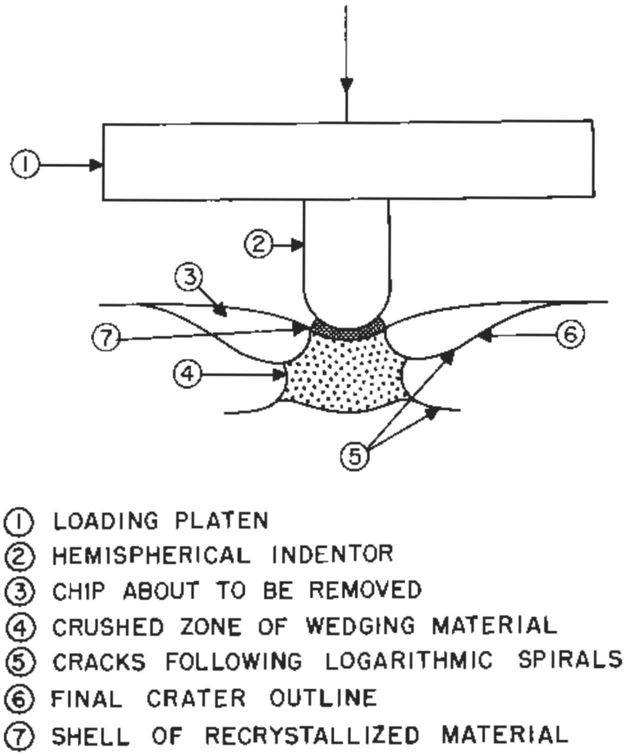

Figure 23. Idealized indentor cratering model.

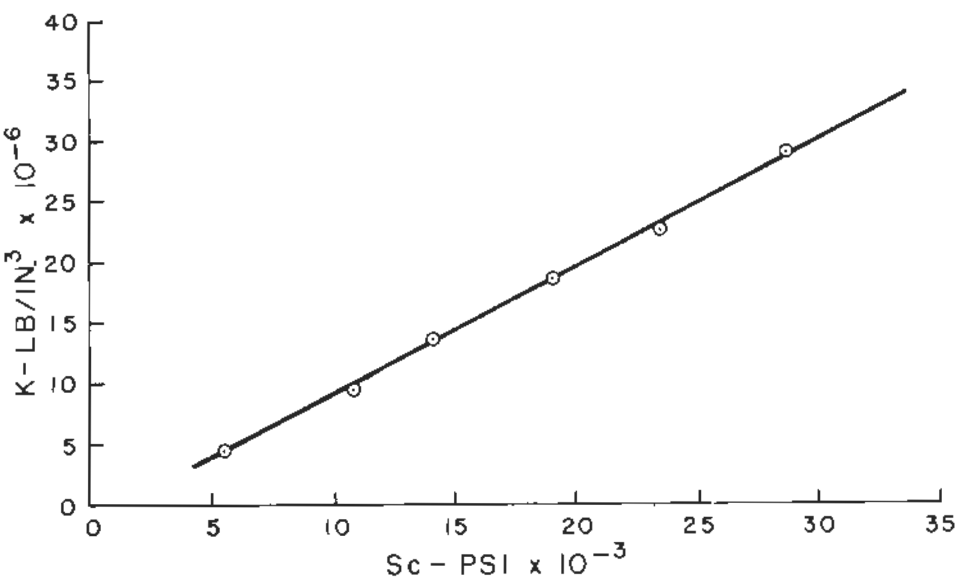

Figure 24. Rock penetration constant vs uniaxial compressive strength.

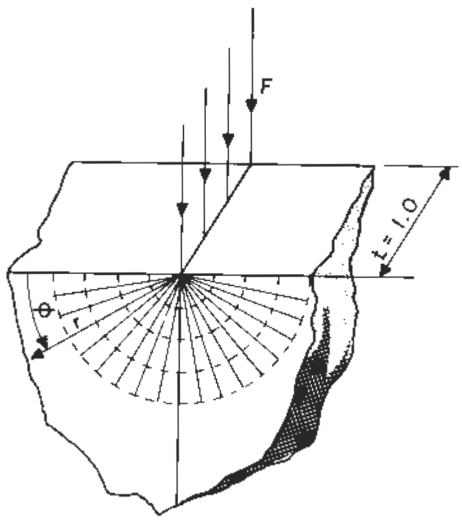

r, θ -- POLAR COORDINATES
SOLID LINES ARE σ_r ISOSTATICS
DOTTED LINES ARE σ_θ ISOSTATICS

A

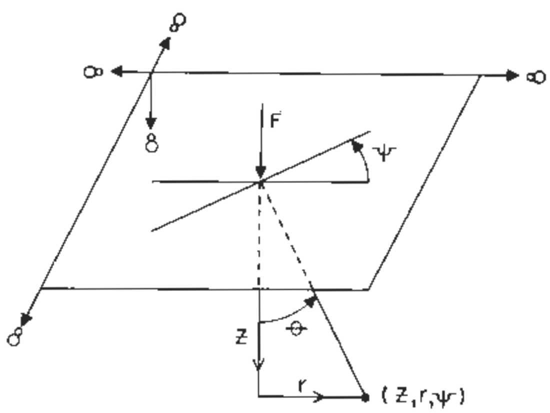

B

Figure 25. A - Line load acting on the edge of a semi-infinite plate, B - Point load acting on the surface of a half-space.

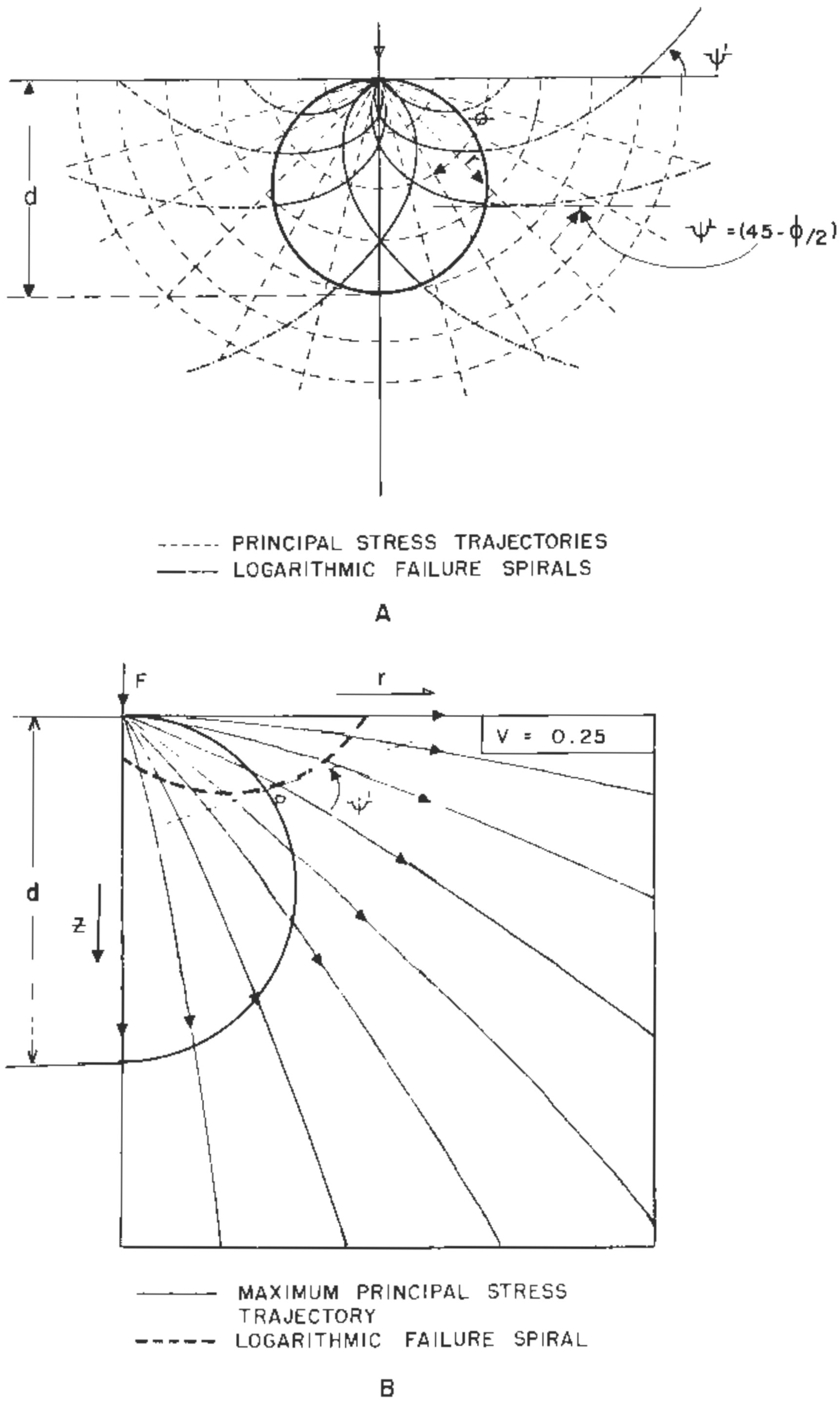

Figure 26. **Stress distributions and failure spirals associated with A, a line load and B, a point load.**

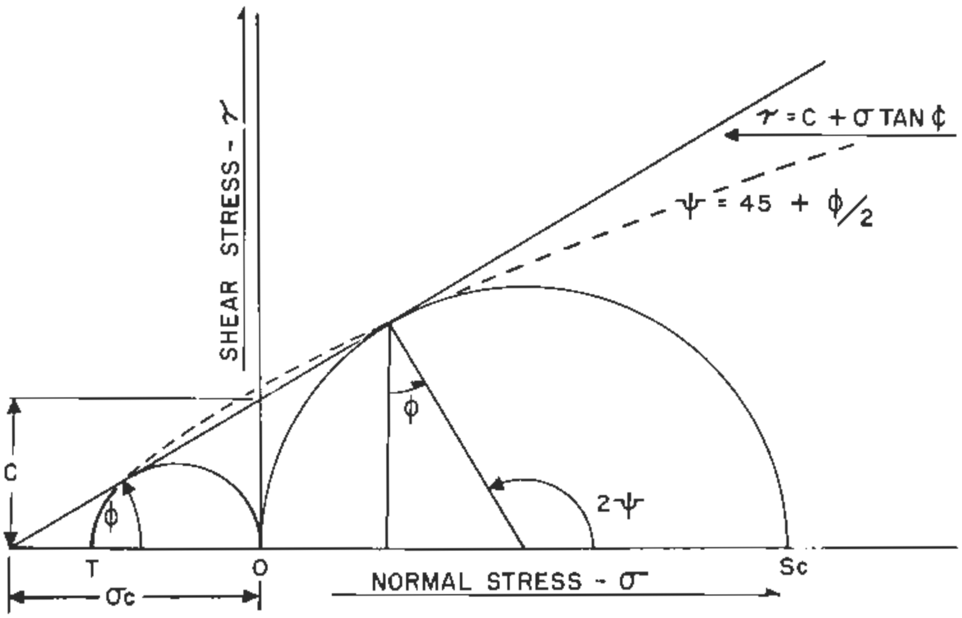

Figure 27. Representation of the Mohr-Coulomb failure theory.

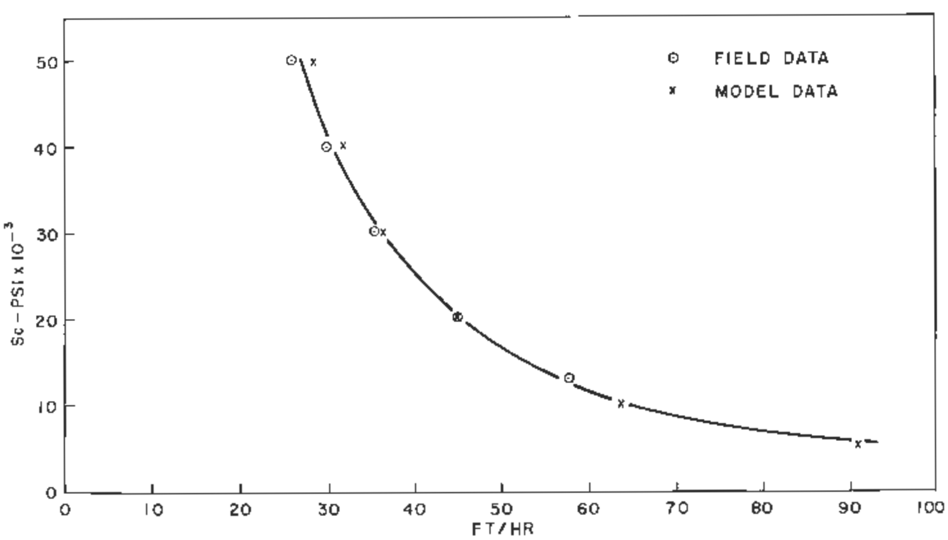

Figure 28. Comparision of field drilling rates with values calculated using rotary drilling model.

CONTROL OF GROUND MOVEMENT AT THE GECO MINE

*R.C.E. Bray**

Introduction

The lessons in ground control at the Geco Mine have been learned by experience. From the behaviour of the ground in the first block of stopes mined, certain assumptions were made for the design of the second block of stopes. The adverse effects which resulted from this mining program necessitated modifications in the dimensions of subsequent stope layouts, but also resulted in the evolution of a shrinkage-blast hole type of mining which has been used very successfully since.

In this paper, the early mining efforts are described as well as the subsequent modifications which were adopted to correct the faults in these initial efforts.

The Mine Property

The Geco Mine, a division of Noranda Mines Limited, is a base-metal operation in northwestern Ontario, 50 miles north of Lake Superior and midway between the cities of Port Arthur and Sault Ste. Marie. From the commencement of production in September 1957 to the end of 1966, a total of 828,700 tons of copper concentrate, 688,600 tons of zinc concentrate and 14,570 tons of lead concentrate have been produced from milling 12,141,600 tons of ore. The current rate of production is 4,000 tons/day. Three quarters of this comes from blast hole stopes and the remaining quarter from cut-and-fill stopes, and stope preparation (both blast hole and cut-and-fill). The details of the mining operations have been described by McLeod (1), Marshall (2), and Brooks (3) and are therefore dealt with only briefly.

*Noranda Mines Limited, Geco Division, Manitouwadge, Ontario.

The paper by Brown and Bray (4) gives a detailed description of the geology of the mine and need not be repeated here. Certain features of the structural geology which have a bearing on the mining operations are of interest.

The Geco orebody, in common with other known orebodies of the Manitouwadge area, is associated with a dragfold on the south limb of the Manitouwadge syncline. This major geological structure, the nose of which is about five miles west of the Geco plant, has an easterly plunge, and all the orebodies have a similar plunge.

The Geco ore occurs in a quartz muscovite schist, having developed along an east-west fault which parallels the axial plane of the dragfold. The orebody consists of a core of massive sulphides (chalcopyrite, sphalerite, pyrite, pyrrhotite) partly surrounded by an envelope of disseminated sulphides (chalcopyrite, pyrite, pyrrhotite). It forms a tabular mass lying more or less vertical, and raking eastward at from 20° to 30° (Figure 1). In cross-section, the orebody has the shape of an onion, with the bulbous bottom portions conforming to the curvature of the dragfold.

The grade of the ore averages better than 2 per cent copper, 4 per cent zinc and 2 oz/ton silver. There is a rough zoning of the ore at right angles to the line of the rake, with copper concentrated at the deeper horizons and zinc at the shallower. Where the widths are large (up to 200 ft in places), blast hole mining is used, but where the ore narrows to 25 ft or less it is necessary to change to a cut-and-fill method. The differences in the grades of the ore being mined are averaged out by random distribution of the crushed ore as it is fed into the four 2,000 ton bins in the concentrator.

As previously mentioned the host rock for the ore is a quartz muscovite schist - a metamorphosed quartzite. As a result of the regional folding, this schist has a pronounced foliation in an east-west direction. Narrow quartz diorite dykes have been intruded into the schist at a small angle to the plane of the schistosity.

Coarse and fine grained pegmatite dykes, striking generally north-east, south-west and dipping west, have also intruded the schist. Later faulting along the axial plane of the dragfold has offset these pegmatites. The introduction of the sulphides forming the orebody, filled this fault zone, and although fragments of pegmatite are found within the massive sulphide core, the pegmatite dykes cannot be traced across the massive sulphides.

Late diabase dykes fill north-south fractures with the broader dykes crossing the orebody, while some of the narrow ones (less than 12 in.) pinch out within the ore zone. The diabase is itself extensively jointed, and hence is a structurally weak rock. Post-intrusion faulting has caused crushing along some dyke contacts with the development of gouge.

Multiple folding in the ore bearing schist, transverse to the main drag folding, aggravates the ground weaknesses induced by faulting and fracturing, and in some places increases the tendency to slough.

As a rule, the pegmatite dykes are not mineralized, except where in contact with the massive sulphide core. They are, therefore, rarely included in a stope, but may form a stope wall. Since the large dykes (over 3 ft) are extensively fractured, they tend to slab and break off when exposed over a wide surface. By contrast, the massive sulphide core of the orebody is relatively free from joints and fractures and has been observed standing solidly over horizontal lengths of 70 ft and vertical heights of over 300 ft. Thus the structural weaknesses of the ore bearing formation consist of:

(a) Foliation and some faulting in an east-west direction.
(b) Jointing and minor faulting in a north-south direction.
(c) Weak contacts along diabase dykes and along quartz diorite/quartz muscovite schist contacts.
(d) Regional, drag and cross folding.
(e) Irregular fractures and joints in broad pegmatites.

Stoping Practices

The orebody is divided into blocks for convenience of identification (Figure 2).

"A" block extends 1,000 ft eastward from the point where the bottom of the orebody reaches the surface to the Fox Creek fault. The presence of a 100-ft-wide north-south diabase dyke 150 ft west of the fault made it necessary to restrict the mining to the portion of the orebody lying to the west of this dyke.

"B" block extends from the Fox Creek fault about 750 ft eastward to another transverse diabase dyke, the so-called Shaft Diabase (since it crosses the orebody close to No. 1 shaft).

"C" block includes the next 950 ft east from the shaft diabase.

"D", "E", and "F" blocks are arranged in order to the east and each has a horizontal (strike) length of 1,000 ft. To date, mining has been carried out in "A", "B", "C", "D", and "E" blocks. The first production came from "A" block. Except for a 50-ft-long, 45-ft-high unmined portion, purposely left against the west side of Fox Creek diabase to prevent sloughing of the diabase and also possible flooding from Fox Creek, and the 150-ft portion between the Fox Creek diabase and the Fox Creek fault, all the ore has been extranted from "A" block.

Mining of "A" Block

Mining of "A" block was accomplished by alternate stopes and pillars laid out across the orebody. Most of the stopes (and pillars) were 50 ft in strike length, about 300 ft high and an average width of about 65 ft. The stopes were blasted through to surface and pulled empty, then the intervening pillars were blasted into these holes. All the blasting was accomplished in 36 months and no pillar was left standing exposed for more than seven months. As was expected, some sloughing of the stope walls occurred, and a surface pillar above the easterly stopes collapsed. From a position on the west end of this open pit, the gradual disintegration of this pillar was observed. As a succession of chunks (not over 4 cu ft in size approximately) fell from the originally flat stope back, a well defined arch was formed. Presumably the nearly vertical inclination of the formations prevented the "key stones" of this arch from resisting the vertical forces on them, and so the pillar collapsed. Since the greater part of this sloughed material was of ore grade, it did not seriously dilute the previously blasted ore on which it fell.

Mining of "B" Block

Influenced by the successful mining in "A" block, and also by the configuration of the orebody, the first stopes to be mined in "B" block were increased in length to 70 ft (for optimum economy of stope preparation advances), and in vertical height to 500 ft.

Six stopes with intervening pillars were laid out. In four of these stopes, numbers 10-19.5, 10-21, 10-22 and 10-23.5, the slot was cut out for the full height of the stope. This slot blasting started in January 1960 and was completed in all the stopes by the following October (Figure 3).

In that month, a small amount of sloughing occurred on the north side of 10-21 stope. This was followed in November by extensive cracking in 10-21.5 and 10-23 pillars (between 10-21 and 10-22 stope, and 10-22 and 10-23.5 stope respectively). The walls of the 21.5 pillar cross-cut on the 850 level, about the centre of the stoping block, required extensive scaling followed by timbering to prevent additional loose from falling. Subsequent to the blasting of a ring of holes north of the slot in the 10-21 stope, the lower parts of two rings fell from the north wall of 10-22 stope. Then in December, the 10-21.5 pillar failed from the 7A to the 5A sublevels (the upper half of the pillar) and the 10-23 pillar was reduced in size by sloughing at the 650 level.

By the next month, sloughing had produced a hole completely through this pillar. It must be emphasized here that the rock which sloughed in these stopes was mineralized schist of ore grade (Figures 3, 3A, 3B, 3C).

Corrective action was started immediately. A fill raise was driven to surface from above 10-22 stope, and access headings were driven, on all the affected levels, around to the south of the stopes. New slots were cut in the unblasted portion of the stopes to create voids into which the remaining stopes and pillars could be blasted.

Additional blast hole drilling was also necessary to ensure good fragmentation when this ore in place would be blasted.

By March 1961, the 10-22 stope had caved to the elevation of the 450 level, mainly as a result of the drop raise which had been drilled from the bottom of the new fill raise to surface, but the waste rock fill, quarried on surface and dumped down the new fill raise, helped to prevent further sloughing in 10-22 stope (Figures 4, 4A, 4B).

Blasting of the ore in the south half of the stopes, into the new slots and against the broken ore and waste of the north half took place in August 1961 (Figure 5). Fragmentation was excellent. In September, sloughing on the west side of 10-20.5 pillar (facing 10-19.5 stope) had created a breakthrough to the pillar cross-cut on the 650 level but there was very little additional sloughing here for the next seven months. Ore was withdrawn from the 10-21, 10-22, and 10-23.5 stopes during this period. Simultaneous dumping of waste rock kept the stope excavations almost completely full of material which gave support to the walls and prevented more sloughing.

Caving of the unsupported portions of the back continued however, and in April 1962, the sloughing took out part of the 450 level cross-cut over 10-20 stope and part of the 4-22 scram drift, 30 ft above the level.

Within the next two months, all the broken ore had been removed, and classified tailings were being poured in to sandpack the coarse rock fill. Although a reasonably steady flow of tailings was maintained, the unsupported back on the north side continued to slough until, in October 1963, it had reached to 250 level and cut out a section of the 250 cross-cut down the centre of the stoping block (Figure 6). Tailings were immediately diverted to this level and by March 1964, the hole was full and the track in the 250 cross-cut was relaid over the backfill. This ore recovery and back filling operation has been most successful.

So tightly has the tailings sand packed around the coarse rock fill that it has been possible to mine up against it. A cut-and-fill stope at the east end of the excavation has exposed stope backfill which stood unsupported over a vertical height of over 10 ft (Figure 9).

Mining of "C" Block

"B" block mining experience suggested that a stope height of 500 ft was too high and that simultaneous mining of four adjacent stopes was unwise. In "C" block, therefore, the first part to be mined, the so-called 30.5 stoping block was 230 ft long (strike length) from 40 ft wide at the top, to 200 ft wide at the bottom and extended from 60 ft below the 850 level to 40 ft above the 1250 level, a vertical distance of 300 ft.

The 230-ft length was divided into two 60-ft-long stopes, separated by a 110-ft pillar. The two stopes were mined out by the blast hole method and pulled empty. Then the central pillar was blasted into the two voids. Waste rock, quarried on surface, was delivered to the top of the 30.5 stope by means of fill raise and dumped on top of the broken ore. Careful control of the rate and sequence of extraction of the broken ore ensured that the broken waste - broken ore interface descended horizontally and that piping above any one box hole was prevented.

The rate of extraction was co-ordinated with the rate of waste filling, so that the stope excavation was kept as full of muck as possible all the time. In this way the walls of the stope were supported and sloughing prevented or retarded.

Some waste is unavoidably pulled along with the ore, but by careful study of the draw zone for each draw-point, the amount of ore to be obtained can be estimated. In this way, the total number of tons to maintain the ore-waste interface horizontal is estimated. A daily schedule is drawn up and the scram operators required to adhere to it. Regular grab sampling of the ore in the draw-points determines when the grade has dropped below the economic cut-off.

While the broken ore in the upper section of this panel was being withdrawn, two stopes were being mined out of the middle section of the panel (40 ft above the 1650 level to 60 ft below the 1250 level). These stopes had been mined and pulled empty by the time all the broken ore had been removed from the upper section. Blasting of the vertical pillar separating these two stopes, plus the horizontal pillar enclosing the 1250 level filled the excavations with broken rock. Dumping of waste was resumed and ore removal on the 1650 level commenced.

The lower and final section of this stoping panel was developed and blasted in the manner described above after all possible broken ore had been withdrawn on the 1650 level. Withdrawal of this final portion of broken ore is nearly finished. About two million tons of ore have been pulled from the 30.5 stoping panel. When the extraction of the ore is completed, cemented tailings fill is introduced to sandpack the coarse rock fill. On consolidation, this fill is expected to provide sufficient support for blasthole mining operations which will be carried out on the adjacent panels (Figure 7).

Ground Movement in the 30.5 Stope Area

In February 1963, when the central pillar in the part of 30.5 stope between the 1250 and 850 levels was blasted, east-west cracks developed parallel to the foliation in 10-1 east drift and 10-30.5 cross-cut. The former heading lies 100 ft north of the stope, while the latter leads south from 10-1 east drift, down the centre of the pillar (Figure 10).

The plan of filling the void above the broken ore in the stope before pulling any of the broken ore, had to be set aside for production reasons, and ore removal began at once. The back of the stope was about 100 ft above the muck at this time and this distance had increased to about 125 ft before backfilling commenced. During this period, the cracking, which had been observed before the pillar blast, increased as the north wall of the stope moved southward into the stope. Also at this time, a slowly descending slab from the north wall of the stope blocked off the 30.5 pillar cross-cut. Once the level of the muck in the stope had been raised to within 20 ft of the back, movement on these cracks was reduced to measurable but insignificant amounts. By November 1963, all the ore had been withdrawn and the stope was filled to refusal with quarried waste rock. During this last quarter of the year, sloughing of the stope back continued at a slow rate. In a pillar raise from the 850 level down to the back of the stope, there was evidence of stress, walls slabbing and diagonally opposite corners cracking.

While the broken ore was being removed in the 1250 level scrams, a second pair of stopes extending from 40 ft above the 1650 level to 60 ft below the 1250 level were developed, mined and pulled empty on either end of the 110-ft pillar. This stoping increased the stresses on the back of the stoping block immediately below the 850 level. Prior to blasting, this rib pillar and the 1250 sill pillar (including the 1250 scrams), the ground above the back of the stope was reinforced with additional tensioned cable bolts, which were installed at 10-ft intervals in the sill pillar over top of the stope for the full length. Some cable bolts were also installed in holes drilled from the scram above the 850 level over the 30.5 stope back. Also a 4-ft-thick pad of concrete, reinforced with stressed cable bolts was poured in the 8-2 east drift north of the stope over a length of 60 ft from the fill raise westward, that is opposite the west half of 30.5 stope (Figure 8).

It was feared that to blast the 110-ft-long 16-30.5 rib pillar and the 230-ft-long 1250 sill pillar in one millisecond delay blast, might cause severe sloughing at the back of the stope. To minimize the shock, the west half of the rib pillar was blasted first into the void of the west stope, filling it to about 80 per cent capacity. Then the east half of the rib pillar and the 1250 sill pillar above it were blasted together. The muck dropped about 60 ft after this blast, but was restored to normal level by dumping waste rock before any ore was removed.

The stope back was comparatively stable during the withdrawal of the ore at the 1650 level scrams. Minor sloughing from the back persisted however, adjacent to the fill raise and the pillar raise at the south wall. Because of this, more standard rock-bolts were placed in the back of the stope during the lull in ore withdrawal, which occurred when all the ore in the stope above the 1650 level had been pulled, and before the bottom portion of the stope, the 18-30.5 rib pillar and the 1650 sill pillar, had been blasted. These two pillars were left, of course, when two stopes between the 1850 and 1650 levels were mined out and pulled empty on either end of the stoping panel.

Subsequent to the final blasting of the 18-30.5 rib pillar and the 1650 sill pillar, the caving around the fill raise was accelerated. It broke through the 8-32 scram drift and continued to at least 50 ft above the 850 level. The concrete bulkheads in the sill and the scram of the 8-28 stope (west of the 30.5 stope) were exposed. Some tensioned cable bolts in the vicinity of the fill raise were pulled out and others had their anchorage cut. Some became ineffective when the surrounding rock shattered and fell away from the bolt. Beyond the immediate area of the fill raise, that is, beyond a distance of 50 ft east and west of the raise, the stress bolts held the back and prevented the sloughing from spreading.

Mining in "D" and "E" Blocks

Most of the current mining in these two blocks is of the cut-and-fill type because the ore is narrow and has irregular outlines but is of sufficient grade to offset the higher mining cost.

The present practice in developing a cut-and-fill stope is to cross-cut from the service drift to the orebody, then drive a raise up to 30 ft alongside the ore. From the top of this raise, a subdrift is driven along the ore for the full length of the stope. A small scraper is used to slush the broken ore back to the raise. A mucking machine is used on the level to load this ore into cars for tramming to the ore pass. Where necessary, the walls of the subdrift are slashed to the ore limit. Knowing the details of the configuration of the ore, it is now possible to drive a straight tramming drift and then put up manway and millhole raises to the sublevel as required. Under-cutting, arc-gate, air-operated chutes are installed at the bottom of the millholes.

Continuous laminated stringers (10 in. x 12 in. in cross section) are laid on the floor of the subdrift where it is intended that another cut-and-fill stope will be mined directly below. Round lagging is set on the stringers from wall to wall of the stope, and about 4 ft of cemented tailings poured on top of the lagging and stringers.

The first two lifts in the stope are removed by horizontal breasting and the void filled to within 10 ft of the back with classified mill tailings. Towards the end of each pour, a small amount of cement is added to provide a firm floor for scraping the ore from the next lift. The succeeding lifts are drilled off with automatic-feed, Lyner machines dual-mounted on a rubber-tired base. After blasting, the back is scaled and then reinforced with standard rock-bolts set on a 4-ft pattern. Where necessary, the stope walls also are rock-bolted. In this way, most of the sloughing and slabbing is arrested.

Methods of Back and Wall Support

Rockbolting

Conventional, expansion shell, rock-bolts are used extensively through the mine to strengthen the backs and walls of development headings and cut-and-fill stopes. Experience has taught that a 4-ft-long, 5/8-in. diam, high strength, steel bolt, installed on a 4-ft x 4-ft pattern gives the best results both in development headings and stopes. Occasionally, where it is impracticable to scale the back to solid ground, 6-ft bolts are used, and some of these may be holding loose ground in place. The bolts are tightened with a stoper to 125 to 160 ft/lb torque. If more positive tension is required, an hydraulic ram is used and a tension of about 5 tons is applied.

Tensioned Cable Bolts

Considerable success in preventing or delaying sloughing has been achieved by the use of tensioned cable bolts. Initially, extension steel bolts were installed in the manner described by Marshall (5). The present practice is to use lengths of discarded locked-coil, hoisting cable in place of the much more expensive high test, steel rock-bolts. The 1-1/4-in.-diam cable has proven to be just as effective as the steel bolts. Tensioned cable bolts are used to control the back and, to some extent, the walls of open blast hole stopes. This is done by installing them from drifts, raises or the back of stopes. In blast hole stopes, which have been developed by a cross-cut from the main service drive, followed by fringe drifts along the north and south boundaries of the ore, tensioned cable bolts are installed to strengthen the north and south walls of the stope. Since most of the service headings are driven south of and parallel to the orebody, it is possible to collar a hole for a tensioned cable bolt in the main service drift and drill it through to the south fringe drift. These 2-1/8-in. to 2-in.-diam holes are drilled with a long-hole, percussion drill and spaced at about 10-ft intervals. Bolt holes to reinforce the north wall are drilled north from the north fringe drift, at the same spacing. The current practice for reinforcing the back of a stope is to slash it out to the ore limits at the top, then drill cable holes in both walls and also up into the back. The depth of hole varies according to the expected ground conditions, but would average about 30 ft. The used hoisting cable is cut into specified lengths in the machine shop, and one end fitted with an anchor in the form of a 6-in. length of 3-in.-diam pipe attached to the cable by pouring molten zinc around the expanded strands (Figure 11). The other end is whipped with wire to hold the strands together while the cable is being installed. Punch-lock bands are placed at intervals along the length of the cable to prevent the strands from opening up or "bird-caging" - a tendency which used locked-coil, hoisting rope displays when being handled. Where the cable bolt is to pass from one heading to a parallel one, the collar of the hole at the anchor end is reamed to 4-in. size for a depth of 12 in., to provide a sheltered anchorage. Where the bolt is to be anchored in solid rock, it is necessary to ream the hole to a 3-in.-diam for its full length.

The steel, wedge plate and anchor plate at the collar of the hole are of the same dimensions and design as described by Marshall (5), i.e., the anchor plate is 12 in. x 12 in. x 1 in. steel and the wedge plate is approximately 6 in. x 6 in. x 1-1/2 in. steel. Through the centre of the wedge plate, there is a 2-1/8 in. hole tapered to receive a cone shaped wedge. The 1-5/8-in.-diam hole in the centre of the anchor plate is not tapered. The procedure for installing a cable bolt in a -5° hole is as follows: The cable bolt is pushed to the bottom of the hole and a cement grout is poured in sufficient to cover to anchor plus 10 ft of the cable bolt. This is allowed to harden.

Next the anchor plate and wedge plate are threaded over the protruding end of the cable bolt, and pushed up against the collar of the hole. A 12-in. length of 1/2-in.-diam copper tubing, and a slightly longer length of 1/4-in.-diam plastic tubing are lashed together and bent so that one end will fit in the hole and the other end pass out beyond the side of the anchor plate. The conical wedge, broken into three segments, and held together around the cable by means of an elastic band is pushed into the tapered hole in the wedge plate. The anchor plate is now concreted to the rock wall in a plane at right angles to the centre line of the cable bolt (Figure 12). When this concrete has hardened, two hydraulic jacks are passed onto the cable. One jack faces the wedge plate and exerts pressure (between 15 and 20 tons) on the conical wedge. The other faces away from the wedge (and the hole) and exerts tension on the cable to a limit of 40 tons. These pressures are carefully applied at a slow, uniform rate (Figure 13). Now the cement grout is pumped into the hole via the copper tubing, while the displaced air escapes from the plastic tube. The emergence of grout from the plastic tubing indicates that the hole has been completely filled.

For up holes the procedure is slightly different. Before pushing the cable bolt up in the hole, a plastic tube, as long as the cable bolt, is taped to the cable bolt close to the anchor. Then, except for the 4 ft from the anchor, the cable is given a coating of grease, as it is pushed up the hole. This is to permit free movement of the cable bolt as it is tensioned. At the collar of the hole a wooden plug and a 12-in. length of copper tubing are inserted alongside the cable, and all packed tightly with oakum. A small amount of grout is now pumped into the hole and allowed to set against the wooden plug. This will ensure that the plug stays in place when the rest of the hole is filled with grout (Figure 14). Once the hole has been filled with grout (and a thicker mixture is used for the up holes than for the down holes), and the grout has set, then the cable bolt can be tensioned to 30 to 40 tons as before.

In those places, such as stope walls, where blasting might damage the bearing plate and so reduce or destroy the effectiveness of the cable bolt, the collar of the hole has been countersunk to protect this anchorage arrangement.

Tensioned cable bolts have proven to be effective in preventing or retarding wall sloughing. Where installed in -5° or more steeply inclined holes, in which the cable is not greased, the cement creates a bond between the cable and the walls of the hole. If sloughing should expose the cable bolt anchor, this bonding prevents the complete loss of tension in the unexposed remainder of the cable holt and so part of the bolt's usefulness persists. Unfortunately, this is not the case with up holes where the cable must be greased.

Complete cost figures are not available, but the installation of tensioned cable bolts is known to be less expensive than that of high strength, extension steel rock-bolts. The cable bolts are of equal or greater effectiveness.

Observation of Cracking and Sloughing

Regular inspection of the workings adjacent to the blast hole stopes excavations is carried out by members of the Geology Department and has been conducted since October 1960 when the sloughing in the "B" block stopes attracted attention. Equipped with prints of the geological plans of the headings accessible to the stopes and the surrounding areas, the geologists examine the walls and the backs of the headings and the walls of the open stopes, looking for signs of ground movement. New cracks, or new movement on old cracks, loose in the back or walls of the drifts, or appreciable increase (or decrease) in the flow of water from cracks, are all recognized as evidence of ground movement. Regular measurement, with feeler gauges, of the width of selected prominent cracks is also done to obtain some indication of the rate of movement. The results of these inspections are passed to the Mine Superintendent for necessary action, such as additional rock-bolting or timbering. The crack measurements have shown that some cracks expand for a period then contract. The greatest movement has been in east-west cracks parallel and close to the sides of the stope excavations (Figure 15).

Measurement of Movement of Drift Walls

A turnbuckle micrometer gauge modified from the one designed by Professor E. L. J. Potts of Durham University, England, and illustrated in "Rock Pressures in Mines" by E. de St. Q. Isaacson is used to measure the movement of drift walls in mining areas. Stainless steel, survey spads, welded to 3-ft lengths of 1/4-in.-diam steel reinforcing rods, serve as measuring points. The rods are cemented to the bottom of holes drilled in opposite sides of the drift, with the survey spad set flush with the collar of the hole. These measuring stations are set at 50-ft spacings to coincide with the mine sections and facilitate plotting of the results. Specially prepared wires of known length are hooked on the spads in each wall and then to opposite ends of the gauge. Constant tension of the spring in the gauge is obtained by turning the micrometer screw until the centring mark on one end of the gauge is centred. The difference between successive readings is a measure of the wall movement (Figure 16).

Readings have been taken with this instrument with semi-regularity for a period of 2-1/2 years. Sharp changes up to 0.30 in. have been recorded, particularly in headings close to stopes in which large size blasts have been detonated. More gradual changes have been noted in those measuring stations opposite partially filled stope excavations.

A study of results shows that the greatest amount of movement has occurred in those headings closest to the stope excavations, which was to be expected. However, a further observation shows that the most prominent cracks and the stations showing greatest movement lie on an elliptical path surrounding the stope excavations. The stations of least movement and the areas of weaker cracking lie outside this elliptical path.

While most of the measured wall movements have been expansions, a few of the stations, particularly those in pillars between stopes, have registered contraction. The expansion suggests a movement of the drift wall towards the stope excavation. The contraction may be because of the squeezing of the walls as a result of a buttress action on the pillar.

Criticism of Results

Since the measuring stations are anchored a scant 3 ft in the drift wall, any cracking of the walls at a greater depth would not be detected. Nor is it possible to be sure which wall is moving inwards or outwards. Despite these shortcomings, this type of measuring will give forewarning of possible danger and is being continued with the expectation of proving more valuable as the mining proceeds and the goal of total extraction is approached. Such forewarning will be extremely useful in indicating the need for additional reinforcing in certain headings, or the need for alternative headings to give access to other stoping areas.

Rock-bolt Extensometers

Acting on the advice of D. F. Coates, Head of the Mining Research Laboratories, Department of Energy, Mines and Resources, a set of twelve rock-bolt type extensometers were installed to monitor the ground movement in the vicinity of the 12-30.5 stope, the uppermost portion of the 30.5 stoping block. Six pairs of extensometers were set in holes in the walls of headings paralleling the long axis of the stope.

North of the stope, two pairs of holes were drilled in the south wall of 10-1 east drift, a heading which lies 40 ft from the stope. The holes, 10 ft and 20 ft deep, and about 2 in. diam in every case, were drilled on section 28+65 east (on the centre line of the 120-ft-long pillar lying west of the stope), and on section 29+20 east (opposite the west end of 30.5 stope). The third pair of holes were drilled east of the stope along the centre line. The fourth, fifth, and sixth pairs of holes were drilled in the north wall of a by-pass drift which parallels 30.5 stope about 175 ft south of it (Figure 1).

Description of Extensometers

The working drawings for these extensometers were provided by the Mining Research Laboratories. They are of a standard design, each instrument consisting of a series of 3/4-in.-diam steel rods connected by couplings and anchored to the bottom of a hole by an expansion shell cemented in place. Short discs of rubber, set at intervals along the rods, prevent the rods from touching the sides of the hole, yet allow free movement. Except for the movable measuring bar which is attached to the protruding end of the rod, and the stationary, wall plug, measuring point, all parts of these instruments were made in the mine machine shop. Measurements of ground movement are read on this type of instrument by means of an inside micrometer gauge (Figure 17).

Results Obtained

The first set of readings was taken in November 1963. Late in the following month the 16-30.5 central pillar and the 12-30.5 sill (horizontal) pillar were blasted - a total of 164,400 tons. As expected, the No. 2 station extensometers were affected the most, both bolts moving 0.011 in. towards the stope. The changes on the other ten instruments were negligible (less than 0.005 in.). Since January 1964, the No. 2 extensometers have continued to show the greatest movement - almost always towards the 30.5 stope. Blasting in other stopes above and to the west of the Nos. 1 and 2 extensometers stations has affected these extensometers about equally until April 1966 when the combined effect of final blasting in the 30.5 stope block and in a 1450 level to 1250 level stope 250 ft to the west, increased the movement of the No. 2 station from -0.002 in. to a maximum of -0.026 in.

Discussion of Results

The anchor end of the 20-ft extensometer bolt in the No. 2 stations is only 50 ft from the north wall of the 30.5 stope, while the ends of the corresponding bolts at stations Nos. 4 and 5 are 140 ft away from the south wall of the stope. This doubtlessly accounts for the marked difference in the readings.

A continuous decrease in the No. 2 station readings suggests that the ground on the north side of the 30.5 stope is moving southward towards the excavation. The protruding ends of the No. 3 station extensometers were unfortunately struck by a loaded ore car eight months after their installation, so a measure of the movement of the rock off the end of the stope excavation was not obtained. During the time when both bolts were usable, they showed no significant movement.

Other Rock-bolt Extensometer Installations

Movement of ground around other stope excavations is being tested by rock-bolt type extensometers, installed in specially drilled, EX size, diamond drill holes collared on the 650 and 1250 levels. The design of these extensometers, also provided by the Mining Research Laboratories, was changed from that used on the 1050 level to facilitate reading the measurement. The portion of the rock-bolt protruding from the hole was passed through an aluminum plug at the collar of the hole. The hollow plug was cemented in place, but the rod moved freely through it. A brass gauge seat bracket was fastened to the plug by one end. A gap measuring plate was attached to the rock-bolt and positioned by means of set screws. A dial gauge micrometer, inserted through a hole in the gap plate to touch the gauge seat bracket, was used to measure the distance between the two (Figure 18).

Location of Rock-bolt Extensometers on the 650 Level

Extensometers were installed in 1966 on the 650 level as follows:

Section	Length of hole	Dip	Direction	Location of collar
23+00 E	78 ft	-5°	South	6-1 South X-C
23+50 E	8 ft	+0°	North	6-1 East Dr.
23+50 E	29 ft	+0°	South	6-1 East Dr.
27+30 E	85 ft	-20°	South	6-1 East Dr.
28+65 E	8 ft	+0°	South	6-28.5 X-C.

The extensometers on sections 23+00 E and 23+50 east are opposite the "B" block stope excavation described earlier. The bottom of the 23+00 east hole is 100 ft (approximately) from the north wall of the stope excavation, while the bottom of the 23+50 east (south) hole is approximately 50 ft away.

The cumulative difference in the readings after ten months of regular reading on the 23+00 east extensometer station is -0.007 in., and on the 23+50 east station it is -0.005 in. This would seem to indicate that the walls of the stope are not moving.

The 27+30 east extensometer is located in the 40-ft-wide pillar between two mined out stopes, Nos. 8-27 and 8-28. The 8-27 stope was mined by the blast hole, open stope method from 20 ft above the 850 to the 450 level, a vertical height of 380 ft, then filled with classified tailings.

The 8-28 stope was also mined by the blast hole, open stope method, through a similar vertical extent. It has been filled with classified tailings to the 650 level. The observed differences in periodic readings for the first ten months were only a few thousandths of an inch, but for the most part positive, so that the cumulative difference is +.01 in.

The fifth extensometer on the 650 level is located in the face of short cross-cut driven south from 6-1 east drift on section 28+60 east. The bottom of this extensometer is approximately 40 ft from the north wall of 8-28 stope, which, as noted above, is a mined out but partially filled stope. The monthly differences measured have been positive for the most part, and the ten-month cumulative total is +0.007 in. This suggests a very slight movement of the ground southward towards the stope excavation.

Location of Rock-bolt Extensometers on the 1250 Level

Ground movement above a cut-and-fill stope is being measured by five rock-bolt extensometers installed in 1-1/2-in.-diam holes drilled with a diamond drill from 12-1 east drift. This heading lies about 60 ft south of the south wall of the stope. The stope extends from section 36+50 east to section 41+50 east, a horizontal distance of 500 ft, and the stope back at the end of 1966 was 100 ft below the 1250 level.

Rock-bolt extensometers were installed as follows:

Section	Length of hole	Dip	Horizontal distance from extensometer anchor to expected stope wall
37+00 E	43 ft	−35°N	15 ft
38+00 E	43 ft	−35°N	15 ft
39+00 E	43 ft	−35°N	20 ft
40+00 E	64 ft	−35°N	20 ft
41+00 E	71 ft	−35°N	15 ft

Results Obtained

After ten months of observation, the cumulative differences vary from −0.005 to +0.010 in. – very slight differences in themselves and showing no definite trend in their distribution. As mining continues and the stope back comes closer to the extensometer, the information provided by these instruments will become more significant.

Conclusions

1. It has been observed that the wall in stopes remote from the bottom of the orebody are more stable than those near the bottom. This is partly because the ore limits, and hence the stope walls, tend to be more nearly vertical and of uniform strike high up in the orebody. Those stopes near the bottom of the orebody have flatter dipping walls and less regular ore outlines, a reflection of the drag folding and strike faulting which has localized the ore. In addition to these reasons, it may be that the folding of the rocks in the formation of the drag fold has reduced their cohesion in some way so that they tend to slough more easily. This same reasoning may be applied to the other places higher up in the orebody where cross folding occurs. Further study is required here.

2. The blast hole mining method which has been evolved at Geco, whereby the stope is kept full of broken rock, has been quite successful. The production rate has been maintained at a high level and sloughing has been greatly reduced. The fact that a cut-and-fill stope was successfully mined against the sand packed, coarse rock fill of the "B" block stopes indicated that this material gives adequate support. The addition of cement to the tailings in future filling operations is expected to give considerably greater support.

3. The use of rock-bolts and tensioned cable bolts has prevented sloughing in some places and delayed it in others. In the 30.5 block, there was a great deal of evidence that the ground at the 850 level, and at the top of the stope some 55 ft below the level, was under increasingly heavy stress; cracks were widening and timbers in the pillar raise on the south side of the stope were cracking. The back held, however, until the 18-30.5 stope undercut, near the bottom of the stoping panel, was blasted. The rate of sloughing was accelerated and when the 18-30.5 rib pillar and the 1650 sill pillar were blasted, the back sloughed upward to about 50 ft above the 850 level. Only then did the cable

bolts break or lose their anchors. It is quite possible that the ground between the cable bolts became so fractured because of the increased stresses that it fell off in pieces around the cable bolt, rendering the bolt useless.

4. The true value of the wall closure measurements being taken with the turnbuckle micrometer gauge is hard to assess. However, there has been sufficient reaction on those stations closest to the working (i.e., producing) stopes to warrant continuing to collect these measurements. They may well give warning of excessive cracking in, and hence the need for special attention to, certain headings.

Perhaps the most useful information is that supplied by the rock-bolt extensometers, particularly those installed close to operating stopes. Experiments with multi-wire borehole extensometers just recently initiated here, may give more reliable data on ground movement.

With experience, all such data will be more confidently correlated with the mining events and ground movements may be anticipated as mining proceeds. Preventive measure may then be taken well in advance of possible danger.

Acknowledgments

I am indebted to Noranda Mines Limited for permission to present this paper and to Mr. J.A. Graham, Manager of the Geco Division for helpful criticism and advice in its preparation. I also wish to thank Mr. L.S. Brooks, Mine Superintendent, Geco Division, for information on the mining procedures. Mr. T. Bakker, of the Mine Geology staff has been most helpful in the preparation of the ground movement measurement data, while other Geology staff members, Miss I. Meyers and Mr. G. Todd assisted in the preparation of the illustrations.

References

(1) McLeod, P.C.
1958: The underground phase of the Geco project, Trans. Can. Inst. Mining Met. v. LX.

(2) Marshall, G.M.T.
1959: Blasthole mining at Geco mining engineering, August.

(3) Brooks, L.S.
1964: Mining at Geco, Proc. Lakehead Branch Can. Inst. Mining Met. Minnesota Section AIME Pub. by Univ. of Minnesota.

(4) Brown, W.L., and Bray, R.C.E.
1960: Trans. Can. Inst. Mining Met v. LXIII.

(5) Marshall, D.
1963: Hanging wall control at Willroy, Bull. Trans. Can. Inst. Mining Met., April.

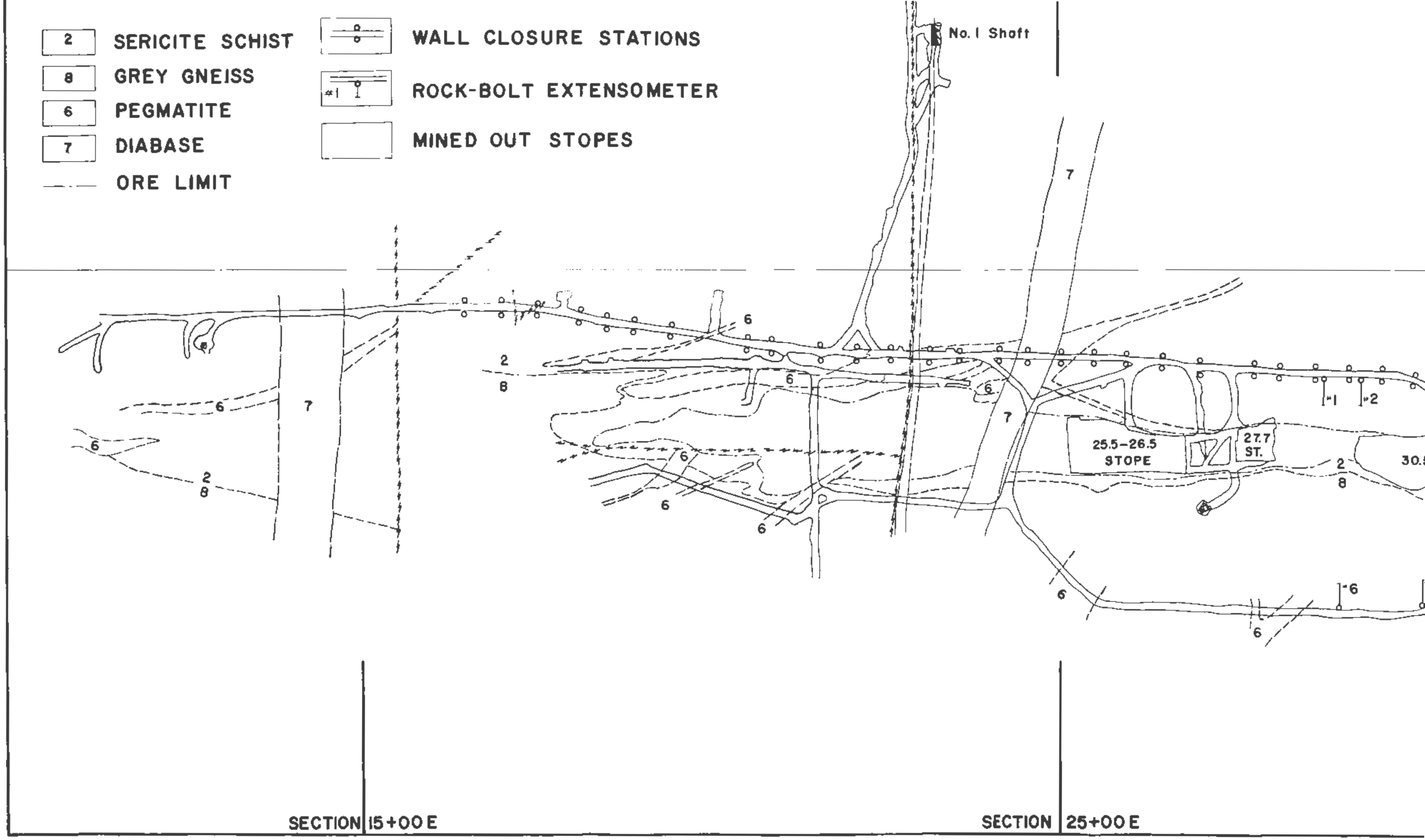

Figure 1. Geological plan of the 1050 level.

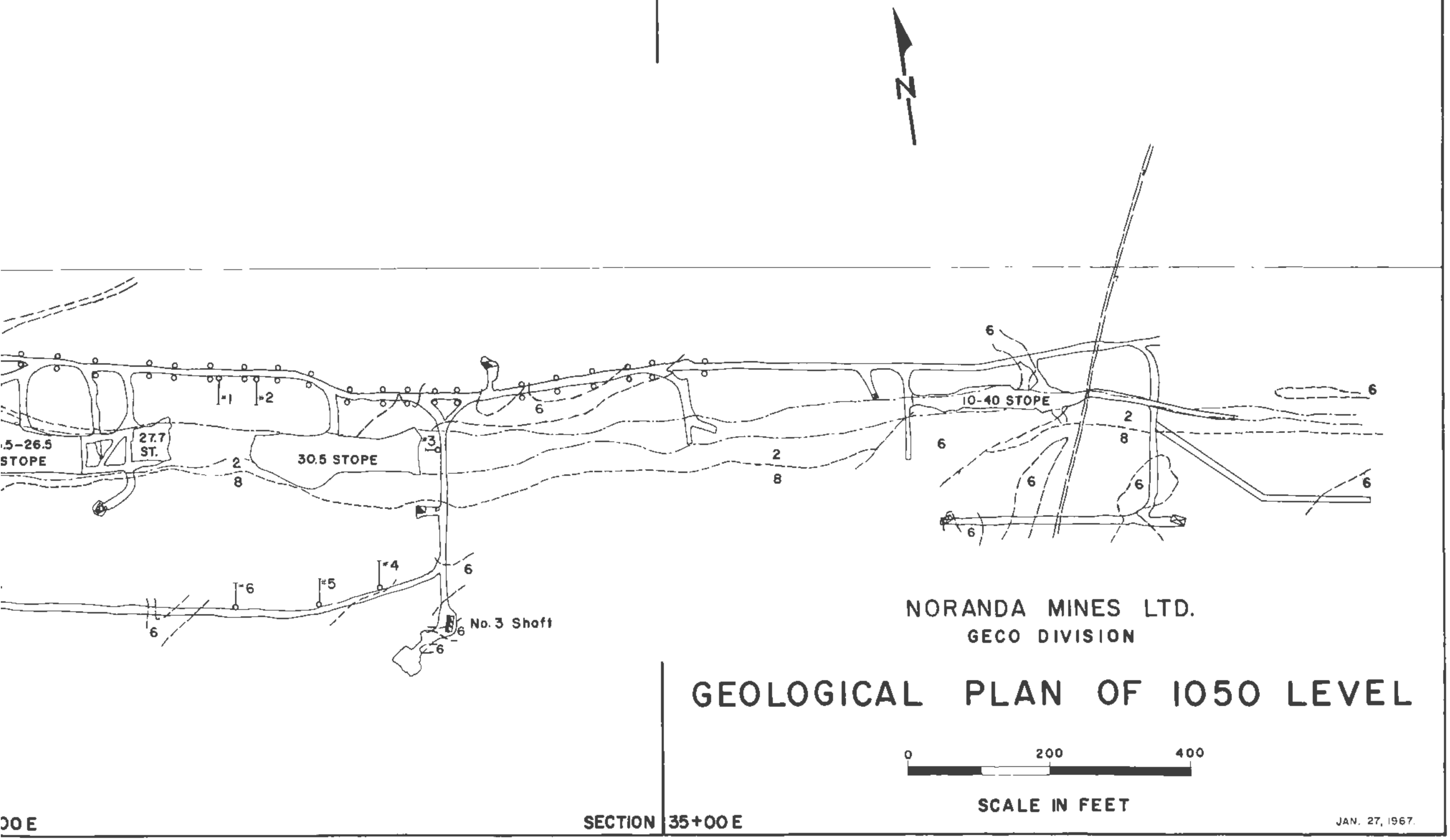

Figure 1. Geological plan of the 1050 level.

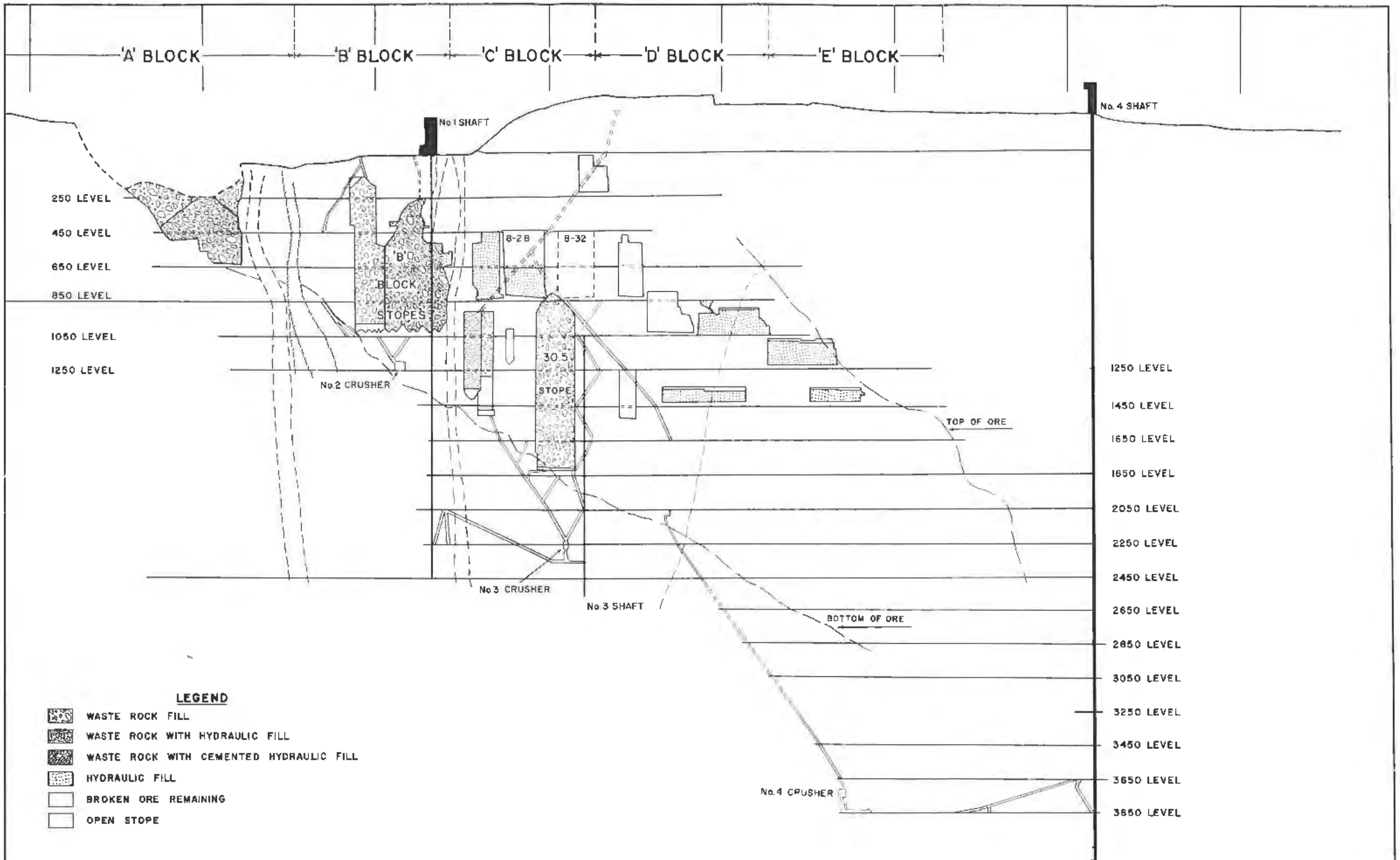

NORANDA MINES LIMITED

GECO DIVISION

LONGITUDINAL SECTION

SHOWING STOPES

0 500 1000

SCALE IN FEET

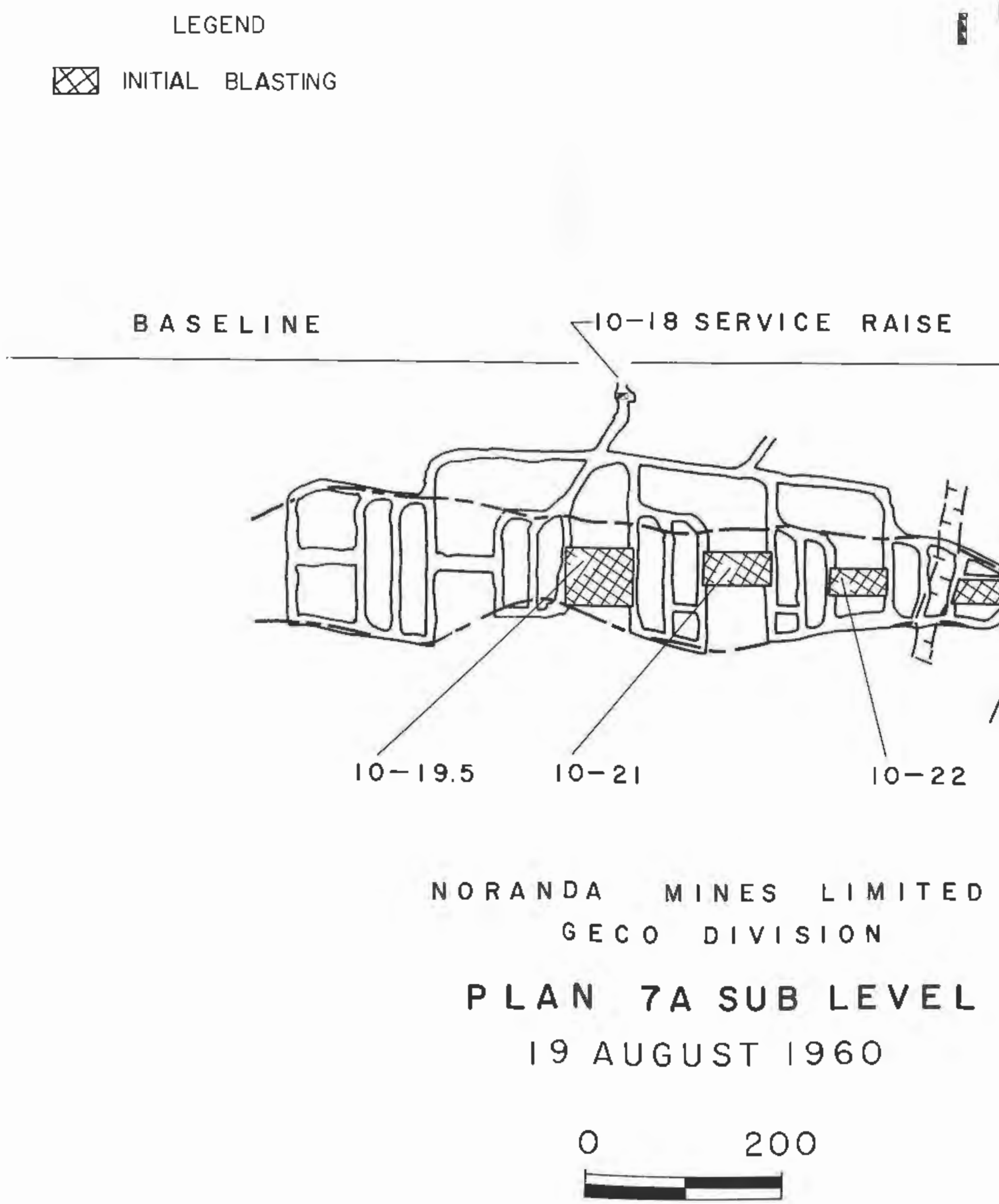

Figure 3. "B" block mining - 7A sublevel at 19 August 196

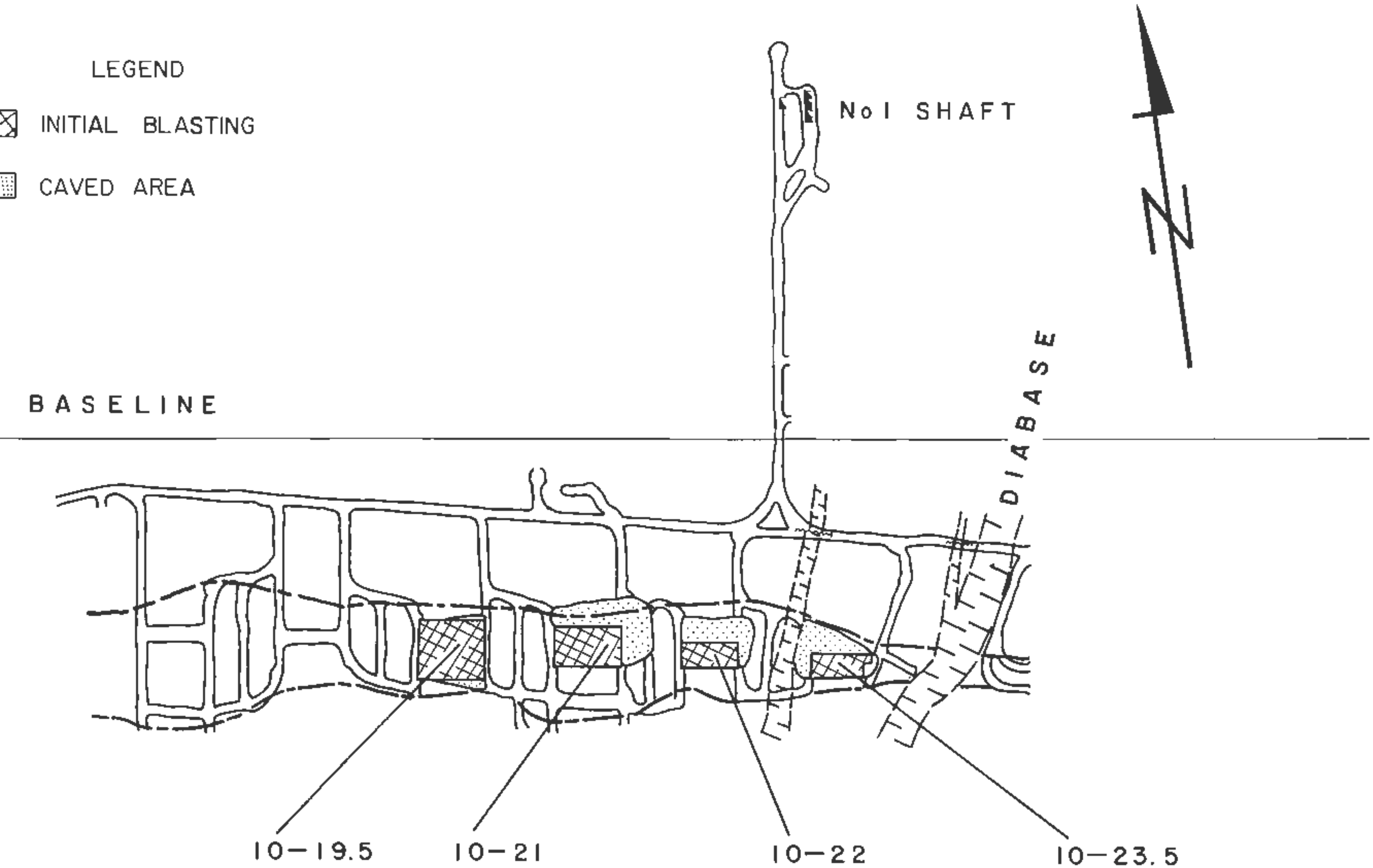

NORANDA MINES LIMITED
GECO DIVISION

PLAN 650 LEVEL

19 DECEMBER 1960

0 200

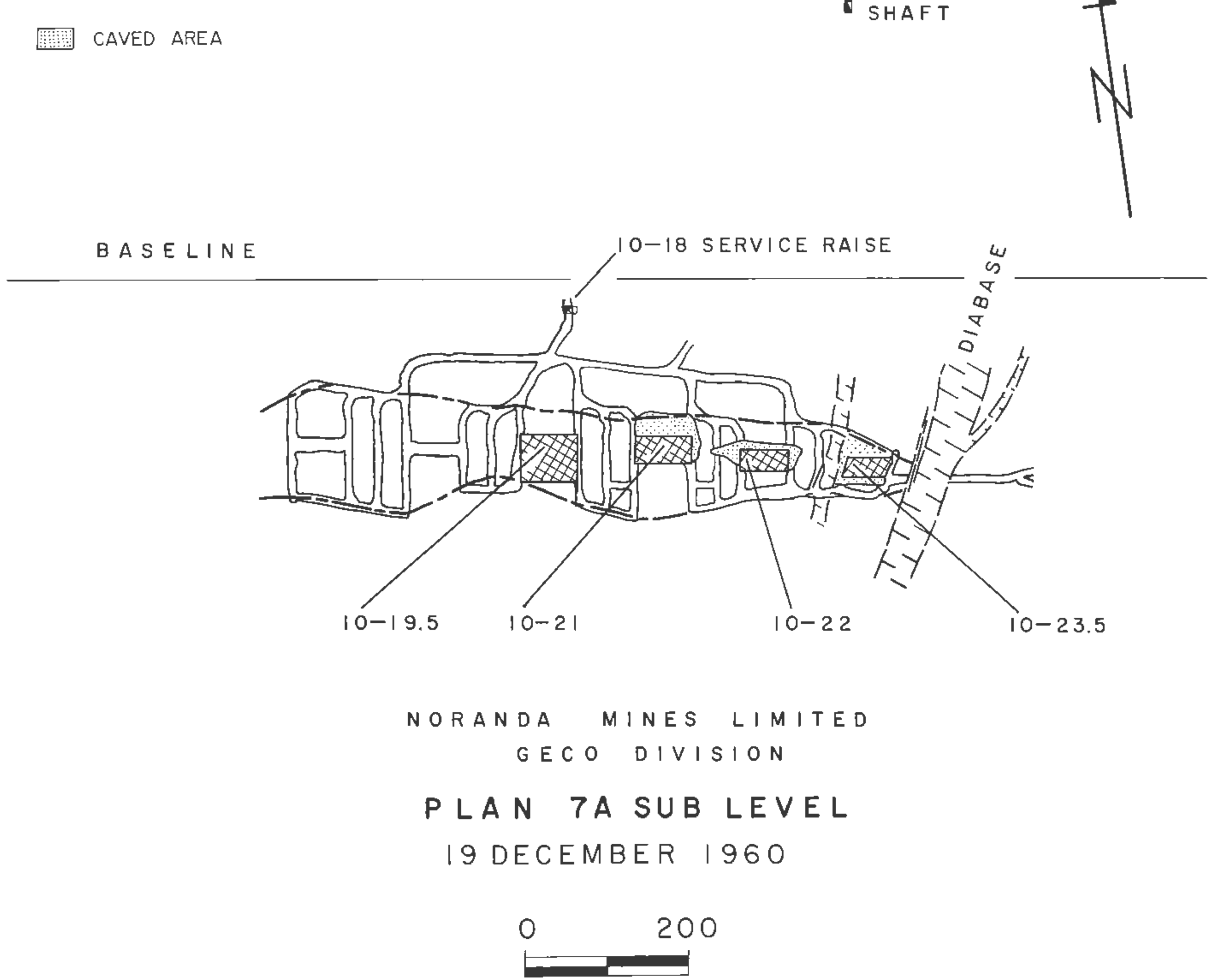

Figure 3B. "B" block mining - 7A sublevel at 19 December 1960.

NORANDA MINES LIMITED

GECO DIVISION

LONGITUDINAL PROJECTION

SHOWING STOPING & SLOUGHING

19 DECEMBER 1960

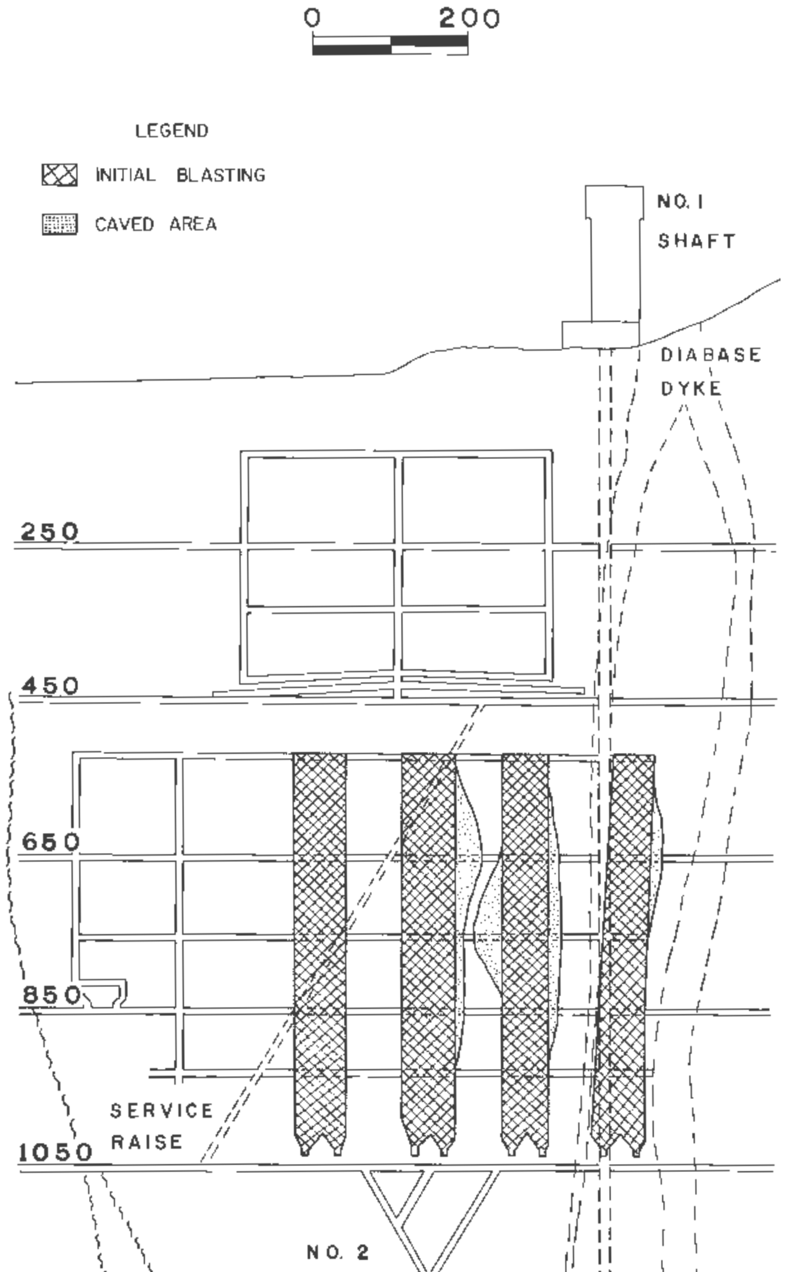

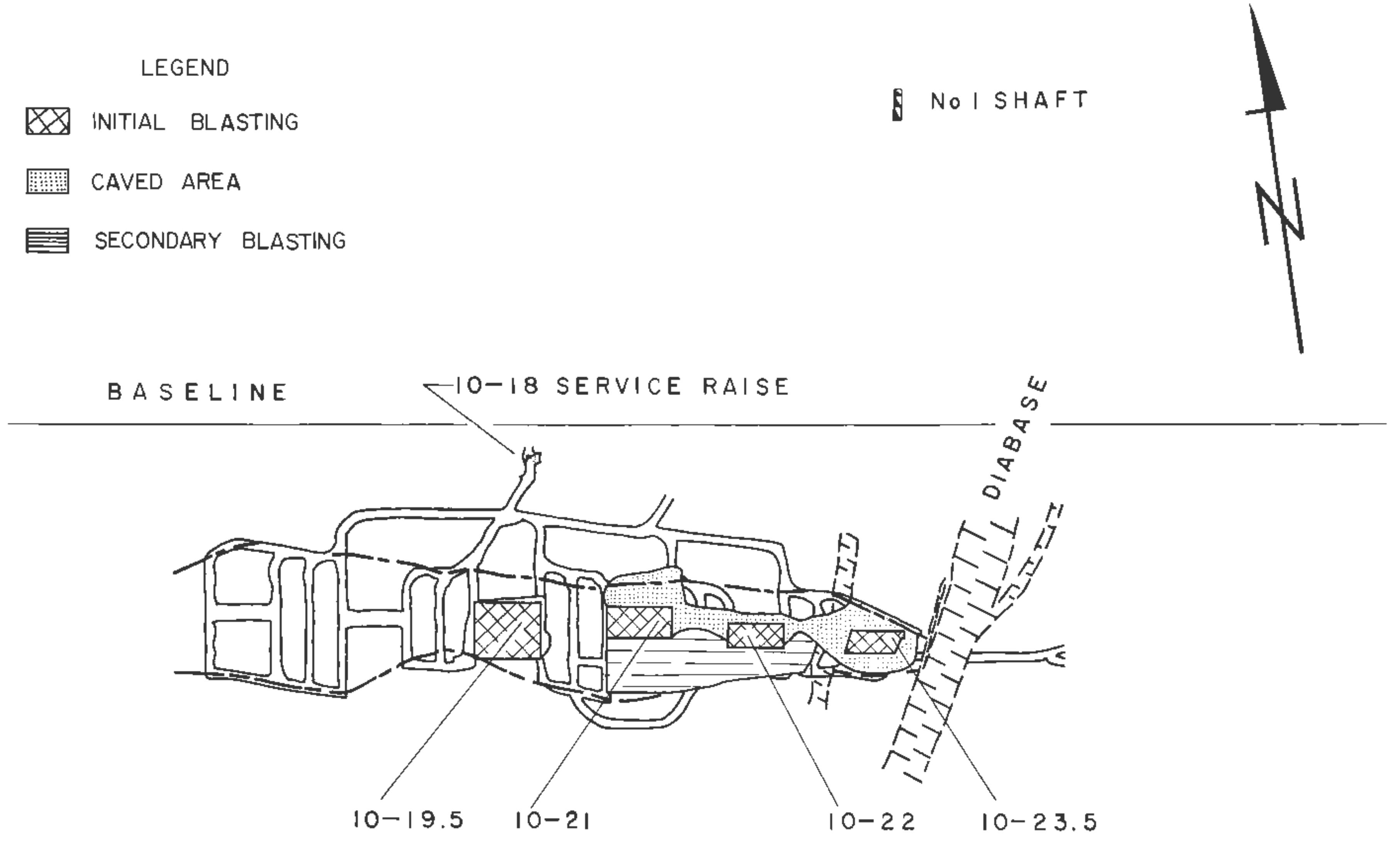

NORANDA MINES LIMITED
GECO DIVISION

PLAN 7A SUB LEVEL

29 AUGUST 1961

0 200

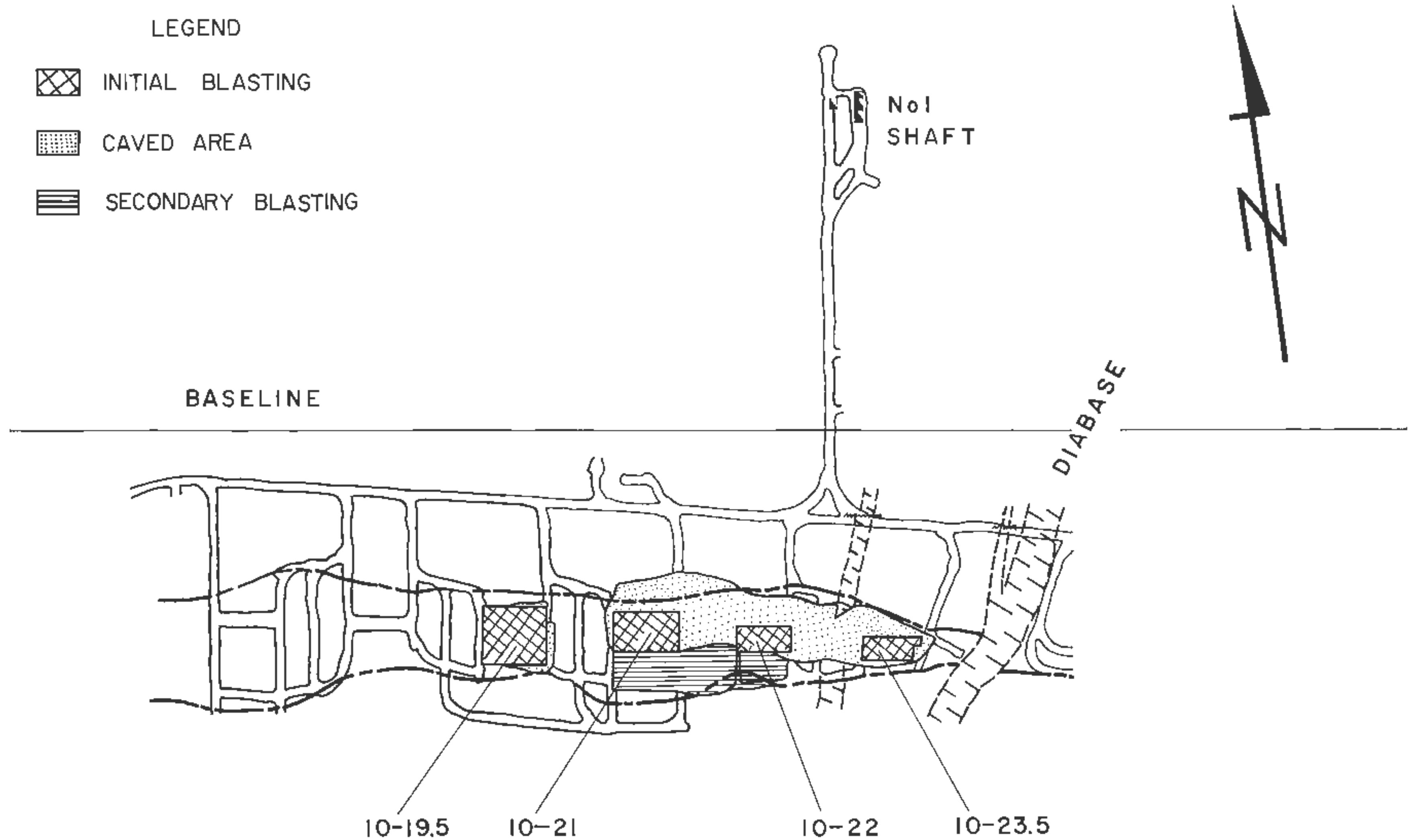

NORANDA MINES LIMITED
GECO DIVISION

PLAN 650 LEVEL

29 AUGUST 1961

0 200

NORANDA MINES LIMITED

GECO DIVISION

LONGITUDINAL PROJECTION

SHOWING STOPING & SLOUGHING

29 AUGUST 1961

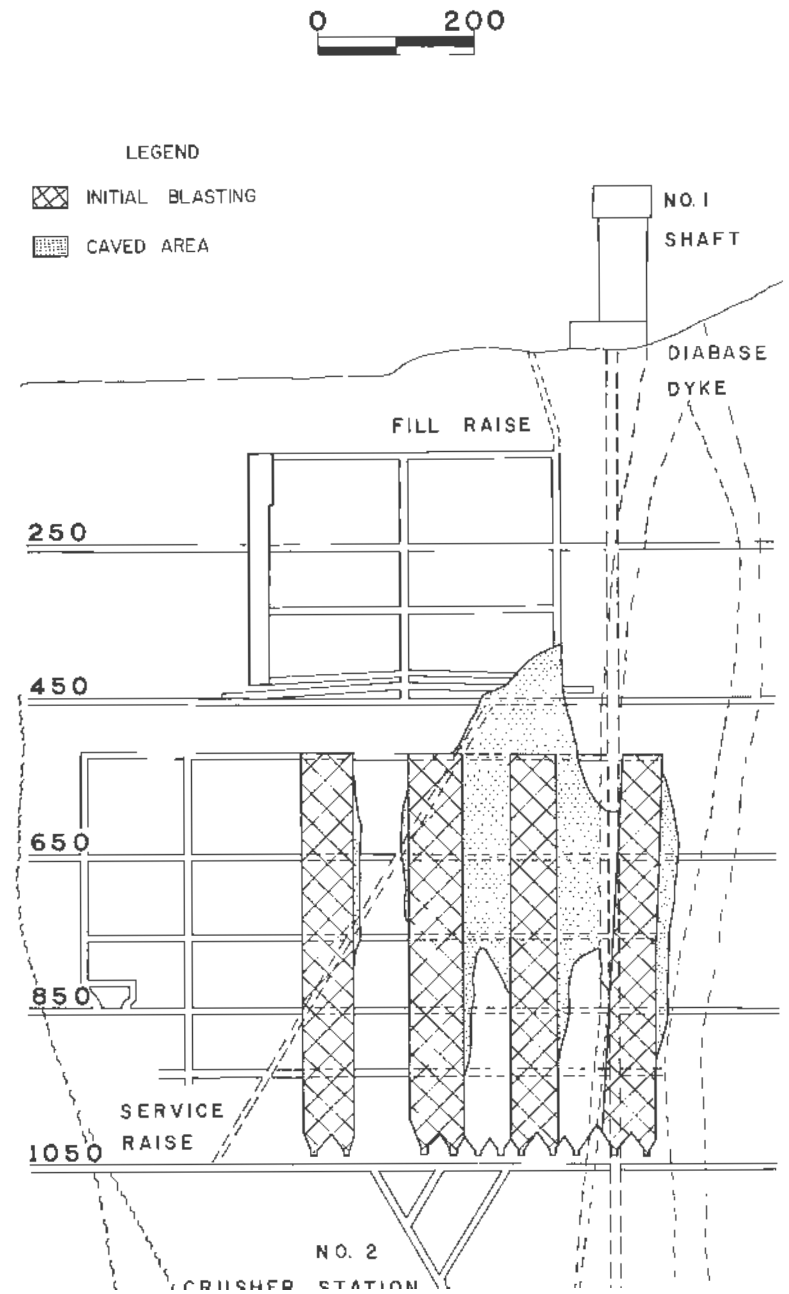

NORANDA MINES LIMITED (GECO DIVISION)

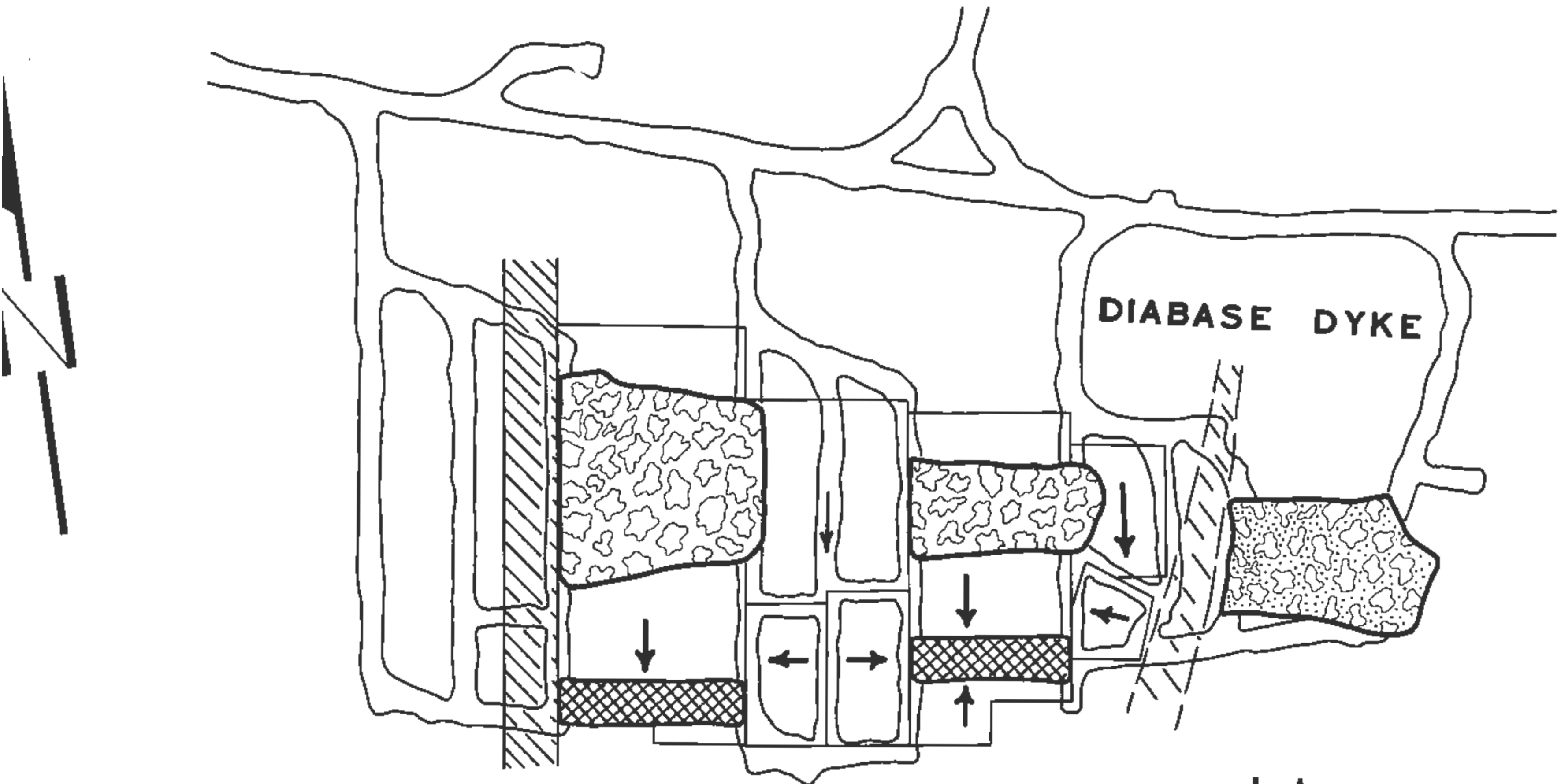

'B' BLOCK
SECONDARY
BLASTING
29 AUG 61

0 50 100

LEGEND

IB PILLAR
ROKEN ORE
ASTE FILL
XCAVATED STOPE

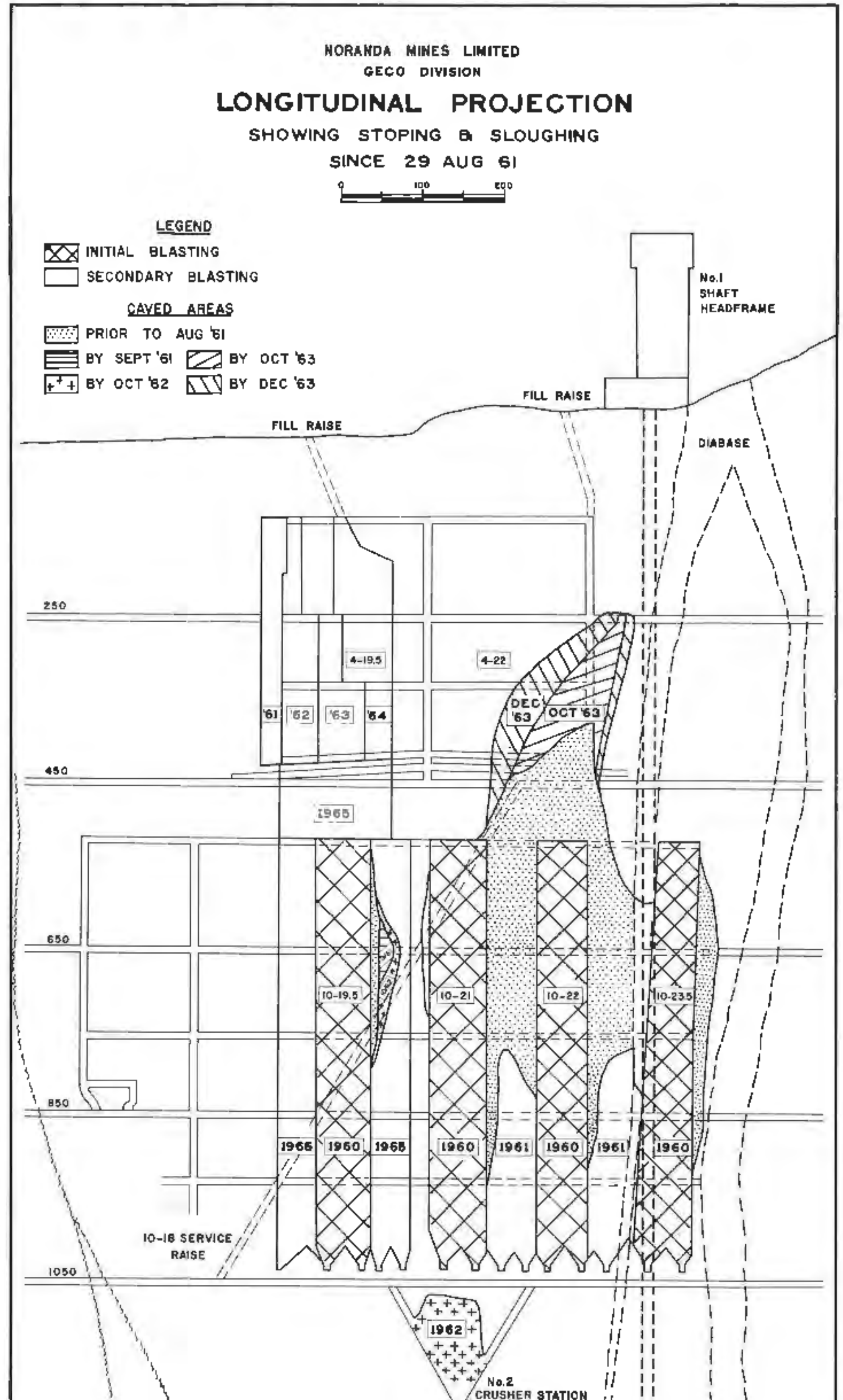

NORANDA MINES LIMITED
GECO DIVISION
LONGITUDINAL PROJECTION
SHOWING STOPING & SLOUGHING
SINCE 29 AUG 61
0
100
200
LEGEND
INITIAL BLASTING
SECONDARY BLASTING
CAVED AREAS
PRIOR TO AUG '61
BY SEPT '61
BY OCT '63
BY OCT '62
BY DEC '63
No.1 SHAFT HEADFRAME
FILL RAISE
FILL RAISE
DIABASE
250
450
650
850
1050
4-19.5
4-22
'61
'62
'63
'64
DEC '63
OCT '63
1965
10-19.5
10-21
10-22
10-23.5
1965
1960
1965
1960
1961
1960
1961
1960
10-18 SERVICE RAISE
1962
No.2 CRUSHER STATION

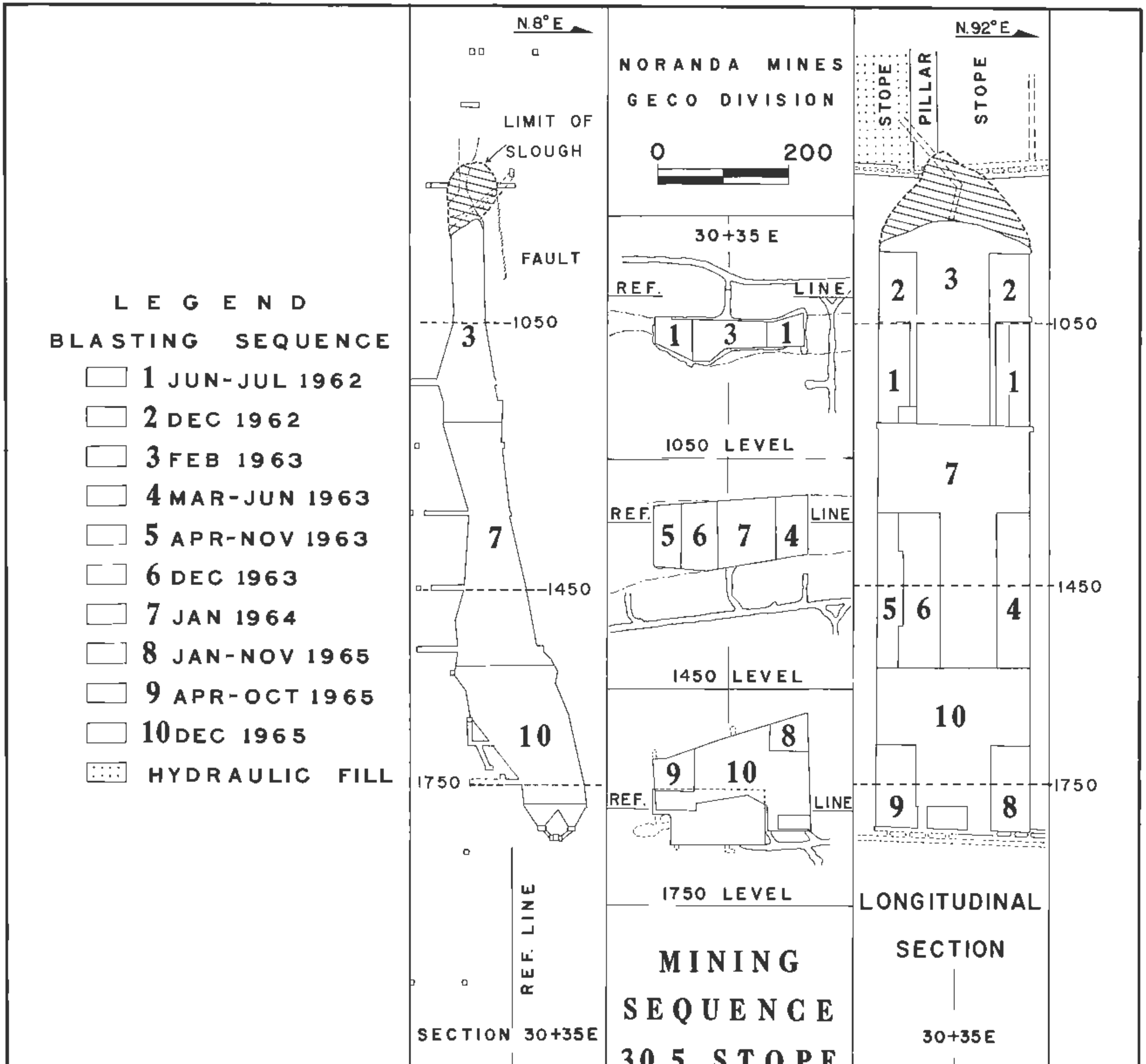
LEGEND
BLASTING SEQUENCE
1 JUN-JUL 1962
2 DEC 1962
3 FEB 1963
4 MAR-JUN 1963
5 APR-NOV 1963
6 DEC 1963
7 JAN 1964
8 JAN-NOV 1965
9 APR-OCT 1965
10 DEC 1965
HYDRAULIC FILL
N.8° E
LIMIT OF SLOUGH
FAULT
1050
1450
1750
REF. LINE
SECTION 30+35E
NORANDA MINES
GECO DIVISION
0
200
30+35 E
REF.
LINE
1050 LEVEL
1450 LEVEL
1750 LEVEL
MINING
SEQUENCE
30.5 STOPE
N.92° E
STOPE
PILLAR
STOPE
LONGITUDINAL
SECTION
30+35E

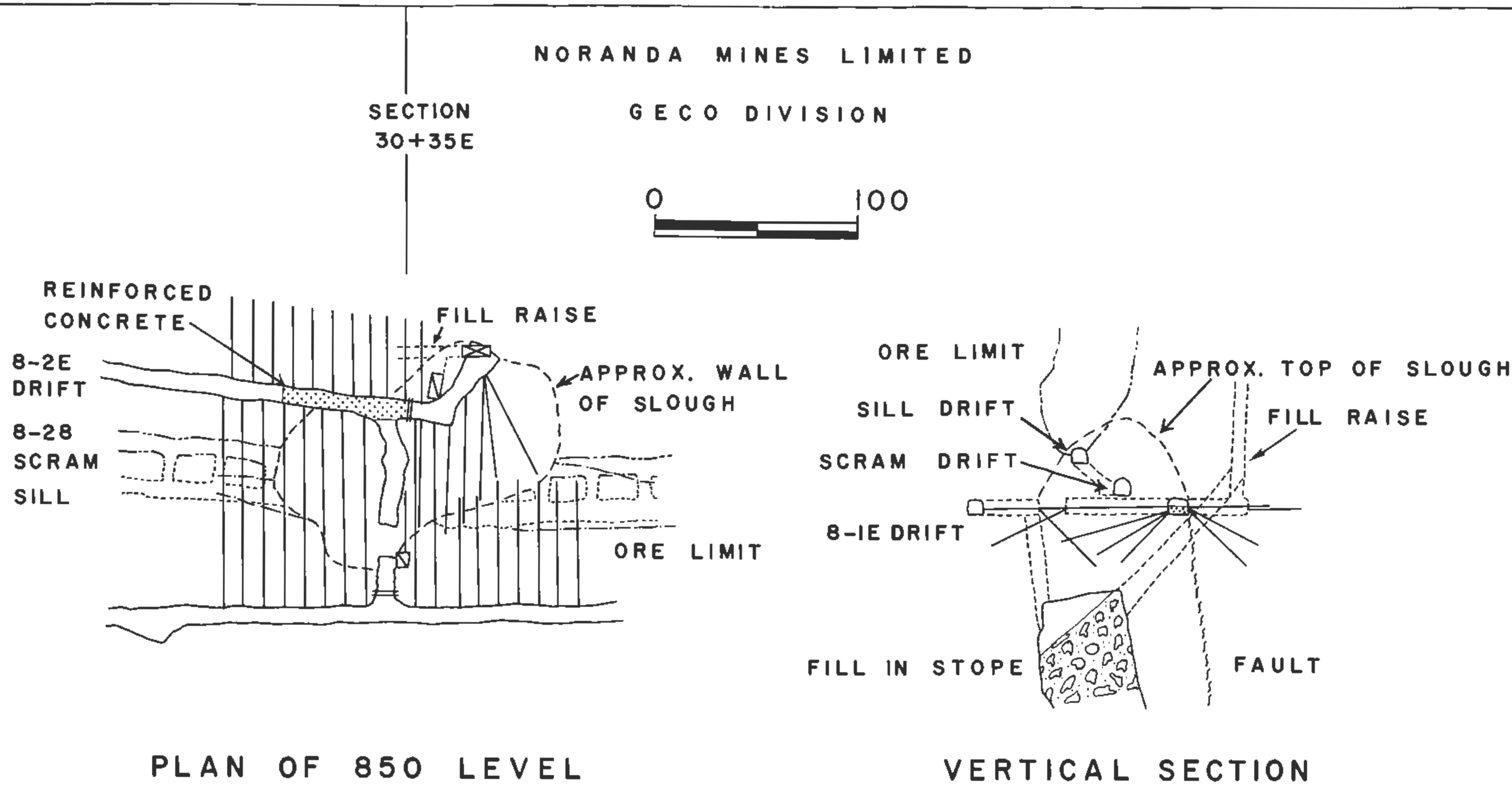

TENSIONED CABLE BOLTS
ABOVE
30.5 STOPE

Figure 9.
Cut and fill stope showing sand-packed coarse rock fill over a vertical height of 10 ft.

Figure 10. Cracking in south wall of 10-1 east drift opposite the central pillar of 30.5 stope, north of stope. (White horizontal band is a 6-ft rule folding at 1/2 ft intervals.)

Figure 11. Anchoring button.

Figure 12. Installation of tension cable bolt in a -5° dipping hole. Note: Copper tube and plastic bleeder tube. (Scale 6-ft folding rule with 1/2 ft sections.)

Figure 13. Twin hydraulic jacks applying tension on a cable in a -5° dipping hole.

Figure 14. Tension cable bolt held in an up-hole by a wooden plug. Note: Plastic tube rising up to the left of the cable and the copper tube just visible under the cable.

Figure 16. Turnbuckle micrometer gauge set up to measure wall movement.

Figure 15. 1350 level: 30.5 stope, central pillar cross-cut, west wall, showing cracking on south side of stope. One arm of the 'V' of the angle rule is 6 in. long.

Figure 17. Rock-bolt extensometer installation in 10-1 east drift - south wall.

Figure 18. Dial gauge: measuring movement on a rock-bolt extensometer, 650 level.

ROCK MECHANICS FIELD MEASUREMENTS IN NORTH SWEDISH SULPHIDE MINES

H.K. Helfrich and N. Krauland**

Abstract

The rock mechanics field-tests, which were undertaken by the Boliden Company in the sulphide mines of North Sweden, represent an endeavour to provide mining operators with guidelines which can be used in judging the stability of cavities and pillars. Special account is hereby taken of their function and lifespan.

The tests cover the following methode of investigation: geological structure analysis, probing of boreholes, deformation measurements, stress measurements, microseismic measurements, visual inspection of the rock condition and determination of pillar index numbers. Moreover, laboratory tests were also undertaken, which are not further described herein. The test results available to date indicate the feasibility of supplying the operating engineer with data which provide an additional basis for judgment in mine planning. Their economic value increases with the certainty with which the rock properties can be predicted; this in turn can only be achieved by the most appropriate combination of measuring techniques under optimum economic conditions.

Introduction and Definition of Problem

The rapid progress in depth of modern mining, the increasing rate of mining as well as the increasingly larger underground areas involved require a more exact knowledge of rock properties and behaviour around the workings and in pillars, not only qualitatively but also quantitatively.

---

*Mining Divisions, Boliden Aktiebolag, Boliden, Sweden.

In Sweden too, ore mining operations took due account of these requirements (19). In the large mining companies rock mechanics working groups were formed which collaborate with the central research organizations of the Swedish Mining Association, with the Engineering Academy and with the Mining Institute at the Technical University in Stockholm.

This paper describes the methods of operation and measurements in the rock mechanics field, used in the Boliden Company, as regards their implementation and purpose. In this respect reference is made to the fact that rock mechanics work has been sporadically undertaken already for a long time (8, 11). Since the individual deposits of the company under reference have a different character as regards dip, geology and structure, the following groups must be distinguished:

a. Horizontal - flat orebodies with rooms and pillars.
b. Sloping orebodies with room and pillars.
c. Steeply dipping orebodies, worked with or without backfill.

In line with this grouping the rock mechanics problems are also of various nature. However, the object is the same in each case: optimalization of rooms and pillars as regards their function and lifespan.

The work described hereunder has not so far yielded any conclusive results. Therefore only methods of work and part results can be reported. So far our work is limited to measurements which indicate, directly or indirectly, the rock behaviour; at a later date it is to be extended so that it will be possible to make a field analysis of the stress condition and of its variation in time around excavations and in pillars, due to mining operation.

Survey of Methods of Investigation

1.0 Geological Structure Analysis

A knowledge of the geological rock structures according to their material, stratification and general condition is a prerequisite for judging the strength of the rock mass in question (9, 12 and others). The term rock mass does not refer to large geographical or tectonic units, but to the rock formations within the area of mining and other engineering structures.

In order that the relationship of the geological field measurements to the stability problems of mining may be covered functionally, it must be included in a general concept which takes account of the relationship between rock properties and rock mass properties. Let us first sketch the outlines of this concept:

1.1 A survey of the field-geologic and mining-geologic work already completed.

1.2 A description of the condition of the area surveyed (mine, surface structures, etc.): photo-geology, morphology, geology, methods of mining, stability conditions, water economy.

1.3 Petrography and texture analysis, rock sample, rock formation.

1.4 Tectonic analysis and synthesis, the extent of the homogeneity and isotropy domain, characterization of the manner of deformation and of the fabric types within the rock mass, an attempt at reconstructing the functional fabric, the stress field and the force distribution on hand of the conditions after deformation.

1.5 Blasting - tectonics.

1.6 Hydrogeology

Within the framework of this paper only the working methods of the tectonic analysis will be detailed; mention will also be made of the grain texture analysis which controls it. The former is of essential importance as a direct field measurement and the latter as an indirect in situ measurement.

The planar and axial structures are taken stock of as shown in Figure 1, which represents a modification of the form proposed by Müller (24). The "textural data" are evaluated by Sander's method (28) and the textural diagrams are incorporated in the mine plans (Figure 2).

In this way the rock mass is three-dimensionally defined within the area of the deposit according to its degree of homogeneity and isotropy (20). As a result one obtains a division of the deposit-range into structurally equivalent sub-ranges. The structural analysis is supplemented by a fissure count (Figure 3) which in turn can be combined with a description of the rock condition to form a classification scheme (Figure 4). This classification is also taken from Müller (24), and modified for the special rock conditions encountered in our mines.

Since however these geological field measurements of the mega-fabric can only be controlled by the petro-fabric which itself features as a factor strength (6), it is necessary to refer to Sander's methods in this connection (28). Both the mega- and micro-fabric are indicators of the geological deformation field and can be considered as signals of the possible presence of tectonic stresses (latent or residual stresses) (7, 13).

The example of a recording of the s-planes in the floor of the Renstroem mine clearly shows that both the frequency of the s-surfaces per unit area as well as their orientation are subject to variation. The s-strike oscillates around a steep axis both in a vertical and horizontal direction (Figure 2), which would not have shown up on a surface recording. The prerequisites are there for this kind of tectonically prestressed rock mass to become destressed during shaft sinking and drifting operations. This destressing is assisted by the accumulation of potential energy, which can lead to rock-bursts (12). In such cases the given tectonic structure serves as an additional energy factor. The like applies also to the analysis of the ac-fissures, which also exhibits a characteristic anisotropy of direction and distribution. The fabric characterizes the structural properties of the rock mass; it must therefore serve as the basis for all rock mechanics observations and investigations. Simultaneously one obtains a measure of the degree of the loss of the overall strength of the rock mass. The recording must be made immediately following a mining advance, since afterwards the openings are disguised by injected concrete. The room-and-pillar structure in the Laisvall mine serves as an example of a fissure survey (Figure 5), in which the number of fissures per linear meter (Figure 3) are determined. These numbers provide a measure for comparison of the fissured character of the rock mass. In the given case (Figure 3) one may first observe a decrease of the fissure intensity to the right. The fissures are grouped in bundles, which is expressed by a frequency maximum on a 3 to 6 cm interval. In most cases by far of fissuring the fissure distance is 50 cm and more. In the second sub-section there is a decrease in the fissure intensity, with a corresponding increase in the fissure distance and a larger scatter in the fissure bundles. In the third section it follows from the absolute fissure numbers and interval frequencies that one again observes a concentration of fissure bundles with relatively large fissure numbers. The distance between individual fissure bundles has increased. These fissure data rate first, together with fissure orientation, as important factors when evaluating and determining pillar orientation; they may necessitate a change of the latter, even if such may not always be feasible due to technical operating reasons. Particularly interesting in this connection are the fissure numbers and fissure distances in the roof which, incorporated in a system, are to serve as the basis for the roof anchoring plans. A knowledge of the magnitude of the homogeneity and of the isotropy domains, to which specific stress and loading conditions are often also to be assigned, is of great significance in judging the stability of a mine workings.

2.0 Visual Inspection of Rock Condition - Determination of Pillar Stability Evaluating Points

In order to objectively judge the stability of pillars it is necessary to observe and comprehend a series of factors which influence it. Therefore, from an early date on, such factors have been regularly obtained in our mines. These so-called rock mass inspections are carried out according to principles described by Helfrich and Stephansson (15). They refer to a quantitative, respectively semi-quantitative determination of dimension, form, position of construction and cohesion, as well as of the fissure picture. The distinguishing characteristics of these determining groups are given in Figure 6. Their evaluation is carried out on a point system. The classification is presented in mine plans (Figure 7). It enables the operating engineer to objectively follow the alteration in the condition of the pillars and to correlate same with the current stability situation. Furthermore the conclusion is drawn that this observation basis can be considered as a quasi in situ measurement; it must be considered as a most essential prerequisite in all types of rock mechanics measurements, even though this method is subject to all the limitations of the classification systems (Trollope 31). Supplemented by, as an example, a wave velocity measurement across the pillar, as described by Bernabini, Esu, Martinetti and Ribacchi (2), or possibly by in situ tests according to Salamon and Oravecz (27), the stability or the degree of damage (31) should be predictable with a large degree of certainty.

3.0 Probing of Boreholes

Borehole investigations yield interesting quantitative results; they are either aimed at obtaining structural data for judging the strength of the rock mass, or else they permit a direct observation of the rock and simultaneously a running control of it (measurement of fissure movements).

3.1 Determination of Rock Strength by Means of a Core Factor

Hansagi (10) refers to relationships between the strength of a rock sample and of a rock mass, which can be determined by simple means. Drill cores of various length are obtained by means of diamond drilling. These are grouped in classes and the number of drill cores per meter is referred to an idealized body of rock entirely without jointing. From these relationships a correction factor C_1 is obtained, which is always less than 1. On comparing the number of test samples of given length, which may be expected on the basis of the core lengths, with the number which could be expected from the idealized rock mase, a correction factor C_2 is obtained which is also always less than 1.

On cutting out test pieces from the drill core with a saw, the number of test pieces actually obtained does not tally with the intended amount; hence the correction factor C_3 is obtained, which again is less than 1. By means of the coefficient C_3 one modifies C_2 according to the expression.

$$C_3 \times C_2 = C_4$$

Now Hansagi determines a factor of structure C_g, which will be referred to herein by the more appropriate term of core-factor, on taking the arithmetic mean:

$$C_g = \frac{C_1 + C_4}{2} \leq 1$$

The strength values obtained in the laboratory, $F_{(lab)}$, are multiplied by the core-factor to obtain a reduced rock strength value $F_{(geb)}$:

$$F_{(geb)} = F_{(lab)} \times C_g$$

Although this method includes certain sources of error, it seems to be a suitable method for obtaining quasi in situ values of the rock mass strength quickly and relatively cheaply. Several references have already been made in the literature to the importance of rock mass strength, when solving stability problems (3, 5, 22, 24).

The values obtained by the above described method are introduced as strength data in calculating, for example, roof spans and pillar dimensions.

Simultaneously, by means of a planned array of core drilling, one obtains a detailed profile of the deposit, supplemented naturally on hand of the underground workings. As an example, from the detail profile obtained in the Laisvall mine (Figure 8), one obtains the following core-factors for the individual horizons:

D1a	0.28
D1-3	0.43
D4-8	0.34
D1-2	0.29
F	0.39

In the given case the experimental borings were driven at right angles to the almost horizontal bedding. The respective core-factors clearly reflect the lithologic and facial conditions.

From the foregoing discussion it is obvious that this method represents one approach which can provide a relatively simple relationship between the rock and rock mass strengths.

Perhaps Hansagi's method also contributes to the solution of the problem of functional rock classification (1).

3.2 Optical Borehole Probing

An optical borehole probe (30 mm diam) of the Hagconsult Company, Stockholm (23), is being used for the optical investigation of the rock mass's degree of fissuring. It consists of a Hensold telescope with a sharpness of focus permitting observation up to 8 to 10 metres, a built-in mirror, a low voltage bulb and a micrometer graduation. One metre long tubes are being used for extension pieces, which carry a decimeter graduation (Figure 9). It is possible to accurately examine the interior of pillars with these borehole probes. Moreover, for a continuous operational control, the measurement of fissure movements can also be undertaken.

In our mines the optical borehole probe is used to assist in determining pillar stability. Thereby it was, for example, possible to establish extensive fissuring inside pillar beams which seemed whole from the outside. On the other hand rock mass parts, which figure as future pillars in plans, can be continuously pre-examined. Thereby it is possible to make statements about the structure of the rock mass already at an early stage.

Furthermore, it is important to mention that every borehole, which is to be used for any type of rock mechanics measurement, be exploited for examination of the rock structure with the probe. The geologic conditions within the vicinity of the measuring instrument's position could be of great interest when evaluating the resulting measurements.

Simple though the instrument may be, it has proved itself in use and shown that it is suitable for a number of possible applications. In this connection it may be considered, whether it might not be advantageous to obtain a TV equipped probe especially if same is also to be used in other kinds of investigations as, for example, in geophysics, for the investigation of long boreholes.

4.0 Deformation Measurements

The deformation measurements are to serve the following purposes:

1. To determine the characteristics of the deformation properties of pillars.
2. To monitor the stability of pillars.

At Laisvall the measurements are concentrated on the following deformation processes:

1. Convergence, respectively lengthwise pillar extension.
2. Crosswise pillar extension.
3. Roof sagging

    a. locally: in the sill - between the pillars;
    b. across the whole width of the mined area.

4. Exfoliation of beds.
5. Movement on fissure surfaces.
6. Subsidence at ground level.

When selecting the measuring equipment attention was primarily paid to the large dimensions of the mine rooms and pillars, while the effect of blasting (1,500 metric tons of ore per blast) could also not be overlooked.

Today mining at the Laisvall mine proceeds in two sections of the ore-body (Central and Kautsky ore). Presently the centre of mining activities is in the Kautsky ore, because the Central ore is mostly mined out. However, measurements are also undertaken in the Central ore, to monitor stability.

From among the two possible principles of measuring device selection - namely either very accurate, but expensive instruments or less accurate but cheap ones - the latter principle was adopted at Laisvall, because this permits a large number of measuring locations.

Measuring Instruments and Measuring Techniques

Presently the following four types of measuring devices are used:

4.1 Measuring with Long Wires

Since a very long measuring base is required for measuring convergence in rooms, roof exfoliation, as well as vertical and crosswise deformation of pillars, long wires are being used for this purpose.

Figure 10 illustrates the schematic arrangement of the entire equipment and the measuring principle.

The following comments apply to the construction:

1. The wire is to be of high-quality stainless steel.
2. The wire loading, achieved by means of the weight (respectively spring), should be far below its yield point.
3. Only the bearing surfaces of the dial-gauge and the guide collar of the wire must be accurately machined and need to be made of stainless steel.

With this type of arrangement any number of measuring points can be served with a single dial-gauge.

Measuring accuracy is $\pm$ 0.01 mm. Naturally the length of the wire is temperature dependent. Temperature correction is expensive, especially in case of very high rooms; at Laisvall therefore temperature correction is omitted, because the temperature induced error rectifies itself in time (the temperature variations amount to 3 degrees at most).

The following deformation measurements are undertaken with devices constructed in accordance with the foregoing principles:

1. Convergence measurements inside rooms (see measuring set-up in Figure 11).
2. Measurement of the vertical deformation in pillar beams (Figure 12).
3. Roof sagging and exfoliation (the same analogously for the floor) (Figure 13).
4. Crosswise deformation of the pillars (Figure 14).

Table 1 lists the usual measuring distances over which the deformations are measured at Laisvall.

TABLE 1

Deformation Measurement	Measuring Distance
Convergence in rooms	up to 24.0 m
Vertical pillar deformation	up to 24.0 m
Roof sagging and exfoliation	up to 12.0 m
Crosswise pillar extension	up to 15.0 m

These simple devices too have their weak points such as, for example, that they cannot be used close to blasting operations; nonetheless these devices have proved to be suitable for our purposes, namely as regards their function and also the cost of installing and operating the measuring stations.

A number of convergence points were laid out in a profile transversely across the width of the mined area. The measuring instruments were installed at a time when the mined area had already reached its full width. Nonetheless the following results were obtained on evaluating the convergence velocities, measured during a period of six to nine months:

1. The average convergence velocity amounted to 0.003 to 0.025 mm per day.
2. The convergence velocity attained its maximum value at approximately the centre of the mined area and decreased towards the periphery.
3. The strength of the roof underpinning by means of pillars could also be clearly discerned: in the neighbourhood of pillar beams the convergence velocity reached lower values, and in the vicinity of pillars with reduced carrying capacity it reached higher values.

4.2 Measuring Rods

In the immediate vicinity of blasting operations it is advisable to measure the roof deformations and the pillar cross extension by means of measuring rods in boreholes. Figure 15 illustrates the principle of the measuring arrangement. The advantage of this construction is that no part of the measuring apparatus protrudes from the borehole, so that blasting operations cannot damage the measuring devices.

A disadvantage is that in practice only one measuring rod can be placed in each borehole so that to determine the exfoliation of the roof several boreholes are required.

4.3 Measurement of Movement on Fissures

The purpose of these measurements is to determine on fissures the velocity and the direction of relative movement.

The simplest arrangement, and one which is satisfactory for operating purposes, consists of three fixed points, two of which are secured on one side of the fissure and the third on the other. Thus the movement is measured in the plane defined by the position of the three fixed points.

The measuring points are marked by means of steel pins, which are cemented into the rock mass. The measurement is made on steel balls, which are welded onto the steel pins (Figure 16). The measurements are taken with an accuracy of $\pm$ 0.01 mm. The length of the side of the triangle amounts to approximately 230 mm, i.e., it is very large compared to the amount of deformation (a maximum of 3 mm measured so far), and thus the graphical representation of the measuring results is greatly simplified.

It was found that, in case of one pillar for example, the movement is usually restricted to one fissure, even when more are present. In order to determine the right fissure, and thus also the proper location of a measuring station, all fissures are covered by a thin layer of cement at one point. From ruptures in this cement layer one can determine which of the fissures moves most intensely.

The results of these measurements can be summarized as follows:

1. The movements on the fissures are not necessarily in direct relation with the convergence. Often one can observe relatively large (usually horizontal) movements without a correspondingly large change in the convergence velocities.
2. The measurement of fissure movements can therefore, with certain presuppositions, be used as a measure for judging the stability of pillars.
3. Under certain circumstances the movement on the fissures may be tied in with blasting.

4.4 Precision Levelling

Surface subsidence is measured by precision levelling (Zeiss Ni II plane plate micrometer, accuracy of reading 0.01 mm).

Although for additional measurements it will be necessary to improve the marking (moraine masses, severe climate) and the closeness of the points, the results obtained to date already display a description of the subsidence characteristic which agrees with the measurements obtained in the mine.

It is planned to use precision levelling underground as well, namely for:

1. Roof deflection between two pillar beams.
2. Deflection of the hanging-wall across the entire width of a mined area.
3. As a complement to the other types of deformation measurements, which will serve both for localizing and rendering precise these deformation measurements and also for their control.

5.0 Stress Measurements

No additional determination of the prevailing stress conditions in pillars has been performed to date, since the stress measurements undertaken by Hast (11) in 1952 and 1961 at Laisvall.

However field tests were undertaken with two types of measuring cells within the framework of the Swedish mining research program, viz. with a rigid (KTH-2) and with an axial measuring cell.

Rigid Measuring Cell

The principle and construction of this measuring cell are further described in reference (29). An indication shall merely be given here, that one is dealing with a passive, rigid measuring cell. This measuring cell was built as a prototype for developing the KTH-1 measuring cell; for its measuring medium it is equipped with swinging wires instead of an extension sensing transmitter; thus it attains a considerably higher degree of sensitivity. It is thus possible to determine the stress conditions of the rock mass in the vicinity of the measuring cell, given suitable creep properties of the rock mass.

Test measurements undertaken at Laisvall to date with seven cells extended over approximately one and a half years.

Unfortunately however, it transpired that the creep properties of the sandstone are not adequate for determining the stress conditions in the case of this particular measuring cell. It is now to be investigated though how well this measuring cell is suited for determining the stress variations under the conditions at Laisvall.

The reliability of this cell must, however, be termed as good, since no cell has so far failed.

Axial Measuring Cell

The function of this cell corresponds to that of an extensometer, with which extensions can be measured along the axis of a borehole (18). A soft ring serves as a measuring medium, equipped with four extension sensing transmitters. The ring is equipped with two arms, each of which carries a cylinder at its end. These cylinders are cemented into the borehole with epoxy resin. The distance between the two rings thus corresponds to the measuring base, which amounts to 200 mm (Figure 17).

Three of these extensometers, in horizontal boreholes, were built into two pillars which had not as yet been exposed by mining operations. These, and a few bordering pillars, were exposed after installing the extensometers. The changes in the pillar loading which thus arose could be clearly determined; however a quantitative evaluation could not so far be performed because of an insufficient knowledge of the deformation characteristics of the rock mass and of the pillars.

Future plans include measurements with the South African measuring cell "Doorstopper".

6.0 Selfregistering Microseismic Measurements

A few years ago the method of microseismic measurements (seismo-acoustic self-impulse method) was introduced on an experimental basis for current control of rock mass destruction (14). At present the measurements are exclusively adjusted to register microseismic activity, timewise distribution of impulses, and to determine impulse rates. Presently there are no plans for analyzing impulse records on magnetic tapes as to amplitude, impulse forms, and timewise alteration of the relative impulse energies respectively frequency spectra, possibly following methods of seismic models in situ as performed, for example, at the Institute for Applied Geophysics of the Mining Academy at Freiberg and at the regional office in Freiberg of the "Geodynamik Jena" of the German Academy of Science (26).

In our mines the measurements are performed on a selfregistering basis by the following equipment (manufactured by the firm of Adelta AB, Stockholm): electromagnetic geophon with preamplifier, counting device with three stage transistorized amplifier (connections to main and battery), Esterline - Angus recorder (Figure 18). This combination of the measuring installation permits of an objective measurement, automatic count and registering of the timewise impulse distribution. Measuring results are recorded either in 5 minute diagrams or hour diagrams, with values presented as impulse/min. Roofs, intermediate floors and pillars, in areas either being mined or already worked out, are being checked.

The microseismic measurements, undertaken according to the self-impulse method, are used for:

1. Accidental, sporadic, local control of rock mass destructions.
2. Current, continual, local control of rock mass destructions.
3. Pin-pointing rock destructions in the mine workings.

Two examples are listed hereunder. Figure 19 illustrates two measuring regions. "A" represents an annual diagram of a pillar in the Lindsköld mine, on which sporadic control measurements were undertaken. Two impulse peaks show up here, of which the latter coincides with rock mass movements, as determined by convergence measurements. "B" represents an hourly measurement, recorded in the roof of the Laisvall mine. Here too, one finds agreement of convergence phenomena between roof and floor, and increased impulse rate. True enough the latter arises suddenly without prior warning, while "A" recorded an extended increase of the impulse rate.

The two examples show the limited possibilities for applying the seismo-acoustic direct-method, as described already in (14). It is primarily limited to measurements extending over longer periods of time and to movements of a relatively slow type. This limitation is because, not in the least, of the given method of evaluation which limits itself to the number of impulses and their timewise sequence alone. In concluding it may be said that by means of the self-impulse method it is possible to determine the onset of rock mass destructions at an early stage. In combination with other measuring methods the monitoring of microseismic activity is an effective stability control. At present a new automatically registering instrument is in preparation (by the firm of Adelta AB). It will permit of a considerably larger number of measurements with the same number of personnel, so that it appears that a more meaningful evaluation of the measuring results will be possible which, after all, is to be used as a basis for the operating point control.

Conclusions and Future Aims

The following final conclusions can be drawn from the rock mechanics methods of investigation presented by way of a few examples:

The rock mechanics field measurements, undertaken in the complex way described, provide information about rock mass properties, their ways of behaviour and existing stability conditions. On the one hand they provide the prerequisites for various types of model-tests (inter alia 25), and on the other they provide, on a broad basis, quantitative data about the stability of cavities and pillars. Furthermore, these data may be useful in conducting present day mining operations. In the long run these investigations provide complementary results for future operational planning.

However, a prerequisite for this is that an optimal method combination be used, which may be a different one for each case involving a rock mechanics problem. Above all it should be noted that the rock mass is subject to geological space – time requirements. A mathematical handling of the various problems must also depart from this hypothesis. Looking at it in this way it follows that the rock mass must be treated as an in situ body.

From the practical operating person's point of view, the research effort and the degree of investigation must be functionally coordinated with the lifespan and the purpose of the mine installation.

The difficulty in satisfying this requirement is the problem of how to achieve optimum ore exploitation at still satisfactory stability conditions.

The authors wish to express their sincere thanks to director Fred Agri of the Boliden Company, Mines Administration, for permission to publish this paper, and also to all collaborators who have participated in producing this article.

Bibliography

(1) Bergman, S. G. A.
1965: Funktionell bergklassificering. IVA Meddelande, Stockholm.

(2) Bernabini, M., Esu, F., Martinetti, S., and Ribacchi, R.
1966: On the stability of the pillars in an underground quarry worked through soft pyroclastic rocks. Proc. First Cong. Int. Soc. Rock Mech., Lisboa.

(3) Clar, E.
1963: Gefüge und Verhalten von Felskörpern in geologischer Sicht. Felsmechanik 1 : 1.

(4) Coates, D. and Ignatieff, A.
1966: Prediction and measurement of pillar stresses. Can. Mining Jour., Jan.

(5) Denkhaus, H. G.
1963-64: Gebirgsfestigkeit und Gesteinsfestigkeit. Bericht über das 5. Ländertreffen des Internationalen Büros für Gebirgsmechanik, Leipzig, Nov. 1963, Berlin 1964.

(6) Dreyer, W.
1966: Quantitative Untersuchungen über die Festigkeit einfach strukturierter Gesteinsarten in Korrelation zu den Gefügeparametern und dem Mineralgehalt der Accessorien. Proc. First Cong. Int. Soc. Rock Mech., Lisboa.

(7) Friedman, M.
1963-64: Petrofabric techniques for the determination of principal stress directions in rocks. State of stress in the earth's crust. Int. conf. Santa Monica, California 1963, New York 1964.

(8) Grip, E. und Wirstam, Å.
1949: Hållfasthet, spricksystem och ras i nordsvenska sulfidmalmsgruvor. Jernkontorets annaler 133, 12.

(9) Hagerman, T. H.
1966: Rock bodies and particular zones in rock. The geological structure as a factor in rock stability. Proc. First Cong. Int. Soc. Rock Mech., Lisboa.

(10) Hansági, I.
1966: Bergmännisches Verfahren der Gebirgsfestigkeitsbestimmung und der gebirgsklassifizierung. Proc. First Cong. Int. Soc. Rock Mech., Lisboa.

(11) Hast, N.
1958: The measurement of rock pressure in mines. Part 1 - 6. Sveriges geol. Undersökning (SGU), Ser. C, no. 560.

(12) Helfrich, H.K.
(In press) Geological aspects of strength of rock and rock maases with illustrations from Renström, Adak and Laisvall. Engineering Geology .

(13) Helfrich, H.K.
1965: Zur Gefügeanisotropie des Granites der Bleierzlagerstätte Laisvall und deren Beziehung zu den horizontalen Hauptspannungsrichtungen, Felsmechanik, v. III/2.

(14) Helfrich, H.K.
1966: Selbstregistrierende mikroseismische Messungen. Felsmechanik IV:1.

(15) Helfrich, H.K. und Stephansson, O.
1966: Eine Kennziffer für die Stabilität von Pfeilern im Kammerbau. Proc. First Cong. Int. Soc. Rock Mech., Lisboa.

(16) Höfer, K.H.
1958: Beitrag zur Frage der Standfestigkeit von Bergfesten im Kalibergbau. Freiberger Forschungshefte A 100.

(17) Höfer, K.H., und Menzel, W.
1962: Vergleichende Betrachtungen über die mathematisch und aus Messungen unter Tage ermittelten Pfeilerbelastungen im Kalibergbau. Bericht über das 4. Ländertreffen des Int. Büro f. Gebirgsmechanik, Leipzig.

(18) Jacks, G.
1965: Axiell mätcell. Diskussionbeitrag in IVA-meddelande 142, Stockholm.

(19) Janelid, I.
Bergmekaniken och dess betydelse vid plane ring av gruvor och hergrum (Die Bedeutung der Gebirgsmechanik fur die Planierung von Gruben und Hohlräumen Untertage). IVA-meddelande no 142.

(20) Karl, F.
1964: Anwendung der Gefügekunde in der Petrotektonik, Teil 1: Grundbegriffe, Tektonische Hefte. 5, Clausthal - Zellerfeld.

(21) Kvapil, R.
1961: Natürliche Gesteinszerstörung. Freiberger Forschungshefte A 156.

(22) Kvapil, R.
1963-64: Veränderlichkeit der Festigkeitseigenschaften von Gebirgskörpern in Abhängigkeit von natürlichen Bedingungen Ber. über das 5. Ländertreffen des Int. Büro für Gebirgsmechanik, Leipzig 1963, Berlin 1964.

(23) Morfeldt, C.O.
1965: Granskning av borrhål i berg och betong. Väg- och vattenbyggaren no. 4/1965, Stockholm.

(24) Müller, L.
1963: Der Felsbau. 1. v. Ferdinand Enke Verlag, Stuttgart.

(25) Ramberg, H, and Stephansson, O.
1965: Note on centrifuged models of excavations on rocks. Tectonophysics, v. 2, no. 4, Oct.

(26) Rotter, D.
1965: Die Eigenimpulsmethode, ein geophysikalischer Beitrag zur geomechanischen Forschung, Monatsber. d. Deutsch. Akad. d. Wiss. zu Berlin, Bd. 7, Heft 3.

(27) Salamon, M.D.G., and Oravecz, K.I.
1966: Displacement and strains induced by bord and pillar mining in South African collieries. Proc. First Cong. Int. Soc. Rock Mech., Lisboa.

(28) Sander, B.
1948-50: Einführung in die Gefügekunde der geologischen Körper. Teil I und II, Springer Verlag Wien und Innsbruck.

(29) Sundkvist, H.
1965: Stel mätcell. IVA-meddelande 142, Stockholm.

(30) Tincelin, E., und Sinov, P.
1960: Der Einsturz des Hangenden bei Orterbau. Int. Kongress für Gebirgsdruckforschung, Paris.

(31) Trollope, D.H.
1966: Underground excavations and deep borings - General report of theme 7. Proc. First Cong. Int. Soc Rock Mech., Lisboa.

		Date		
		Mine: Level: Drift:		
		Range of Homogeneity		
		Current No.		
		Fissure-, s-surfaces, Dislocation-, type of fracture a. o.		
		Strike		
		Dip		
		Level	Overall	Condition
		Uneven		
		Wavy, dislocated		
		Smooth	Detail	
		Rough		
		Wavy, humped		
		Type	Linear, etc.	Harnish
		Strike		
		Dip		
		Gap, in mm		
		Fill material		
		Water economy		
		Length of outcrop (m)		
		No. of outcrops/m		
		No. of fissures m^2/m^3		
		Mean of normal distance between fissures 'd' (cm)		
		'd' min, 'd' max (cm)		
		Size of fissured body		
		Class of rock mass		
		Other Observations		

Figure 1. Scheme for taking stock of rock mass structures (modified form after L. Müller 1963, p. 212).

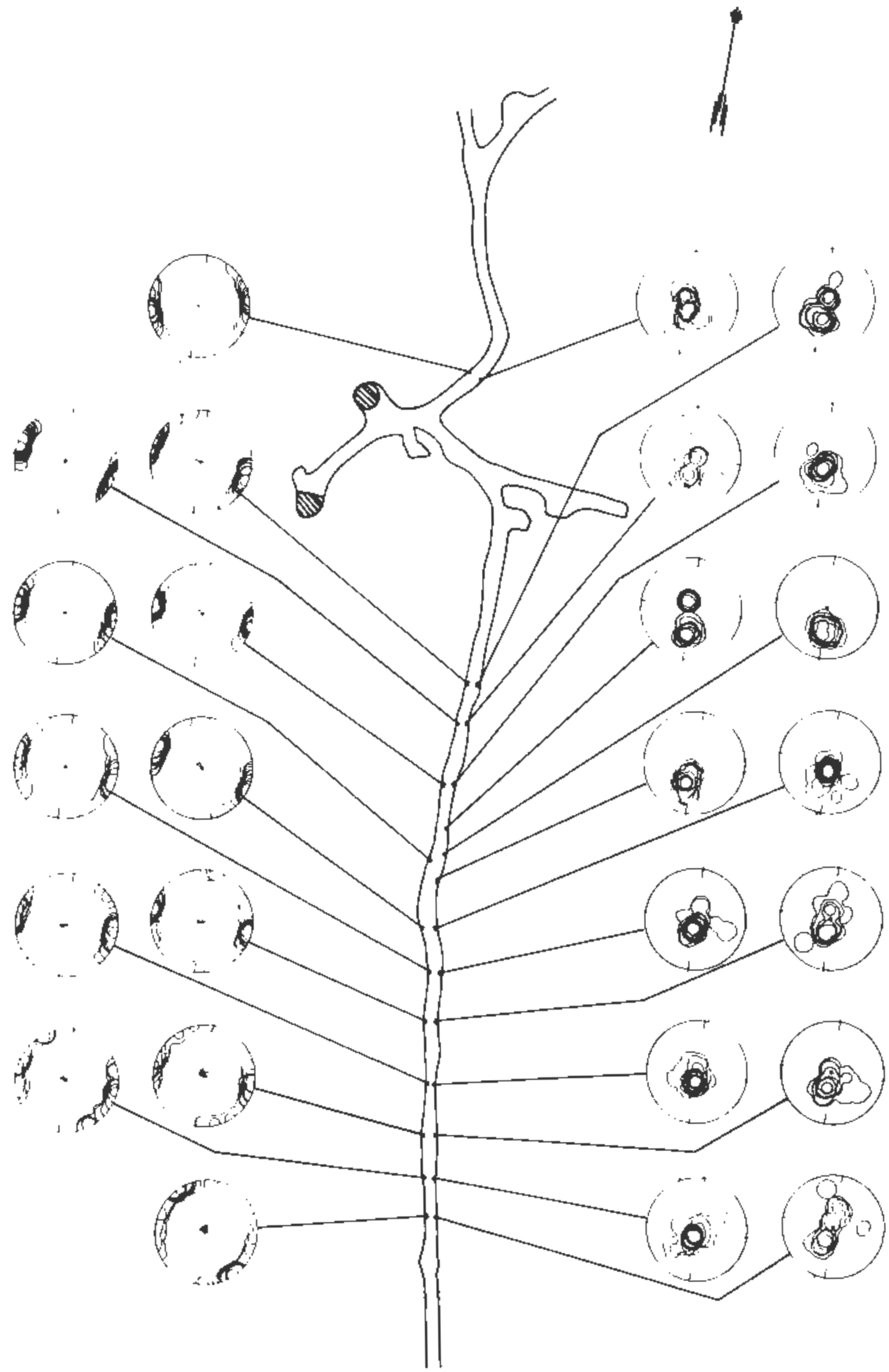

Figure 2. Texture analysis for typifying and classifying the tectonic structure and rock mass strength.

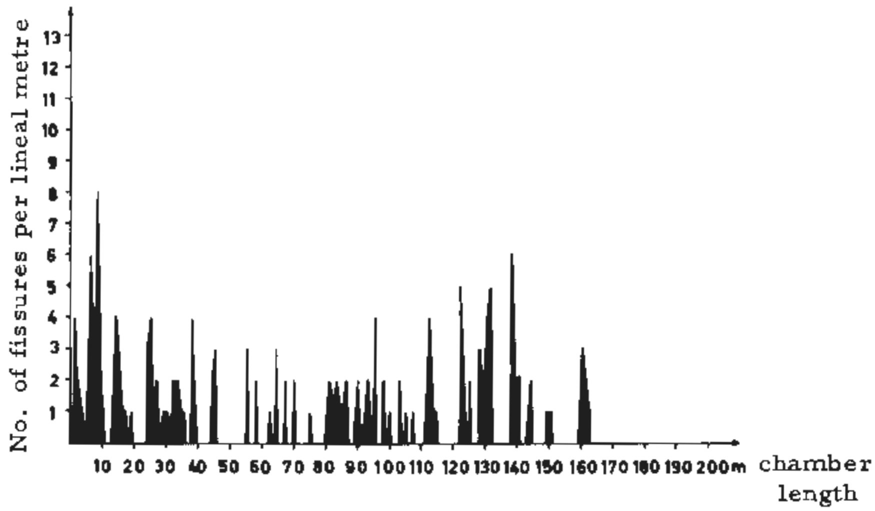

Figure 3. Fissure count per lineal metre along a working face and frequency analysis of fissure distances:

Fissure Distance, in cm	0–50 m	Length of Room 50–100 m Fissure Frequency in %	100–150 m
0 – 1	0	0	0
1 – 3	4,8	0	0
3 – 6	14,3	5,9	2,0
6 – 10	11,1	5,9	7,8
10 – 15	11,1	11,8	19,6
15 – 25	4,8	17,6	13,7
25 – 50	9,5	5,9	11,8
50 – 100	22,2	5,9	19,6
100 – 700	22,2	47,0	25,5

	Fissuring / Degree of loss of strength	Fissure distance > 1 m A	Fissure distance 10 cm - 1 m B	Fissure distance 1 cm - 10 cm C	Brecciated Mylonitized D
I	Fresh				
II	Weathered				
III	Slightly altered				
IV	Greatly altered				
V	Greatly weathered and altered				

Figure 4. Rock mass classification in accordance with fissuring and degree of loss of strength (modified table after L. Müller 1963, p. 246).

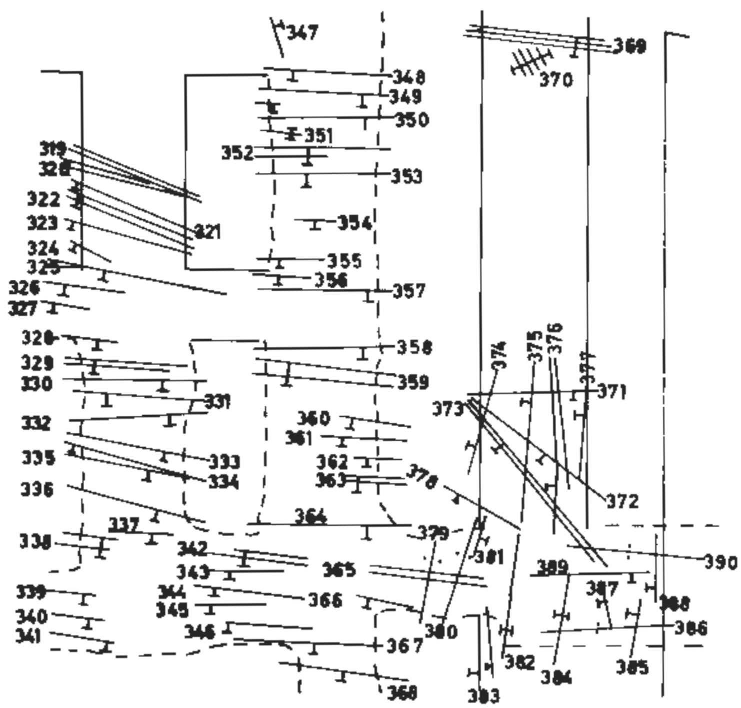

Figure 5. Example of fissure recording in room-and-pillar mining (fissure designation: current number).

Determining Group	Distinguishing Characteristics	Point Rating			
		0	1	2	3
Dimension	Height	0-8	8-12	12-20	> 20
	Effective pillar area (m^2)	>40	30-40	20-30	< 20
	Roof area to be supported (m^2)	<150	150-250	250-350	> 350
Form	Horizontal section	round, beam-shaped	elliptic	square	non-symmetrical
	Vertical section	uniform	conical	hour-glass shaped	non-symmetrical
	Outer surface	smooth	wavey, irregular	s-surface following	overlapping unterminated
Position	Deviation from the roof-normal	0°	$5-10^{\circ}$	$10-15^{\circ}$	$> 15^{\circ}$
	Pillar base-floor	horizontal	inclined	forming a working edge	sill forming
	Pillar head-roof	horizontal	inclined	stepped	Forming working periphery
Construction and Binder	No. of geological beds	1	2	3	> 3
	Weathering	absent	local	affecting outer layer	extensive, deep
	Contact:Pillar-Roof/Floor (%)	100-90	90-70	70-50	$< 5^{\circ}$
Fissure picture	Fissuring	0	Fissure distance (cm)		
			100-10	10-1	< 1
	Fissure length	0	Fissure length in relation to pillar height		
			1/4	1/2	1
	Gap width (mm)	0	0-2	2-8	> 8

Sum of evaluating points (a maximum of 9 points per determining group) = index number.

0- 5	excellent	0
6-10	very good	1
11-15	good	2
16-20	satisfactory	3
21-25	reasonable	4
26-30	deficient	5
31-35	bad	6
36-45	very bad	7

Figure 6. Table for determining pillar evaluating points.

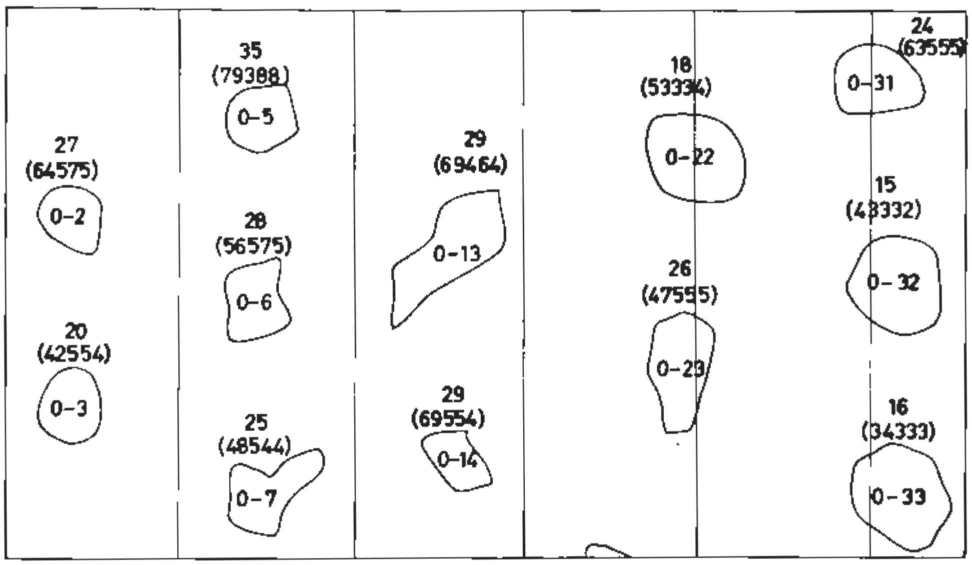

Figure 7. Scheme of pillar classification with evaluating points.

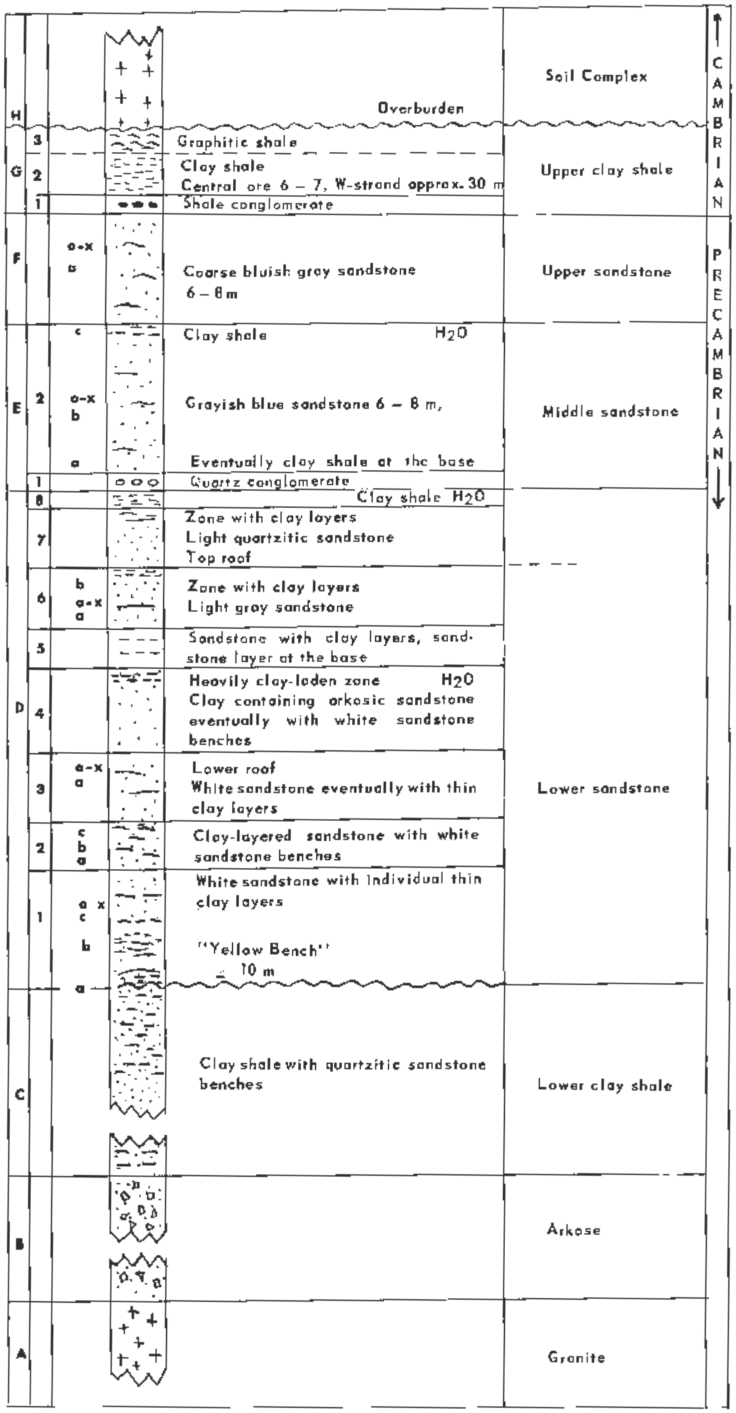

Figure 8. **Stratigraphic-petrographic table of the galena mine at Laisvall.**

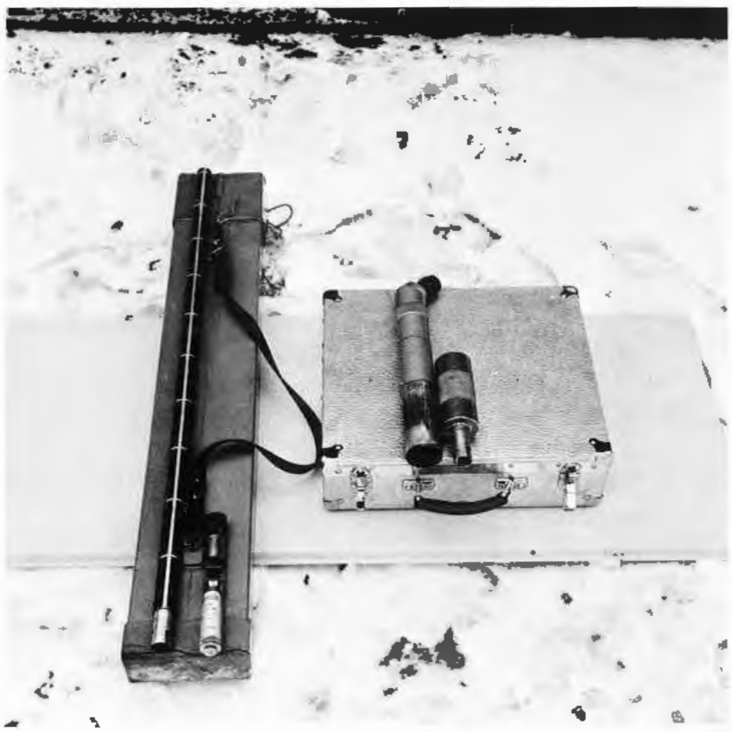

Figure 9. Optical borehole probe of the firm Hag-consult (Stockholm).

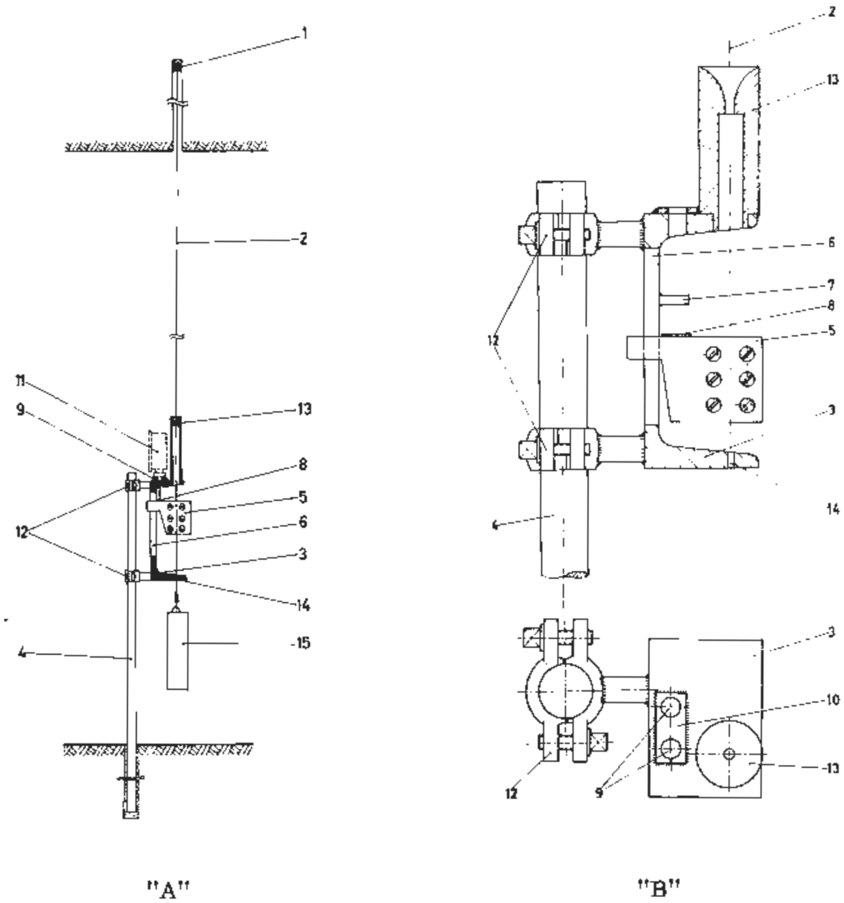

Figure 10. Measuring installation for long wires (per R. Kvapil's suggestion, Royal Technical University, Stockholm).

"A" 1) anchoring of wire, 2) steel wire, 3) U-shaped channel iron, 4) foundation pipe (cemented into borehole), 5) measuring mark, clamped onto wire, 6) slot for measuring mark, 7) reference plate, 8) stainless steel measuring plate, 9) drill holes for dial-gauge (deformation and reference measurement), 10) bearing surface of dial-gauge (stainless steel), 11) dial-gauge, 12) clamps, 13) guide collar (stainless steel), 14) guide hole, 15) weight (may be replaced by loading-spring if necessary).

"B" illustrates details of the construction in plan view and elevation.

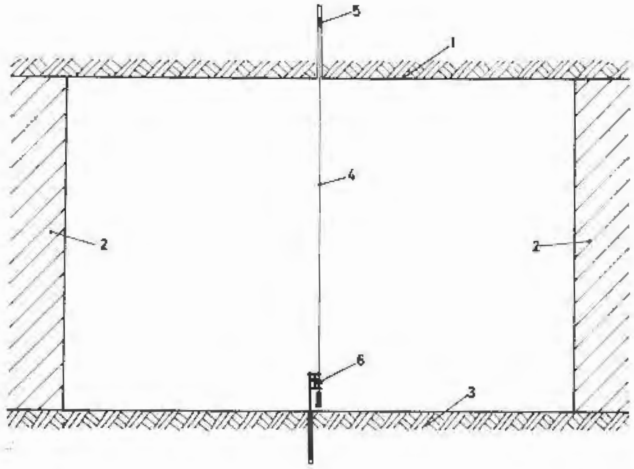

"A"

"B"

Figure 11. Convergence measurement in a room.
"A" illustrates the principle of the convergence measurement 1) roof, 2) pillar, 3) floor, 4) measuring wire, 5) anchoring of the measuring wire in the roof, 6) measuring stand, cemented into the floor.

"B" illustrates a convergence measuring station in the pit.

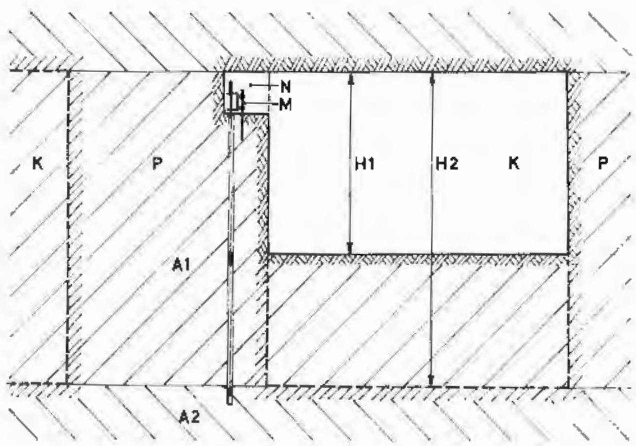

Figure 12. Measurement of vertical deformation in pillar beams.

K – room
P – pillar beam
H1 – room height during the first stage of mining
H2 – room height during the second stage of mining
A1 – anchoring of the first wire for measuring the deformation brought about by the first stage of mining
A2 – anchoring of the second wire for measuring the deformation brought about by the second stage of mining
M – measuring stand
N – recess in pillar beam, required for sinking the borehole and to accommodate the measuring stand

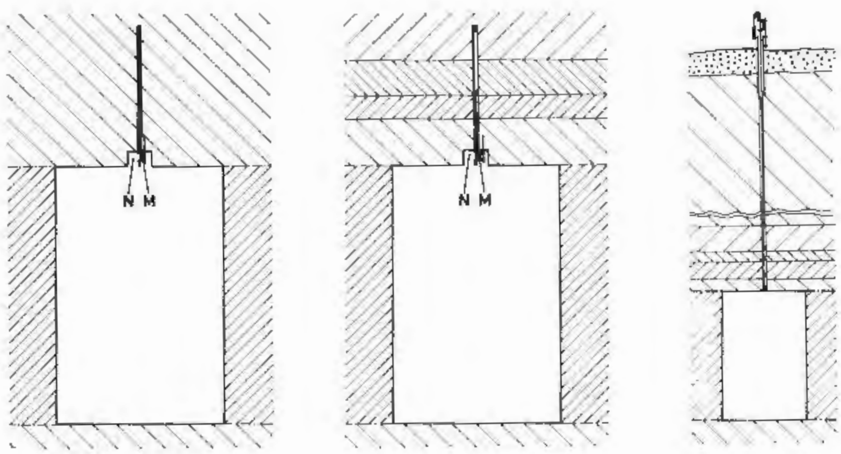

"A" "B" "C"

Figure 13. Measurement of roof sagging and exfoliation.

"A" illustrates measurement of roof sagging.

"B" illustrates measurement of roof sagging and exfoliation, wherein a wire is attached to each layer by means of an anchor. The measurement proper occurs on the measuring stand M inside the recess N, which can be sealed with a steel lid, to protect the measuring stand from damage. In this case the wires are kept tight hy means of springs.

"C" illustrates measurement from ground level of sagging and exfoliation. By this means it is possible to check the roof even after complete backfill of the workings.

Figure 14. Measurement of crosswise pillar deformation.

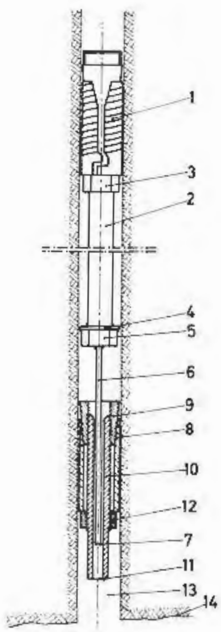

Figure 15. Construction of measuring rods 1) expansion sleeve, 2) anchoring rod, 3) stop nut, 4) centring ring, 5) nut for tightening expansion sleeve (1), 6) measuring rod (stainless steel), 7) bearing surface for dial-gauge point, 8) expansion sleeve (with spring clamp removed), 9) cone of expansion sleeve (8), 10) sleeve (stainless steel), 11) bearing surface for dial-gauge sleeve, 12) nut for tightening expansion sleeve (8), welded to sleeve (10), 13) borehole, 14) surface of rock mass.

Figure 16. Measurement of movement on a fissure surface (per R. Kvapil's suggestion, Royal Technical University, Stockholm).

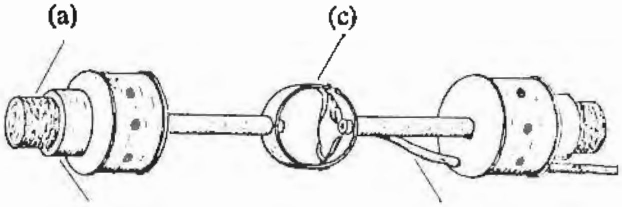

Figure 17. Axial extension meter (per G. Jacks, in 18).

(a) piston for extruding epoxy-resin from container (b) through radial holes in (b).

(c) ring with extension sensing transmitters.

(d) cable.

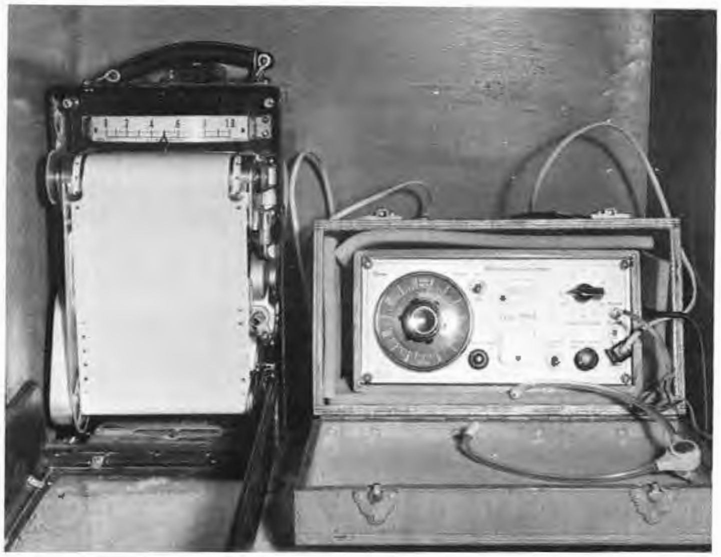

Figure 18. Selfregistering microseismic equipment of the firm Adelta AB, Stockholm, consisting of a geophon, counting and recording device.

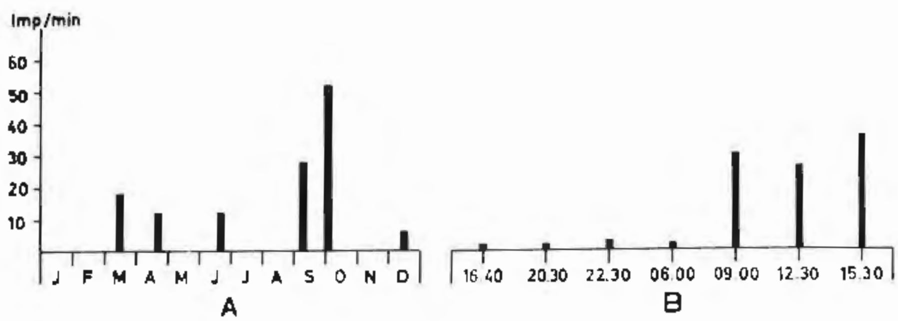

Figure 19. "A" example of a sporadic microseismic long-term time control (12 months).

"B" example of a short-term series measurement (24 hours).

COMPARATIVE STRESS MEASUREMENTS AT ELLIOT LAKE

W.L. van Heerden and F. Grant***

Abstract

As part of an extensive program of measuring rock stresses, a series of comparative measurements were made in a Canadian uranium mine by means of a strain cell developed at the South African Council for Scientific and Industrial Research and of a borehole deformation meter developed at the U. S. Bureau of Mines. An analysis of the results, taking account of certain sources of error, shows that there is satisfactory agreement between the results obtained with the two methods.

Introduction

During recent years increasing consideration has been given to the problem of measuring the stress in rock around underground excavations. Leeman (1) has published an excellent review of the instruments and techniques available for this purpose. In Canada an extensive program has been pursued since 1963, and this paper, in effect, is a second progress report (the first having been published last year (7)).

---

*Exchange Research Officer from National Mechanical Engineering Research Institute, South African Council for Scientific and Industrial Research, Pretoria, South Africa, at Mines Branch, Department of Energy, Mines and Resources, Ottawa, Canada.

**Scientific Officer, Mining Research Laboratories, Fuels and Mining Practice Division, Mines Branch, Department of Energy, Mines and Resources, Elliot Lake, Canada.

The instruments that are most often used today can be divided into two classes. One class, the borehole deformation gauge, measures the changes in length of one or more diameters of a borehole drilled in the rock when the stress in the rock surrounding the gauge is relieved by drilling an annular groove concentric with the borehole. Because the overcoring hole is usually 6 in. or more in diameter, the method is expensive and practical drilling difficulties restrict the depth at which a measurement can be obtained.

The second class of instrument, which takes the form of a so-called strain cell containing electrical resistance strain gauges or a photo-elastic disc, is glued on the flattened end of a borehole drilled in the rock. It measures the change in strain of the rock on which it is glued when the stress is relieved by extending the length of the borehole by means of a coring drill. The small size of the hole required and the simplicity of the overcoring and installation procedure make it possible to obtain measurements at a considerable depth inside the rock mass.

In this paper the results obtained using a borehole deformation meter developed at the U.S. Bureau of Mines (2) (referred to as a deformation meter in this paper) with the results given by a borehole strain gauge device (1) developed at the South African Council for Scientific and Industrial Research (referred to as a strain cell in this paper) are compared.

Both instruments were tested in the laboratory (3, 4) and were found to perform satisfactorily under uniaxial and biaxial loading conditions. In this paper the performance of the two instruments, under the more complex stress conditions which are encountered underground, are compared.

Description of the Instruments

The instruments used for the measurements have been described elsewhere (1, 2) so that only a brief description will be included here.

U.S. Bureau of Mines Borehole Deformation Meter

The borehole deformation meter which was developed in the U.S. Bureau of Mines measures the changes in length of a single diameter of a borehole. The measuring element is a beryllium copper cantilever on which four resistance strain gauges are mounted and connected to form a Wheatstone bridge. The cantilever also produces the force required to keep the piston in contact with the sidewalls of the borehole.

When the deformation meter is installed in a borehole, any change in diameter of the borehole is transmitted via the piston to the cantilever.

The change in bending strain produced in the cantilever is measured on a conventional strain indicator. Changes in diameter of as little as 50 micro in. can be measured with this meter. The reference diameter of the instrument can be changed by changing either the piston length or the spacing stud directly opposite the piston. This allows the meter to be adjusted for use in an oversize hole. The gauges on the cantilever are waterproof and dust proof, and the meter has a temperature sensitivity of less than 10 micro in. per °F.

CSIR Strain Gauge Strain Cell ("Doorstopper")

This strain cell was developed at the South African Council for Scientific and Industrial Research. It measures changes in strain in three directions on the end of a borehole. The measuring element is a conventional rectangular strain gauge rosette, the individual gauges of which are oriented to measure changes in strain in the vertical, 45° and horizontal directions. The leads from the gauges are connected to four pins in an insulated connector plug. Both the plug and the gauges are encapsulated in a silicone rubber compound which provides physical protection as well as waterproofing for the strain gauges.

The strain cell is installed into the borehole by means of a special installating tool (5, 6). In this method the rock on which the cell is cemented is stress-relieved by extending the length of the borehole.

Method of Measurement

Theoretical

In using either of the methods described above, the principal stresses, σ_1 and σ_2, acting in the plane normal to the borehole, are obtained by measuring the deformation or strain in at least three different directions. The calculation of the magnitudes and directions of σ_1 and σ_2 from the measurements depends, in general, on the assumption that the measurements are insensitive to any normal stress parallel to the direction of the borehole.

For purposes of comparing the two instruments underground, the boreholes in which the measurements were made were drilled parallel to each other. Thus at any depth of the boreholes the stresses to be measured could be considered to be the same. Any differences could only be the result of inaccuracies introduced by the instruments, inaccuracies in determining the elastic constants of the rock and inaccuracies due to the degree to which the above assumption was not fulfilled.

U.S.B.M. Deformation Meter. The formulae to calculate the stresses from borehole deformation measurements obtained with the U.S.B.M. deformation meter were derived by Merrill and Peterson (3). They are as follows:

If,

u_1	=	deformation measured across a diameter of the borehole (see Figure 1)
u_2	=	deformation measured in a direction 60 degrees anticlockwise from u_1 (usually the vertical direction)
u_3	=	deformation in a direction 120 degrees anti-clockwise from u_1
θ_1	=	angle measured anticlockwise from σ_1 to the direction of u_1
D	=	diameter of the borehole
E	=	modulus of elasticity of the rock

then,

$$\sigma_1 + \sigma_2 = \frac{E}{3D} \quad (u_1 + u_2 + u_3)$$

$$\sigma_1 - \sigma_2 = \frac{\sqrt{2}\,E}{6\,D}\left[(u_1 - u_2)^2 + (u_2 - u_3)^2 + (u_1 - u_3)^2\right]^{1/2}$$

from which the magnitudes of σ_1 and σ_2 can be determined. The direction of σ_1 is given by:

$$\tan 2\,\theta_1 = \frac{-\sqrt{3}\,(u_2 - u_3)}{2\,u_1 - u_2 - u_3}$$

CSIR Strain Cell. The formulae used to calculate stresses from strain measurements obtained with the CSIR strain cell are well known strain rosette equations derived from the theory of elasticity. They were included in a recent publication by Leeman (4).

Let the difference in the strain readings in the vertical, 45° and horizontal directions before and after overcoring be e_V, e_{45} and e_H respectively.

The principal strains in the rock on the end of the borehole are given by:

$$e_{1,2} = 1/2\left[(e_H + e_V) \pm \sqrt{\{2\,e_{45} - (e_H + e_V)\}^2 + (e_H - e_V)^2}\right]$$

The principal stresses σ_1' and σ_2' in the rock on the flat end of the borehole are:

$$\sigma_1' = \frac{E}{1 - \nu^2} (e_1 + \nu e_2)$$

$$\sigma_2' = \frac{E}{1 - \nu^2} (e_2 + \nu e_1)$$

where

E = modulus of elasticity of the rock

ν = Poisson's ratio of the rock.

The principal stresses σ_1 and σ_2 in the rock surrounding the borehole can be obtained from

$$\sigma_1 = \frac{1}{1.53} \sigma_1', \quad \sigma_2 = \frac{1}{1.53} \cdot \sigma_2$$

The direction of σ_1 can be determined from:

$$\tan \theta = \frac{2 (e_1 - e_H)}{2 e_{45} - (e_H + e_V)}$$

where θ is measured anticlockwise from the horizontal direction (see Figure 2).

Experimental

U.S.B.M. Deformation Meter. The procedure used to install the deformation meter and to relieve the stress in the rock surrounding it involves the following sequence of steps.

A 6-in. hole is drilled sufficiently far into the rock to get beyond the fractured zone near the rock face. The core is removed, and guides are placed in the hole to centre the EX core barrel. An EX hole is then drilled into the centre of the end of the 6-in. borehole to a depth of 10 ft or more ahead of the end of the 6-in. hole.

The deformation meter is placed in the EX hole 6 to 9 in. from the end of the 6-in. hole and oriented to measure changes in the vertical diameter of the borehole. The cable from the meter is brought out through the drill rods and connected to a strain gauge bridge, an initial reading is taken, and the 6-in. drill is advanced. Readings are taken at regular intervals until the meter is overcored. A final reading is taken and the core is removed.

The difference, u_1, between the initial reading and the final reading during the overcoring operation is a measure of the borehole deformation in this direction.

The meter is then installed deeper in the EX borehole and oriented to measure changes in diameter in a direction 60 degrees anticlockwise to the direction of the u_1. It is again overcored, and a measurement u_2 is obtained.

The CSIR Strain Cell. To use this strain cell a BX size (2-3/8-in.-diam) borehole is drilled into the rock to the depth at which the stresses are to be determined.

The end of the borehole is ground flat and smooth with a square faced diamond bit and a flat faced diamond impregnated bit. The end of the borehole is dried by wiping it with a piece of cloth soaked in a suitable solvent.

The strain cell to be used is cleaned, plugged into the installing tool and smeared with a uniform layer of glue. The complete assembly is pushed up to the end of the borehole.

On reaching the end of the borehole the tool is oriented and the cell is pushed against the and of the hole by applying sufficient pressure on the installing rods.

Once the glue has set and the strain readings become constant, the tool is removed, leaving the strain cell adhering to the end of the borehole.

The drill using a BX coring bit is inserted in the borehole, and the rock to which the strain cell is attached is cored out. On removai from the borehole the strain cell, adhering to a length of core, is plugged into the installing tool and a final strain reading is taken. The strain resulting from the stress-relieving operation is the difference between the initial and final strain readings.

The end of the hole is flattened and the procedure repeated.

Tests Performed on 6-in. Core Samples. Each of the 6-in. core pieces in which a deformation meter measurement was obtained was returned to the laboratory. Cylindrioal specimens with their axes parallel to the directions in which field measurements were taken were prepared from tham.

Simple uniaxial compression tests were performed on these specimens from which the modulus of elasticity of the rock was determined. Lateral strain gauges were glued to some of these specimens in order to determine the Poisson's ratio of the rock.

Tests Performed on BX Core Samples. As a confirmation that the strain cells were properly glued to the rock, tests were conducted on 1/2-in.-thick discs cut from the ends of the core to which the strain cells were attached.

Compressive loads were applied to the cylindrical surface of the discs at two diametrically opposite points and parallel to, say, the vertical strain gauge in the rosette. Readings from all the strain gauges were taken at fixed increments of load.

The response of the gauges was plotted against the applied load, and if there were no pecularities in the curves it was assumed that the bond between the strain cell and the rock was adequate. The modulus of elasticity and the Poisson's ratio of the rock were obtained from the core by means of uniaxial compression tests in the laboratory. Unfortunately some of the core pieces were not recovered and others were not suitable for compression testing so that these tests were performed at about half the stress-relieving stations.

Description of the Test Sites

Test Site 1 - Measurements in Rock Undisturbed by Stoping

Measurements were made with both instruments in No. 14 extension drift in the hangingwall of the mine. The drift is 1,400 ft below surface and the average dip of the formation is 14°.

Three horizontal boreholes were drilled in the sidewall of the drift as shown in Figure 3. Borehole No. 1 was used for deformation meter measurements and boreholes Nos. 2 and 3 for strain cell measurements.

Test Site 2 - Measurements in Pillars

Both instruments were used to determine the stresses in several narrow pillars in a mined-out area of the mine. The ore is mined on a room-and-pillar system (7). The stopes are approximately 250 ft long on dip by 140 ft wide and are separated by pillars 10 ft wide.

Holes for the strain cell measurements were drilled parallel and close to holes in which the deformation meter measurements were taken. The pillars in which measurements were taken as well as the general layout of the stopes are shown in Figure 4.

Experimental Results

Field Stresses, Test Site 1

The results of the measurements made with each instrument in the 14 level extension drift are given in Table 1 and Figures 5, 6 and 7. Figures 5 and 6 show the variation, with distance into the solid, of the major and minor principal stresses (σ_1 and σ_2) respectively. Figure 7 shows the variation of the major principal stress direction with distance into the solid.

In analyzing the deformation meter results, two obviously erroneous results were rejected. Plots were made of borehole deformation u_i ($i = 1, 2, 3$) versus distance from the collar of the borehole for each orientation of the meter in the borehole. Values for the borehole deformations u_1, u_2 and u_3, determined at intervals, along the length of the borehole, by interpolation from these plots were used to calculate the deformation meter results shown in Figures 5, 6 and 7.

The strain cell results in Figures 5, 6 and 7 are the average of measurements made in boreholes Nos. 2 and 3. Except for the first 10 ft the scatter in the results obtained in these two boreholes was less than 10 per cent. The scatter in the results over the first few feet can be attributed mainly to the fact that these measurements were obtained during a period when the strain cells and installing equipment were undergoing initial evaluation tests when the underground crew was not yet fully acquainted with the installation procedure.

Measurements were obtained in borehole No. 2 for a distance of 80 ft into the solid. Since the deformation meter measurements were discontinued at a depth of 30 ft, the strain cell results between 30 and 80 ft could not be used for comparison purposes and are, therefore, not included in this paper.

As can be seen from Figure 7 both methods showed that the major principal stress is acting in a direction of between 70 and 100 degrees from the vertical direction (i.e., close to the horizontal direction). The magnitudes of both major and minor principal stresses as determined with the deformation meter are consistently higher than those indicated by the strain cell. It is believed that some of the reasons for this are as follows:

1. In most cases the deformation meter may have been installed too close to the end face of the 6-in. overcoring hole when the initial reading was taken. For this reason the diameter of the hole at the point of measurement may have been affected by the stress concentration ahead of the 6-in. overcoring hole. Although a distance of 6 in. (one diameter) was used, a decrease in the borehole diameter was detected as soon as the overcoring hole was advanced. This might mean that the deformation meter was not completely outside the zone of influence of the overcoring hole; thus the measurements would be, therefore, slightly high because the stress concentration effect is included in the reading.

2. in some cases the overcoring operation had to be discontinued while the diameter of the borehole was still changing. This resulted in measurements which were either too high or too low depending on the direction in which they were taken (9).

3. The construction of the strain cells used in these tests was such that the strain had to be transmitted to the strain gauges via a thin piece of "Araldite" shim. This resulted in strain readings which were as much as six per cent too low.

These errors increased the difference between the results obtained with the two instruments.

Pillar Stresses, Test Site 2

The results of the strain cell and deformation meter measurements are shown in Tables 2 and 3 respectively. Since the three readings u_1, u_2 and u_3 required to complete a deformation meter measurement were obtained over a distance of approximately 3 ft, fewer measurements could be obtained in the narrow pillars with this method. Average values of u_1, u_2 and u_3 were, therefore, determined to calculate the stresses in the pillars.

Table 2 shows that the strain cell results are fairly consistent over the centre section of the pillar in which measurements were obtained. In view of this and the fact that few deformation meter results were obtained, it was considered reasonable to compare average values of the stresses and their directions in the pillars. The results are compared in Table 4.

Both methods showed that the major principal stress acts in an up-dip direction approximately 45 degrees from the vertical direction. The magnitudes of the major principal stresses as obtained from deformation meter measurements were again slightly higher than those obtained from strain cell measurements. The difference in the magnitudes of the minor principal stresses obtained with the two methods is much greater. In some cases the deformation meter values are three times as high as the strain cell values.

It is believed that this difference is because of errors which were introduced in the u_3 deformation meter measurements taken in a direction 120 degrees from the vertical direction. As a check, the stress values obtained from the strain cell measurements were used to calculate the deformations of an EX borebole in the three directions in which deformation meter measurements were taken. The calculated values of u_1, u_2 and u_3 and those measured by the deformation meter are given in Table 5. These clearly indicate that the agreement between the calculated and measured u_3's are generally poor. On the other hand the agreement between the calculated and measured values of all u_1's and u_2's is satisfactory with only one exception, namely, in borehole 9W9-2L. Thus it can be concluded that, had the u_3 measurements been more satisfactory, the stresses obtained by the deformation meter would have conformed even more closely with those given by the strain cells.

Rock Properties

The uniaxial compression tests performed on BX core samples which were obtained from overcoring tests with the CSIR strain cell produced values of the modulus of elasticity and Poisson's ratio of the rock with a standard deviation of less than five per cent. The following mean values were obtained:

Modulus of elasticity 11.5×10^6 psi

Poisson's ratio 0.2

All the results, except the values of Poission's ratio, were obtained from compression tests on specimens prepared from the 6-in. overcoring cores (8).

Although the same mean values were obtained, the standard deviation was found to be 15 per cent for the modulus of elasticity and 25 per cent for Poisson's ratio.

When analyzing strain or borehole deformation measurements, obtained from overcoring tests, the results are usually more accurate if the elastic constants (E and ν) obtained at each measuring station are used for the calculation of the stresses at that point. However, since the constants could not be determined at every overcoring station, it was considered reasonable to use the mean values given above for all calculations in this paper.

Conclusions

Both instruments show the same general variation of σ_1 and σ_2 with distance from the sidewall of the 14 level extension drift. At distances of between 20 and 25 ft from the sidewall the difference between the results is large. However, considering the accuracy with which the elastic constants of the rock could be determined, the inherent accuracy of the instruments and other errors, the results obtained with the two methods are generally in good agreement.

With the exception of the u_3 measurements all other measurements (u_1 and u_2 measurements) obtained with the deformation meter in the pillars are in good agreement with measurements obtained with the strain cell. The directions of the principal stresses obtained at both sites using the two instruments are in good agreement.

The results of these experiments are a good indication of the reliability of both instruments for determining the stresses in unfractured hard rock.

The deformation meter has the advantage that it can be used under wet conditions. It has the disadvantage that it is not rigidly fixed in the hole during the overcoring operation and it can, therefore, move while being overcored.

The strain cell has the advantage that more measurements can be obtained with it within a given distance. Although it has the disadvantage, at the present time, that it can only be used on dry rock, chemicals are now available for improving the bond of cements to wet surfaces which may solve this problem.

Acknowledgments

This work is part of an extensive program of stress measurements being conducted in Canada under the supervision of D. F. Coates. The assistance of J. St. Onge, W. Zawadski, A. V. St. Louis, H. Montone, W. Timms and P. Pike of the Mining Research Laboratories at Elliot Lake as well as the assistance of W. M. Gray in editing the paper are acknowledged.

The co-operation and assistance of the mining officials at the Nordic Mine of Rio Algom Mines Limited was much appreciated.

The permission of the Canadian Department of Energy, Mines and Resources and the South African Council for Scientific and Industrial Research to publish this paper is gratefully acknowledged.

References

(1) Leeman, E.R.
1964: The measurement of stress in rock - Part II: Borehole rock stress measuring instruments, Jour. SAIMM, v. 65, no. 2, pp. 48-81, Sept.

(2) Obert, L., Merrill, R.H. and Morgan, T.A.
1962: Borehole deformation gauge for determining the stress in mine rock, U.S. Bureau of Mines Rept. of Investigation 5978, 11 pp.

(3) Merrill, R.H. and Peterson, J.R.
1961: Deformation of a borehole in rock, U.S. Bureau of Mines Rept. of Investigation 5881, 32 pp.

(4) Leeman, E.R.
1964: The measurement of stress in rock - Part I: The principles of rock stress measurements, Jour. SAIMM, v. 65, no. 2, pp. 82-114, Sept.

(5) Instruction Manual for the Use of the CSIR Strain Gauge Strain Cell
1966: ("Doorstopper") Equipment Using the Manually Operated Installing Tool, Rep. S. Afr. Counc. Sci. Indust. Res., no. MEG 417, Feb.

(6) van Heerden, W.L., Szombathy, C. and St. Louis, A.V.
1966: A new strain cell installing tool, Mines Branch Report FMP 66/37-MRL, Dept. Energy, Mines and Resources, Ottawa.

(7) Coates, D.F. and Grant, F.
1966: Stress measurements at Elliot Lake, Bull. CIMM, v. 59, no. 649, May.

(8) Parsons, R.C. and Sullivan, J.D.
1965: Moduli determinations for the Elliot Lake stress relief overcoring work, Mines Branch Report FMP 65/137-MRL, Dept. Energy, Mines and Resources, Ottawa.

TABLE 3

Results Obtained from Deformation Meter Measurements in the Pillars

Hole Number	Depth of Hole (inches)	Deformation Measurements (10^{-4} inches)		
		u_1	u_2	u_3
9W9-1C	37	28	--	--
"	63	--	--	4.8
"	80	--	12	--
MEAN		28	12	4.8
9W9-2C		Core disced all the way		
9W9-2L	21	--	21	--
"	31	32	--	--
"	44	--	--	2.8
"	55	--	14	--
"	77	32	--	--
"	89	--	--	18.2
MEAN		32	17.5	10.5
9W9-3L	22	--	2.9	--
"	34	48	--	--
"	46	--	--	29
"	68	--	33	--
MEAN		48	31	29
9W9-1R	72	--	18.0	--
		Core disced most of the time		
9W9-2R	33	--	8.0	--
"	45	36.63	--	--
"	58	--	--	0
"	80	--	19.0	--
MEAN		36.63	13.5	0
9W9-3R	42	--	12	--
"	53	48	--	--
"	66	--	--	3.6
"	76	--	19.2	--
MEAN		48	15.6	3.6
11W9-2C	30	--	23.3	--
"	46	32.4	--	--
"	59	--	--	-0.7
"	72	--	--	-1.4
"	80	--	--	0
"	92	44.0	--	--
"	102	--	14.5	--
MEAN		38.2	18.9	-0.7
11W9-3C	24	--	20	--
"	41	33	--	--
"	54	--	--	0
"	65	--	20	--
MEAN		33	20	0

TABLE 4

Comparison of the Magnitudes and Directions of the Principal Stresses as Determined with Each of the Methods in the Pillars

Borehole Number	Type of Measuring Instrument	Principal Stresses (psi)		Angle from Vertical to Direction of Maximum Principal Stress (deg.)
		Maximum	Minimum	
9W9-1C	Strain Cell	7610	1014	44
"	Deformation Meter	8680	3220	53
9W9-2C	Strain Cell	8210	1075	45
"	Deformation Meter	--	--	--
9W9-2L	Strain Cell	7400	1858	38
"	Deformation Meter	10475	5425	50
9W9-3L	Strain Cell	13930	5400	36
"	Deformation Meter	16800	12000	57
9W9-1R	Strain Cell	10210	342	44
"	Deformation Meter	--	--	--
9W9-2R	Strain Cell	10750	1415	43
"	Deformation Meter	11640	3220	44
9W9-3R	Strain Cell	13000	1410	47
"	Deformation Meter	14000	3600	52
11W9-2C	Strain Cell	10437	1546	42
"	Deformation Meter	11975	3025	45
11W9-3C	Strain Cell	9710	1744	41
"	Deformation Meter	11500	2600	42

TABLE 5

Comparison of the Changes in Diameter of an EX Borehole as Measured with the Deformation Meter and as Calculated from Measurements Made with the Strain Cell

Borehole Number	Principal Stresses Determined from Strain Cell Measurements (psi)		Borehole Deformations Calculated from Strain Cell Measurements (10^{-4} inches)			Borehole Deformations Measured with the Deformation Meter (10^{-4} inches)		
	Maximum	Minimum	u_1	u_2	u_3	u_1	u_2	u_3
9W9-1C	7610	1014	26.0	11.8	-3.9	28	12	4.8
9W9-2C	8210	1075	30.0	12.0	-6.5	--	--	--
9W9-2L	7400	1858	23.0	15.7	-2.3	32	17:5	10.5
9W9-3L	13930	5400	40.7	30.4	3.8	48	31	29.0
9W9-1R	10210	342	35.6	14.6	-8.9	--	18.0	--
9W9-2R	10750	1415	35.8	17.4	-5.9	36.6	13.5	0
9W9-3R	13000	1410	45	16.5	-6.2	48	15.6	3.6
11W9-2C	10437	1546	38.0	18.1	-5.6	38.0	18.9	-0.7
11W9-3C	9710	1744	31.0	18.0	-4.35	33	20	0

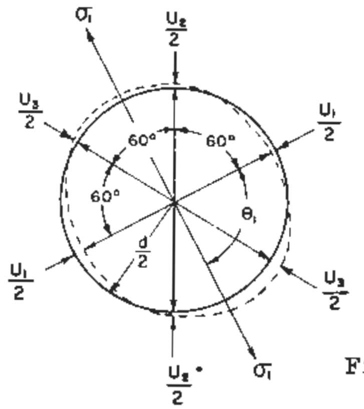

Figure 1. Directions of stresses and deformations (U.S.B.M. deformation meter).

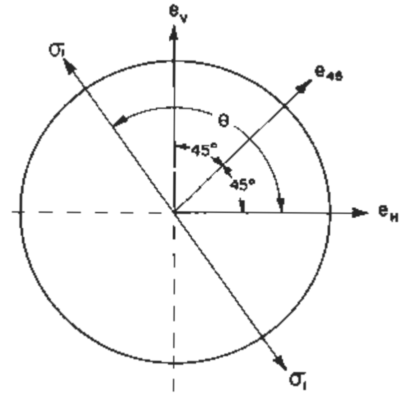

Figure 2. Directions of stresses and strains (C.S.I.R. strain cell).

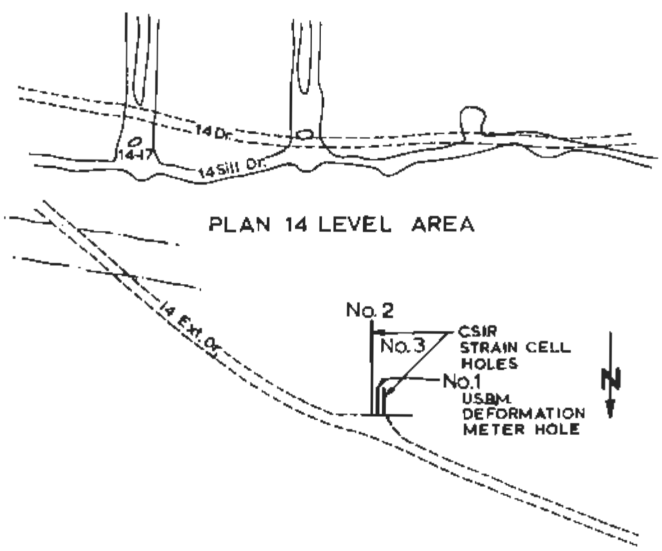

Figure 3. Position of the boreholes in the 14 extension drift.

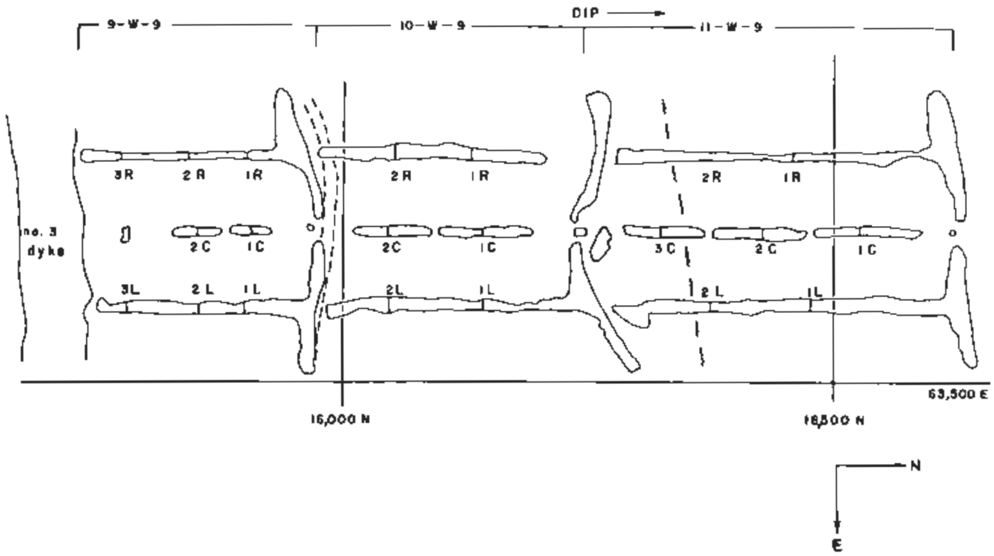

Figure 4. Plan of stopes showing pillars in which measurements were taken.

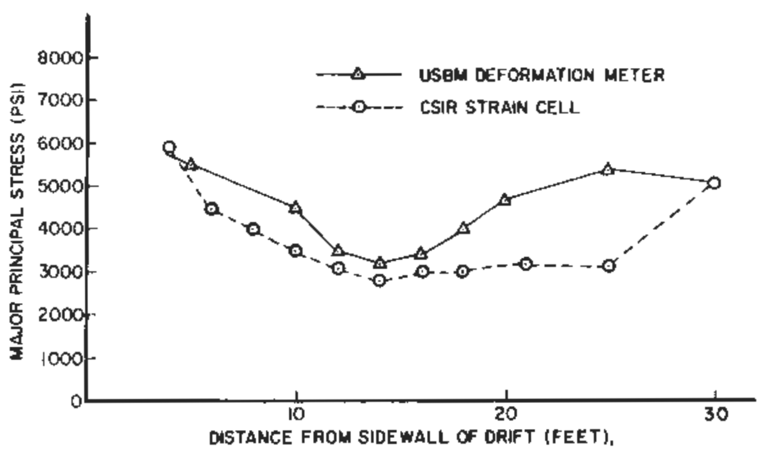

Figure 5. Graph showing variation of major principal stress (as determined with each of the two methods) with distance into the solid.

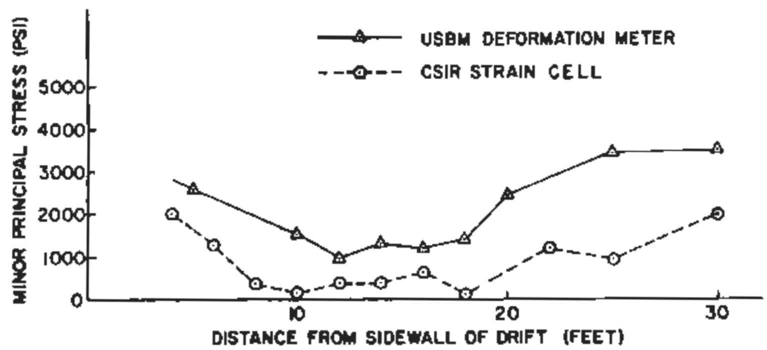

Figure 6. Graph showing the variation of the minor principal stress (as determined with each of the two methods) with distance into the solid.

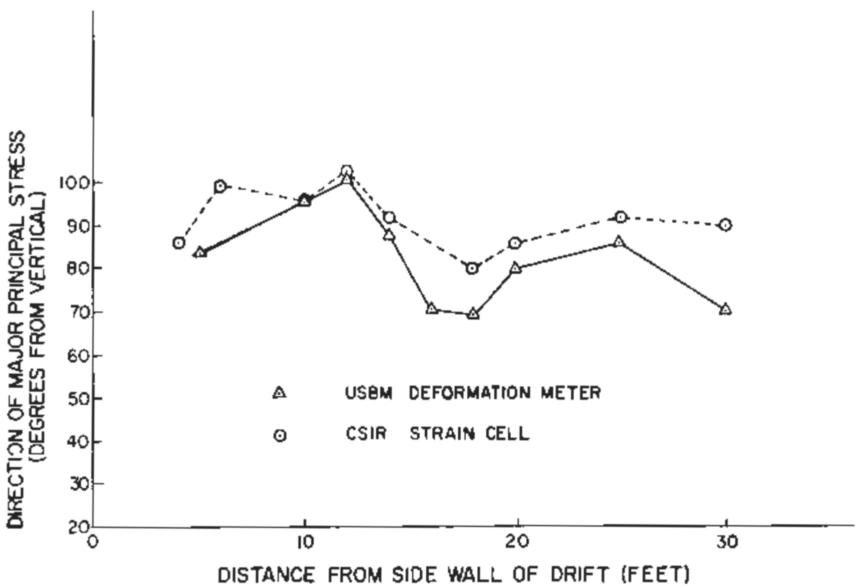

Figure 7. Variation of the major principal stress direction with distance into the solid.

AN APPRAISAL OF CONVERGENCE MEASUREMENTS IN SALT MINES

*D.G.F. Hedley**

Introduction

In salt mines the rock-mass movement because of mining does not occur instantaneously, but over a long period of time. Consequently, salt pillars which appear to be stable immediately after mining often deteriorate with time and may ultimately fail. Pillar failure can take place over a range of vertical compressive stresses. At high stresses failure occurs earlier than at low stresses. It has been suggested (1, 2, 3) that a criterion of failure based on a limiting vertical deformation would be more realistic than one based on stress, and the value of deformation at which the deformation rate starts to accelerate is chosen as the point between stability and instability. The time taken by a pillar to reach an unstable condition can be calculated from an experimental value of the maximum permissible vertical deformation and the rate of convergence measured in situ.

The rate of convergence is the best parameter for comparing the relative stability of the pillars at different mines or sections of mines. The higher the convergence rate the less time it takes for the pillars to reach instability.

This paper discusses the factors which have been found to affect convergence measurements. Convergence rates measured at five salt mines in England, Canada and the United States are presented. These measurements are analyzed and a relationship between convergence rate and calculated pillar stress is evaluated.

*Post Doctorate Research Fellow, Mining Research Laboratories, Fuels and Mining Practice Division, Mines Branch, Department of Energy, Mines and Resources, Elliot Lake, Ontario.

An example of the convergence profile across the centre panel at the Meadowbank Mine is shown in Figure 2 and the position of the stations in Figure 5. In this instance the area was mined previous to 1939 and the rate of convergence at each station is now approximatoly constant. The convergence is a maximum at the centre and decreases almost symmetrically towards the solid boundary.

Height of the Pillars

For a given stress acting on a pillar the greater the height the greater is the vertical deformation. As a first approximation it can be assumed that the deformation per unit height (strain) remains constant. Therefore if the height of the pillar is doubled the amount of vertical deformation is also doubled.

Geological Structure of the Salt

It has been observed (1, 4, 5) that the presence of impurities and the size of the salt crystals affects both the compressive strength and creep characteristics of salt. The presence of impurities, especially anhydrite, increases the compressive strength and decreases the rate of deformation at a constant stress. However, salt becomes more brittle with the presence of impurities and therefore exhibits less deformation before failure.

Salt specimens composed of large crystals have been found to deform at a faster rate than those composed of small crystals.

Temperature and Humidity

An increase in temperature increases the rate of convergence (6, 7). An example of the effect of temperature on convergence at an experimental site at the Lyons Salt Mine, Kansas, is shown in Figure 3. These measurements are part of an experiment, conducted by the Health Physics Division of the Oak Ridge National Laboratory, into the disposal of radioactive waste in salt mines. The rate of convergence increased rapidly when the temperature of the heaters was increased te over 100°C.

The effect of humidity on convergence is less well known. Salt is a hygroscopic material and absorbs moisture from the atmosphere. How far this moisture penetrates into the salt is unknown and it may he only a surface effect.

In summary, when the local sag of the roof and floor heave are not significant then the convergence rate in the rooms reflects the stress acting on the pillars. The magnitude of the convergence rate is affected by: time since mining, depth below surface; extraction ratio; position within the workings; pillar height; temperature and humidity; and geological factors. Of these probably the most important factors are depth below surface and extraction ratio, which determines the stress acting on a particular pillar, and the time which has elapsed since mining.

Analysis of Convergence Rates

The rates of convergence measured at Meadowbank Mine, Cheshire, England (1), Sifto Mine, Ontario, Canada (8), Ojibway Mine, Ontario, Canada (9), Lyons Mine, Kansas, United States (10, 11), Hutchinson Mine, Kansas, United States (10, 11), are given in Table 1 together with the percentage extraction, estimated pillar stress and age of the opening. The locations of the convergence stations at these mines are shown in Figures 5, 6, 7, 8 and 9. Also a brief description of each mine is given in the Appendix. All the mines are similar in that the salt beds are approximately horizontal and a room and pillar system of mining is employed.

When comparing the convergence measurements at these mines it is not possible to equate all the factors affecting convergence. The mines have been in operation for different periods of time and the convergence rates at some are constant, while at others they are still decreasing.

In obvious cases where the roof or floor have separated from the surrounding strata the results have been rejected and are not included in Table 1. Also, where possible measurements near the centre of an excavation or panel have been chosen, since these are the maximum values. However, at most mines only a limited number of measurements have been taken, in which case all the measurements are included. To take into account the varying working heights of the different mines, each convergence rate has been divided by its respective room height.

The stresses acting on the pillars were estimated from the weight of the overburden and the percentage extraction, using Equation 1. However, in irregular room and pillar workings, as in the centre panel at the Meadowbank Mine and in parts of the Lyons and Hutchinson mines, the percentage extractions were estimated. At high extraction ratios any small error produces relatively large errors in the evaluated pillar stress. The density of the overlying strata at the Meadowbank, Sifto and Ojibway mines was obtained from surface drill holes, while at the Lyons and Hutchinson mines it was assumed to be equivalent to 1 psi per ft depth.

The graph of convergence rate versus estimated pillar stress is shown in Figure 4. As expected there is a considerable amount of scatter of the results. However, the general trend indicates that as pillar stress increases the convergence rate also increases.

A number of different types of mathematical functions could be fitted to the data. The most common, laboratory determined, relation between vertical pillar strain rate (or convergence rate) and pillar stress is in the form of a power function.

TABLE 1

Comparison of Convergence Rates at Five Salt Mines

Mine	Station Number	Convergence Rate in/in/day x 10^{-6}	Type of Flow	Nominal Percentage Extraction	Estimated Pillar Stress psi	Age of Opening Years	Comments
	6	2.6	constant	85	3000		
	11	1.2	constant	85	3000		
	12	1.3	constant	85	3000		Depth
	17	1.7	constant	85	3000	30	
	28	2.7	constant	85	3000		450 ft.
	29	2.0	constant	85	3000		
Meadowbrook	33	2.3	constant	85	3000		Overburden
	C2	1.1	decreasing	75	1800		weight
Cheshire	C4	1.2	decreasing	75	1800		
	C7	1.2	decreasing	75	1800		1.00 psi/ft depth
	C8	1.4	decreasing	75	1800	3	
	C9	1.4	decreasing	75	1800		
	C10	1.3	decreasing	75	1800		
	23	0.6	decreasing	75	1800		
	24	0.5	decreasing	75	1800		
	25	0.7	decreasing	75	1800	8	
	26	0.6	decreasing	75	1800		
	N5C	5.2	decreasing	40	3400		Depth
	N5W	5.6	decreasing	40	3400	3	
Sifto	N5E	4.1	decreasing	40	3400		1760 ft.
	S4C	6.4	constant	35	3200		Overburden
Ontario	S4W	5.8	constant	35	3200	4	weight
	S4E	5.9	constant	35	3200		1.16 psi/ft depth
Ojibway, Ontario		0.3	decreasing	57	2300	7	Depth 960 ft. Overburden weight 1.04 psi/ft depth
	1	2.7	decreasing	60	2600		Depth
	7	2.9	decreasing	60	2600	70	1024 ft.
	10	2.9	decreasing	60	2600		
Lyons,	13	2.3	decreasing	60	2600	60	Overburden
	14	4.5	decreasing	58	2450		
Kansas	15	2.3	decreasing	58	2450		weight
	16	2.2	decreasing	59	2500		1.00 psi/ft depth
	20	1.8	decreasing	59	2500	30	assumed
	24	1.4	decreasing	59	2500		
	33	1.2	decreasing	59	2500		
	T1	1.5	decreasing	59	2500		
	5	0.3	decreasing	70	2150		Depth
	9	0.4	decreasing	70	2150	40	650 ft.
	10	0.2	decreasing	70	2150		
Hutchinson	6	5.7	decreasing	83	3600	16	
	7	3.4	decreasing	83	3600	11	Overburden
Kansas	2	2.4	decreasing	77	2600	7	weight
	3	3.5	decreasing	78	3000	10	1.00 psi/ft depth
	4	1.6	decreasing	74	2500	28	assumed
	1	3.2	decreasing	78	3000	2	

$$\dot{\epsilon} = A \sigma^{n} \qquad \ldots\ldots 3$$

where $\dot{\epsilon}$ = vertical strain rate or convergence rate

σ = stress

A and n = constants.

A regression line, which is the best statistically fitted equation assuming a power function, is drawn on the graph in Figure 4 and on either side of the regression line are drawn two arbitrary lines at ± 50 per cent. The values of the constants "A" and "n" for the regression line are

$$\dot{\epsilon} = 15 \times 10^{-8} \ \sigma \ 2.7 \qquad \ldots\ldots 4$$

where $\dot{\epsilon}$ = convergence rate in/in/day x 10^{-6}

σ = pillar stress

These values are very similar to those obtained by Obert (3) and Bradshaw, et al., for laboratory model pillars,

$$\dot{\epsilon} = 9 \times 10^{-8} \ \sigma^{\ 3.1} \ t^{0.6.} \qquad \ldots\ldots 5$$

when t = time since mining hrs.

A time factor was introduced into this equation to take into account a decreasing convergence rate.

In the following sections the convergence measurements at each mine are examined to determine whether the time, position and geological factors, if they were taken into account, would reduce the scatter of the results.

Meadowbank Mine

The measurements in the centre panel are mainly below the regression line as shown in Figure 4. The convergence rates are approximately constant and are unlikely to decrease substantially with time. However, the lower convergence rates are at stations situated near to the periphery of the panel, while those near the centre correspond very closely with the regression line. Convergence rates in the west panel are close to the regression line. Although the convergence rate is still decreasing, the difference from year to year is very small. Those measurements in the east panel are all above the regression line. However, the openings are only three years old and it is expected that the convergence rate will decrease with time and approach the same value as those measured in the west panel. The salt at this mine contains a number of impurities which would tend to depress the convergence rates.

Sifto Mine

All the convergence rates measured at this mine are above the regression line. Those measured at the N5 site are decreasing with time and will approach the regression line. But the convergence rates measured at S4 are constant and furthermore the site is on the periphery of the workings. Consequently, it would be expected that the convergence rates measured at this site would be less than those measured at N5. One possible explanation is that the mining height at S4 is 20 ft compared to 40 ft at N5 and any local sag of the roof will have double the effect on the convergence rate at S4 to that at N5. This anomaly will be clarified since site S4 is presently being re-mined to a height of 40 ft. Therefore it will be possible to compare the convergence rate for 20 ft and 40 ft heights at the same site. In addition, convergence stations have been installed to check the accuracy of the measurements at N5. The salt at this mine has a high purity which would tend to elevate the convergence rates.

Ojibway Mine

The one convergence measurement at this mine is considerably below the regression line, and the rate is still decreasing with time. There is no obvious reason why this is the case, even though it is situated 350 ft away from a relatively large shaft pillar. Also the salt bed is of a high purity which should tend to elevate the convergence rate. However, too much reliance should not be placed on one measurement and it would be preferable if it had been substantiated by other measurements.

Lyons Mine

Most of the convergence rates measured at this mine are reasonably close to the regression line. An exception is the rate measured at station 14, which is considerably higher, possibly because of local separation of the roof strata. The age of the opeoings at this mine is at least 30 years and the convergence rate is decreasing very slowly with time.

Hutchinson Mine

In general the convergence rates measured at this mine are evenly distributed about the regression line. The exceptions are those, measured at stations 5, 9 and 10 which are considerably lower. However, these stations are located very near to the shaft pillar, hence the results are not unexpected. Many of the measuring stations at this mine are located near the periphery of the workings. Consequently, the convergence rates at these sites would be expected to be lower than those near the centre.

It can be concluded from the qualitative deductions that in most cases, if the time, position and geological factors could have been standardized, then the scatter of the results would have been considerably reduced.

Conclusions

Convergence rates measured at five salt mines are in reasonable agreement with each other. As a first approximation the relation between convergence rate and pillar stress can be expressed by:

$$\dot{\epsilon} = 15 \times 10^{-8} \quad 2.7$$

where $\dot{\epsilon}$ = convergence rate in/in/day x 10^{-6}

σ = pillar stress psi

This equation gives an average quantity which covers a time period from 2 to 70 years and a variation of positions within an excavation or panel. If the time, position and geological factors could have quantitatively been taken into account, then the scatter of the results would have probably been substantially reduced.

One of the acceptable principles of room-and-pillar design is the direct comparison of conditions at similar mines. Room-and-pillar dimensions which have been found to be stable in one part of a mine, or in another mine with similar conditions, can be applied to a new area of extraction with slight modifications, depending on local conditions. The convergence rates measured at the five salt mines indicate that there is a general consistency between the results. The pillars at these mines are still standing, in some cases for over 70 years, and there has been no major pillar failure. Consequently mines which have low convergence rates could theoretically increase their extraction, and hence pillar stress, so that the convergence rates are comparable with other mines and still retain stable pillars. However it would be unwise to extrapolate and try to predict convergence rates for pillar stresses beyond the range of the measured results.

Appendix

Meadowbank Salt Mine, Imperial Chemical Industries, England

The Meadowbank mine is situated in Cheshire and is the only operating salt mine in the United Kingdom. The reddish brown salt deposit, situated in the Keuper Marl formation, extends over a large portion of Cheshire and consists of two main beds. The uppermost of these is not worked, mining being confined to the best quality salt found in the bottom 20 ft of the 80-ft-thick lower bed, some 470 ft below the surface. In the vicinity of the mine the salt beds are almost horizontal.

A plan of the mine and a geological section of the strata is shown in Figure 5. Mining commenced in the centre panel over 100 years ago, leaving irregular shaped pillars at irregular intervals and taking between 80 and 90 per cent extraction. The more recent west, north-west and east panels were mined on a regular room-and-pillar basis taking 75 per cent extraction. A barrier pillar approximately 400 ft wide was left between the centre and other panels.

Convergence measurements were initiated by the mine during the early 1940's. These and other types of measurements were expanded during the late 1950's when a research project was started with the Mining Department at Newcastle-upon-Tyne University.

Sifto Salt Mine, Domtar Chemicals Limited, Canada

The Sifto mine is located at Goderich, Ontario on the north-eastern rim of the Michigan Basin. The salt deposit which forms part of the Salina formation, extends over a large area of south-western Ontario and to the western border of Michigan State. Although several salt beds are present at Goderich, mining operations are confined to one of the lower beds of high quality salt at a depth of 1,760 ft. The bed in the vicinity of the mine is horizontal and is 80 ft thick, of which the bottom 42 ft is mined. The salt is almost pure white with small lateral dark bands of dolomite and anhydrite running through it at 3 to 8-in. intervals.

A plan of the mine and a geological section of the strata is shown in Figure 6. Mining commenced in 1960 on a regular room-and-pillar basis mining rooms 60 ft wide, 42 ft high and leaving pillars 210 ft square, giving an extraction rate of approximately 40 per cent. Convergence measurements were initiated during 1962-63 by the Department of Mines and Technical Surveys, Ottawa in co-operation with the mine. These types of measurements were expanded during 1966.

Ojibway Salt Mine, Canadian Rock Salt Company, Canada

The Ojibway mine is located near Windsor, Ontario, on the eastern rim of the Michigan Basin. The salt deposit is in the same formation as that at Goderich, but at Ojibway one of the upper salt beds, at a depth of 950 ft is mined. This bed is 27 ft thick of which 18 te 21 ft is mined leaving 6 ft of salt in the roof. The bed is horizontal and the appearance of the salt is similar to that at Goderich.

A partial plan of the mine and a geological section of the strata is shown in Figure 7. Mining commenced in 1955 on a regular room-and-pillar basis. At present pillars 60 ft x 70 ft are left and rooms 50 ft wide and cross-cuts 30 ft wide are mined. The overall percentage extraction in the panels is approximately 57 per cent. The mine installed one convergence station near to the shaft pillar during 1958.

Lyons Mine, The Carey Salt Company, Kansas, United States

The Lyons mine is located near the city of Lyons, Kansas. The salt beds which are part of the Wellington formation underlie central Kansas. At the Lyons mine there is 300 ft of nearly horizontal beds of salt, shale and anhydrite overlain by shales and occasional limestones. Mining is carried out at a depth of 1,024 ft in one of the lower beds in the Wellington formation, taking a working height of 12 ft and occasionally 17 ft. The salt occurs in relatively pure layers one to six in. thick, separated by small clay and shale laminae. Above and below the workings are shale beds several inches in thickness.

A plan of part of the mine showing the locations of the convergence stations is shown in Figure 8. Mining commenced in the 1890's taking 60 to 70 per cent extraction in the older parts of the mine and about 60 per cent in the more recent workings. Production mining ceased in 1948 although the mine is still being used as an experimental site for the disposal of radioactive waste. Convergence measurements were started by the Oak Ridge National Laboratory after 1959.

Hutchinson Mine, The Carey Salt Company, Kansas, United States

The Hutchinson mine is located approximately 30 miles to the southeast of the Lyons mine. The same salt formation is being mined as at Lyons, but the depth below surface is 650 ft.

A plan of the mine indicating the locations of the convergence stations is shown in Figure 9. Mining commenced in the 1920's leaving long narrow pillars in a number of panels and taking about 70 per cent extraction. More recent panels were mined leaving square pillars and taking either 75 per cent or 80 per cent extraction. The working height varies from 6 ft in some panels to 10 ft or 12 ft in other panels. Convergence measurements were commenced during 1959 by Serata and the Oak Ridge National Laboratory.

References

(1) Hedley, D.G.F.
1965: Deformation and failure characteristics of rock salt and potash. Ph. D. Thesis, Univ. of Newcastle-upon-Tyne, February.

(2) Potts, E.L.J.
1964: An investigation into the design of room and pillar workings in rock salt. Trans. Inst. Min. Engrs., v. 124, no. 49, October.

(3) Obert, L.
1964: Deformation behaviour of model pillars made from salt, trona and potash ore. 6th Sym. Rock Mech., Univ. of Missouri, Rolla.

(4) Sen, G.C.
1961: An investigation into the stability of room and pillar workings in rock salt. Ph. D. Thesis, Univ. of Durham, May.

(5) Reynolds, T.D. and Gloyna, E.F.
1961: Creep measurements in salt mines. 4th Sym. Rock Mech., Penn. State Univ., March.

(6) McClain, W.C.
1966: The effect of nonelastic behaviour of rocks. 8th Sym. Rock Mech., Univ. of Minnesota, Minneapolis, September.

(7) Bradshaw, R.L., Lomenick, T.F., McClain, W.C. and Empson, F.M.
1966: Model and underground studies of the influence of stress, temperature and radiation on flow and stability in rock salt mines. 1st Cong. Int. Soc. Rock Mech., Lisbon, September

(8) Muir, W.G. and Cochrane, T.S.
1966: Rock mechanics investigations in a Canadian salt mine. 1st Cong. Int. Soc. Rock Mech., Lisbon, September.

(9) Rice, W.M.
Private communication.

(10) Bradshaw, R.L., Boegly, W.J., and Empson, F.M.
1964: Correlation of convergence measurements in salt mines with laboratory creep test data. 6th Sym. Rock Mech., Univ. of Missouri, Rolla.

(11) McClain, W.C.
Private communication.

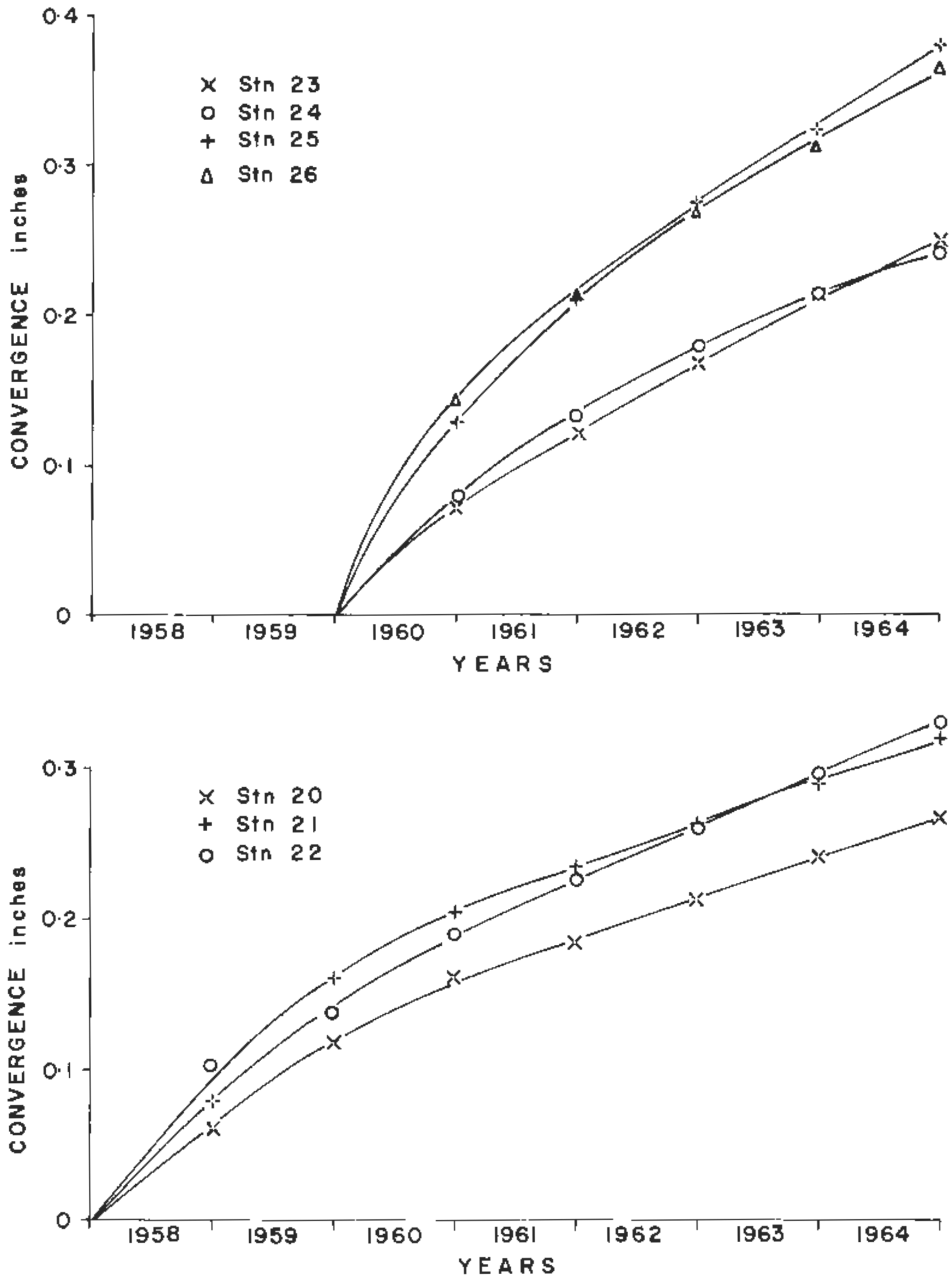

Figure 1. Convergence in west panel, Meadowbank Mine, Cheshire.

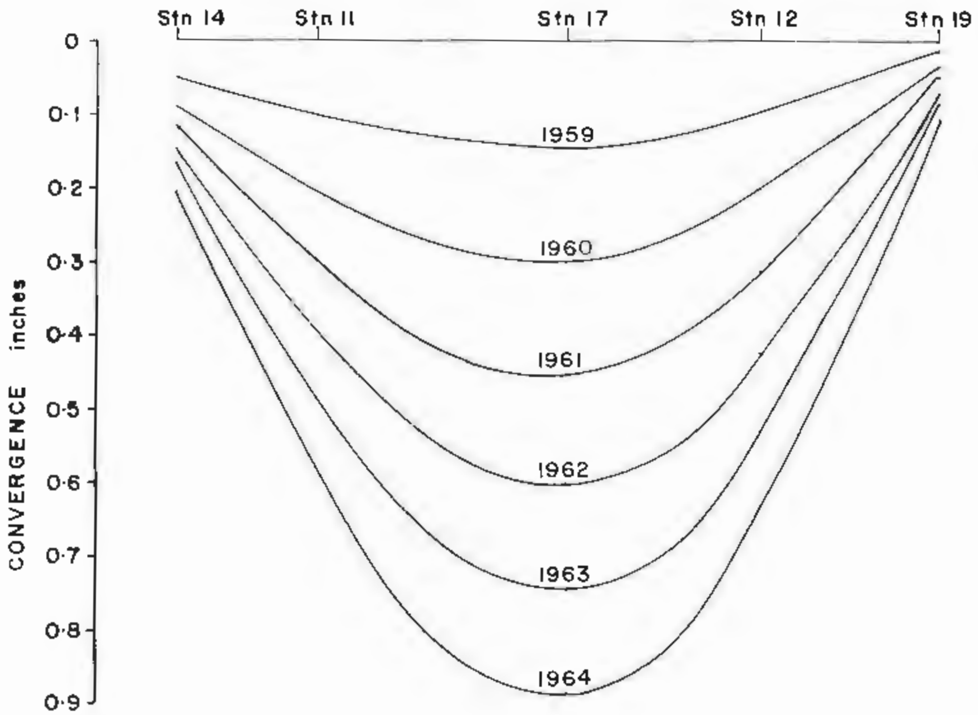

Figure 2. Convergence profile across centre panel, Meadowbank Mine, Cheshire.

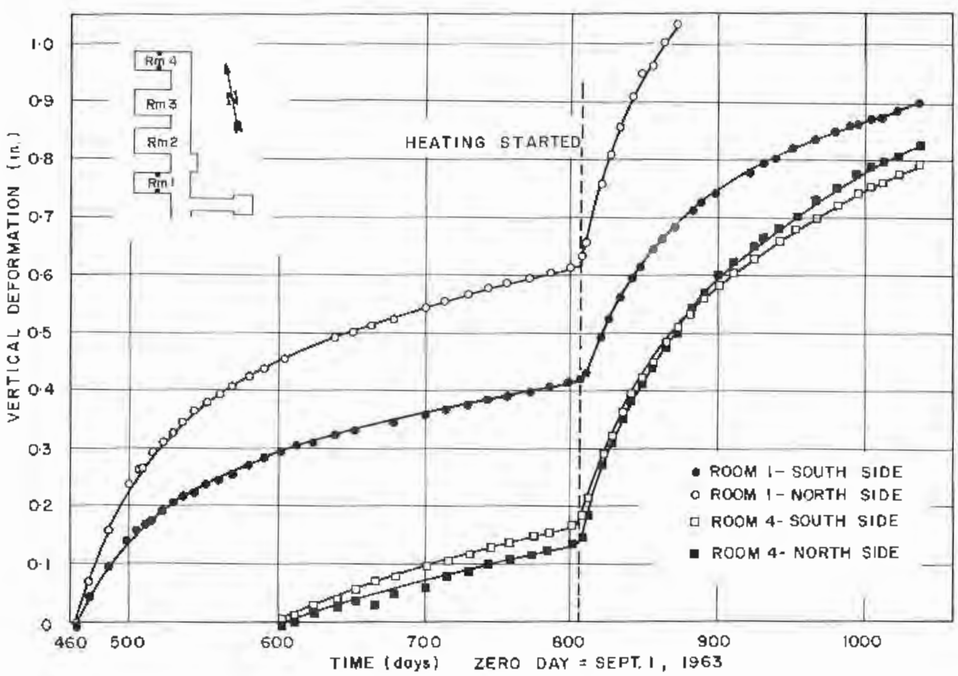

Figure 3. Effect of temperature on convergence (after McClain).

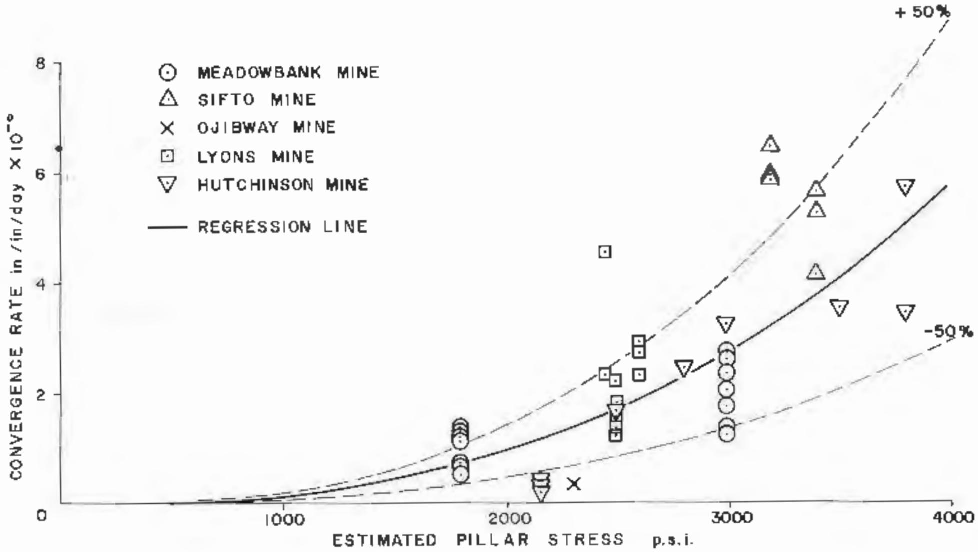

Figure 4. Relations between convergence rate and pillar stress.

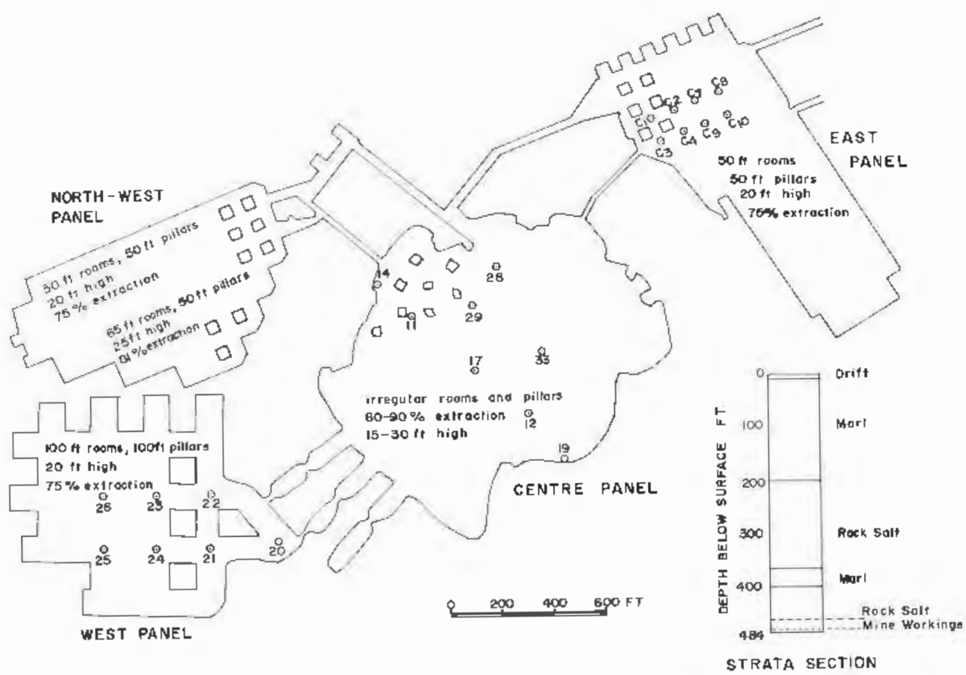

Figure 5. Plan of Meadowbank Mine, Cheshire, showing position of convergence stations.

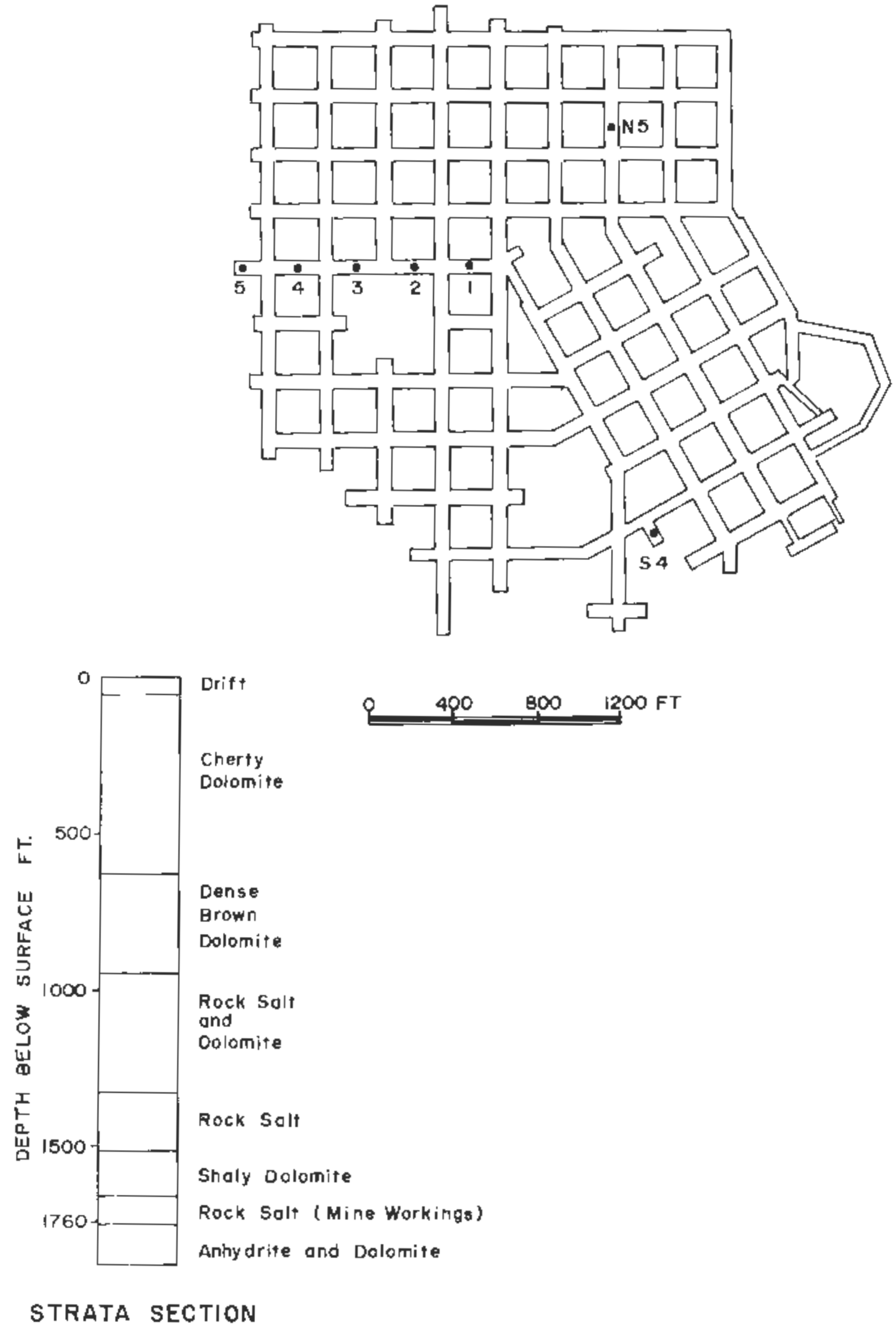

Figure 6. Plan of Sifto Salt Mine showing position of convergence stations.

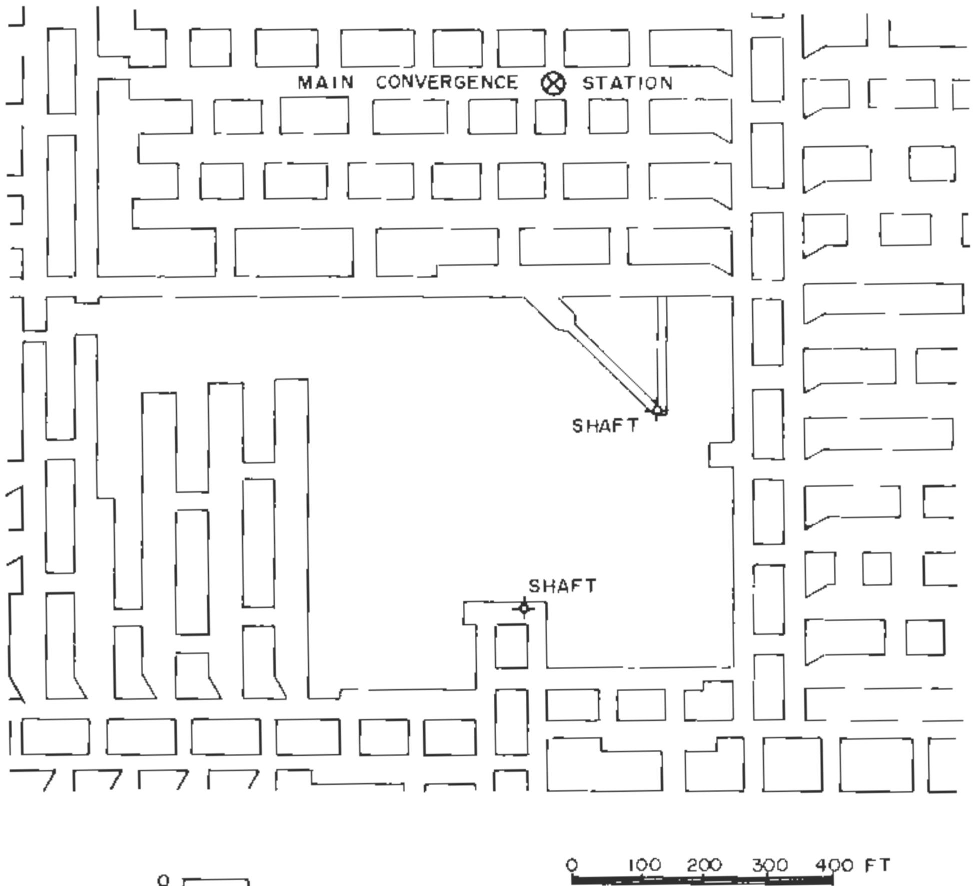

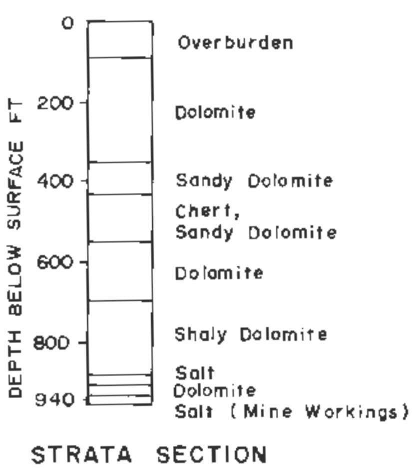

Figure 7. Partial plan of Ojibway Mine, Ontario, showing position of convergence stations.

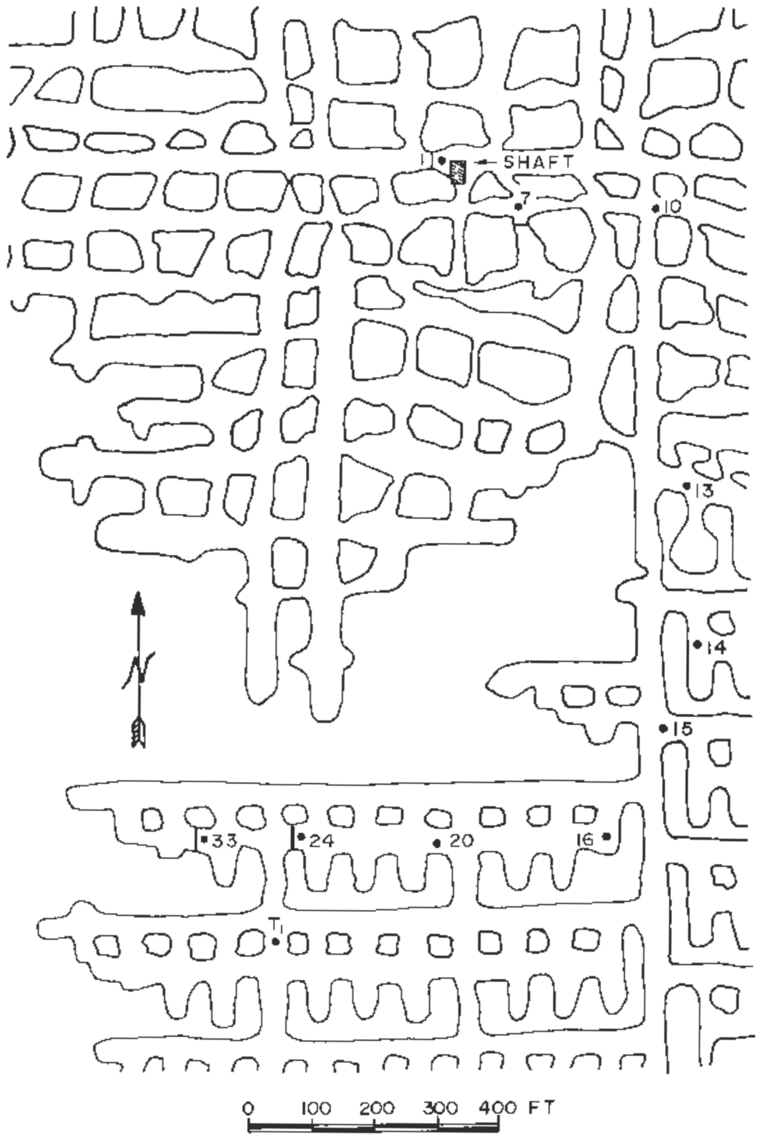

Figure 8. Partial plan of Lyons Mine, Kansas, showing locations of convergence measuring stations. (After Bradshaw et al.).

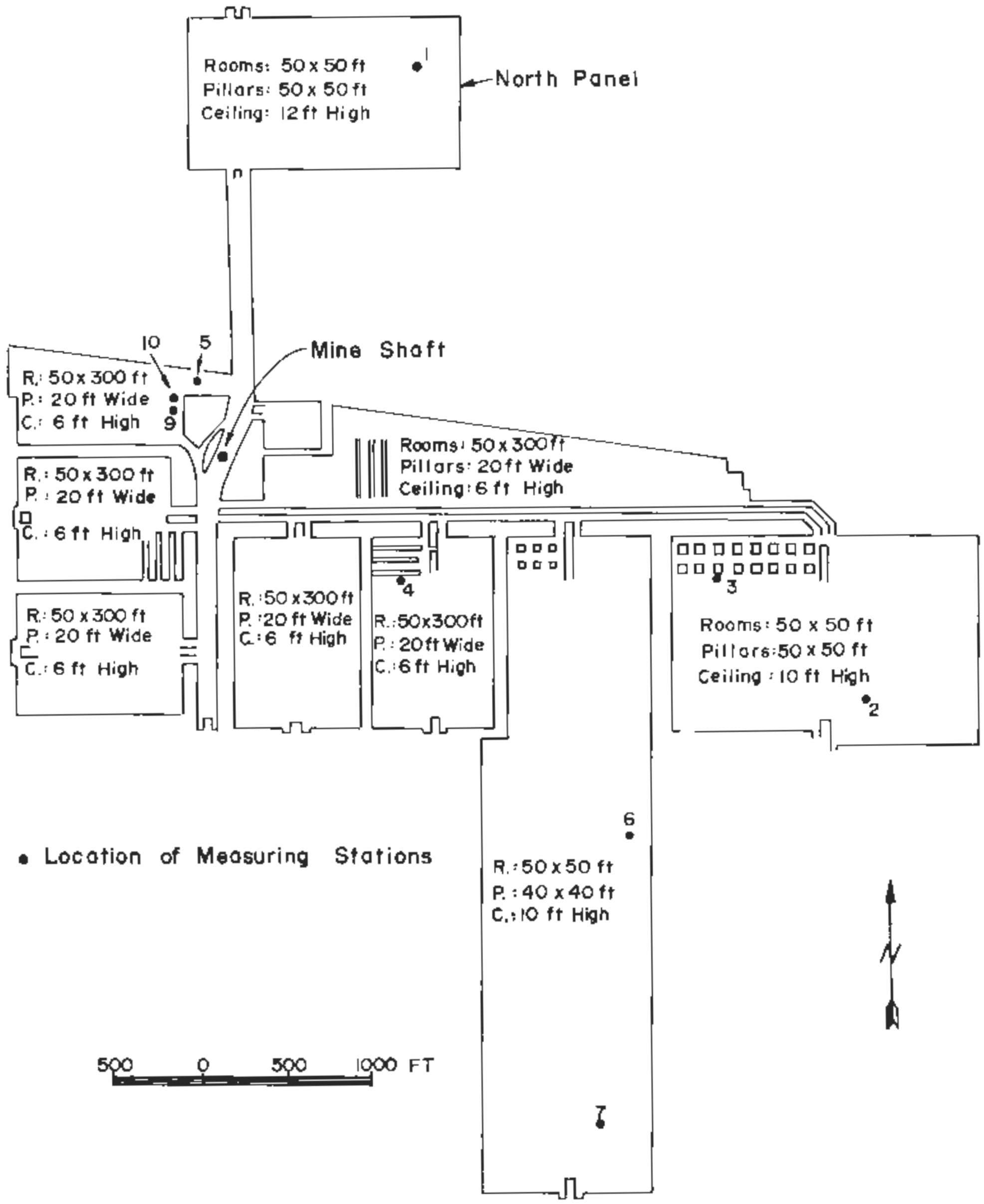

Figure 9. Plan of Hutchinson Mine, Kansas, showing location of convergence measuring stations. (After Bradshaw et al.).

IN SITU STRESSES ALONG THE APPALACHIAN PIEDMONT

V.E. Hooker and C.F. Johnson**

Abstract

The U.S. Bureau of Mines has used the borehole deformation overcoring technique for measuring stresses in rock outcrops and dimension stone quarries along the Appalachian Piedmont from Northern Vermont to Central Georgia. The data show that secondary principal stresses in a horizontal plane near the surface are compressive and are 500 to 4,000 psi. Stresses were measured in granites, gneisses, diabases, and dolomite.

Introduction

The existence of high horizontal stresses in massive rock formations near the earth's surface has been suspected and/or hypothesized by geologists and geophysicists for more than a century. According to Bucher (2) tangential compression dominates the whole record of earth deformation and throughout recorded geologic history the earth's crust has been under tangential compression.

A review of geologic literature concerned with the Appalachian Piedmont shows that many phenomena have been observed that could only be accounted for by the existence of high horizontal stresses. For example, Dale (6) observed visually the deformation of drill holes and the closing of channels in dimension stone quarries and from this information deduced that compressive

*Research geophysicist, Denver Mining Research Center, Bureau of Mines, U.S. Department of the Interior, Denver, Colorado.

stress in New England ranged from an east-west to a north-south direction. White (20) reported expansion cracks and rock bursts in the granite quarries at Barre, Vermont. Lowry (10) reported the formation of expansion domes and shear cones in the granite at Mt. Airy, North Carolina. Niles (14) observed spontaneous fracturing of rock in a granite quarry near Monson, Massachusetts. Some of this fracturing occurred with explosive force, causing dust and debris to be thrown into the air. In one instance he reports that by using several hundred wedges a bed of rock 354 ft long, 11 ft wide, and 3 ft in thickness was freed from the rock mass except that it still remained firmly attached at one end. Although no movement was perceptible, the corresponding halves of drill holes revealed that 1-1/2 in. of expansion had taken place over the total length of 354 ft. E. C. Robertson of the U. S. Geological Survey has attempted to use strain gauges to measure the changes in strain that occurred in a granite in Massachusetts while the rock was being mined by wire sawing in place. The attempts were not too successful.

The recent development of the borehole gauge has made possible the evaluation of underground and near-surface stresses. Underground measurements have shown that abnormally high horizontal compressive stresses exist in a limestone in Ohio (16), in Precambrian Proterozoic rocks and diabase dykes at Elliot Lake, Ontario (4, 5), and in other Precambrian rocks (15) in Ontario, Canada. Since the overcoring technique can readily be applied for near-surface measurements, the Bureau of Mines has begun an investigation into the nature and extent of near-surface horizontal stress fields.

Stress relief measurements were obtained in vertical boreholes located in dimension stone quarries or rock outcrops of granite, gneiss, diabase, and dolomite. Drill holes ranged from 1-1/2 to 8 ft in depth. Some of the holes were located on the surface of the rock mass and others in the bottom of dimension stone quarries which had been mined to a depth of 300 ft.

Test Sites

The test sites consisted of three outcrops, 13 dimension stone quarries, and one shallow underground site. Test site areas are shown in Figure 1. Rock outcrops which are badly weathered and fractured are difficult to evaluate as to the probability of obtaining stresses or reliable information. The three outcrops selected for stress relief measurements showed some effects of weathering. Although macrofractures can be seen in the overcores, the specimens remained intact during the in situ overcoring and laboratory testing. Two separate test holes were drilled approximately 200 ft apart in the same dolomite outcrop near Proctor, Vermont.

A dome-shaped rock mass as reflected by the topography with horizontal sheeting in which the sheets thicken downward has long been recognized as a phenomenon associated with high compressive strains (6, 20). This type of sheeting was usually strongly developed in most of the granite and gneissic rock masses. The thickness of sheets showed considerable variation, ranging from several inches at the surface to several feet or more at depth. Sheeting in the granite at the Oak Hill quarry in Massachusetts is shown in Figure 2.

Dimension stone quarries are usually located in this type of structure and provided test sites free of weathered and broken rock. Where possible, more than one site was selected in an area to provide relative information regarding the effect of depth on the horizontal stress field. Figure 3 is a typical view of a deep quarry near Barre, Vermont. Stress relief measurements were also made in one underground site near Tewksbury, Massachusetts. Excessive core breakage was encountered over the first few feet of this hole owing to the angle of foliation in the gneiss.

Stress relief sites at Mt. Airy, North Carolina, were spaced over about one-third of a mile. Some of the measurements were made pertaining to an enclosed fragment of pre-existing rock (a xenolith) which was exposed on the surface of the quarry floor. The xenolith, which was approximately 5 ft diameter and 1-1/2-ft-thick, is shown in Figure 4.

The initial measurements at the Rapidan, Virginia, test site were made in October 1965. The quarry was relatively new, having just been started. On May 29, 1966, an earthquake of Richter magnitude 4.5 was recorded with the epicenter located just 50 miles south-east of this site. To enhance our knowledge of the nature of these near-surface stresses, a second set of stress relief measurements was made in August 1966. The two sets of measurements were made in holes located 3 ft apart in the quarry where the existing stress field was probably not influenced by mining during the time between measurements. A vertical view of these hole locations is shown in Figure 5.

Test holes in quarries were located to minimize effects of stress concentrations. Surface holes near the quarries were located at least one diameter of the mined opening away from the quarry. Holes in quarry floors were located away from corners and other probable stress-concentrated areas. All of the boreholes were located on a relatively large free surface so that any vertical component of stress should be near zero. The calculated stresses are thus representative of those existing in the horizontal plane of measurement.

Instrumentation and Experimental Procedure

Measurements were made at each test site using the overcoring stress relief technique. The changes in borehole diameter were measured with Bureau of Mines single-component and three-component deformation gauges (18). Either gauge fits into a 1-1/2-in. gauge hole and offers negligible resistance to borehole deformations. The gauge sensitivities range from 5 to 10 microinches. The drill used for most of the tests is shown at a typical outcrop setup in Figure 6. The drill is skid-mounted and could be detached from the truck and lowered by boom to the floor of dimension stone quarries which were not accessible by road.

The overcoring procedure for obtaining the borehole deformations was essentially the same as that described in detail by others (4, 8, 12, 13). Only minor adjustments in this procedure were made when applying it to near-surface measurements. Since the borehole gauge was normally lying in the sun or on a hot rock surface, care had to be taken to allow ample time for temperature equilibrium to be reached as indicated by zero drift on the strain gauge indicator. In some instances it was necessary to continue drilling until the overcoring was 2-1/2 to 3 in. beyond the point where the piston of the gauge was in contact with the rock before complete relief was accomplished. Although the three separate measurements with a single-component gauge were made over a distance of 12 to 18 in., they were considered to be in the same plane for calculation purposes. The overcored rock in each hole was broken loose and returned to the laboratory for testing.

The modulus of elasticity was determined in the laboratory from the overcored rock samples taken from each test site. Samples were prepared for testing in a triaxial device described in detail by Obert (17). A borehole gauge was inserted into the test specimen and oriented to the corresponding direction in which the in situ deformation was measured. The overcore was then subjected to a lateral pressure on the outer boundary, causing a greater borehole deformation than the in situ recorded value. After three cycles, the stress-deformation data were recorded. This procedure was repeated for each of the orientations from which in situ borehole deformations were obtained.

The resulting stress-deformation curves were mostly nonlinear and showed hysteresis. For the specific triaxial cell used, the minimum axial load that could safely be used with radial loads corresponded to an axial stress, σ_2, of 1,000 psi. A typical curve is shown in Figure 7. Since overcoring completely relieves the rock from a stressed condition, the secant moduli are believed to be the most representative of this effect. Secant moduli were calculated from the equation (17)

$$E = -\frac{4ab^2p_o}{(b^2 - a^2)\,U} \qquad \ldots\ldots 1$$

where E = modulus of elasticity, psi,

a = radius of hole in specimen, inches,

b = outer radius of specimen, inches,

U = in situ borehole deformation,

and p_o = latsral pressure from the unloading curve at the in situ deformation value.

An arithmetic average secant modulus was calculated from the three moduli obtained from each rock type.

The secondary* principal stresses, P and Q in the horizontal plane, were calculated using the plane stress equations for an isotropic, homogeneous medium for a 60° rosette and average secant modulus (11):

$$P+Q = \frac{E}{3d}(U_1 + U_2 + U_3), \qquad \ldots\ldots 2$$

$$P-Q = \frac{E\sqrt{2}}{6d}\left[(U_1 - U_2)^2 + (U_2 - U_3)^2 + (U_1 - U_3)^2\right]^{1/2}, \qquad \ldots\ldots 3$$

and $$\tan 2\Phi = \frac{\sqrt{3}\,(U_2 - U_3)}{2U_1 - U_2 - U_3}, \qquad \ldots\ldots 4$$

where d = diameter of the borehole

Φ = the angle from U_1 to P measured counterclockwise as positive, and U_1, U_2, U_3 = deformation of borehole across diameters 60° apart.

Summary of Stress Data

Data from the present investigation are given in Table 1. The stress magnitudes and directions vary considerably along the Appalachian Piedmont; however, horizontal stresses were found to exist in all rock types tested. Measurements at Barre, Vermont, West Chelmsford, Massachusetts, and Tewksbury, Massachusetts, indicate that increase in horizontal stresses with depth is much greater than expected from overburden pressure and any stress concentration because of the quarry configuration. This increase in stress with depth agrees with the data given at the end of the table which were previously obtained in rock masses in Georgia. The largest stresses were obtained in the Fletcher quarry floor which was approximately 250 ft below the original surface of the rock mass.

The maximum stresses at the Mt. Airy, North Carolina, site range from about 1,650 to 4,000 psi, compressive, over the total quarry surface area measured. Yet the direction of P seems fairly consistent for all of the measurements. The calculated stresses in the xenolith are not significantly different in either magnitude or direction from those existing in the enclosing granite.

Data obtained at Rapidan, Virginia, 10 months apart indicate that changes in stress conditions took place during this period. The ratio P/Q changed significantly. The average ground stress (P+Q)/2, also increased 59 per cent. Comparison of the data from this test site, which were obtained by both single- and three-component borehole deformation gauges, shows that in competent rock such as this the measurements with either gauge are equally reliable. The most recent measurements, from 2 ft to nearly 5 ft, indicate a

*The term "secondary" is used since τ_{zx} and τ_{zy} are not necessarily equal to zero.

slight decrease in the horizontal stress field with depth. This suggests the possibility that rock temperature may be influencing these relative measurements, thus overcompensating for an increase in magnitude expected with depth.

Effect of Temperature

Rock temperature data have been given by Forbes (7) in which seasonal variations were recorded in a traprock near Edinburgh, Scotland, at depths of 3, 6, 12, and 24 ft along with the corresponding air temperatures measured 6 in. above the surface. Temperature variations at 48 ft are usually not detectable. To evaluate the effect of temperature variation with time and depth of measurement, the graph shown in Figure 8 was plotted from the original rock temperature data. The four curves shown represent the maximum (70° F), minimum (30° F), fall (55° F), and spring (55° F) air temperatures. The maximum and minimum curves show that at a depth of 1 ft a 19° variation in rock temperature can occur.

According to the U.S. Weather Bureau the average mean temperature in Richmond, Virginia, was 56° F in October 1965 and 78° F in August 1966. Both of these dates are in the post-heating cycle time of year. Through the use of additional data (3, 7), representative rock temperature values were obtained for these corresponding air temperatures. These data are shown plotted in Figure 8 and indicate a 4° F rock temperature variation at 1 ft.

The change in rock stress due to a change in rock temperature can be calculated from Equation 5.

$$\sigma_h = -\frac{\alpha E(T_1 - T_\circ)}{1-\upsilon}, \qquad \ldots\ldots 5$$

where σ_h = horizontal stress because of temperature change,

α = thermal coefficient of expansien for rock,

$T_1 T_\circ$ = temperature change, degrees F,

and υ = Poisson's ratio.

Using the thermal coefficient of expansion for diabase (1) and a modulus of elasticity of 8.74×10^6 psi, the calculated increase in stress because of temperature variation should be about 260 psi for the measurements obtained in August 1966 as compared with those obtained in October 1965. Further calculations show that changes in rock stress could be more than 1,000 psi for a maximum rock temperature change of 19° F near the surface.

Calculated stresses and directions from data which were obtained in holes using only the single-component gauge are valid since these measurements were made where the local near-surface rock temperature gradient was near zero. Comparative deformation data were obtained with the three-component gauge in several holes which were drilled when local temperature variations would have influenced the near-surface stress gradient.

Conclusions

The calculated stresses given in the report are compressive and range from 500 to 4,000 psi. Compressive stresses were found to exist in sedimentary, metamorphic, and granite rocks of Paleozoic and Triassic Age. No measurement of tensile horizontal stress was obtained during this series of tests. These data, along with those of others, are compatible with theories of tangential compression in the earth's crust for the areas described in this report. On the basis of these data, compressive stresses may be expected to be found in any competent rock in which the stresses can be contained.

If a condition of stress equilibrium is assumed for an isotropic, homogeneous mantle under tangential compression, the horizontal compressive stresses would be expected to be nearly equal in all directions. The data show that most of the stresses determined along the Appalachian Piedmont are of an unequal biaxial nature. In addition, for a given area, significant variations in stress directions were found. These facts may indicate that the magnitudes and directions of horizontal stresses are subject to local variations because of structural or anisotropic anomalies.

Seasonal and diurnal rock temperature variations can be significant, and in the future all near-surface stress relief measurements must take into account the changes in stress magnitudes because of these variations.

At the Rapidan, Virginia, site, however, the effect of temperature does not account for the total increase in stress magnitude or for the change in the state of stress from an unequal biaxial stress field to a nearly equal biaxial stress field. It cannot be determined from these data whether the earthquake was a contributing factor to these changes.

References

(1) Birch, Francis, Schairer, J. F., and Spicer, H. Cecil
1942: Handbook of physical constants. G.S.A. special paper 36, January 31.

(2) Bucher, W.H.
1951: Fundamental Properties of Orogenic Belts. Trans. A.G.U., v. 32, no. 4, August, p. 514.

(3) Carslaw, H.S., and Jaeger, J.C.
1959: Conduction of Heat in Solids. Oxford Univ. Press, Amen House, London, 2nd ed.

(4) Coates, D.F., and Grant, F.
1966: Stress Measurements at Elliot Lake. Canadian Min. and Met. Bull., v. 59, no. 649, May, pp 603-613.

(5) Corlett, A.V.
1966: Letter to author. Denver Mining Research Center. September 27.

(6) Dale, T. Nelson.
1923: The commercial granites of New England. U.S. Geol. Survey Bull. 738.

(7) Forbes, James D.
1849: Account of Some Experiments on the Temperature of the Earth at Different Depths. Trans. Roy. Soc. Edinburgh, v. XVI, pp. 189-236.

(8) Hast, Nils.
1958: The Measurement of Rock Pressure in Mines. Sveriges Geologiska Undersokning Arsbok 52, Series C, no. 3, P.A. Norstedt and Sonner, Stockholm, Sweden, pp. 12-16.

(9) Hooker, Verne E., and Duvall, W.I.
1966: Stresses in rock outcrops near Atlanta, Ga. BuMines Rept. of Inv. 6860, 18 pp.

(10) Lowry, W.D.
1959: Expansion Domes and Shear Cones in Mt. Airy Granite. VPI Mineral Ind. J., v. VI, no. 4, pp. 1-6.

(11) Merrill, R.H., and Peterson, Jon R.
1961: Deformation of a borehole in rock. BuMines Rept. of Inv. 5881, 32 pp.

(12) Merrill, R.H., and Hooker, V.E.
1960: Static stress determinations and crushed zone measurements site Hobo. BuMines, College Park, Md., Rept. APRL-E 38-7.1, 15 pp.

(13) Merrill, R.H.
1960: Static stress determinations in salt. Project COWBOY, Final report APRL 38.3.1, July 29, 13 pp. (BuMines, College Park, Md.)

(14) Niles, W.H.
1871: Some Interesting Phenomena Observed in Quarrying. Proc. Boston Soc. of Nat. Hist., v. XIV, pp. 80-87.

(15) Nyland, E., and Blanchard, J. E.
1965: A Determination of Tectonic Stress in the Canadian Shield. Trans. A. G. U., v. 46, no. 1, March.

(16) Obert, Leonard.
1962: In situ determination of stress in rock. Mining Eng., August.

(17) ________
1964: Triaxial method of determining the elastic constants of stress relief cores. BuMines Rept. of Inv. 6490, 22 pp.

(18) Obert, Leonard, Merrill, R. H., and Morgan, T. A.
1962: Borehole deformation gage for determining the stress in mine rock. BuMines Rept. of Inv. 5978, 11 pp.

(19) Timeshenko, S. and Goodier, J. M.
1951: Theory of Elasticity. McGraw-Hill Book Co., Inc., New York, 2nd ed.

(20) White, Walter S.
1946: Rock bursts in the granite quarries at Barre, Vt. U.S. Geol. Survey Circ. 13.

TABLE 1

Calculated secondary principal stresses

Location and Quarry or deposit	Rock type	Depth to collar of hole, feet	Depth of gage, feet	Modulus of elasticity, 10^6 psi	P, psi	Q, psi	Direction of P
Barre, Vt.:							
E. L. Smith	Granite	0	0.5 to 1.5	2.84	298	82	N37°E
		300	0.8 to 2.0	4.63	2,453	1,286	N13°W
Proctor, Vt.:							
Outcrop	Dolomite	0	0.5 to 1.8	6.41	1,427	470	N5°E
		0	0.5 to 1.8	6.66	1,132	517	N24°W
West Chelmsford, Mass.:							
H. E. Fletcher	Granite	250	0.5 to 1.5	4.93	4,234	2,312	N50°E
Guilmette	Granite	30	0.5 to 1.8	4.86	1,491	453	N41°E
LaMasurier	Granite	0	1/ 6.0	4.90	448	279	N31°W
R. Morris	Granite	4	3.0	4.90	1,213	528	N37°E
			3.5	4.90	1,303	538	N39°E
V. Morris	Granite	50	2.0	4.90	1,534	1,278	N61°W
			2.5 to 3.7	4.90	1,451	1,151	N71°W
			4.2	4.90	2,300	1,483	N84°W
Oak Hill	Gneiss	70	2.0	4.90	2,897	1,907	N60°E
			2.5 to 3.7	4.90	2,942	1,552	N64°E
			4.2	4.90	3,016	1,993	N55°E
Tewksbury, Mass.:							
Outcrop	Paragneiss	0	4.0 to 5.0	5.30	347	134	N4°W
Underground	Paragneiss	40	4.7	5.30	770	665	N12°E
			5.6	5.30	684	419	N31°W
			6.9	5.30	564	496	N13°W
			7.5	5.30	770	407	N to S
			8.0	5.30	1,110	577	N17°W
Nyack, N.Y.:							
Outcrop	Diabase	0	0.5 to 1.5	2.84	173	68	N2°E
St. Peters, Pa.:							
Fr. Cr. Granite Co.	Diabase	0	4.3	8.74	565	205	N7°E
			4.8	8.74	522	210	N12°E
Rapidan, Va.:							
Buena black	Diabase	2/ 6	0.5 to 1.7	8.76	1,124	789	N5°W
		2/ 6	0.5 to 1.5	8.71	965	524	N9°E
		3/ 6	2.0	8.74	1,660	1,510	N17°W
			2.5	8.74	1,621	1,444	N10°E
			3.5 to 4.3	8.74	1,550	1,495	N63°E
			4.9	8.74	1,503	1,424	N11°E
Mt. Airy, N.C.:							
N.C. Granite Co.	Granite	50	1.0 to 3.0	5.08	3,977	976	N87°E
	In xenolith	30	0.5 to 1.5	3.52	1,885	1,000	S76°E
	Below xenolith		1.7 to 2.5	3.48	2,174	1,139	S84°E
	Beside xenolith	30	0.5 to 1.5	3.67	1,667	918	S84°E
		30	0.5 to 1.5	4.62	2,705	1,835	S84°E
		30	0.5 to 1.5	4.39	1,840	1,744	N71°E
Stone Mountain, Ga. (9):							
Stone Mtn. Granite Co.	Granite	10	0.5 to 1.5	2.65	1,525	1,080	N10°E
Lithonia, Ga. (9):							
Consolidated	Gneiss	0	0.5 to 4.2	3.32	1,373	792	N50°E
		0	23.0 to 28.5	3.32	2,211	1,173	N55°E
Douglasville, Ga. (9):							
Consolidated	Gneiss	0	0.5 to 1.5	3.26	500	235	N55°W

1/ Indicates a 3-component gage reading, all elements at the same depth.
2/ Measurements made on October 21, 1965.
3/ Measurements made on August 9, 1966.

Note: P and Q are compressive stresses.

Figure 1. Test site areas.

Figure 2. Sheet structure at Oak Hill Quarry, West Chelmsford, Massachusetts.

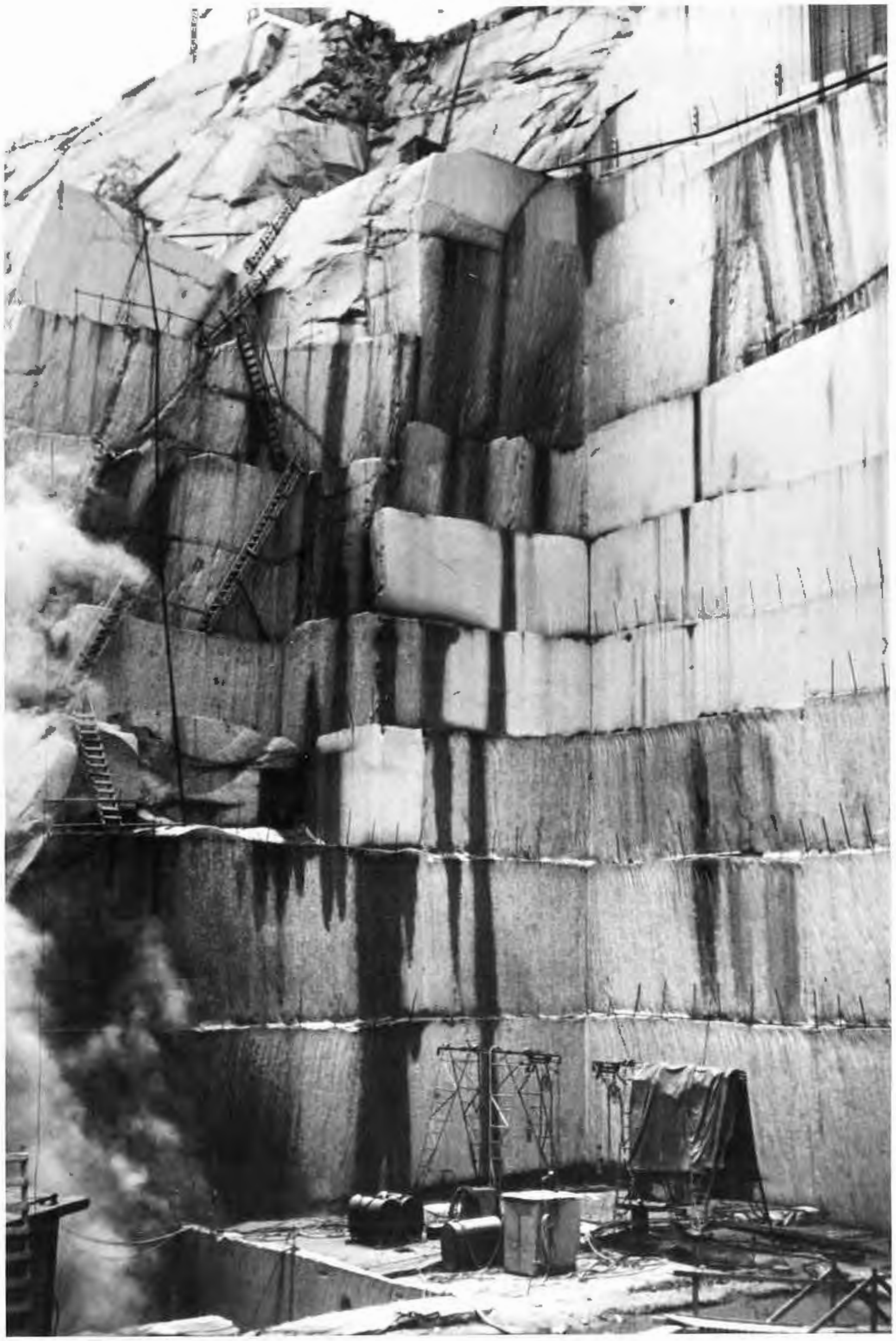

Figure 3. Deep quarry near Barre, Vermont.

Figure 4. Xenolith at Mt. Airy, North Carolina.

Figure 5. Showing hole locations 3 ft apart at Rapidan, Virginia.

Figure 6. Typical setup on rock outcrop.

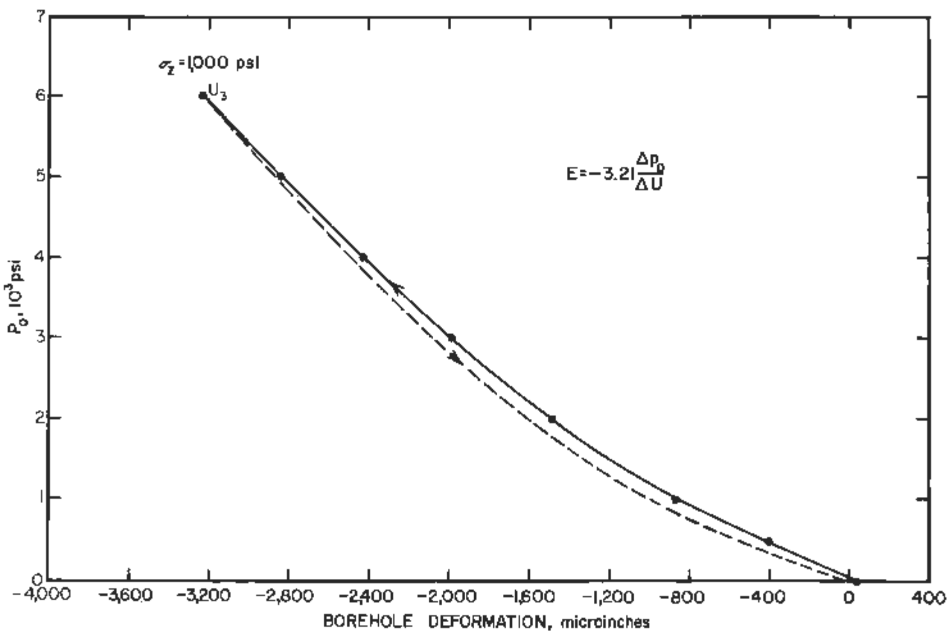

Figure 7. Typical stress versus deformation curve.

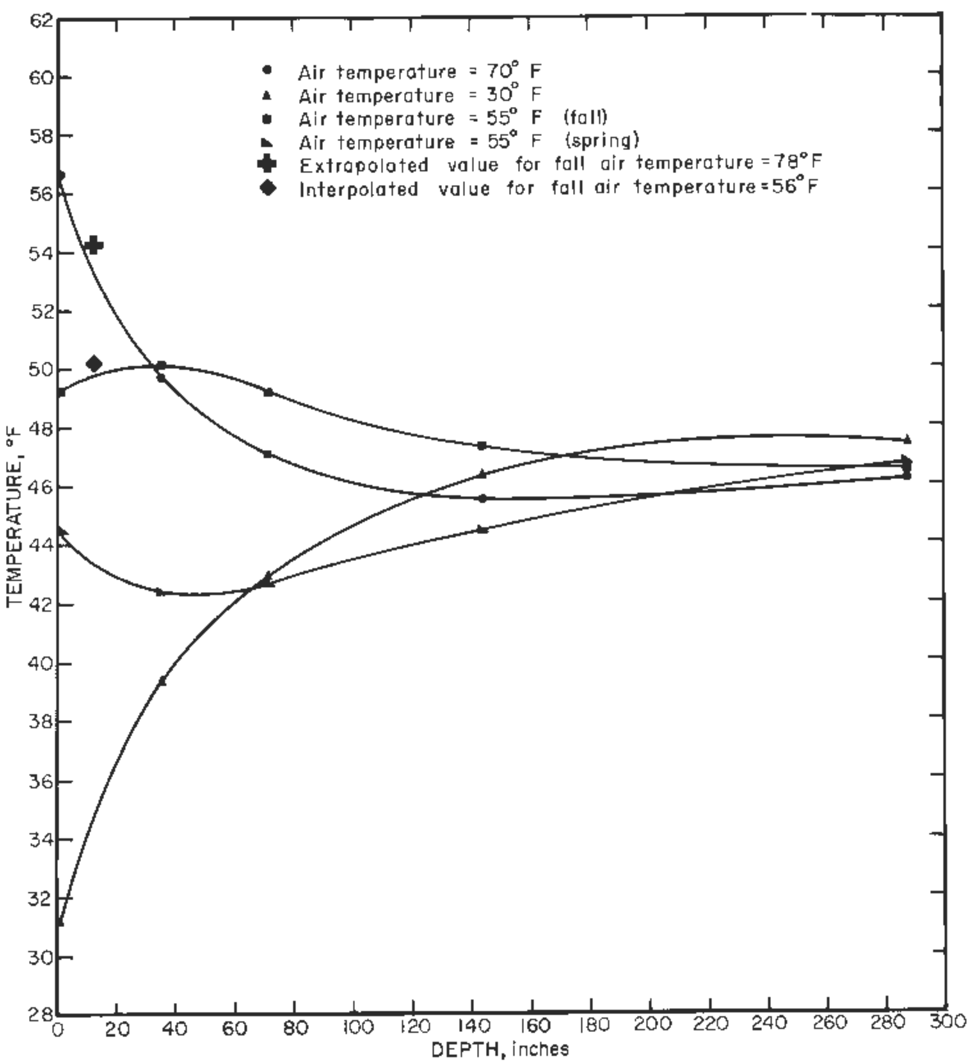

Figure 8. Graph of near-surface rock temperature data in Traprock (7).

STRESS CHANGES DURING UNDERCUTTING FOR BLOCK CAVING AT THE GRÄNGESBERG MINE

J. Hult[1] and H.W. Lindholm[2]

Abstract

The changes in rock pressure have been continuously recorded at a site below the proceeding undercut during a block caving operation. The purpose was to test the long term stability of a new simple rock pressure gauge and to study the stresses induced by such a large scale underground process. The results indicate that the gauge was intact during all the 14 months of the test, and that the recorded stress history agrees well with theoretical results, based on the theory of elasticity.

Introduction

The continued increase in depths of mining is creating a growing need of knowledge regarding rock pressure. Several field studies have already been performed, Hast (2), Leeman (5), which show that measured rock pressure data may deviate considerably from those obtained by theoretical analysis. This discrepancy may be attributed to two main reasons:

1. The analysis is usually based on simplifying assumptions, such as isotropy and homogeneity of the rock material, in order to make possible a quantitative estimate of the stresses.
2. A regional, often horizontal, rock pressure component is sometimes present, which may not be determined from an analytical study, ultimately attributing rock pressure to gravitational forces. It may then be concluded that field measurements will continue to be the main source of knowledge regarding rock pressure for a long time to come.

---

[1]Chalmers University of Technology, Gothenburg, Sweden.
[2]Grängesberg Mine, Sweden.

The various special requirements to be fulfilled by rock pressure gauges depend on the intended use, cf. Hult, Kvapil and Sundkvist (3). Irrespective of this some general requirements may be stated. The gauges should be mechanically robust, and their zero drift should be kept within prescribed limits.

The design should be such that all the equipment and necessary tools may be carried by hand in the mine drifts. Full protection against moisture and corrosive atmosphere must be ensured. It is an advantage if the gauge may be used in conjunction with commercially available standard electronic equipment, and if the cost of the gauges in particular is kept low. The large scale measurements, which are necessary in order to get a complete picture of the stress field in a mine, do necessarily require a pressure gauge and a measuring technique, which are much simpler and less costly than many of those used so far in various research projects.

The question of long term stability of rock pressure gauges is of secondary importance in the overcoring method, where a stress change is recorded during a rather short interval of time. In certain cases, however, it is desirable to follow the consecutive changes in rock pressure at certain fixed points in a mine. This may of course be done by repeated use of the overcoring technique, but the cost would then soon become prohibitive.

In addition the various overcoring measurements would have to be performed at different sites in the area of interest. Since the required minimum distance between two such sites is of the order of one metre (3 ft), one cannot guarantee that the same rock pressure is measured in all instances. A much simpler way is to insert pressure gauges in boreholes at the points of interest and then read these gauges at consecutive intervals. Such measurements reveal the changes in rock pressure occurring at the site, but do not disclose the absolute magnitude of the rock pressure. The latter may, however, be determined after termination of measurement program by overcoring the gauge as a final step.

It is obvious that this type of continuous stress recording is preferable compared to repeated overcoring. The number of error sources is much less and the total cost of the whole program is considerably smaller.

A case where rock pressure changes are of main interest is when mining is performed by means of block caving. Here large changes in rock pressure are actually aimed at, and further development of this technique would therefore be facilitated by detailed knowledge of how the stress pattern develops.

A joint research program, established between the Grängesberg Company and the Chalmers Institute of Technology, was directed towards the development of a simple rock pressure gauge intended for long term recordings. Field tests were to be carried out in conjuction with a block caving operation in the Grängesberg mine.

Rock Pressure Gauge

A ring type transducer gauge, cf. Griswold (1) or Leeman (5), was chosen to be used on account of its simplicity and high sensitivity. Steel rings were designed to fit into a 40 mm diam borehole, and each ring carried four micro-type foil resistance gauges, as shown in Figure 1. In order to simplify the design as far as possible the gauges were not placed in a housing, but were mounted directly in the borehole by means of a special detractable tool. The bottom 100 mm of the borehole were ground to conical shape by means of a diamond reamer. Three gauges were then inserted into this part, and their measuring axes were arranged at 60° intervals. The required pre-load was achieved by pushing each gauge sufficiently far down the conical part; the measuring bridge, type Peekel B 103 U, was connected to the gauge leads all during this operation.

Before the field tests took place, the gauges had been calibrated in a rock prism loaded in a hydraulic press. Simultaneous readings of compressive load and bridge strain indication had shown a linear relationship in the whole range of interest. Hence a constant gauge factor was determined for each gauge, which would translate the bridge strain reading into rock pressure in the field tests.

The gauges were sealed against moisture by means of a preparation trade-marked "Bostik", which was generously applied to the foil gauges as well as to the leads.

Site of Measurement

The orebody at Grängesberg has the shape of a lens with the total length of 1,500 m. The dip angle is 65-70°.

About 2/3 of the orebody is mined by block caving in one continuous block. The average width is 50 m; maximum 100 m and minimum 25 m. A length section is shown in Figure 2. The height of the block is 45 m, see cross-section in Figure 3. The plan of the loading level is shown in Figure 4.

From a drift in the footwall cross-cuts are made at every 16th m. In these there are loading points at every 8th m. These funnel-shaped craters emerge into cross-cuts situated 5 m above. These are used for undercutting operation. In Figure 5 the exact situation of the cross-cuts is shown as well as the drilling plan for the undercutting. The distance between each row is 1.25 m, the angle 80°. Two or three rows are blasted simultaneously.

A plan of the undercutting level is shown in Figure 6. The front line is kept at an angle of about 45° to the horizontal main axis of the lens. The undercutting starts in the middle of the ore body and proceeds towards the ends.

It may be added that the undercutting starts at the hangingwall at a narrow magazine running along the hangingwall. This magazine is 15 m high and 2.5 m wide.

Three gauges were inserted on May 30th, 1963, at a depth of ca 2.5 m in the borehole shown in Figures 4, 5 and 6.

Measurement Program; Results

The gauges were read at continuous intervals all during the undercutting operation, which continued for 14 months. The horizontal distance b between the edge of the cut, first approaching and then leaving the site of measurement, was recorded simultaneously, cf. Figure 12. In Figures 7, 8 and 9 is shown the recorded variation in the gauge readings. Figure 10 shows the estimated variation of the distance b during the six months which were most relevant in the test.

It is seen that gauge No. 1, which was oriented in a vertical direction, indicated a continuously increasing vertical pressure around the borehole as the undercutting edge was approaching. A sharp maximum was reached when the edge was just above the gauge; then the pressure fell very sharply. This development is at least qualitatively in agreement with the prediction of a simple theoretical argument. The three pictures in Figure 11 show the vertical pressure field lines at the beginning, the middle, and the end of the undercutting operation. The sharp rise in vertical pressure is an obvious result of the stress concentration in front of the moving edge.

The two other gauges, marked No. 2 and No. 3, show only a slight change in reading during the phase of interest. This tends to indicate that the direction of the rock pressure change induced by the undercutting operation is essentially vertical. A purely vertical pressure gives rise to such a change in the borehole cross-section, that the diameters in the $\pm 60^\circ$ directions remain unchanged.

For a quantitative judgment of the recorded data a theoretical analysis of the stress field around a propagating edge is required.

Theoretical Analysis

The following problem will be analyzed, cf. Figure 12. An infinitely extended elastic medium carries a uniform uniaxial pressure p. A rectangular coordinate frame Oxy is located with Oy parallel to p, and G denotes a fixed point (corresponding to location of gauge) with coordinates $x = c$, $y = d$. Starting at a certain time a slot is being cut with infinite extension perpendicularly to the Oxy-plane. The width of the slot, denoted 2a, increases continuously, while one edge, located at 0, is held fixed. The problem is to determine the stress $-\sigma_y$ at G, corresponding to the pressure recorded by gauge No. 1.

The slot may be regarded as an ellipsoidal contour, where the minor axis is zero. The stress field around such an opening, first determined by Inglis (4), may be found in the standard literature on elasticity, e.g., Savin (7).

There results

$$-\sigma y/p = \text{Re} \left\{(z - a)/\sqrt{z(z - 2a)}\right\} \qquad .....1$$

where $z = x + iy$ and re denotes "the real part of".
Introducing here

$$\theta = d/c, \qquad \epsilon = a/c \qquad ...2, \; ...3$$

the expression 1 takes the form

$$2(\sigma_y/p)^2 = 1 + \epsilon^2 (1-2\epsilon - \theta^2) \;/\; \left\{ (1-2\epsilon + \theta^2)^2 + 4\epsilon^2\theta^2 \right\} +$$

$$+ \; \left\{(1-\epsilon)^2 + \theta^2\right\}/\sqrt{(1-2\epsilon+\theta^2)^2 + 4\epsilon^2\theta^2} \qquad .....4$$

Here ϵ is a dimensionless measure of the slot width, such that $\epsilon = 1/2$ denotes the case when the moving edge is exactly above G. A plot of $-\sigma_y/p$ versus ϵ for $\theta = 0.004$, which corresponds to the location of G in the field test, is shown in Figure 13 as the dotted curve. The full curve is a replot of Figure 7, and it is observed that the two curves agree fairly well in shape. As to the magnitude of the pressure the following estimate may be made.

The maximum pressure at the gauge point, as found from Equation 4, is very closely equal to 2p. When ϵ increases beyond 1/2, the pressure $-\sigma_y$ decreases very rapidly, when $\theta \ll 1$. The change in σ_y from $\epsilon = 0$ to $\epsilon \approx 1$ is closely equal to the pressure p, i.e., the undercutting operation causes an almost total deloading of the gauge. The recorded change in σ_y as shown in Figure 7 is approximately 130 kg/cm^2. In case of vertical principal stress direction such a pressure at the 345 m level would correspond to an average density of the rock and ore material amounting to 3.75 kg/dm^3. This figure is slightly higher than the real density at Grängesberg, but the discrepancy is not too large.

Finally it should be mentioned that observations similar to those reported here have in the meantime been reported by Merrill and Johnson (6) after field studies at the San Manuel copper mine in Arizona.

Acknowledgments

The authors are indebted to B. Börjesson, G. Dryselius and S. Nyström for valuable assistance and to C.E. Lengquist for fruitful discussions during this research program. The Grängesberg Company has carried the full cost of the work.

References

(1) Griswold, G.B.
1963: How to measure rock pressures: new tools. Eng. and Mining Jour. 164, 90-95.

(2) Hast, N.
1958: The measurement of rock pressure in mines. Sveriges Geologiska Undersökning, Ser. C, no. 560, Stockholm.

(3) Hult, J., Kvapil, R., and Sundkvist, H.
1966: Function and scope of stress meters in rock mechanics. Int. J. Rock Mech. Min. Sci. 3, 1-10.

(4) Inglis, C.E.
1913: Trans. Inst. Naval Arch., London.

(5) Leeman, E.R.
1964-65: The measurement of stress in rock; parts 1-3 and discussions. J. South African Inst. Min. Met. 65 (1964), 48-114 and 254-284; 66 (1965), 408-423, 656-664; 67 (1965), 109-119.

(6) Merrill, R.H., and Johnson, G.
1964: Changes in strain and displacement created by undercutting in block caving. U.S. Bureau of Mines, Denver, Colorado.

(7) Savin, G.N.
1961: Stress concentration around holes. Pergamon Press, Oxford.

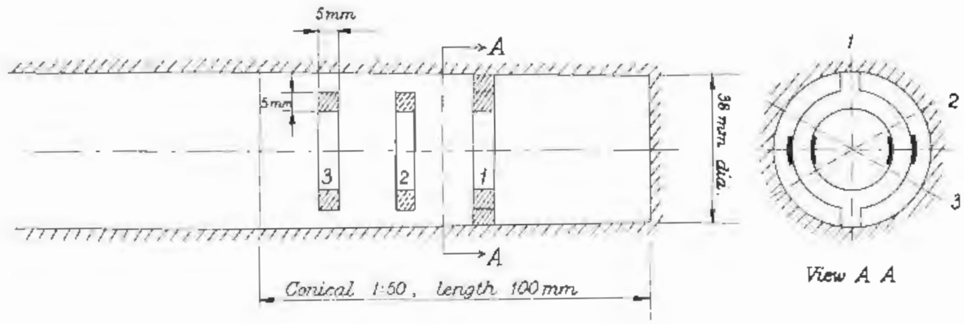

Figure 1

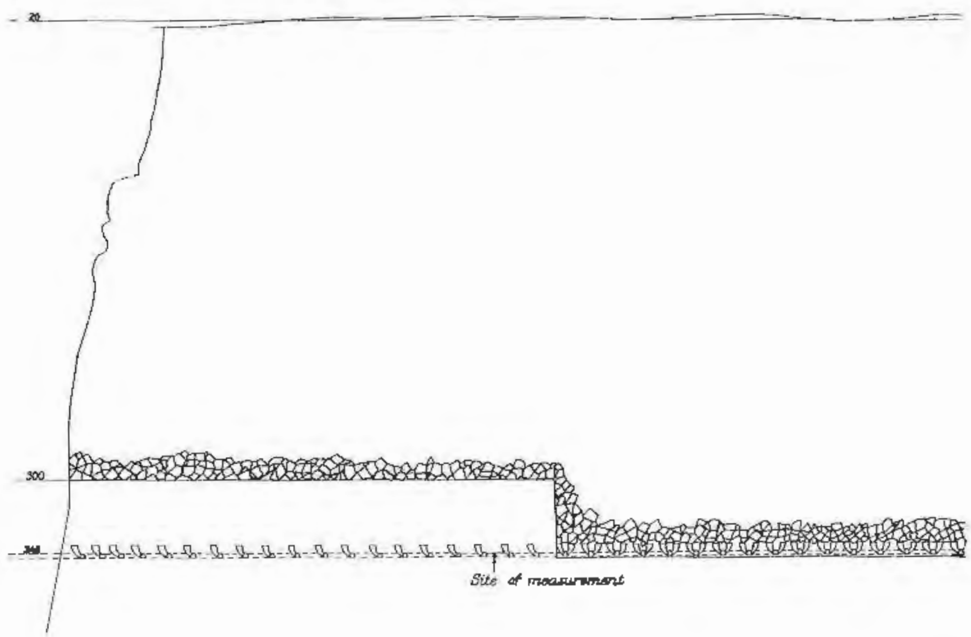

Figure 2

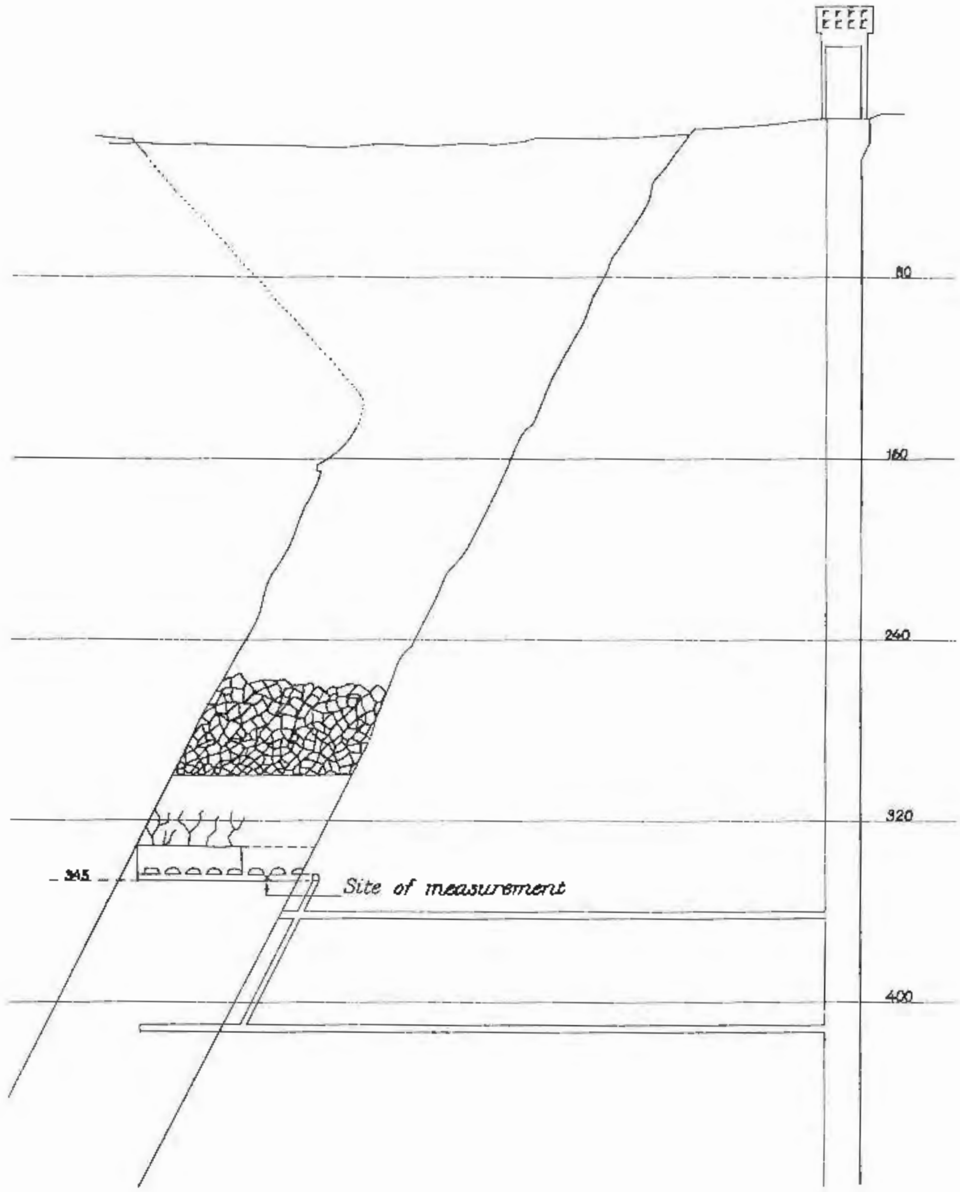

Figure 3

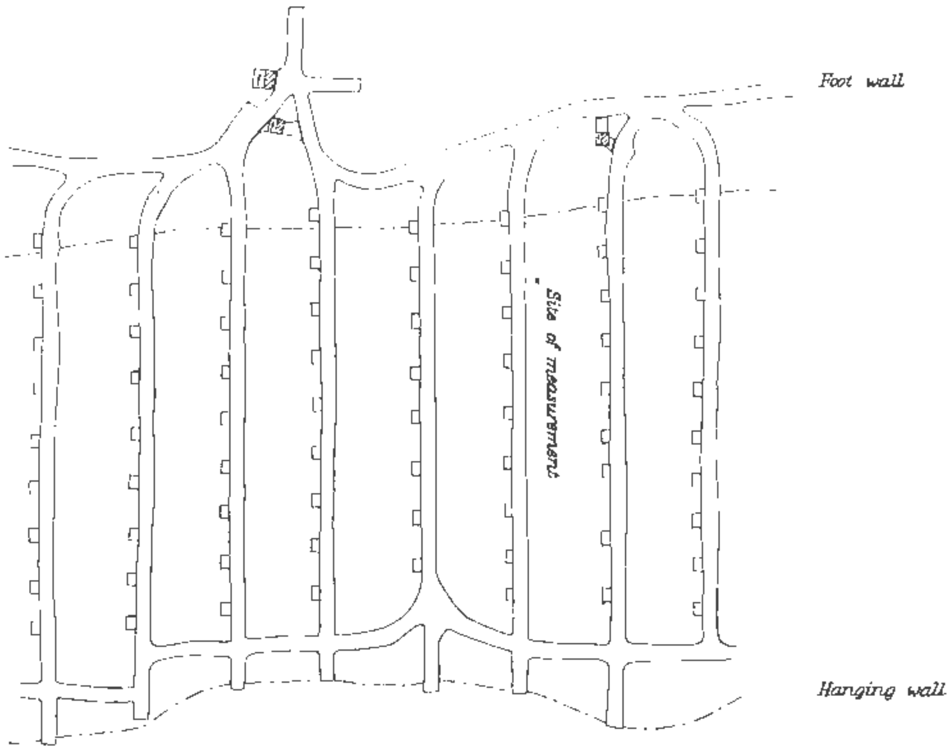

Figure 4

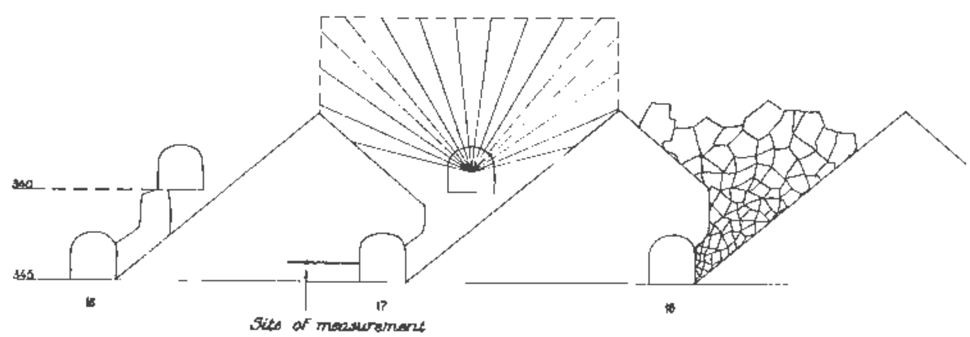

Figure 5

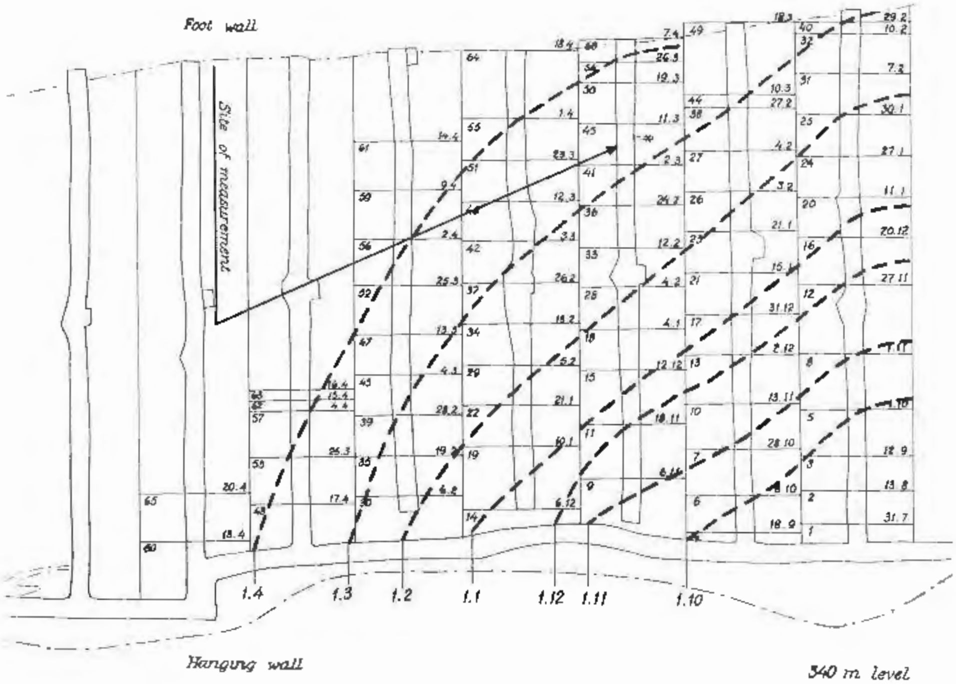

Figure 6

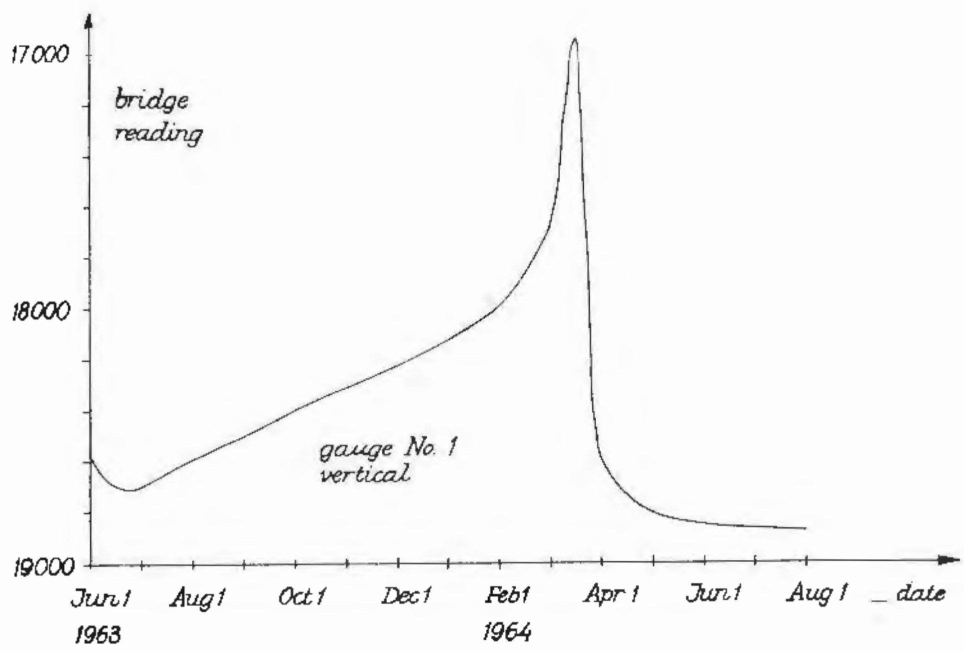

Figure 7

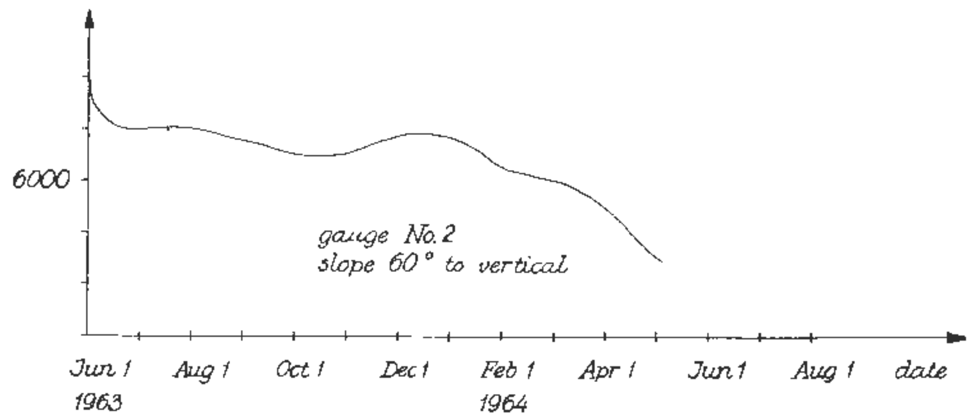

Figure 8

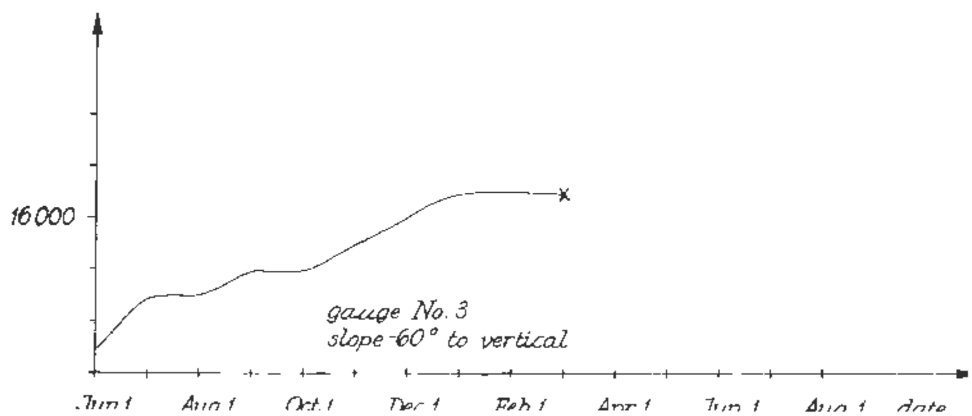

Figure 9

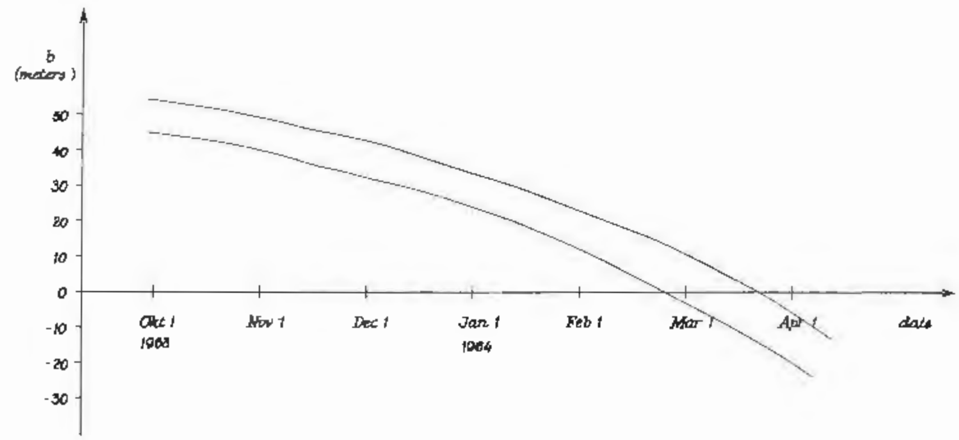

Figure 10

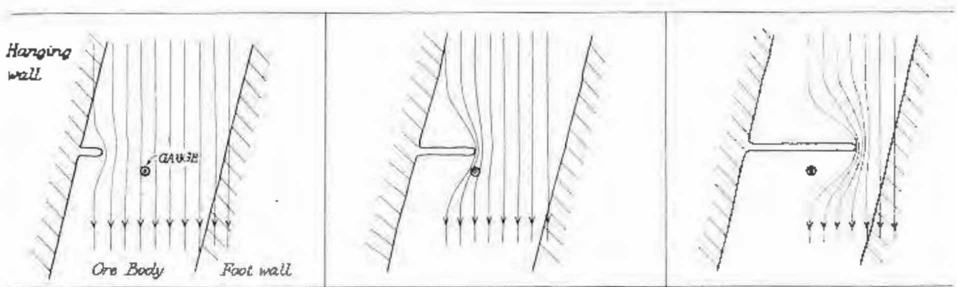

Force lines pass through gauge location almost undisturbed by undercutting edge.

Force lines pass through gauge location very closely, i e high pressure, due to concentration in front of undercutting edge.

Force lines pass beside gauge location due to shading by undercutting edge.

Figure 11

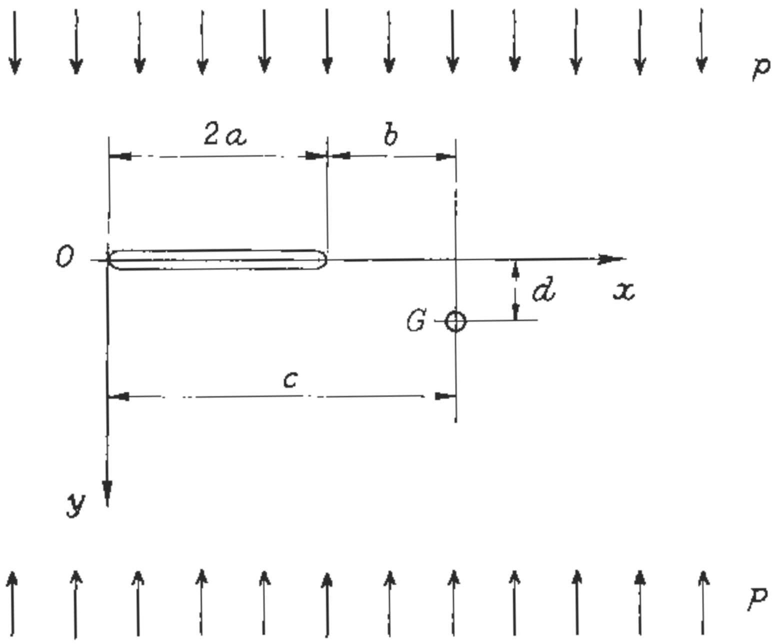

Figure 12

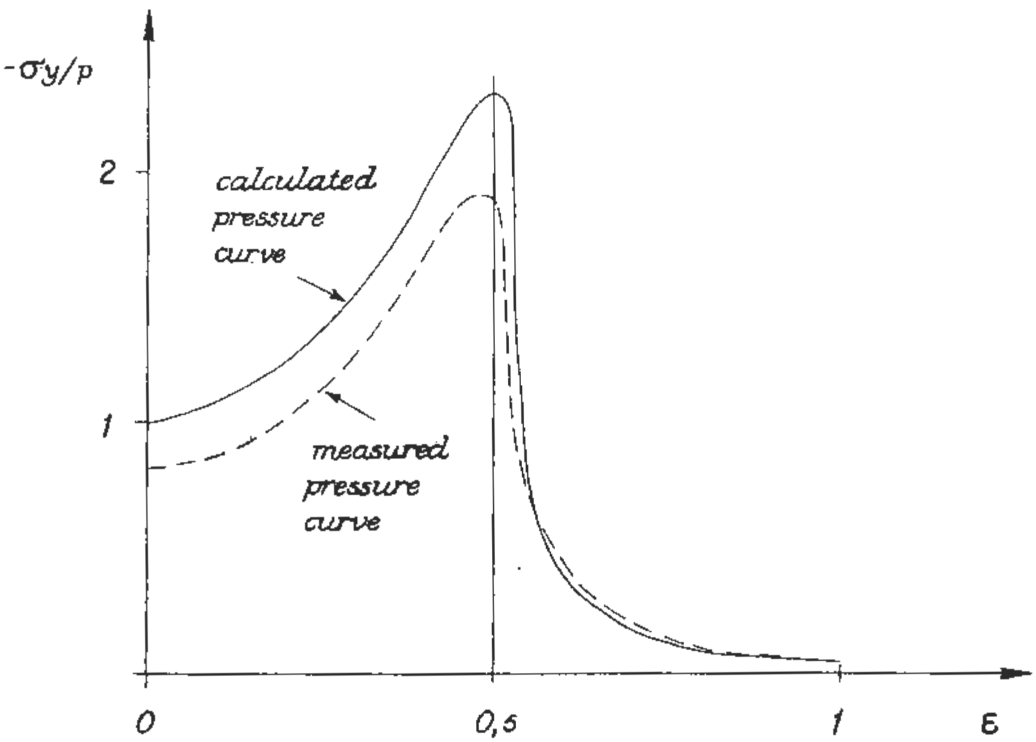

Figure 13

96038—12½

FIELD BLASTING STUDIES

G.E. Larocque[1], K. Sassa[2], J.A. Darling[3], and D.F. Coates[4]

Abstract

Field experiments have been conducted to provide information on the ground motion resulting from detonation of explosive charges in the equivalent of a continuous elastic medium. Such experiments have been completed for two types of explosive placed in a magnetite rock mass. The instrumentation used in these experiments, to sense and record ground motion, is described. The method used to measure detonation velocity of the explosive charges is outlined and a description of the two explosives used is given. Laboratory experiments of the 'Hopkinson Bar' type were carried out to determine the dynamic tensile strength of the rock material involved in the field experiments.

A brief description is given of a previously reported method of analysis which was used, in conjunction with the field data, to determine the stress distributions surrounding the explosive charges with or without the presence of a free face. The results of this analysis have been applied with a tensile strength failure criterion to predict crater dimensions. Initial agreement has been found to be good between predicted and actual craters.

[1,3]Research Scientists and [4]Head, Mining Research Laboratories, Fuels and Mining Practice Division, Mines Branch, Department of Energy, Mines and Resources, Ottawa, Canada.

[2]Department of Mineral Science and Technology, Kyoto University, Kyoto, Japan; former National Research Council of Canada Research Fellow at the Mining Research Laboratories, Mines Branch, Ottawa, 1963–65.

Extending this method of stress analysis to column charges, the direct stress distributions in the vicinity of detonating column charges have been determined. It was found that two-point simultaneous detonation is preferable to single-point bottom detonation, if uniform peak stress along the length of a column charge is desired.

Introduction

The current blasting research project at the Mining Research Laboratories was initiated for the purpose of studying the transmission of explosive energy into hard rock. One of the initial objectives was to establish a means of predicting craters, or the boundaries of broken rock, based upon the properties of the rock and explosive. With satisfactory agreement, it was then anticipated that improvements could be made in predicting ground shock occurring at ranges beyond the crater and also in designing industrial blasts.

The procedure followed has been to select a failure criterion for the rock material and to establish a method for determining the stress distribution resulting from detonation of a contained explosive charge. Field and laboratory experiments were carried out to determine rock and explosive properties required for such an analysis.

In the field, the dynamic properties of the rock mass were determined from experiments with explosives in a configuration equivalent to an infinite mass. These dynamic properties included the attenuation indices of particle velocity and displacement, the intercept values (i.e., at a unit distance) of particle velocity and displacement, the shape of the waves transmitted into the rock and carried by it out to various ranges, and the P-wave and S-wave velocities.

The dynamic tensile strength of the rock was determined by laboratory experiments.

After establishing the method of analysis for a spherical charge, a method was developed to simulate the stress distribution resulting from a column charge. This method of analysis has been used to compare two modes of detonating a column charge.

Field Experiments

Data Required from Field Experiments

The stress distribution resulting from detonation of a contained charge was calculated by superposition, with a computer program, of the stresses caused by three transient stress waves: the direct dilatational wave, the reflected dilatational wave, and the shear wave reflected from the free face. The parameters characterizing a particular explosive and rock combination required for use in this program appear as headings in Table 1. The values obtained from two rock-explosive combinations are listed in the table. Crater dimensions for specified explosive charge weights were also required, to determine whether the boundaries of broken rock could be predicted on the basis of the proposed analyses.

TABLE 1

Table of Rock Constants for Stress Computation

Explosive	C_L(m/s)	C_T(m/s)	ρ(g/cm^3)	A_o(cm)	B_o(cm/s)
Geogel 60% (3,400 g)	6,400	3,420	1.5	40.3	3.36×10^5
Cilgel B 70% (2,950 g)	6,400	3,420	1.2	19.5	1.36×10^5
Explosive	n	m	ι	ι'	
Geogel 60% (3,400 g)	1.4	1.4	1.0	1.0	
Cilgel B 70% (2,950 g)	1.3	1.3	1.0	1.0	

Derived Rock Constants:

Lamé's constants $\lambda = 6.25 \times 10^{11}$ dyne/cm^2,

and $\mu = 4.15 \times 10^{11}$ dyne/cm^2,

Young's modulus (E) = 10.6×10^{11}dyne/cm^2 = 1.1×10^6 kg/cm^2,

Poisson's ratio (v) = 0.30.

Glossary of Symbols:

C_L - dilatational wave velocity.

C_T - shear wave velocity.

ρ - density.

A_o - peak displacement intercept value at equivalent charge radius.

B_o - peak particle velocity intercept value at equivalent charge radius.

n - exponent of power law relationship describing peak dilatational wave displacement attenuation with distance.

m - exponent of power law relationship describing peak dilatational wave particle velocity attenuation with distance.

ι - similar to n but for a shear wave.

ι' - similar to m but for a shear wave.

Description of Field Experiments

Three distinct field experiments were carried out to obtain the required data: two array arrangements and a series of crater tests. A normal linear array was used to determine all factors with the exception of ι, ι', and C_T. A non-linear array was used to determine the factors ι, ι' and C_T.

The Linear Array

Figure 1 is an idealized section of the linear array, showing the gauge and shot holes. All gauge holes were located in the same plane, approximately 28 ft below surface. The shot holes were drilled approximately 2 ft deeper. This was done to allow two shots to be fired in one shot hole; for the second shot the hole was filled with tamping sand, to a level 3 ft above the original depth, before the charge was placed. Since it was required that the path between the shot and gauge holes be unobstructed by other shot holes, the shot holes were drilled toward the gauge holes as the experiment progressed. W and E refer to shot holes drilled to the west and east of the linear array gauge holes. The bottoms of all shot and gauge holes were accurately located by survey for the exact determination of the distances between explosive charges and accelerometers. Accelerometers were used as sensing devices in all gauge holes.

With the exception of ι, ι' and C_T, parameters in Table 1 were determined from acceleration waveforms of the direct dilatational wave, measured at the gauge holes in the linear array experiment. The depths of the shot and gauge holes were selected to allow, under the worst conditions, 3.0 millisecs before the shear wave reflected from the surface would interfere with the direct dilatational wave being sensed at the gauge holes. While the reflected dilatational wave in these experiments arrived at the sensing elements within 3.5 millisecs of the arrival of the direct dilatational wave, its contribution was considered negligible.

Shear Array

Figure 2 is a plan diagram of the shear array. In this experiment some AX gauge and shot holes of the linear array experiment were used as gauge holes. A shot hole, G6, 10 ft in depth was offset from G5 and the line of the gauge holes by 3 ft. This provided transmission paths between shot and gauge holes which were independent of other gauge holes. Sensing devices, for this experiment, were installed in the same plane as the bottom of the shot hole.

Crater Studies

For the crater studies, shot holes were drilled to the required overburden depth W at an angle of 45° to the free face. It had been planned to use HM holes in this part of the field project, and the same charge weights as used in the linear array. The diamond drilling machine, however, was incapable of drilling the necessary holes at a 45° angle to the surface. Ultimately, an air track drill was used to provide 3 in. diam shot holes. The explosive charges maintained the original geometrical length-to-diameter ratio used in the linear array. Initially, the critical depths for the two explosives were determined. This was followed by the production of a set of craters.

Sensing Devices

Accelerometers and Mounting Assemblies

Accelerometers were used as sensing devices in both types of array experiments. From the recorded acceleration records, the various parameters required from the field experiments were determined. Endevco 2231 accelerometers were used in the linear array, and Clevite 25D21 in the shear array. Their pertinent characteristics under the conditions used are given in Table 2.

TABLE 2

General Characteristics of Accelerometers Used in Field Experiment

	Voltage Sensitivity	Capacity Frequency Response	Cross Sensitivity	Peak Shock
Endevco 2231	10pk-mv/pk-g	1000 pf 5cps - 10kc	3%	16,000 g
Clevite 25D21	25pk-mv/pk-g	1300 pf 1cps - 6kc	3%	10,000 g

The mounting assembly used to wedge the accelerometers in place is shown in Figure 3A; Figure 3B is an idealized section diagram of the mounting assembly. An hydraulic hand pump, on surface, was used to force the accelerometer mount in place. Extension of the hydraulic piston spreads the tapered half-sleeves, binding the unit against the walls of the drill hole. A pressure of 2,000 psi was used to wedge the accelerometer units in place.

The accelerometer sleeves and wedges were made of aluminum to provide an approximate acoustical match between the accelerometers and rock mass. For the linear array experiments the accelerometers were mounted in wells in the wedges with their sensitive direction perpendicular to the main axis of the accelerometer mount. For the shear array experiments, the accelerometers were mounted in the wells with their sensitive axis parallel to the main axis of the accelerometer mount assembly.

Explosive Probe and Constant Current Supply

An explosive probe was used in the linear array experiment. It provided, for recording purposes, a trigger pulse at the beginning of explosive detonation and a voltage step waveform from which detonation velocity of the explosives could be determined. A constant current supply was used in conjunction with the current probe section of the explosive probe, to provide voltage step waveforms. The current probe consisted of a chain of 22 ohm 1/2 watt resistors, spaced 1 in. apart along the axis of the explosive probe, wrapped in a brass foil. The trigger probe, of the ion gap type, consisted of two insulated open ended wires running to the tip of the unit.

Originally the resistance chain was not sheathed. Laboratory experiments, however, indicated that the variation in conductivity in the detonation region was such as to produce "noisy" records. The brass foil, which vaporizes as the detonation wave passes, provides essentially a dead short. Figure 4 illustrates the effect of the addition of the foil, and a typical field record is shown. The small indentations in step waveforms results from passage of the detonation zone over a resistor.

Electronic Equipment

Description of Recording Equipment

Consistent with the depth of burial, every accelerometer was terminated in a cathode follower with the shortest possible length of cable between the accelerometer and cathode follower. For this purpose, the Endevco 2608 cathode followers used were mounted on insulated boards in weatherproof boxes. A series of potted high-quality capacitors is contained in each of these boxes for the purpose of changing accelerometer voltage sensitivity.

Figure 5 is a block diagram of the recording system. The recording apparatus in operation is entirely controlled by a 10-second, "one cycle and stop" timer, initiated by a momentary closing of a push-button contact.

At the beginning of a cycle, the tape recorder is placed in the record mode in order to provide the 4 seconds required for the tape transport to reach 60 ips. Two seconds later the paper transport of the paper oscillograph unit is started. At 4-1/2 seconds after the cycle has started, the detonator is fired by a cam on the one-cycle timer. From 0 to 8 seconds after the start of the cycle the firing pulse, trigger pulse and output of five accelerometers are recorded by the seven-channel tape recorder. Eight seconds after the start of the cycle, the timing and switching units transfer all seven inputs of the tape recorder to an oscillator which supplies a known amplitude, known frequency sinewave voltage to all seven channels. Shortly before the end of a cycle the switching unit is returned to its original condition, the tape recorder is stopped, and the transport of the paper tape is turned off.

Only four galvanometers were available for use with the paper oscillograph unit. They were used to provide instant records of the output of three of the accelerometers, and the trigger pulse as recorded by the F.M. recorder. In this way, immediate assessment was made of the record resulting from a particular test shot. Thus, in this application the paper oscillograph has functioned as a monitoring unit; possessing only a 0-5 kc bandwidth, the galvanometers were incapable of reproducing with fidelity the output of the tape channels.

Prior to a field test shot, a dummy run of the entire recording equipment was made by disconnecting the detonator circuit. The paper tape record provided a quick check on the operational condition of the equipment.

The detonation velocity of the explosive of each test shot was determined by insertion of a current probe. The characteristic voltage step waveform of this probe was photographed for each test shot hy means of an oscilloscope and attached camera.

Certain safety features were built into the recording equipment. A safety plug must be inserted into the timer panel before the detonator is connected to the firing circuit, and the current probe to the constant camera supply. To make firing of the explosive a deliberate act, a normally open push-button must be held down during the cycle if the explosive is to be detonated.

Information Playback Procedure

The purpose of the trigger pulse on one of the channels of the tape recorder was to provide, on playback, an external trigger to the oscilloscope. The firing pulsc, also recorded by the tape recorder, supplied an alternate signal for external triggering of the oscilloscope.

On playback the outputs of the accelerometers were analyzed one at a time. For this purpose a Tektronix Model 555 oscilloscope was equipped with a type-O operational preamplifier, a type-C.A preamplifier, and an oscilloscope camera. Initially the acceleration waveform and the particle velocity waveform were reproduced, using one integrator of the type-O operational amplifier. This was followed by reproduction of the calibration sinusoidal waveforms appended on the tape at the ond of a test shot. In subsequent reruns of the tapes, hy double integration the particle displacement records and calibration voltage records were produced. These displacement records were accompanied by repeat particle velocity records.

Explosives and Shear Wave Generation

Selection of Explosives

Two explosives were required for the field program with a low and a high detonation velocity. It was necessary for these explosives to be sufficiently plastic to be tamped in place and to function after submersion in water for short periods. It was also essential that they initiate without the need of booster and reach ideal detonation velocity shortly after initiation. The two explosives that were selected as meeting these requirements were Geogel 60% and Cilgel B 70%.

Geogel 60%, in common with other similar straight gelatins designed for seismic prospecting, is efficiently and reliably detonated under much more extreme conditions than were anticipated with a No. 8 blasting cap and has a velocity of approximately 6,500 metres/sec. In addition, it is waterproof and highly plastic. Cilgel B 70%, one of the more plastic ammonia semi-gelatins with a velocity of detonation of about 4,000 metres/sec, is water-resistant.

Table 3 summarizes the pertinent physical properties of Geogel 60% and Cilgel B 70%. Some of the data therein were calculated from data made available by the manufacturer. Pressure and velocity data were obtained from laboratory experiments.

TABLE 3

Selected Properties of Geogel 60% and Cilgel B 70%

	Geogel 60%	Cilgel B 70%
Density		
a) g/1-1/4 in. cartridge	242	203
b) g/ml (calculated)	1.5	1.2
c) g/ml (bulk tamped)	1.3	1.0
Physical Texture	Plastic Gelatin	Plastic Semi-gelatin
Water Resistance	Excellent	Fair
Power = (Function of Energy x Function of Gas Vol.)		
a) g TNT/g	0.96	1.12
b) g TNT/ml	1.45	1.42
Detonation Velocity - metres/sec	6,500	4,000
Detonation Pressure - kilobars	170*	87*

*Determined by aquarium tests.

Shear Wave Generation

Two methods were used to develop a disturbance containing a shear wave; both involved impacting the bottom of the shear array shot hole. One method was to place a No. 8 detonator, housed in a protective casing with an open end, in contact with the bottom of the shot hole and detonate. The second method involved a gun, mounted to an aluminum conduit, which was used to impact the bottom of the shot hole with a 45-calibre lead bullet. With both methods a thin insulated wire, broken by detonation of the cap or passage of the bullet in the vicinity of the bottom of the shot hole, was used to produce a trigger.

Field Experiment Results

The results of the field experiments have been summarized in a number of graphs and tables. In Table 1, much of the numerical information required in the stress analysis methods employed is presented in a concise manner. Numerical information concerning normalized particle velocity and displacement wave shapes was excluded for the sake of brevity.

In Table 4, statistics concerning the various explosive charges are presented. It is evident from this table that some failures of the explosive probe did occur, with loss of velocity records. The design was subsequently rectified (1).

In Table 5, the average rock density arrived at from density determinations on ore samples from the gauge holes is given. Samples for density determinations were concentrated in two horizons: the 10-ft horizon where shear measurements were made, and the horizon where the direct P accelerometers were installed.

In Table 6 the average dilatational wave velocity of the orebody is given. The acceleration records of gauge holes G1 and G5 from a number of test shots were used in the determination of dilatational wave velocity. These records, all time-referenced to the explosive trigger probe, provided a means of determining transit time over a known path length.

In Table 7 the average shear wave velocity of the orebody is given. Acceleration records made as part of the shear array experiment were used in the determination. A procedure similar to that used in the determination of dilatational wave velocity was used, with gauges placed in the shot holes W_1 and W_2.

In this paper, the wave shape data presented are limited to those resulting from east side HM Geogel 60% and Cilgel B 70%. Complete stress analysis has been limited to east side HM Geogel 60%. Figures 6 and 7 are logarithmic plots of maximum particle velocity and displacement against scaled distance, for east side HM Geogel 60% and Cilgel B 70%. Besides providing for the analysis-required numerical values, these plots are a field confirmation of the power law relationships that were earlier assumed to describe the attenuation of the peak values of particle velocity and displacement with distance.

Figure 8 shows typical oscillograms reproduced from tape recordings. From these records, the smoothed normalized particle velocity and displacement wave shapes shown in Figures 9 and 10 were produced. Reduced to numerical form, the information concerning particle velocity and displacement wave shape contained in Figure 9 was used in the present stress analyses. Figure 11 is a logarithmic plot of peak shear particle velocity against scaled distance. Only two of the five gauges in the shear array functioned properly. Difficulty was realized in separating the shear wave from the tail of the longitudinal wave and from reflection from discontinuities adjacent to some of the wave paths.

Laboratory Experiments

Data Required from Laboratory Experiments

To delineate or predict the boundaries of craters on the basis of the present method of stress analysis, a maximum tensile strength criterion was selected. This required a knowledge of the dynamic tensile strength of the rock as distinct from its static tensile strength, which is in general smaller.

TABLE 4

Explosive Charge Data For Geogel 60% and Cilgel B 70%, 2 in. and 4 in. Shot Holes

Date 1965	Shot No.	Charge Horizon (ft)	Charge Weight (g)	Charge Volume (ml)	Bulk Density	VOD metres per sec	Notes
			4 in. Ø Cilgel B 70%				
May 26	East 6 - No. 1	29.0	2950	3070	0.96	--	Probe failed
May 26	East 6 - No. 2	29.0	2950	3270	0.90	4400	3500 for 3 in.
May 31	East 4 - No. 1	28.0	2950	2960	1.00	3920	Average
May 31	East 4 - No. 2	29.0	2950	--	--	4880	Probe error?
June 2	East 2 - No. 1	27.0	2950	--	--	4120	3500 for 6 in.
June 2	East 2 - No. 1	25.5	2950	3360	0.88	4110	--
	Average: Standard Deviation:				0.94 --	4140 --	
			4 in. Ø Geogel 60%				
May 21	West 7 - No. 1	29.5	3400	2560	1.33	6350	--
May 25	West 7 - No. 2	27.0	3400	--	--	6450	Sand bed settled
May 24	East 7 - No. 1	29.5	3400	2350	1.45	--	Probe failed
May 24	East 7 - No. 2	26.8	3400	2250	1.51	6350	--
May 27	West 5 - No. 1	30.0	3400	2490	1.35	6300	--
May 28	West 5 - No. 2	19.0	3400	--	--	6350	Sand bed settled
May 30	East 5 - No. 1	28.0	3400	2460	1.38	6350	--
May 30	East 5 - No. 2	25.5	3400	2400	1.48	--	Probe failed
May 31	West 3 - No. 1	27.0	3400	2250	1.51	--	Probe failed
May 31	West 3 - No. 2	25.0	3400	2460	1.38	6350	--
June 1	East 3 - No. 1	27.5	3400	2250	1.51	6030	--
June 1	East 3 - No. 2	25.5	3400	2350	1.45	5990	--
June 3	East 1 - No. 1	27.5	3400	2550	1.33	6600	--
June 3	East 1 - No. 2	24.7	3400	2350	1.45	6350	--
	Average: Standard Deviation:				1.41 3.2%	6315 2.3%	
			2 in. Ø Geogel 60%				
May 25	West 6 - No. 1	29.5	425	--	--	--	--
May 25	West 6 - No. 2	26.5	425	--	--	642	Sand bed settled
May 29	West 4 - No. 1	30.3	425	330	1.28	--	Probe failed
May 29	West 4 - No. 2	28.5	425	--	--	5900	Sand bed settled
May 29	West 4 - No. 3	27.0	425	254	1.68	6160	--
June 1	West 2 - No. 1	28.5	425	292	1.45	6050	--
June 1	West 2 - No. 2	26.5	425	292	1.45	6350	--
June 3	West 1 - No. 1 No. 2	28.0 not fired	425	330	1.28	6500	--
	Average: Standard Deviation:				1.43 --	6230 --	

TABLE 5

Density and Location of Specimens from Various Gauge Holes

Gauge Hole and Specimen No.	Approximate Depth (ft)	Specific Gravity	Gauge Hole and Specimen No.	Approximate Depth (ft)	Specific Gravity
G5 - 1	10	3.68	G2' -4	30	3.42
G5 -2	10	3.66	G2' -5	30	3.81
G5 -3	10	3.56	G2' -6	30	3.50
G5 -4	30	3.52	W1 -1	10	4.12
G5 -5	30	3.75	W1 -2	10	3.73
G5 -6	30	3.48	W1 -3	10	3.58
G3 - 1	10	3.55	W1 -4	30	3.80
G3 -2	10	3.59	W1 -5	30	3.27
G3 -3	10	3.76	W1 -6	30	3.89
G3 -4	30	3.56	G1 -1	10	3.41
G3 -5	30	3.73	G1 -2	10	3.39
G3 -6	30	3.17	G1 -3	10	3.54
G2'- 1	10	3.39	G6 -1	10	3.42
G2'-2	10	3.71	G6 -2	10	3.67
G2'-3	10	3.71	G6 -3	10	3.26
Average Specific Gravity = 3.54					

TABLE 6

Dilatational Wave Velocities Determined for the Path Between Gauge Holes G1 and G5 on Various Test Shots

Test Shot	Velocity (metres/sec)
W4(1)	6,700
W2(1)	6,530
E2 (1)	6,350
E2 (2)	6,530
E3 (1)	6,530
E4 (1)	6,180
E5 (1)	6,530
Average Value	6,460

TABLE 7

Shear Wave Velocities Determined on the Basis of the Path Difference Between the Shear Shot Hole G6 and Gauge Holes W1 and W2

Test Shot	Velocity (metres/sec)
G5	3,250
G5'	3,620
G7'	3,250
G7'	3,250
G3'	3,650
G4'	3,650
Average Value	3,450

Description of Laboratory Tensile Tests

The dynamic tensile strength of the rock, used in the analyses, has been determined, using a modified Hopkinson Bar apparatus similar to that used by Attwell (2) in his studies concerning rock. In this type of test, a compressive stress wave is generated in a cylindrical specimen by impacting one of the flat ends with a bullet or explosive; this becomes tensile on reflection at the opposite free face. By determining the free face velocity-time profile and the dilatational velocity, and knowing the spall length, the tensile stress at failure can be determined using the formula

$$\sigma = \rho CV, \qquad \ldots\ldots 1$$

where ρ is the rock's density, C its dilatational wave velocity, and V its particle velocity at failure.

The modified Hopkinson apparatus used consisted of a cylindrical specimen with a detonation apparatus at one end and a displacement-measuring device at the other end, separated by a 3-ft pressure bar.

An end parallel plate capacitance gauge was used to determine the displacement-time profile of the free end of the specimen subjected to explosive attack. The plates consisted of a thin metal foil cemented to the end of the specimen, and a parallel brass plate supported in position by a lucite rod attached to a table-mounted unit. A micrometer on this table unit controlled the axial motion of the brass plate; this allowed accurate adjustment of plate separation. Differentiation of the displacement-time voltage profile of the capacitance gauge provided a free face velocity-time profile for each of the specimens tested. Figure 12 is a typical set of profiles for magnetite specimens, from which dynamic tensile strengths were determined.

The calibration factor relating voltage output and displacement of a parallel plate gauge is normally determined ballistically. In the present study, displacement was directly related to voltage output by use of an auxiliary photo-optical system. With this system a linear relationship was established between voltage output and displacement. By making concurrent, identical displacement measurements with the two systems, the capacitance gauge was calibrated directly.

Tensile Test Results

The results of the tensile tests are summarized in Table 8. A mean value of 130 kg/cm^2 ksc was realized with a standard deviation of 28 kg/cm^2 ksc.

TABLE 8

Table of Results for Hopkinson Tensile Tests Conducted on Magnetite Specimens from Carol Lake, Labrador

Specimen No.	Tensile Stress in Failure Plane (psi)	Mean Tensile Strength and Standard Deviation
6	2,200	
7	2,000	
9	1,500	
10	1,800	
11	2,400	
14	1,200	
15	2,200	
16	2,000	
18	2,500	1,800 $\pm$ 400 or $\pm$ 22%
19	2,000	
20	2,200	
23	1,500	
25	1,100	
30	1,700	
31	1,700	
32	1,500	

Method of Stress Analysis

Historical

The method of stress analysis used to determine the stress resulting from detonation of contained spherical charges in the vicinity of a single free face has been previously reported in detail (3). This method of stress analysis, which was developed at Kyoto University, is briefly outlined below.

Outline of Method of Analysis

It is assumed with this method of stress analysis that the disturbance resulting from the explosion of a spherical charge in a medium which acts in an elastic manner is limited to a radial longitudinal wave. When a charge is placed adjacent to a free face, the stresses at any point near the free face result from passage of the three wave motions shown in Figure 13A: the first is the longitudinal wave travelling directly from the explosion, and the second and third are longitudinal and transverse waves resulting from reflection of the direct longitudinal wave at the free face.

The stress components contributed to the stress conditions at a point such as (A) by the direct longitudinal wave are completely defined in terms of particle velocity, particle displacement, and elastic rock constants.

$$\sigma_{r\,ip} = (\lambda + 2\mu)\left\{\frac{dU_p(r)}{dr} \cdot U_w(T_{ip}) - \frac{V(r, T_{ip})}{C_L}\right\} + 2\lambda\,\frac{U(r, T_{ip})}{r}$$

$$\sigma_{\theta ip} = \sigma_{t\,ip} = \lambda\left\{\frac{dU_p(r)}{dr} \cdot U_w(T_{ip}) - \frac{V(r, T_{ip})}{C_L}\right\} + 2(\lambda + \mu)\,\frac{U(r, T_{ip})}{r}$$

$$\tau_{\theta t\,ip} = \tau_{rt\,ip} = \tau_{r\theta\,ip} = 0. \qquad \ldots\ldots 2$$

Similarly, the stress components resulting from the reflected longitudinal and transverse waves are defined in terms of the direct longitudinal particle velocity and displacement wave shapes and amplitudes as well as elastic rock constants. Displacement U(r, Tip) in the above equations is the product of $U_p(r)$ and $U_w(T_{ip})$, where $U_p(r)$ is a function of r and describes the attenuation of the peak value of displacement with distance, and Uw(Tip) is a function of $T_{ip} = (t - \frac{r}{C_L})$ and indicates the change in the value of the normalized displacement wave shape with time. Particle velocity V(r, Tip) can be described as a product of similar expressions $V_p(r)$ and $V_w(T_{ip})$. For the reflected longitudinal (rp) and shear waves (rs), amplitude and phase adjustments are made on the basis of path length and plane wave reflection theory at a boundary. The latter assumption is one of the limitations of this particular analytical approach.

The stress components in the three sets of Equations 2, 3 and 4 are in polar coordinates referred to origins θ_1, θ_2 and θ_3. These origins are the intersections of the projections of the directions of the wave fronts back to an extension of the normal from the shot centre to the plane of the free surface. The computer program written to handle the synthesis of these stresses provides as an output the time-dependent principal stresses and also their directions referred to origin 0. The user of the program selects the points where the stress conditions are to be determined. In passing, it should be noted that the particle velocity and particle displacement wave shapes for the three wave motions are identical and for computational purposes can be characterized by discrete sets of numerical data concerning wave shape and suitable power law relationships.

Application of Analysis

The analysis was carried out for 3,400 g charges of Geogel 60% and 2,950 g charges of Cilgel B 70%. Depths of burial of 100, 120, 150 and 240 cm were considered. Because of the symmetry with a spherical charge, one of the three principal stresses is always in the θ direction; the direction of the other two principal stresses, which are in the r θ plane, vary with time as shown in Figure 13 B. The principal stress coinciding with the θ direction is denoted as σ_3; σ_1 and σ_2 are the principal stresses in the r θ plane.

$$\sigma_{r\,rp} = (\lambda+2\mu)\left\{\frac{\partial U_{p1}(r_1,\theta_1)}{\partial r_1} \cdot U_{w1}(T_{rp}) - \frac{V_1(r_1,\theta_1,T_{rp})}{C_L}\right\} + 2\lambda\,\frac{U_1(r_1,\theta_1,T_{rp})}{r_1}$$

$$\sigma_{\theta\,rp} = \sigma_{t\,rp} = \lambda\left\{\frac{\partial U_{p1}(r_1,\theta_1)}{\partial r_1} \cdot U_{w1}(T_{rp}) - \frac{V_1(r_1,\theta_1,T_{rp})}{C_L}\right\} + 2(\lambda+\mu)\,\frac{U_1(r_1,\theta_1,T_{rp})}{r_1}$$

$$\tau_{r\theta\,rp} = \mu.\frac{1}{r}.\frac{\partial U_{p1}(r_1,\theta_1)}{\partial\theta_1} \cdot U_{w1}(T_{rp})$$

$$\tau_{\theta t\,rp} = \tau_{rt\,rp} = 0.$$

.....3

$$\sigma_{r\,rs} = \lambda\,\frac{1}{r_2}\left\{\frac{\partial U_{\theta p}(r_2,\theta_2)}{\partial\theta_2} \cdot U_{\theta w}(T_{rs}) + \frac{U_{\theta p}(r_2,\theta_2)}{r_2} \cdot U_{\theta w}(T_{rs})\cot\theta_2\right\}$$

$$\sigma_{\theta\,rs} = (\lambda+2\mu).\frac{1}{r_2}\,\frac{\partial U_{\theta p}(r_2,\theta_2)}{\partial\theta_2} \cdot U_{\theta w}(T_{rs}) + \lambda\,\frac{U_{\theta p}(r_2,\theta_2)}{r_2} \cdot U_{\theta w}(T_{rs})\cot\theta_2$$

$$\sigma_{t\,rs} = (\lambda+2\mu).\frac{U_{\theta p}(r_2,\theta_2)}{r_2} \cdot U_{\theta w}(T_{rs}).\cot\theta_2 + \lambda\,\frac{1}{r_s}\,\frac{U_{\theta p}(r_2,\theta_2)}{\theta_2} \cdot U_{\theta w}(T_{rs})$$

$$\tau_{r\theta\,rs} = \mu\left\{\frac{\partial U_{\theta p}(r_2,\theta_2)}{\partial r_2} \cdot U_{\theta w}(T_{rs}) - \frac{V_{\theta p}(r_2,\theta_2)}{C_T} \cdot V_{\theta w}(T_{rs}) - \frac{U_{\theta p}(r_2,\theta_2)}{r_2} \cdot U_{\theta w}(T_{rs})\right\}$$

$$\tau_{\theta t\,rs} = \tau_{rt\,rs} = 0.$$

.....4

Figures 14A and 14B illustrate the effect of the free face on the principal stresses as determined by the analysis. These are plots of the principal stresses at two locations on the normal from the shot centre to the free face; σ_1 coincides with the normal and σ_2 is at right angles to the normal. In proportion, the maximum compressive segment of σ_1 near the free face decreases because of the existence of the free face while the tensile segment increases. Figures 15A and 15B are examples of compiled principal stresses for points near a free face. The angle α is zero when the direction of the principal stress σ_1 parallels the line between the charge centre and the point of computation; α is positive when σ_1 rotates in a direction tending to parallel the free face.

Assuming tensile failure of the rock, the direction of cracking in the $r\theta$ plane should coincide with the direction of σ_1 and should occur when σ_2 exceeds 130 kg/cm^2. Figure 16 shows the direction of σ_1 and σ_2 when this condition exists for a 3,400 g charge of Geogel 60%, W = 120 cm. In the region $\theta > 45°$, σ_1 curves gradually to parallel the free face, suggesting that crater profiles should be slightly convex. This effect was observed on a number of the craters. Besides the direction of principal stresses, Figure 16 shows the locus of points where σ_2 and σ_3 exceed 130 kg/cm^2. Assuming, then, that the field tensile strength of the rock is 130 kg/cm^2 within the lines (σ_2 max, σ_3 max = 130 kg/cm^2), there is a possibility that cracks caused by the explosion may reach the free face and delineate the surface dimensions of the crater. Superimposed on the stress trajectories of Figure 16 are four half-profiles for craters resulting from 3,400 g charges of Geogel detonated at a depth of 120 cm in this particular rock. Good agreement exists for a field experiment between the surface crater dimensions and those one would expect from a maximum tensile failure theory on the basis that σ_2 or σ_3 exceeds 130 kg/cm^2.

The analysis also provided data on the direct stress wave propagated into the rock mass by the two explosives used. Figure 17 is a plot of peak values of $\sigma_{r\ ip}$ and $\sigma_{t\ ip}$ for the two explosives. From this plot it can be shown that the ratio of peak radial stresses for those two explosives is 1.6 at a distance of 100 cm and 1.5 at a distance of 200 cm. The ratio of detonation pressures for these two explosives, as determined in laboratory measurements, is 1.95. However, by assuming that the acoustic coupling relationship:

$$P_{(t)} = \frac{2\, C_{\ell} \cdot \rho \cdot P_d}{D_{\rho e} + C_{\ell \rho}} \qquad \ldots\ldots 5$$

is applicable to determine imposed or transmitted pressures, a ratio of 1.68 was obtained. In this equation, P_d and P_t are the incident detonation and transmitted pressures, ρ_e and ρ are the densities of the explosive and rock, respectively, and D is the detonation velocity of the explosive. Although the evidence is not substantial, the agreement would suggest that, at least for a quick calculation, the acoustic relation provides relative peak stress levels in the vicinity of different explosive charges for the same rock.

Simulated Direct Stress Resulting From a Column Charge

Method of Analysis

Various patterns can be employed to detonate a column explosive charge. It is of considerable practical interest to know the relative effect of various methods of detonation on the resultant direct stress pattern, if optimum breakage is to be realized. On the basis of a knowledge of the direct stress resulting from detonation of an elemental charge unit, a method of analysis has been developed (4, 5) to simulate the stress distribution in the vicinity of a column charge. To date, simulation of the stress distribution resulting from single- and two-point simultaneous detonation of an explosive column has been completed, using data from the HM Geogel 60% field trials.

Results of Analysis

Charge columns 7 metres in length were considered in the analysis. These columns were simulated by 22 charge elements which in diagrams such as Figure 18 are indicated by location numbers (K). Principal stresses and direction were calculated on lines paralleling the axis of the charges for various distances W from the charge axis. Figures 18A and 18B are plots of location number K versus peak compressive value of PS 1 and peak tensile value of PS 2, the principal stresses, for varions separation distances W with single-point detonation at K = 1. Figure 19 is a companion plot indicating the direction of principal stress when these maximum values have been attained. A negative angle in this plot indicates deviation from the normal towards the charge column in the direction of flow of the detonation front in the column. Figure 20 is a similar plot to Figure 18 but with the peak principal stresses shown for double detonation (with second detonation points of K = 6, 8 and 10) as well as for single detonation. Only one separation distance has been considered in Figure 20, W = 2.5 metres. Figure 21 is a companion plot to Figure 20, showing principal stress directions at peak values. Figure 22 shows the principal stress wave shapes for PS 1 and PS 2, at various locations, for single-point and simultaneous two-point detonations, W = 2.5 metres.

From Figure 18 it is evident that towards the terminal end of a detonating column charge, peak stress in the surrounding rock mass is highest. It is evident from Figure 20 that, in terms of uniformity of peak stress along the explosive column, suitable two-point detonation can produce a considerable improvement. Comparison of Figure 19 with Figure 21 will show that there is little modification in the direction of principal stress at peak values with the various detonation patterns. From Figure 22 it is seen, by comparison with similar wave shapes for single-point detonation, that the increase realized in the peak value of PS 1 in the vicinity of the lower end of the charge column is achieved at the expense of pulse width. The effect of double detonation in this example has been to adjust principal stress wave shapes PS 1 and PS 2, in the area surrounding the initiation section of the charge column, in a manner which improves stress conditions for rock breakage. However, where benches are involved, either two- or single-point bottom initiation of a column charge would appear to have advantages over top initiation. First, the explosive acts as its own stemming material, optimizing any gas effect associated with rock throwing or breakage. Secondly, peak stresses are developed normal to the face in the lower section, optimizing initial tensile breakage as a result of stress wave reflection. Bottom detonation also means that the rock mass forming the bench slab to be blasted is undercut. As detonation proceeds up the column charge with more oblique incidence of the principal stress on the original free face, a second face is provided as a result of undercutting, to which the rock can break. At no time, with bottom detonation, is the principal stress in the vicinity of the free face "pointed" to a continuous elastic mass such as the floor; it is always pointed to a free face.

Conclusions

The radii of the craters seem to be consistent with the calculated stresses and with the use of maximum tension as the failure criterion for the rock material. The results indicate that, although σ_2 (the tensile stress acting in the vertical plane) is probably decisive in shaping the crater, the projection up to the ground surface of the locus of points of σ_3 (the tensile stress acting horizontally), which indicates the extreme lateral position when the tensile strength of the rock is exceeded, best defines the crater radii. It follows from this analysis that a large zone probably exists in the ground around the lower part of the crater, where tensile fractures exist.

The studies also indicated that relative stress levels in elastic rock masses resulting from detonating contained charges can be roughly determined from the dynamic properties of the rock and explosive by use of the acoustical coupling relationship. Further experiments, however, are required for absolute verification.

The limited agreement achieved with this method of analysis, between predicted and actual crater dimensions, provides some justification for using this method of analysis for simulating the stress distribution in the elastic zone around explosive charges of various geometrical shapes. With this substantiation, a study of the stress distribution surrounding column charges was undertaken. From the initial results of this study, it would appear that, to obtain uniformity of peak stress, two-point simultaneous detonation of a column charge is preferable to single-point detonation.

Further field trials are required to augment the data presented here. Larger shots are required to test the effect of scale and of gross structural features. Field work is also required, to verify some of the conclusions concerning column charges that have been arrived at purely analytically. It would be desirable to develop, on the basis of explosive and rock properties, a method of predicting the absolute stress levels that are produced in a rock mass by the detonation of a charge; this method would replace the present methods, which involve an elaborate field experiment.

Acknowledgments

The authors would like to acknowledge the technical assistance provided during the various studies by F. Kapeller, A.V. St. Louis and P. Larsen, of the Mines Branch.

The field study was supported in a generous manner by the Iron Ore Company of Canada. We would like to acknowledge particularly the support the project received from D. Selleck and Dr. A. Bauer*, of the Iron Ore Company of Canada, and B. Pryor of the Quebec North Shore and Labrador Railway.

Financial assistance was provided by the RCAF and the USAF.

* Now with the Department of Mining Engineering, Queen's University, Kingston, Ontario.

References

(1) Larocque, G.E., Kapeller, F., and Darling, J.A.
1966: Système de détermination à distance de la vitesse de détonation de fortes charges explosives, Explosifs, No. 3.

(2) Attwell, P.B.
1963: Dynamic Fracturing of Rocks, Colliery Engineering, Part 1, May 1963, pp. 203-210; Part 2, June 1963, pp. 248-252; Part 3, July 1963, pp. 289-294.

(3) Sassa, K., and Ito, I.
1965: Dynamic stresses induced within rock in case of blasting on one free face. Presented at the Seventh U.S. Rock Mech. Symp., Penn. State Univ., July.

(4) Larocque, G.E.
1966: Stress distribution produced in a continuous elastic medium by detonation of a column charge of explosive at one end, Divisional Report FMP 66/120-MRL (unpublished), Mines Branch, Ottawa.

(5) ————
1966: Stress distribution produced in a continuous elastic medium by two-point detonation of a column charge of explosive, Divisional Report FMP 66/131-MRL (unpublished), Mines Branch, Ottawa.

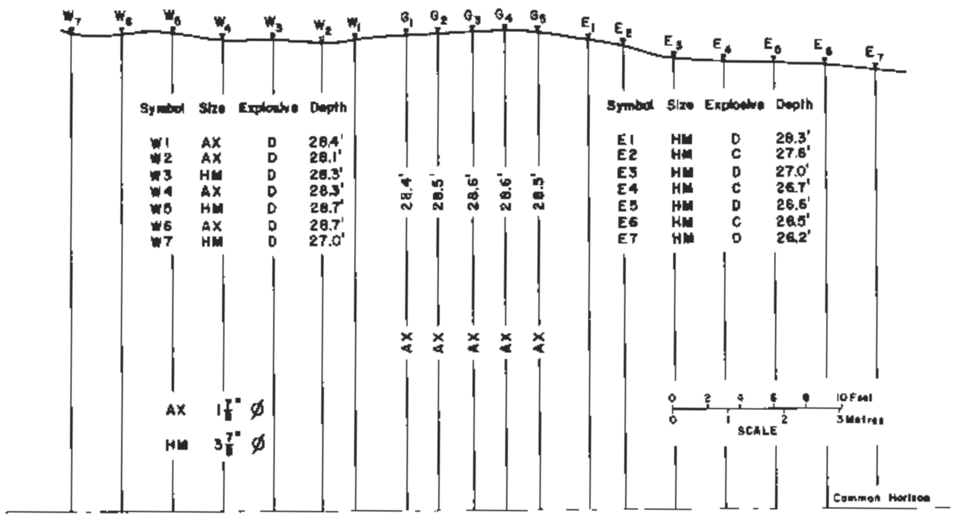

Figure 1. Section diagram of linear array test site, locating gauge and shot holes.

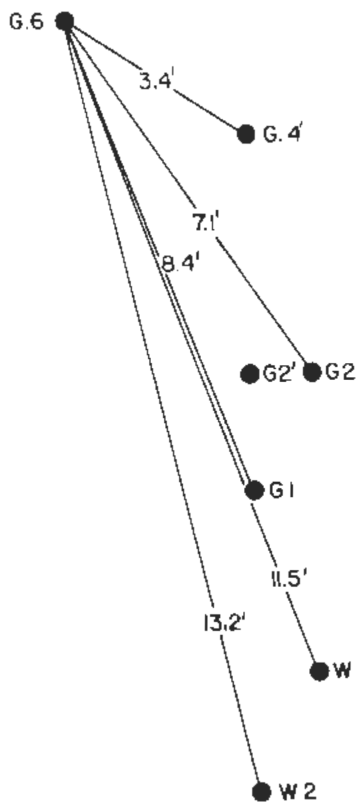

Figure 2. Plan diagram of shear array arrangement.

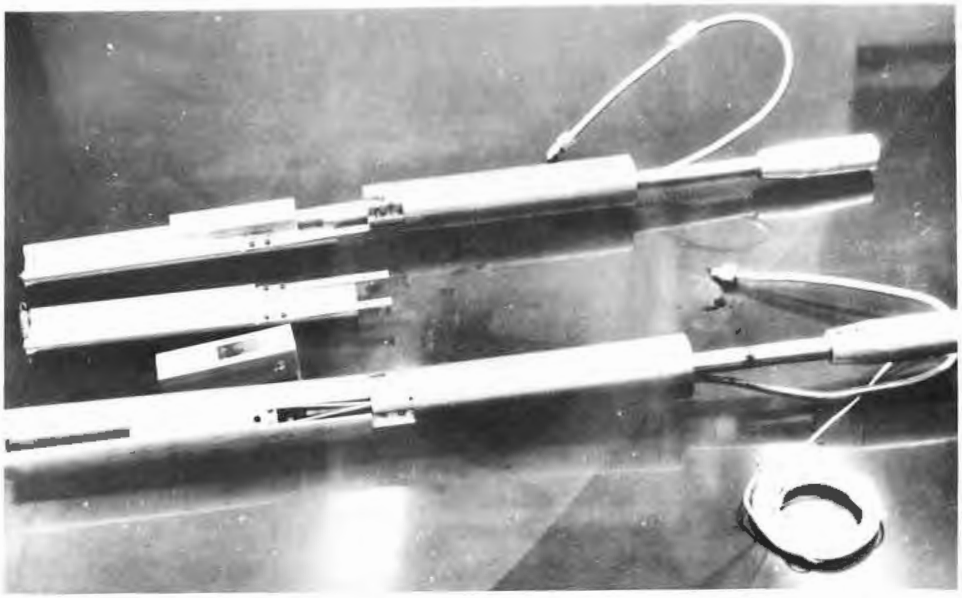

Figure 3A. Photograph of accelerometer mounting assembly assembled and disassembled.

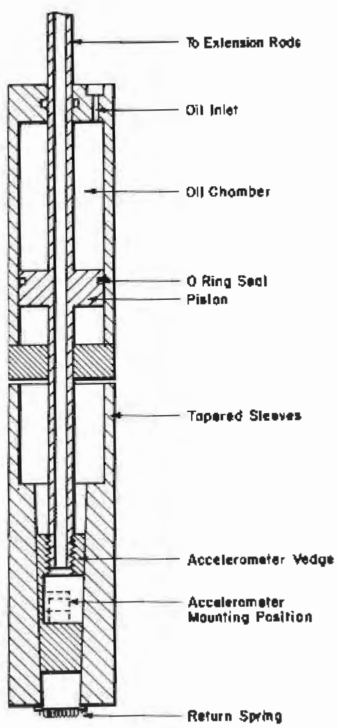

Figure 3B. Section diagram of accelerometer mount assembly.

A

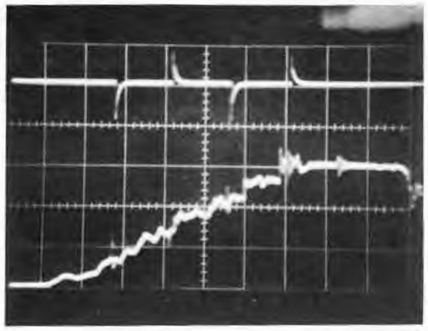

Without foil
(5 μsec/cm, 5V/cm)

B

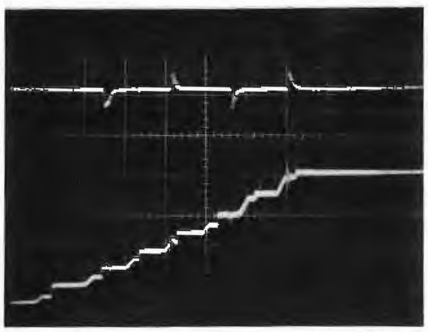

With foil
(5 μsec/cm, 5V/cm)

C

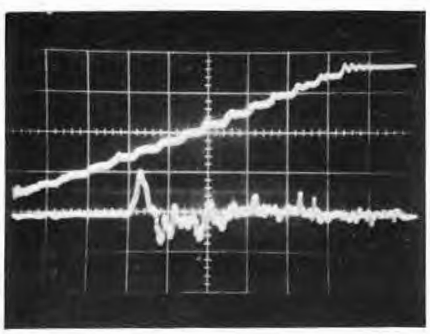

Field test shot E 4.2 250 ft
300 ohm twin lead (10 μsec/cm, 5V/cm)

Figure 4. Photographs illustrating the effect of foil covering on the step waveform of current probes; also a typical field record.

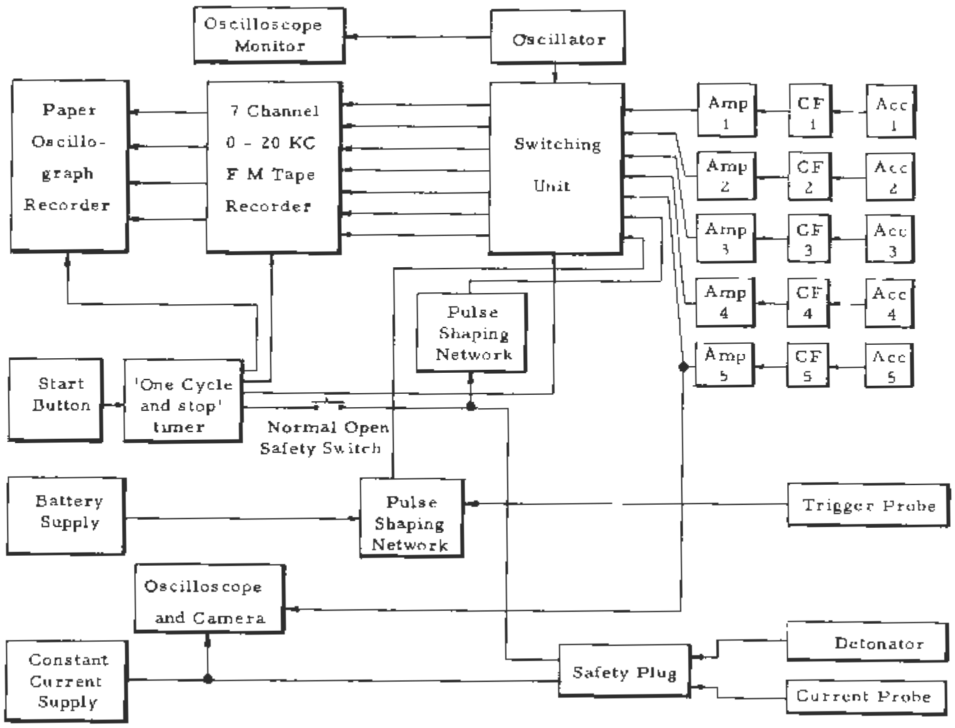

Figure 5. Block diagram of recording system.

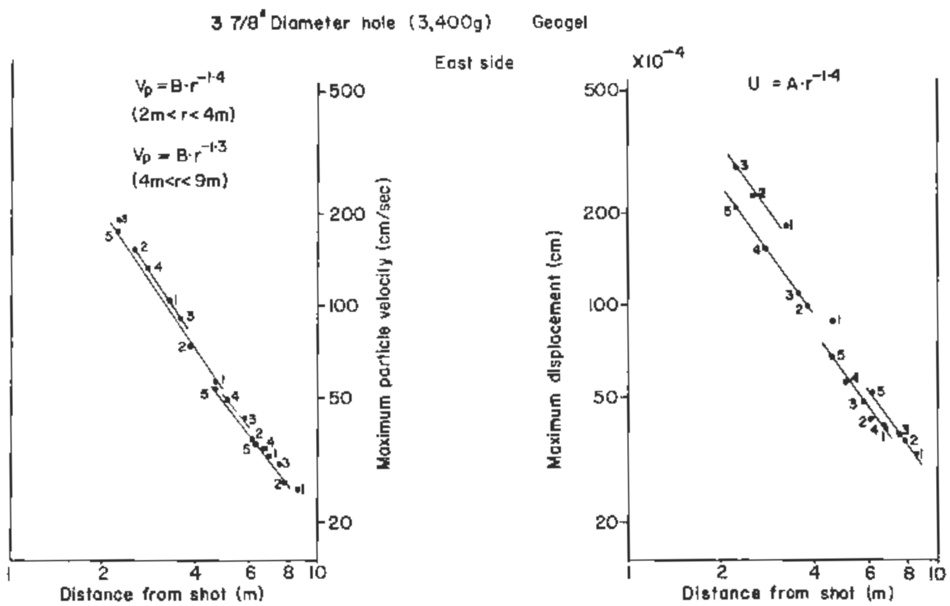

Figure 6. Logarithmic plots of maximum particle velocity and maximum displacement against distance from shot point, for 3,400 g cartridge of Geogel 60%.

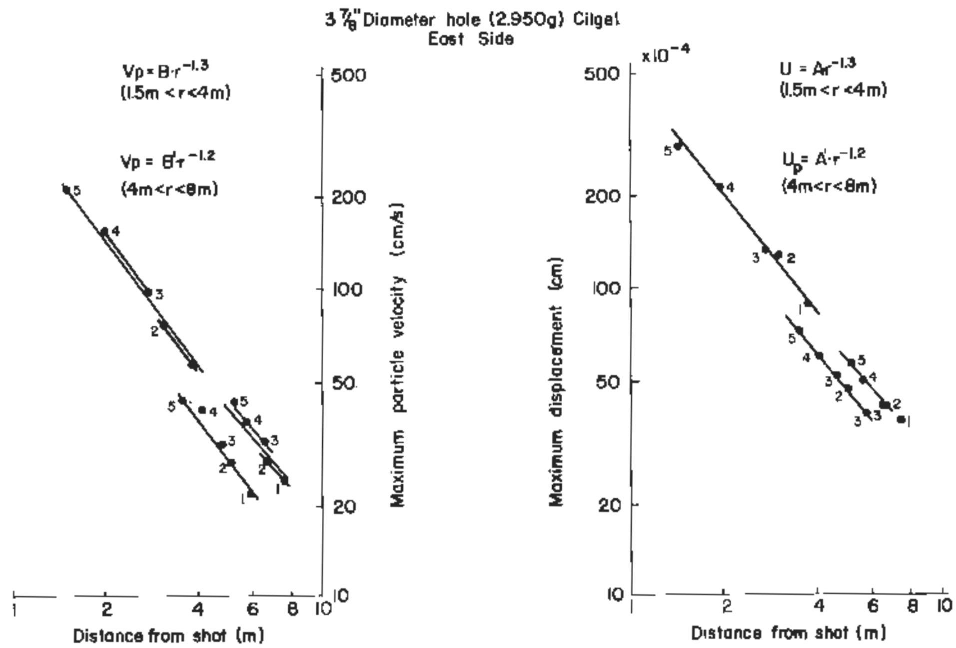

Figure 7. Logarithmic plots of maximum particle velocity and maximum displacement against distance from shot point, for 2,950 g cartridge of Cilgel B 70%.

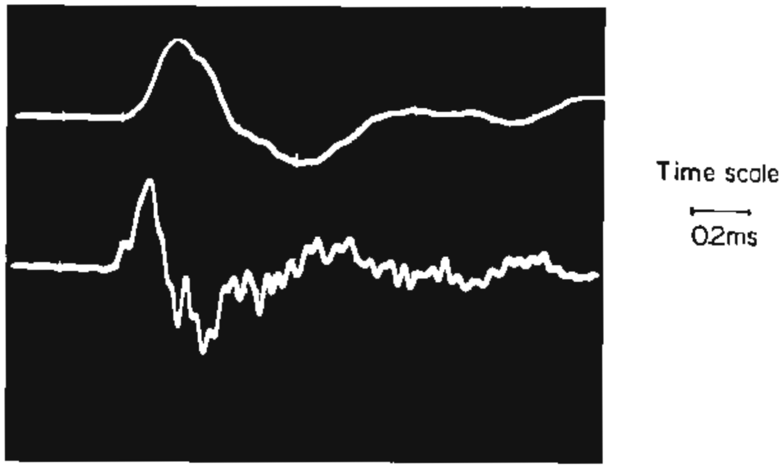

Upper beam: Particle velocity
Lower beam: Particle acceleration

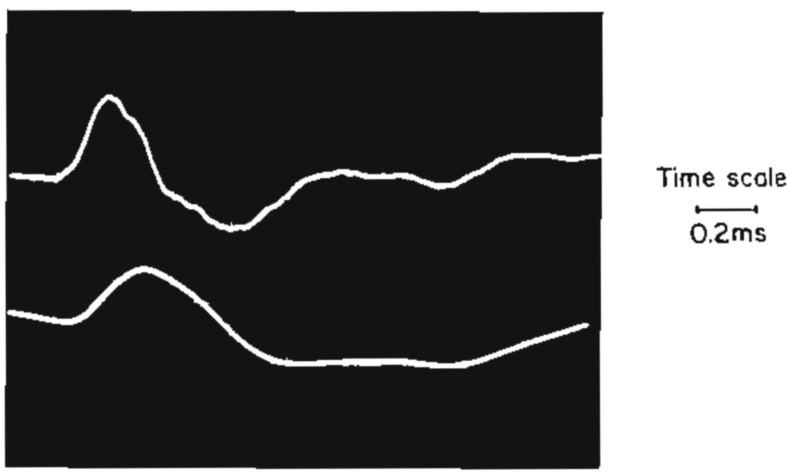

Upper beam: Particle velocity
Lower beam: Displacement

Figure 8. Examples of oscillogram caused by 2,950 g Cilgel B 70% at r = 5.8 metres.

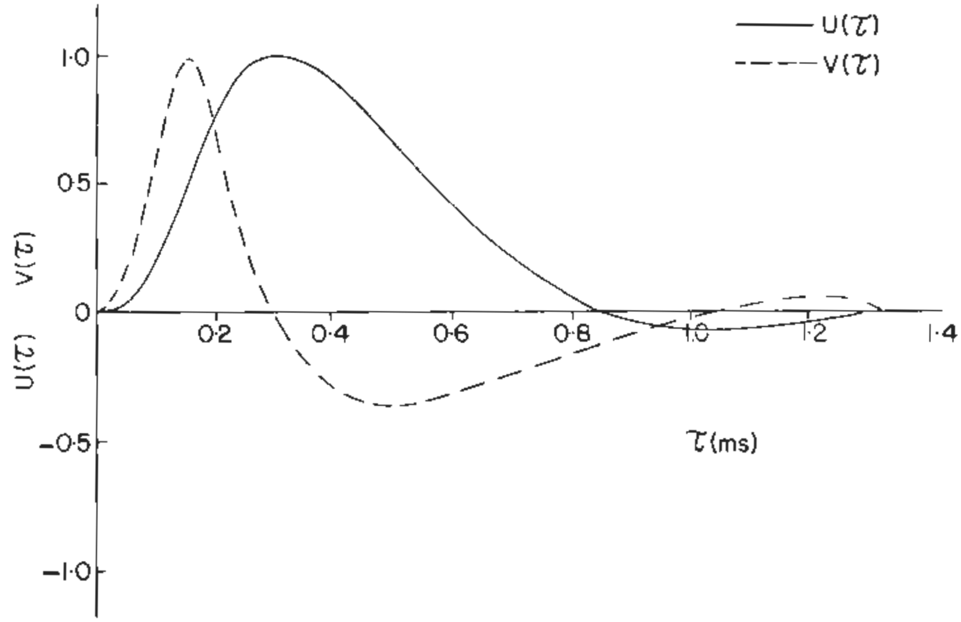

Figure 9. Smoothed wave shapes caused by explosion of 3,400 g cartridge of Geogel 60% at r = 300 cm.

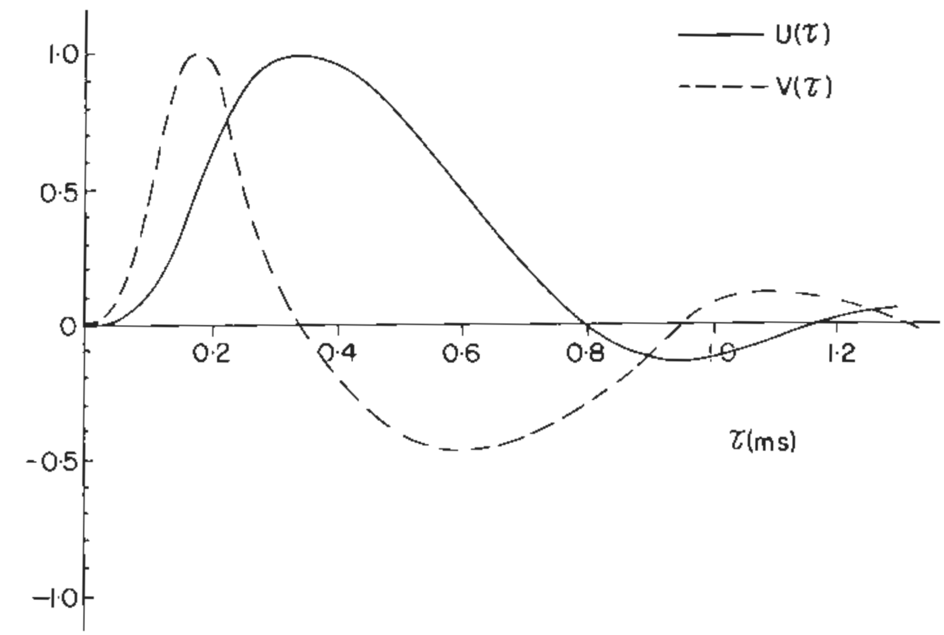

Figure 10. Smoothed wave shapes caused by an explosion of 2,950 g of Cilgel B 70% at r = 200 cm.

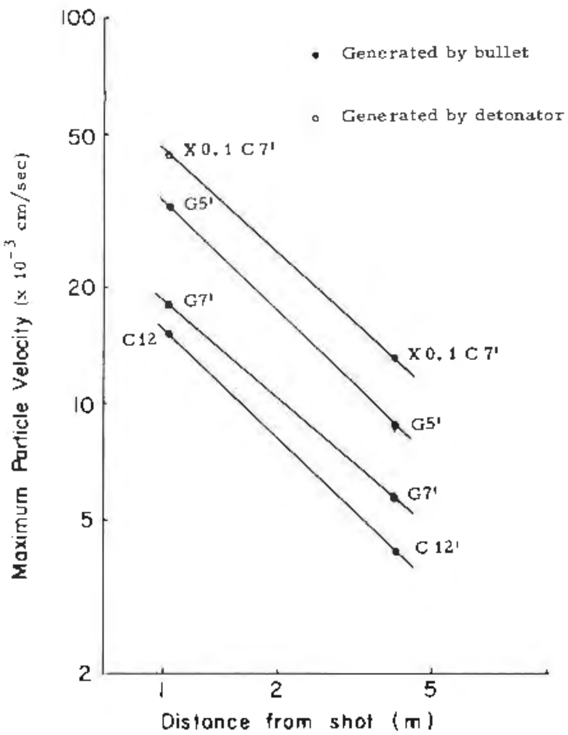

Figure 11. Logarithmic plot of maximum particle velocity caused by shear wave against distance from shot point.

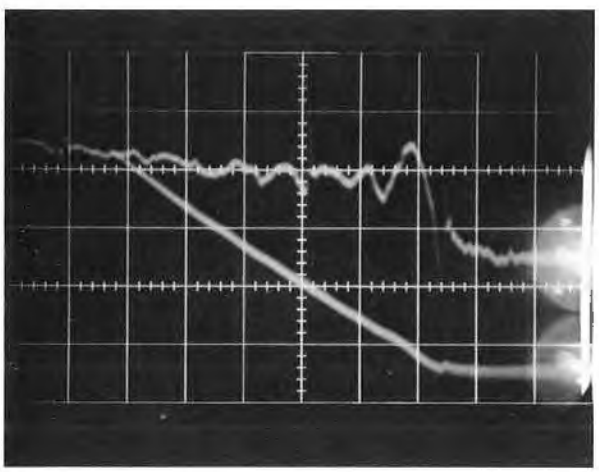

Figure 12. Typical displacement and particle velocity versus time record for magnetite specimens (sweep setting 20 μsec/cm, lower beam displacement record).

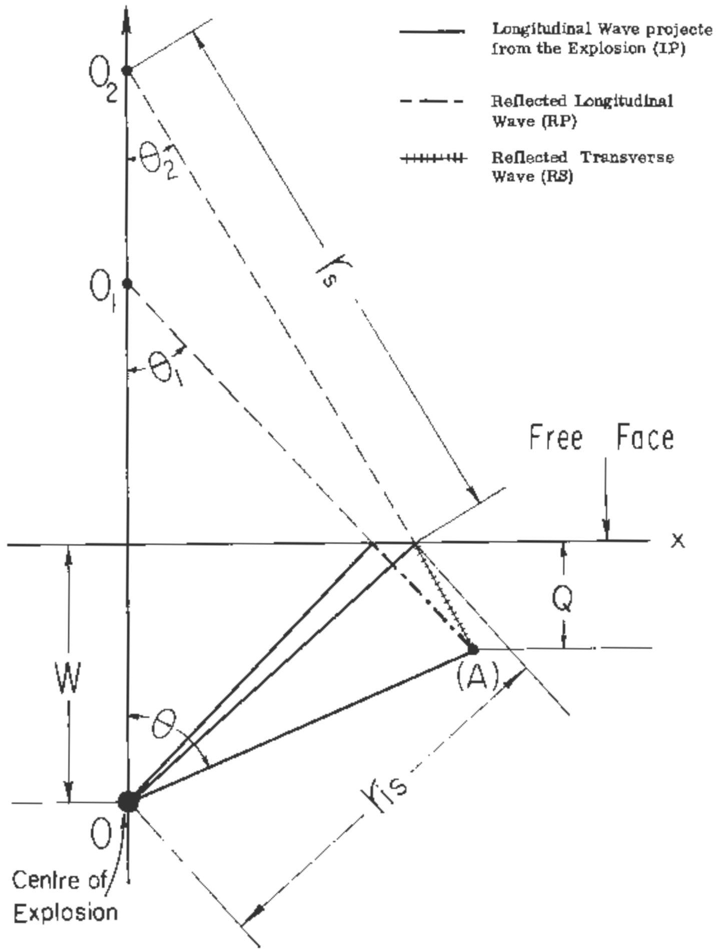

Figure 13A. Spherical coordinate adopted for analyzing the stress near the free face.

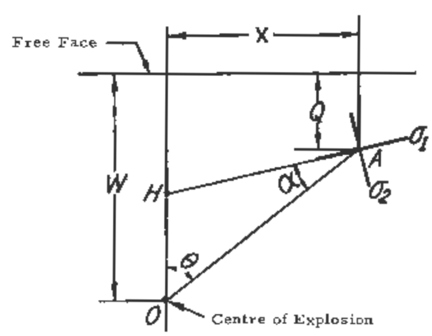

Figure 13B. Explanation of a.

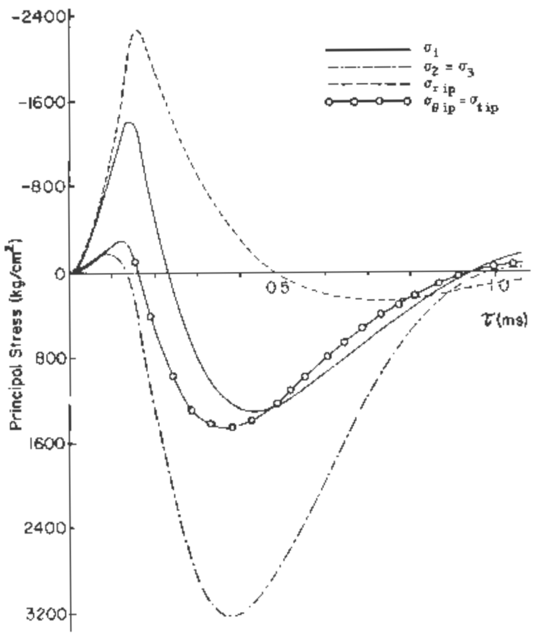

Figure 14A. Principal stresses and the stresses caused by IP at Q = 20 cm, X = 0, for the case of W = 100 cm. (3,400 g Geogel 60%).

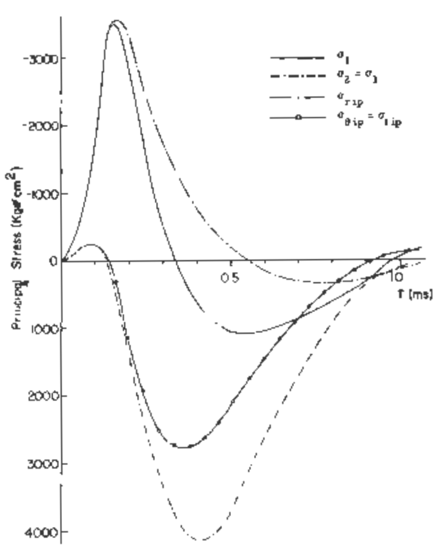

Figure 14B. Principal stresses and the stresses caused by IP at Q = 40 cm, X = 0, for the case of W = 100 cm. (3,400 g Geogel 60%).

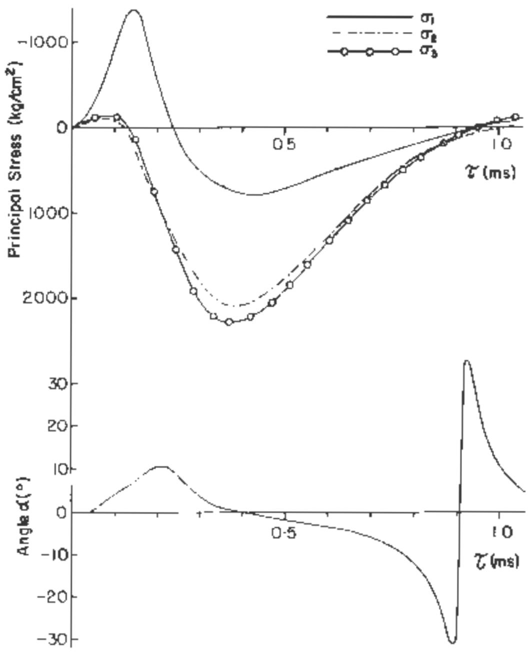

Figure 15A. Principal stresses and direction at Q = 20 cm, X = 40 cm, for the case of W = 100 cm. (3,400 g Geogel 60%).

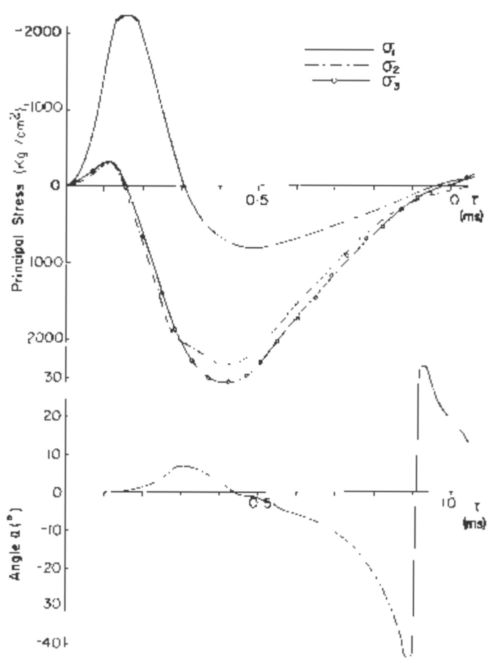

Figure 15B. Principal stresses and direction at Q = 40 cm, X = 46 cm, in the case of W = 100 cm. (3,400 g Geogel 60%).

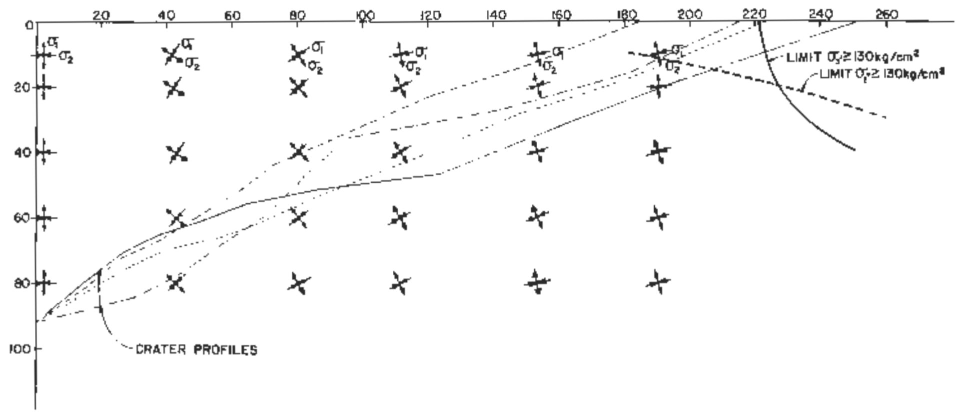

Figure 16. Directions of principal stresses when the tensile value of σ_2 attains 130 kg/cm^2 for 3,400 g Geogel 60%. W = 120 cm.

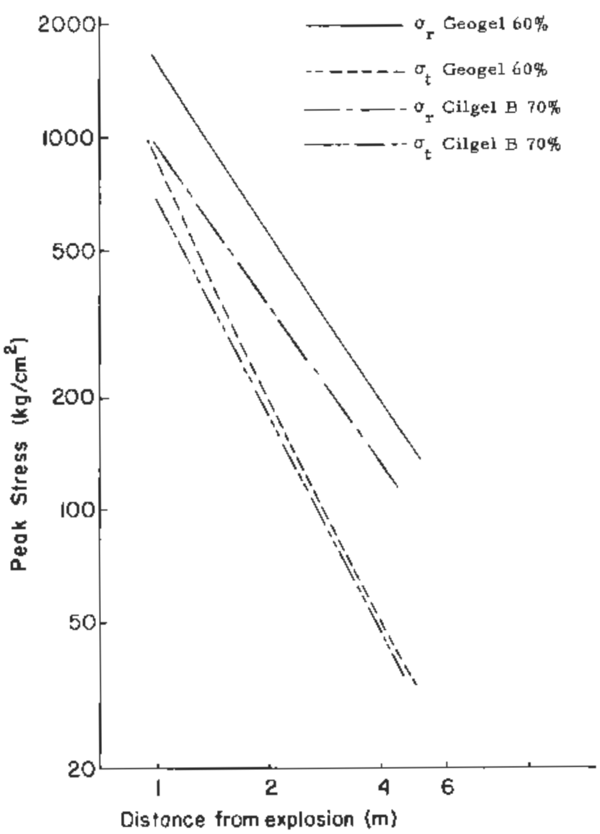

Figure 17. Logarithmic plot of peak values of σ_r and σ_t versus distance for 3,400 g charges of Geogel 60% and 2,950 g charges of Cilgel B 70%.

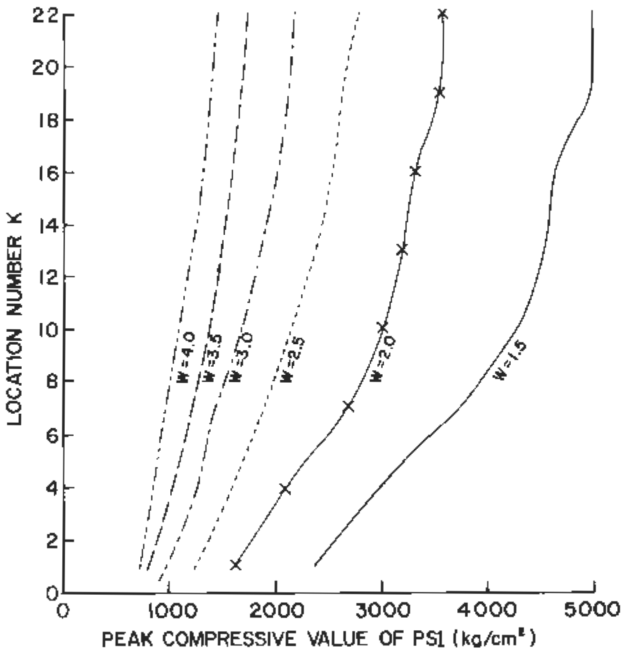

Figure 18A. Location number K versus peak compressive value of PS 1.

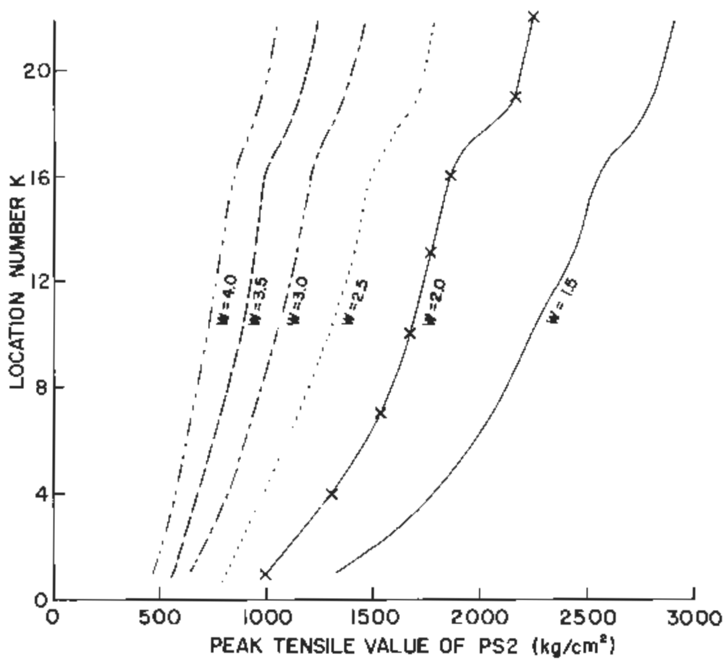

Figure 18B. Location number K versus peak compressive value of PS 2.

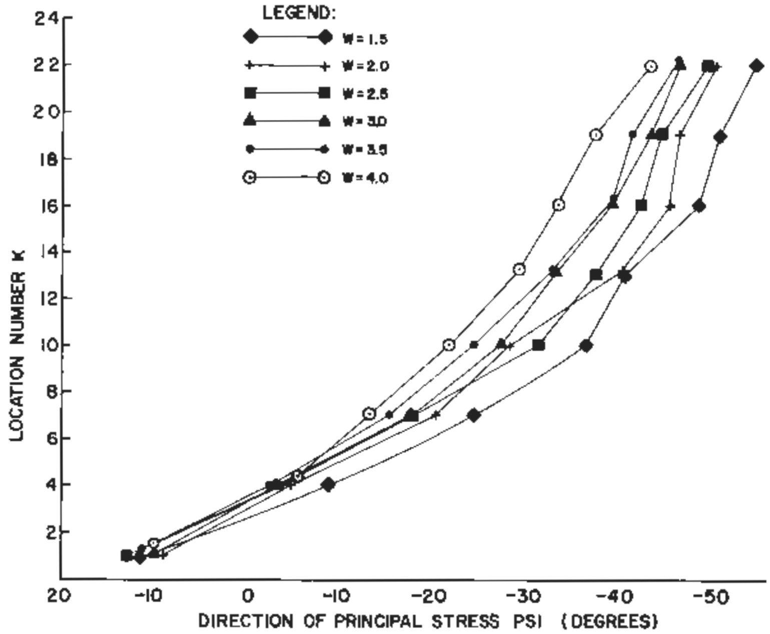

Figure 19. Location number K versus direction of principal stress PS 1 at peak compressive value for various values of W.

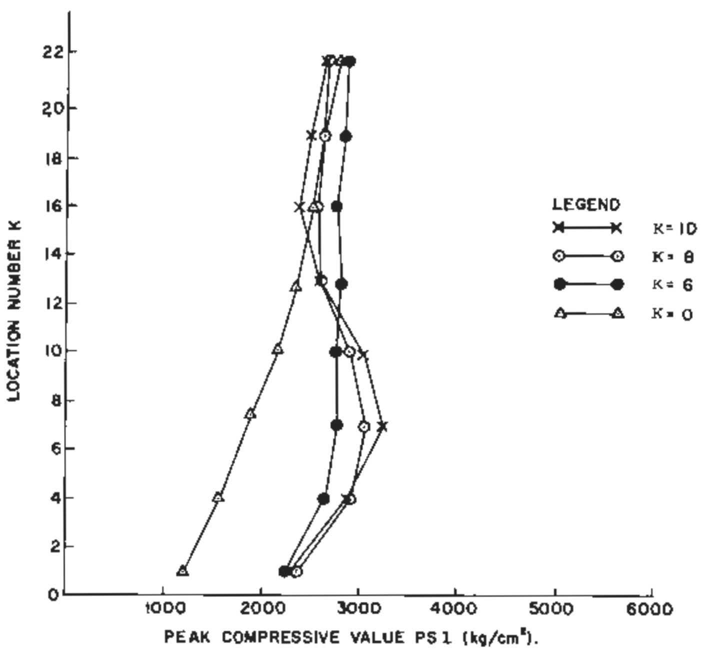

Figure 20A. Location number K versus peak compressive value of PS 1. W = 2.5 metres.

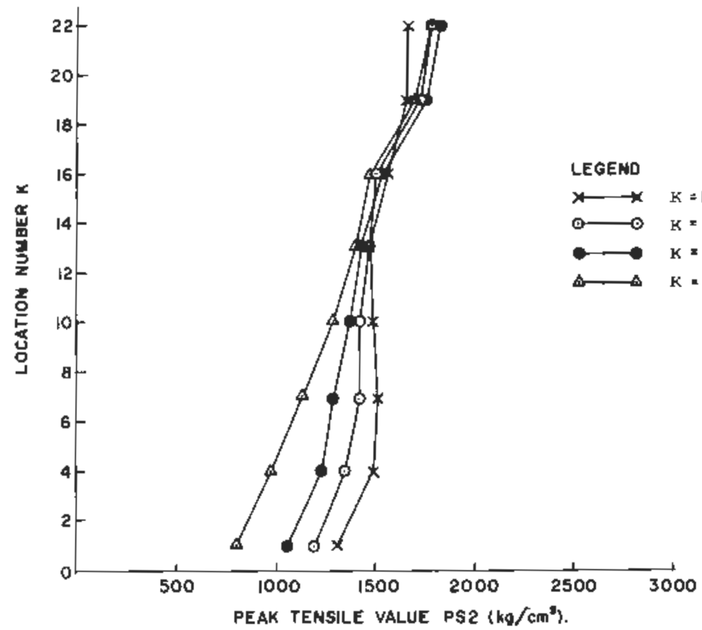

Figure 20B. Location number K versus peak tensile value of PS 2. W = 2.5 metres.

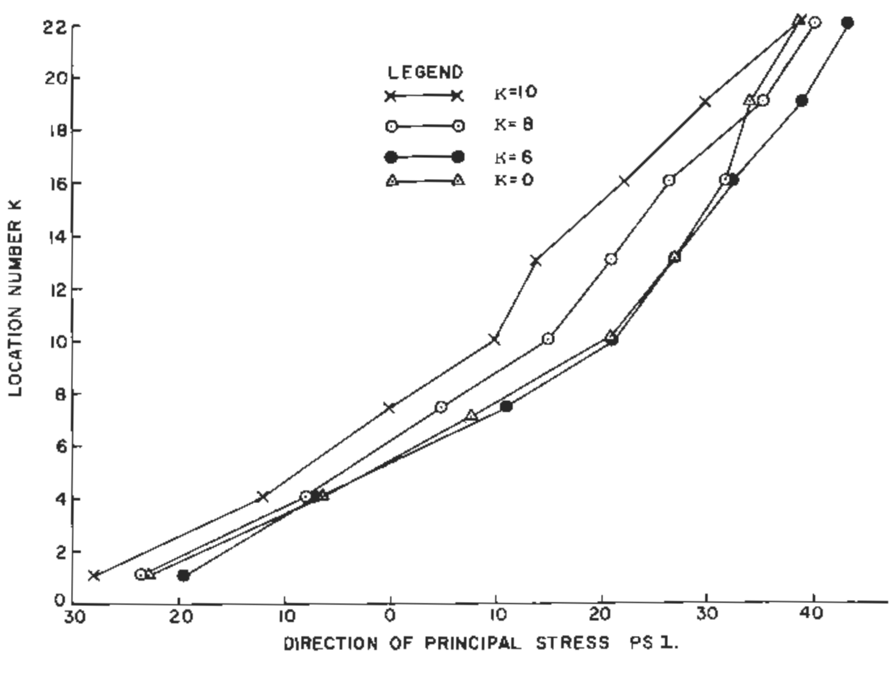

Figure 21. Location number K versus direction of principal stress PS 1 at peak compressive value for various second simultaneous detonation points. W = 2.5 metres.

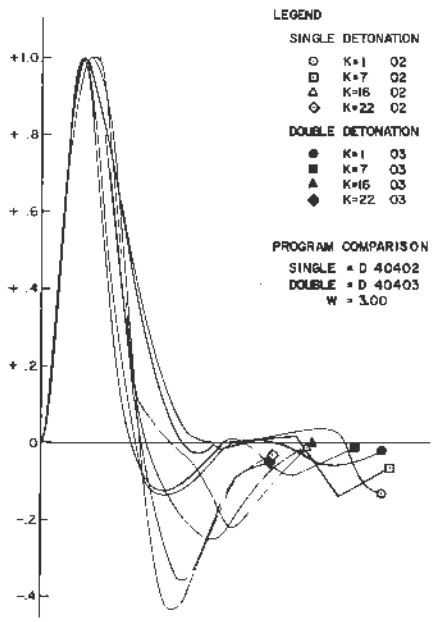

Figure 22A. PS 1 waveform for single detonation at K = 1 and double detonations at K = 1 and K = 8, at various computational points K. W = 3.00 metres.

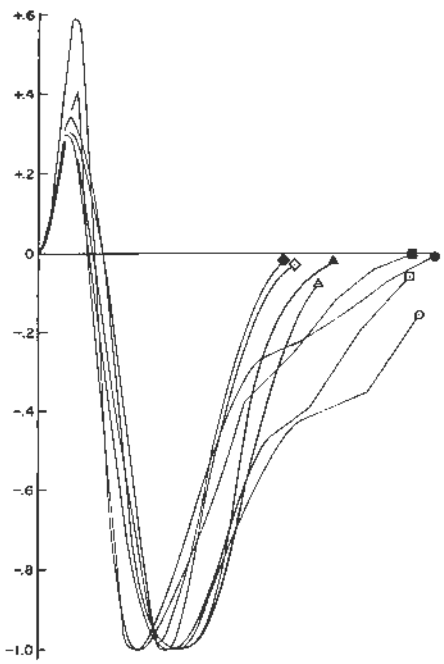

Figure 22B. PS 2 waveform for single detonation at K = 1 and double detonations at K = 1 and K = 8, at various computational points K. W = 3.00 metres.

THE EFFECT OF STOPING ON THE STABILITY OF A REMOTE PRE-EXISTING TUNNEL

*W.D. Ortlepp**

Abstract

The problem of predicting damage in a pre-developed tunnel influenced by stoping, is considered in general terms and illustrated by means of a stress analysis of a specific case.

Knowledge of the stress distribution and of the mechanics of fracture initiation, is shown to be useful, but not sufficient for the prediction of all types of damage. The deficiencies in present knowledge are outlined.

However, certain major decisions were made more readily and with more confidence than would have been possible without the theoretical analysis.

Introduction

The support and layout of tunnels and other long excavations of roughly equi-dimensional cross-section, form the most common of mining problems.

To date, the design of support has been entirely empirical and layout, with respect to the main workings and to neighbouring similar excavations, has been based purely on experience. Whereas the results are often satisfactory, there is seldom any assurance that the most economical solution has been achieved. It is also commonly experienced that excavations have failed in certain instances while in others, similarly dimensioned, the support appears to be redundant.

*Rock Mechanics Engineer, East Rand Proprietary Mines, Limited.

In South Africa, rock mechanics research has been mainly orientated towards the problem of rockbursts. However, much of the fundamental knowledge so gained can be applied to the design and layout of tunnel-like excavations. Together with the results of research more specifically directed towards these latter problems, this provides some hope that the traditional approaches may soon be replaced by more systematic and objective methods.

By describing the results obtained in the analysis of a specific problem, this paper indicates the progress so far made towards this end. It also highlights some of the remaining difficulties which prevent the application of a complete rational design procedure.

Statement of the Problem

The East Rand Proprietary Mines, Limited, is the largest and deepest of the older gold mines in South Africa. The gold bearing conglomerate is one stratum in a succession of strong and massive quartzites of great lateral extent, which are inclined at 25° to the horizontal. The stoping width seldom exceeds 4 ft and dykes and faults, although quite common, do not appreciably disturb the essentially plane and continuous nature of the stoping excavations.

Of the 260,000 tons milled per month, 80 per cent is stoped at a depth greater than 8,000 ft below surface and 10 per cent from below 10,000 ft. The bulk of the total tonnage is produced from five main longwall systems.

The main access and all services to the easternmost of these systems, 'L' longwall, is provided by a single hangingwall haulage on 58 level, 8,000 ft below surface (Figure 1). The haulage is about 12 ft x 14 ft in size and is supported only by rock-bolts except for isolated portions where steel arches have been installed (Figure 2).

Unlike the main connections between the other longwalls, this haulage was developed prior to stoping of the reef below. Consequently it was inevitable that it would be subjected to increasing stresses as the 'K' east and 'L' west longwall faces converge. Since 'L' longwall produces nearly 20 per cent of the mine's total tonnage, any collapse of 58 haulage would have serious economic consequences.

Developing a new haulage through stress-relieved ground already overstoped to the north, would provide a certain but costly way of avoiding these consequences. Alternatively, considerable additional expense might be involved in modifying the stoping layout, or sequence, to minimize the damaging effects on the haulage above. These considerations and the requirements of safety, demanded that an attempt be made to assess the likelihood of collapse of 58 haulage.

The situation was without precedent as the other main connecting haulages are in the footwall and were post-developed in stress-relieved ground, usually about 250 ft below the stoped-out areas. Pre-developed footwall haulages on 68 level at a depth of 9,400 ft, about 160 ft below the reef plane, have suffered considerable damage beneath the advancing longwall. Figure 3 shows the appearance of this tunnel when re-opened after a minor burst.

Because the surrounding argillaceous quartzite is relatively weak, the damage suffered by 68 haulage affords no guide as to the nature or intensity of damage which might occur in the stronger hangingwall quartzites in which 58 haulage is situated 500 to 800 ft above the plane of stoping.

The lack of suitable experience to guide empirical decisions in this instance, made it necessary to adopt a more theoretical approach to the analysis of this problem.

Validation of the Elastic Approach

The theoretical behaviour of quartzites of the South African gold mines has been established by comparing displacements observed underground with those expected from elastic theory - Cook et al. (1). One such comparison was based on observations made on 58 haulage.

Since February, 1962, precise levelling of 23 rock-bolt benchmarks anchored at a depth of 8 ft in the haulage roof (Figure 4), has provided a measure of the vertical differential movement of the rock mass containing the haulage. The changes in elevation observed at 5th July, 1964, and at 23rd October, 1966, are compared with the theoretical changes in elevation of several of the benchmarks (Figure 5). All changes are shown relative to benchmark 15 which is assumed to have behaved according to theory. The detailed history of observed displacements, relative to this benchmark, are shown in Figure 6 together with the corresponding theoretical displacements.

The theoretical displacements were computed from convergence data obtained from the electrolytic analogue described by Salamon et al. (2). The following assumptions were made: -

1. The original vertical stress was equal to the superincumbent load.

2. The horizontal to vertical stress ratio was 'k' = 0.2.

3. The Young's modulus was 10^7 psi and the Poisson's ratio 0.16.

These latter values are typical of the moduli obtained from the testing of small specimens of E.R.P.M. quartzite. Measurements of "convergence" were confined to the areas shown in Figure 4, but the correct boundary conditions were obtained by recognizing, in the analogue model, the existence of all nearby excavations and the limitation imposed upon the convergence distribution by the original stoping width of 4 ft. In addition, the stress gradient associated with inclined excavations was taken into account.

The qualitative agreement is good and quantitative discrepancies are appreciable only at benchmarks 1, 6 and 23. These differences are not easily explained but may be because of: -

a. a real variation in elastic modulus of the rock mass,

b. errors in the stoping widths assumed for the earlier mined portions of K and L longwalls, or

c. variations in the primitive stress distribution.

Measurement of the absolute stress in rock is a difficult process and some uncertainty still attaches to the rather meagre results so far obtained in South African gold mines. However, the indications are that the vertical stress is approximately equal to that, due to the weight of the overburden, and the horizontal components are some fraction of this value.

The magnitude of the vertical displacements are largely dependent upon the magnitude of the original vertical stress and on the value of Young's modulus. The fact that the vertical components are not sensitive to variations in the horizontal primitive stress is demonstrated in Figure 7 where the displacement components for 'k' ratios of 0.1, 0.2 and 0.4 are shown.

The good correspondence between the observed and theoretical displacement may thus be regarded as sufficient proof of the essentially elastic nature of the rock mass behaviour and of the validity of the assumptions regarding Young's modulus and the value of the vertical component of the original stress. It does not, however, throw any light on the values of the horizontal primitive stresses.

The Future Stress Distribution

It was felt that the use of the analogue for the prediction of the stresses that would be induced by the mining of the abutment between K and L longwalls, could be justified provided that the lateral stresses were interpreted with a certain amount of latitude.

The theoretical stress field was determined from the convergence distribution measured on the analogue, in the same way as the elastic displacements were determined. The same constants were used, the same assumptions were made and the same boundary conditions prevailed.

The policy of slightly underhand longwall mining, where individual stope faces are maintained in line and advance in the strike direction at approximately 20 ft per month, leads eventually to the development of a narrow peninsular abutment whose peak moves gradually down dip. Leaving small island remnants such as I and II in Figure 8, where low gold values exist, has been found to give temporary respite from the acute difficulties associated with the mining of the peak. Because of intensive faulting, dykes and low gold content, it was planned to leave another such remnant at III. Leaving the dyke intact above this remnant and so avoiding the considerable difficulties and cost inevitably associated with mining of large dykes, appeared as a very desirable alternative possibility.

Accordingly, two alternative configurations for June, 1967, were recognized in the analogue model of the future mining outlines. Figure 8 shows the five configurations for which the convergence distributions were measured to yield, after digital computation, the future stresses at points A to H on 58 level, and J to L on 68 level.

The principal stresses at each point were evaluated for three values of the original vertical to horizontal stress ratio 'k', viz 0.1, 0.2 and 0.4. The variation, along 58 haulage, in the major principal stresses σ_3 and the minor principal stresses σ_1, are shown in Figure 9 for a 'k' ratio of 0.2. The stresses at F, G and H relate to the "dyke intact" alternative, while the more complete stress profile through A to F, indicates the stresses that would develop as a result of removing the dyke in the course of mining out the peak symmetrically.

The corresponding stress changes at points J, K and L on 68 level haulage are shown in Figure 10. For the sake of clearer presentation the minor stresses have been plotted to a scale twice as large as that used for the major principal stress.

As was the case with the various displacement components, the major, near-vertical principal stresses are insensitive to changes in the k ratio while the values of the minor, near horizontal principal stresses are very dependent on the value of 'k'. This relationship is shown in Figure 11 for two of the points on 58 haulage.

The orientations of the principal stresses are defined, by the digital computer, in terms of direction cosiness with respect to the strike, dip and perpendicular directions of the plane of the excavation. The isometric diagram of Figure 12 shows these reef plane co-ordinate axes X, Y and Z, and the location of 58 haulage above the reef plane. The principal stresses resulting from the symmetrical stoping of the peak are shown as solid vectors and those because of the intact dyke, as broken vectors. The orientations of the principal stresses are also relatively insensitive to variations in the ratio k.

Prediction of Damage

An assessment of the damage that might occur in a tunnel requires a knowledge of the response of a relatively complicated structure to a complex stress situation. The stresses have been approximately specified for the idealized environment and, ignoring the shell of fractured rock that may exist as a result of blasting or previous stresses, the tunnel may be considered as a simple two dimensional void surrounded by solid rock.

With these simplifications the initiation of fracture may be anticipated but the mode of failure remains obscure and gives no hint as to the intensity of damage that may result.

For the prediction of fracture initiation, a "strength" criterion is necessary. It is well known that the strength of a brittle material is not a unique property of the substance but a characteristic whose value depends on the value of the stresses. The most accepted method of determining this relationship is by means of triaxial tests. These tests yield limits which can be represented as a Mohr failure envelope or, perhaps more conveniently, as a plot of the sums and differences of the principal stresses which caused failure.

The results of triaxial tests carried out by Bieniawski and Denkhaus (3), are displayed in this form in Figure 13 for: -

a. a quartzite from E.R.P.M., which is probably representative of the rock surrounding 58 haulage, and

b. a quartzitic shale similar to that encountered on 68 haulage.

Any stresses which plot above this line indicate conditions in which fractures will be initiated while those below the line will be inadequate to promote fracture.

It must be emphasized that the line represents the strength of rock which is as continuous as the small specimens from which the data were derived. If discontinuities such as faults or joints exist in the rock mass, its tensile strength will be zero and the behaviour of the material will be governed by friction only. The lowest strength of the rock mass is thus represented by a parallel line passing through the origin.

Wherever tensile stresses exist then, it is likely that fracture will occur in the rock mass. Even in the absence of discontinuities, fracture can occur if tensile stresses develop even moderate values.

Although obvious, it is perhaps necessary to emphasize at this stage, that the occurrence of fracture does not necessarily constitute a problem in mining. Moreover, fractured material retains, to some extent, the ability to resist load. In other words, its strength does not drop to zero with the onset of fracture.

The fact that fracturing, once commenced, does not proceed continuously until the void is filled by rubble, is shown by Deist (4) to be conclusive evidence that fractured rock possesses appreciable and definable strength.

The complete failure accompanying the onset of fracture in small brittle specimens, has been shown by Cook (5) to result from the energy inherently available in the resilience of conventional testing machines.

In the light of these considerations, the possibility of various types of damage may be examined.

Comparison of Alternative Mining Layouts

Whereas underground excavations cannot suffer damage without the occurrence of fracturing somewhere in the rock mass, it does not follow that fracturing will necessarily cause damage to excavations. This will probably depend on the mode of fracture, its position, velocity of propagation and on the amount of energy released.

This realization makes it difficult to compare the likelihood of damage arising in different situations even where the different stress environments are known. It becomes necessary to attempt to visualize all types of damage that may conceivably occur, and to examine each in the light of the stress situations which exist at various stages in the stoping sequence.

Fracture Initiation in the Rock Mass

The stresses determined from the analogue refer to conditions in the rock mass and ignore the modifying effect because of the presence of the haulage. Although the major principal stresses are relatively low, the minor principal stresses in the strike direction are tensile and of sufficient magnitude to permit failure to initiate in certain instances.

The sums and differences of the principal stresses at the most vulnerable point, F, on 58 haulage for June, 1966, and for June, 1967, with the dyke unmined are plotted in Fignre 13A.

This shows that the intact dyke induces tensile stresses of sufficient magnitude to cause fracture to initiate, even in a rock mass free of discontinuities, provided that the original stress ratio 'k' was 0.2 or smaller.

In the case of symmetrical stoping of the peak, fracture could initiate provided that the ratio between the original horizontal and vertical stresses was as low as 0.1.

Cook (6) has suggested that the original stress ratio cannot be less than about 0.3, and it can be argued that the bulking effect, resulting from the fracture zone developed around the stopes, causes a reduction in the induced tensile stresses. However it is equally valid to claim that the rock mass must contain sufficient discontinuities in the form of faults, dykes or joints to reduce its strength to considerably less than that shown in Figure 13. The fracture locus may even pass through the origin.

In this event fracture would occur even with 'k' ratios of 0.4 or greater; indeed fracture must already have occurred as early as June, 1966, even at points as remote as B. The fact that no noticeable damage has occurred, Figure 2, lends considerable confidence to the suggestion that fracture of the rock mass in a low stress environment does not present any danger to the haulage. This feeling is further reinforced by the disclosure in Figure 13B that stresses in the vicinity of 68 haulage are further removed from the fracture locus than are the 58 haulage stresses, and that the damage caused in 68 haulage was therefore not associated with low stress fracture in the rock mass.

Falls from the Roof

The stress concentration because of the presence of the excavation itself is generally sufficient to cause the initiation of local fracturing which commences at the surface of the walls of a tunnel.

According to theory the first fracture to develop is a tensile crack of limited depth along the centre-line in the roof of the tunnel. This feature, which has been demonstrated in models - Cook et al. (1) page 514, is stable and does not lead to deterioration of the roof. The fact that is has not been observed in tunnels in the South African gold mines suggests that it is of no practical consequence.

Fracturing in the corners of excavations is common and, combined with possible separation along pronounced bedding planes, is frequently the cause of potentially dangerous loose slabs in the roof. These are likely to represent a hazard only if insufficiently supported or, indirectly, if shaken free by the tremor from a distant rockburst or impelled into the excavation by a burst within the walls of the tunnel itself.

While the severity of these roof conditions is likely to be broadly related to the intensity of the environmental stresses, it is probably more influenced by local variables such as geology and shape of the tunnel cross-section.

Since these variables are not recognized by the analogue, the analyses do not permit a comparison of the relative merits of the alternative mining layouts in terms of the probability of roof falls.

Sidewall Slabbing

The most common form of tunnel damage occurs as pronounced slabbing of the sidewalls of the excavation.

Fairhurst and Cook (7), have suggested that these slabs are formed by the extension of Griffith flaws in the direction of the maximum principal stress. The process of slab formation thus requires that the vertical stress parallel to the sidewalls, should exceed the Griffith strength of the rock.

The formation of slabs does not necessarily constitute damage and in certain cases can be inhibited by the restraint imposed by adequate rock-bolting. However, continued increase in the vertical stress can cause damage to the haulage by promoting buckling of the slabs. A particularly dangerous situation will arise if the pressure of the bulging sidewalls displaces the legs of arches or concrete retaining walls which, in turn, are supporting large slabs of loose roof.

According to Fairhurst and Cook, stability of sidewalls is assured in a haulage of optimum shape, where the sides have been cut to a curve of suitable radius and adequately rock-bolted, provided that the vertical component of the field stress does not increase above about one-half of the Griffith strength. In the case of 58 haulage, where the rock has a Griffith compressive strength of 30,000 psi, Figure 13A, vertical field stresses in excess of 15,000 psi are thus likely to cause slabbing of the sidewalls which are insufficiently curved and inadequately rock-bolted.

Obviously the probability of this type of damage is directly related to the magnitude of the principal stress increase. Consequently the stoping sequence which results in the smallest increase, affords the best chance of survival of the haulage. Thus symmetrical stoping of the peak is preferable to leaving the dyke intact since the latter alternative imposes higher stresses on point F during June, 1967 (Figure 9). However, if the haulage is sufficiently rock-bolted to survive this period then the eventual permanent stress field after December, 1969, should not présent a threat to sidewall stability.

Rockburst Damage

Severe rockbursts in stoping areas frequently cause damage to adjacent drives, cross-cuts and haulages in the form of scattered falls of greater or lesser extent. This damage results from the 'shake-up' of potentially dangerous conditions already existing as a result of the roof fracturing or sidewall slabbing processes discussed above.

Rockbursts which are confined to tunnels and are not accompanied by violent damage in the neighbouring stopes, occur less frequently but are usually more severe. The damage shown in Figure 3 is the aftermath of one such event which precipitated a few hundred tons of broken rock into 68 haulage, over a distance of about a hundred feet.

The shape of the zone in which fracturing is initiated around a haulage subjected to some specified field stress, can be defined by a method described by Hoek (8), which involves established elastic techniques and accepted concepts. However this method does not recognize the effect of already fractured material upon the highly stressed solid which is about to fracture, nor does it describe the rate at which the fracture zone propagates.

A non-linear elastic continuum approach described by Deist (4), shows more promise. It recognizes the dynamic reaction, on the unfailed mass, of material which is fracturing and yielding in a known manner and which is all important in controlling further fracture. A reiterative computer program traces out the sequence of stress changes and displacement velocities radiating away from the tunnel void which has suddenly been created in a specified stress field.

For each point in a grid surrounding the void, the computer examines the instantaneous stress values to establish whether the rock has fractured but retains some strength, has broken and is unable to sustain any shear stresses, or has failed and then reverted to elastic behaviour. The analysis is reiterated until stability has been reached. The fracture zone shape, and its rate of change in terms of milli-seconds, can thus be determined and some estimate made of the associated energy changes.

No case-history validation of this approach has been attempted since the values of some of the constants, particularly that which describes the strain-stress behaviour of fractured rock, have not yet been experimentally determined. Furthermore, the computer program, in its present form, considers the case of a tunnel suddenly created in a specified stress field. This differs from the actual situation where an existing tunnel is subjected to an increasing stress field. For these reasons it has not been possible to compare the rockburst-damage potential of the stress situations arising along 58 haulage as a result of the different mining layouts proposed.

Conclusions

The preceding discussion has indicated that the solution of problems involving the layout of tunnels or the design of their support, is assisted by a knowledge of the stress distribution and of the mechanism governing the behaviour of the rock mass.

In South African gold mines, the rock mass has been shown to behave elastically and an analogue technique exists for the prediction of the field stresses. It is evident that, while this knowledge may be necessary, it is not sufficient to solve the crucial aspects of haulage problems. The more obvious deficiencies include: -

a. an inadequate definition of the original state of stress in the rock mass;

b. the unknown effect of the fracture zone, around the main stoping excavations, on the tensile stresses which these excavations theoretically induce in the surrounding rock mass;

c. lack of knowledge regarding the interaction between rock which is already fractured and that which is about to fracture; and

d. uncertainty as to the mode of propagation of the fracture zone, particularly in respect of the energy changes involved.

However it is reasonable to suggest that the use of rational procedures, even if they are not entirely adequate, is preferable to purely empirical approaches. Moreover, comparison of theoretical expectations with actual experience may eventually yield acceptable design criteria.

The results obtained in the analyses of 58 and 68 haulages lead to several useful conclusions.

1. It is possible to develop, at considerable cost, a duplicate haulage which will be entirely safe. However, by the time it is completed the existing 58 haulage will itself be safe, provided it survives the maximum stresses of late 1966, and the duplicate tunnel will not serve any useful purpose.

2. The increased stresses are almost uniformly distributed along a considerable length of the haulage. It would therefore be dangerous to improve the support in only a short portion of the haulage directly above the longwall peak, or above the intact dyke.

3. If part of the considerable cost that would otherwise be involved in stoping the dyke was devoted to improving the support, there is a reasonable chance that the haulage will survive the increased stresses resulting from the dyke remnant.

4. The existing island remnants I and II and the proposed remnant III are so located that they do not directly endanger the haulage.

Acknowledgments

The permission of the management of East Rand Proprietary Mines, Ltd., for the publication of this paper, is gratefully acknowledged.

Most of the displacement data presented are the result of research carried out as part of the Transvaal and Orange Free State Chamber of Mines' program of research into rockbursts and strata control problems.

References

(1) Cook, N.G.W., Hoek, E., Pretorius, J.P.G., Ortlepp, W.D. and Salamon, M.D.G.
1966: Rock mech. applied to rockbursts. J.S. Afr. Inst. Min. and Met., May, pp. 494-499.

(2) Salamon, M.D.G., Ryder, J.A. and Ortlepp, W.D.
1964: An analogue solution for determining the elastic response of strata surrounding tabular mining excavations. J.S. Afr. Inst. Min. and Met., September.

(3) Bieniawski, Z.T. and Denkhaus, H.G.
1966: The triaxial state of stress in rock. Proc. 8th Conf. of the Internat. Bur. of Rock Mech. Leipzig, November.

(4) Deist, F.H.
1965: A non-linear continuum approach to the problem of fracture zones and rockbursts. J.S. Afr. Inst. Min. and Met., May.

(5) Cook, N.G.W.
1965: A note on rockbursts considered as a problem of stability. J.S. Afr. Inst. Min. and Met., March, p. 439.

(6) Cook, N.G.W.
1962: Failure of rock around excavations. Univ. Witwatersrand, Ph.D. thesis.

(7) Fairhurst, C. and Cook, N.G.W.
1966: The phenomenon of rock splitting parallel to the direction of maximum compression in the neighbourhood of a surface. Proc. First Internat. Cong. of the Internat. Soc. of Rock Mech. Lisbon, pp. 687-692.

(8) Hoek, E.
1966: A photo-elastic technique for the determination of potential fracture zones in rock structures. Report of S. Afr. Counc. Sci. Industr. Research., M.E.G. 467, August.

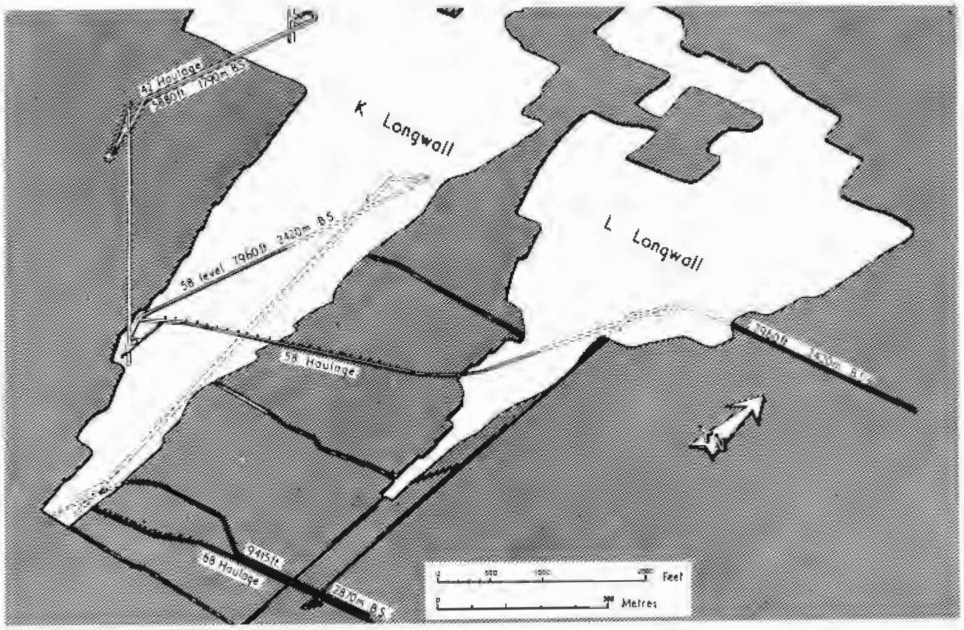

Figure 1. Isometric view of K and L longwalls, E.R.P.M. in March, 1962.

Figure 2. View east along 58 haulage in vicinity of benchmark 15, September, 1966.

Figure 3. View east along 68 haulage showing damage to sidewall and loss of roof as a result of a minor burst, May, 1962.

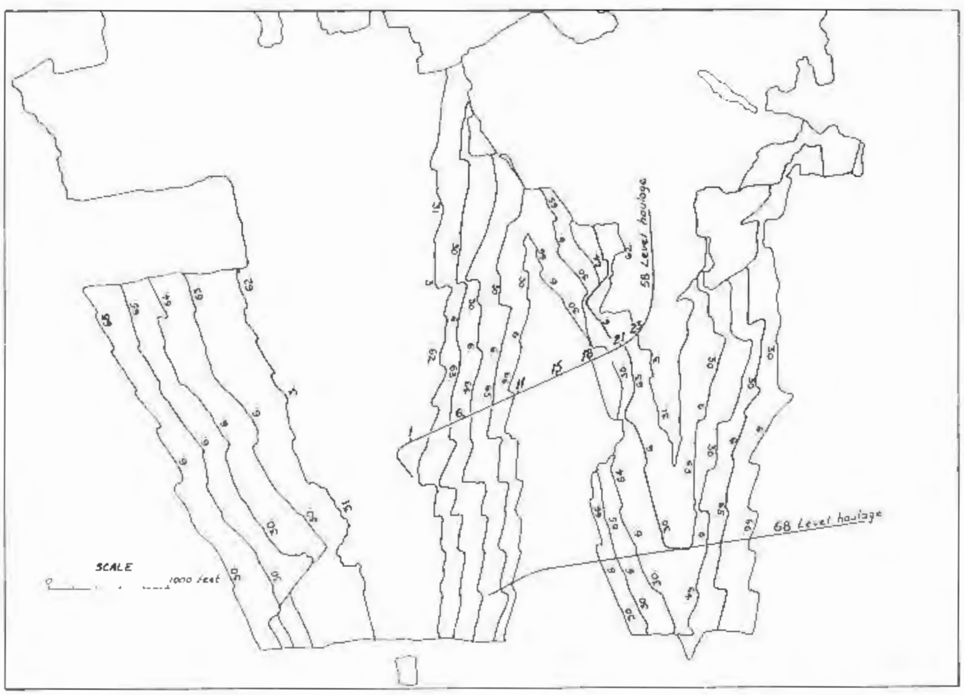

Figure 4. Reef plane projection of K and L longwalls showing the elevation benchmarks and stoping outlines for which the theoretical displacements were determined.

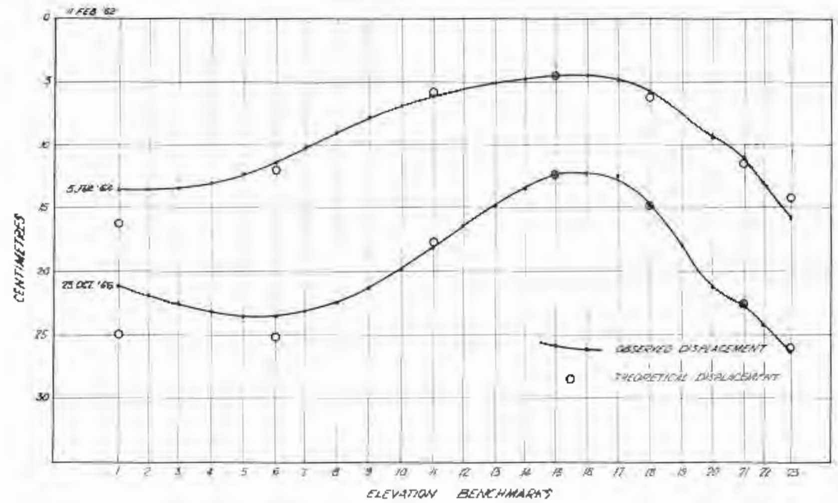

Figure 5. Comparison of theoretical and observed vertical displacements along 58 haulage.

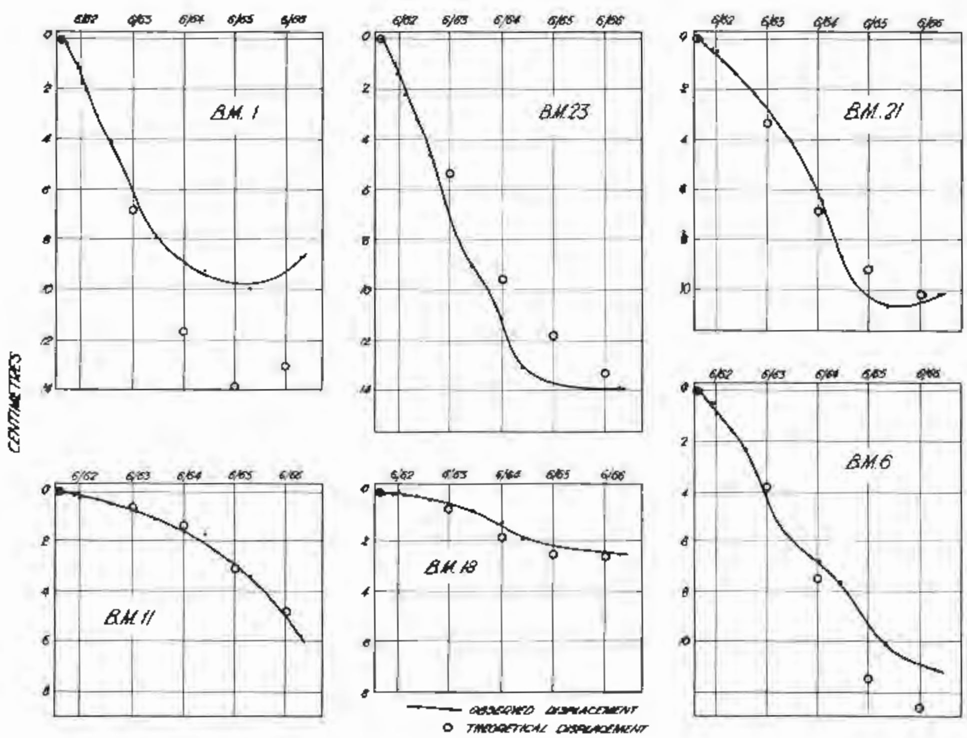

Figure 6. Theoretical and observed elevation histories of benchmarks along 58 haulage.

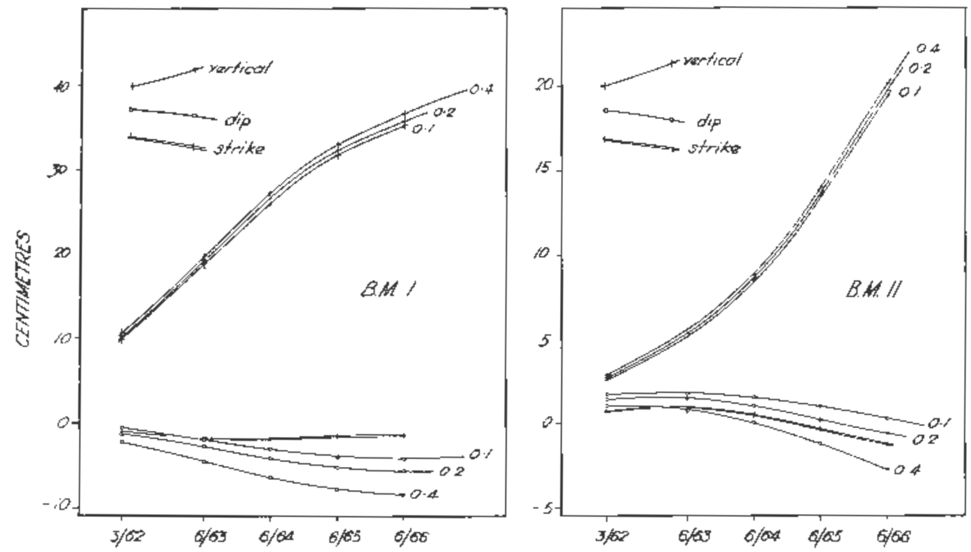

Figure 7. The effect of variation in 'k' ratio on the three components of theoretical displacements.

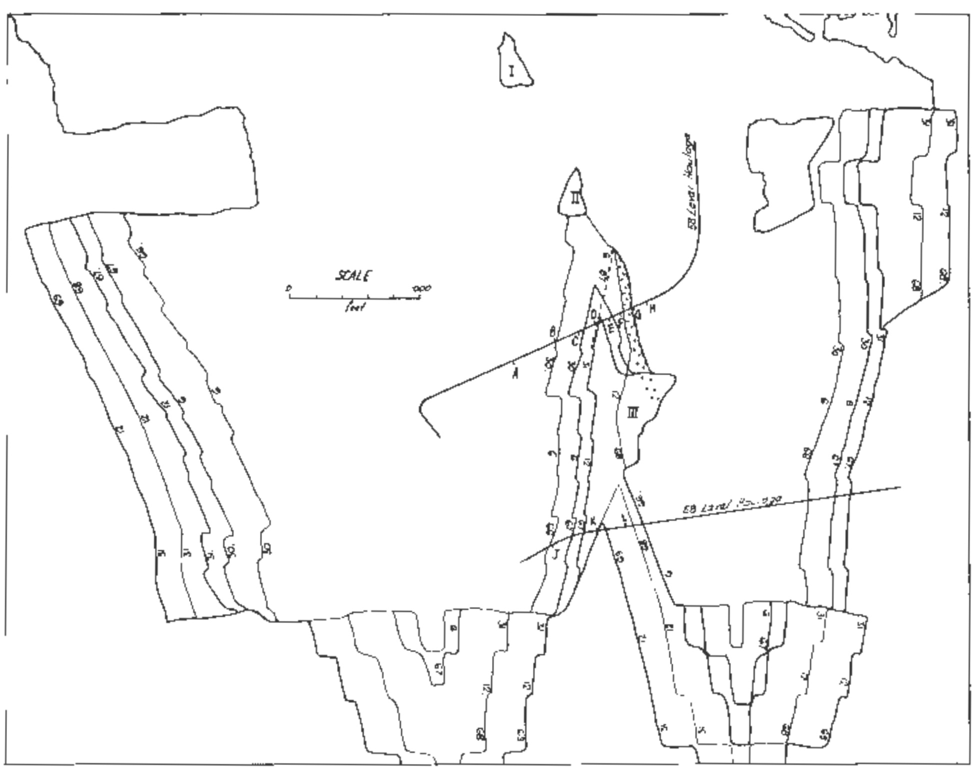

Figure 8. Reef plane projection of anticipated stoping outlines in the K and L longwalls, for which theoretical stresses were determined on 58 and 68 level haulages.

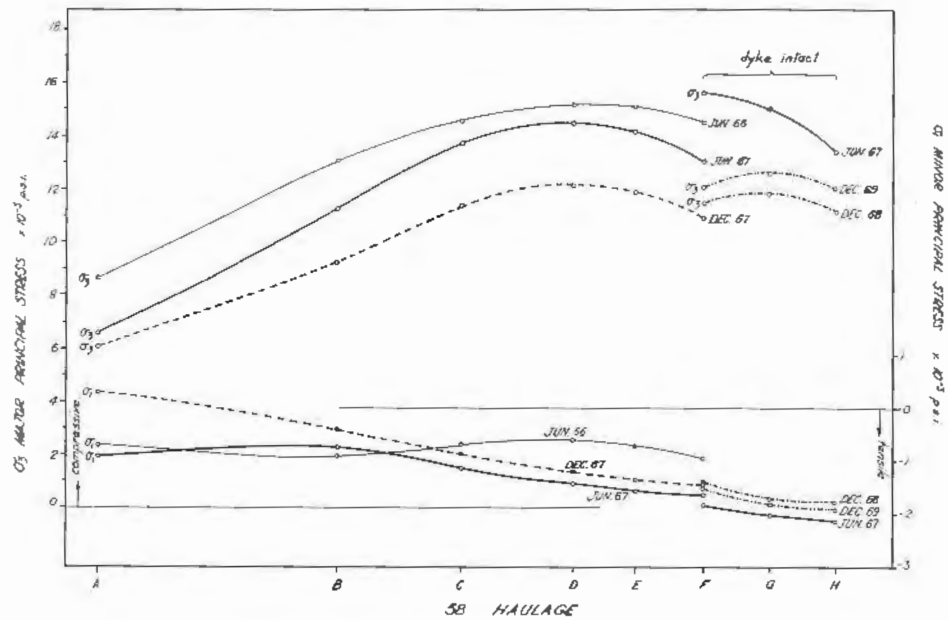

Figure 9. Profiles of the major and minor principal stresses along the line of 58 level haulage.

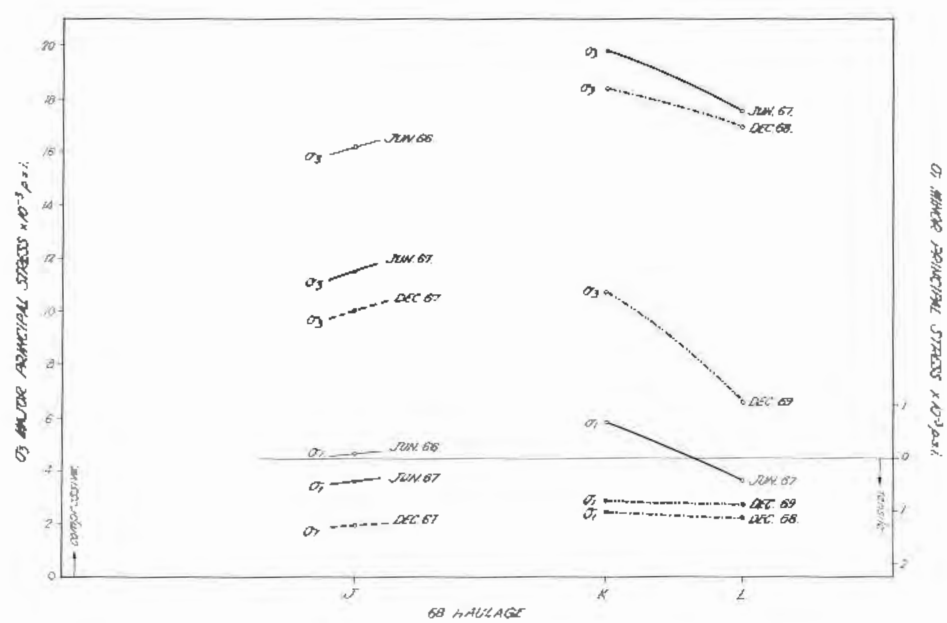

Figure 10. Major and minor principal stresses at points J, K and L on 68 level haulage.

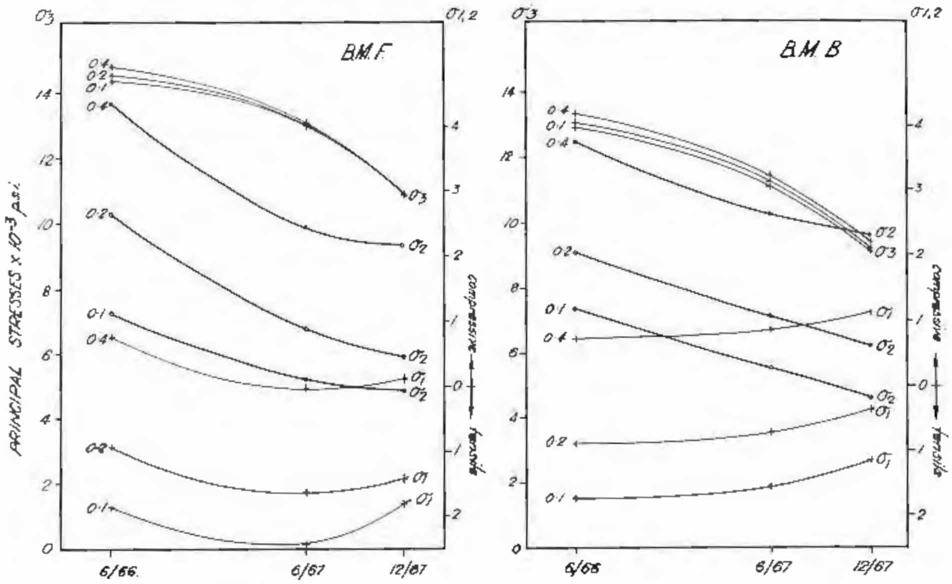

Figure 11. The effect of variation in 'k' ratio on the principal stresses.

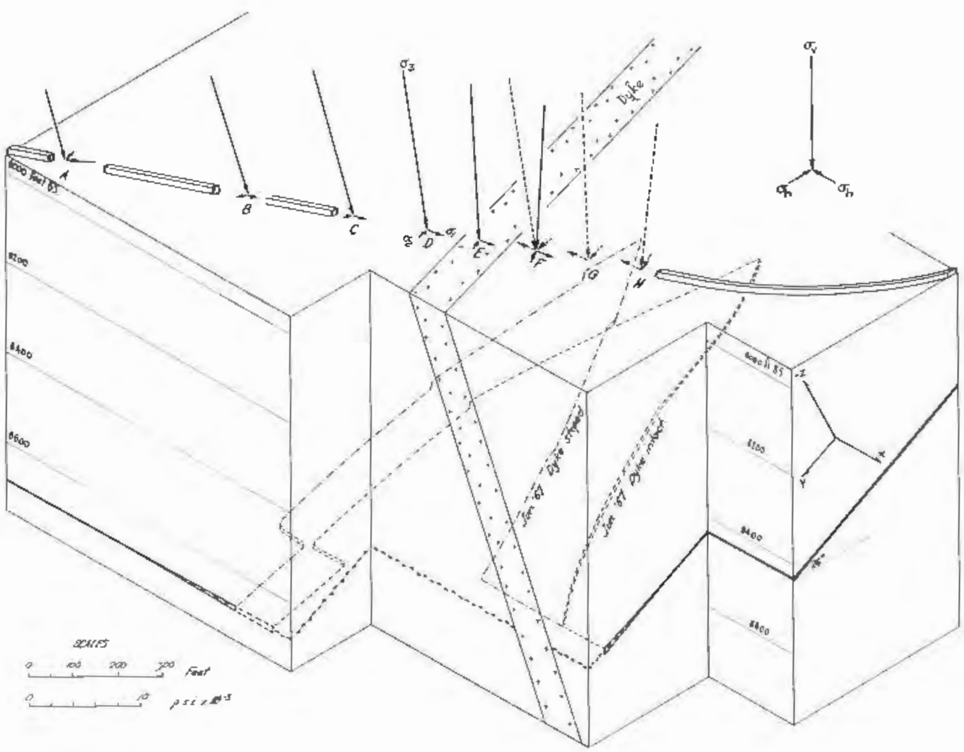

Figure 12. Isometric view of the major and minor principal stress vectors along the line of 58 haulage, in June, 1967.

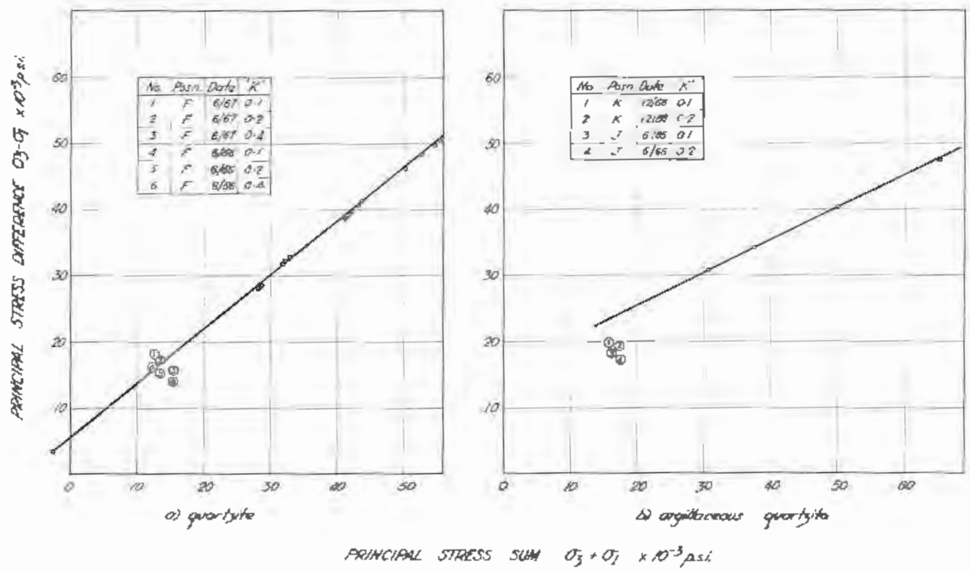

Figure 13. Fracture criteria for quartzite in terms of the sums and differences of the major and minor principal stresses.

EXPERIMENTAL DETERMINATION OF VISCOSITY OF ROCKS BY A SONIC METHOD

Dr. M.H. Rana, and D.W. McKinlay*

Abstract

If the kinematic solid viscosity of rocks can be determined, it may be possible to draw some general conclusions concerning their strength and time-dependent behaviour. Rocks and rock-like materials deform in a viscoelastic manner, approximating to configurations of the Kelvin and Burger types, depending on the range of interest involved concerning behaviour. A rheological model can be used for the determination of viscosity of rocks.

Damping of sonic oscillations in rocks can be determined in situ and in the laboratory. This, in turn, permits calculation of the coefficient of equivalent viscosity, which seems to be a potential future criterion for structural design involving rocks.

The paper deals with analytical considerations pertinent to the present investigation and describes the experimental procedure. The results obtained give an idea of the magnitude of equivalent viscosity at no-load. The results are similar to those obtained sometime ago, concerning structural viscosity.

Solid viscosity is an important rheological parameter in the material behaviour and attempts are now being made at Queen's University to bring the concept into practical viscoelastic structural design involving rocks. The possibilities of this approach are discussed in the paper.

* Assistant Professor, Department of Mining Engineering, Queen's University, Kingston, Ontario.

Introduction

Rocks behave viscoelastically on a time-dependent basis and it is important to evaluate their viscous and viscoelastic parameters in order to design sound engineering structures. A mine designed from a viewpoint of rock mechanics is an engineering structure and an engineer is concerned with its soundness from an operational standpoint. So far, rock mechanics designs have been mostly based on the dynamic and static elastic properties of rocks. It is logical to adopt a viscoelastic approach in rock mechanics, but time and again, the engineer is found helpless in this regard because little, if anything, is reported in the literature on the determination of viscous and other inelastic rock parameters.

The first author (1963) attempted to experimentally determine the coefficients of solid viscosity of rocks using a number of techniques and the results obtained were encouraging. These results have since been published (1965). This work indicated that a coefficient of solid viscosity is a potential future criterion in structural design involving rocks and rock-like materials. Most of the techniques used for these determinations, however, were destructive or semi-destructive. We have felt that a non-destructive approach may be preferable, specially for in situ determinations of solid viscosity, since we are aiming to incorporate the concept in practical design.

A familiar sonic method has been used in an attempt to determine experimentally the coefficient of equivalent viscosity of rocks. This parameter actually is the internal friction encountered by sonic waves of a certain frequency when propagating through a given material. Essentially, the values of viscosity pertain to a no-load condition. As a by-product of this work, in time, a technique may result which would enable a rock mechanics engineer to measure existing state of stress in rocks at depth without changing it in attempts at direct access.

The results obtained are compared with those obtained previously (1963, 1965) and it appears that the coefficient of equivalent viscosity has values similar to those of the coefficient of structural viscosity determined previously. This is despite the differences in the loading conditions and the rock types.

The present work is of preliminary nature. However, the results indicate that it should be possible to determine the coefficient of equivalent viscosity at any load. This is a real possibility in view of a lot of work done in the past on the determination of elastic properties of rocks by sonic methods.

Analytical Considerations

The present investigation is based on the work done by Terry and Morgans (8) who studied the rheological behaviour of coal. The authors' modification of the Terry-Morgans approach consists in taking the work a step further by determining the coefficient of equivalent viscosity which the original authors did not carry out.

The determination of equivalent viscosity is based on the Burger configuration (Reiner, (4)). As is well-known, it is a rheological model resulting from a series combination of a Kelvin solid and a Maxwell liquid conforming to the equation:

$$E(\epsilon + T_k \dot{\epsilon}) = \sigma \frac{1}{+T_m} \int \sigma dt, \qquad \ldots\ldots 1$$

where E = Young's modulus

ϵ = unit strain

$\dot{\epsilon}$ = strain rate

T_k = retardation time

σ = normal traction

T_m = relaxation time

In terms of shears, Equation 1 changes to:

$$G(\gamma + T_k \dot{\gamma}) = \tau + \frac{1}{T_m} \int \tau dt \qquad \ldots\ldots 2$$

where G = shear modulus

γ = displacement gradient

$\dot{\gamma}$ = velocity gradient

τ = shearing traction

Reiner (4) has used a more consistent approach for derivation of the rheological equation of the Burger's body. He considers the displacements of the Maxwell and Kelvin models additive. If $\dot{\gamma}_B$ is the velocity gradient associated with the Burger's body, then, from:

$$\dot{\gamma}_B = \dot{\gamma}_m + \dot{\gamma}_k \qquad \ldots\ldots 3$$

a little analysis yields:

$$\dot{\gamma} = \tau / \eta + \dot{\tau}/G_1 + \frac{d}{dt} \left[e^{-G/\eta \cdot t} \left(\gamma_{os} + \frac{1}{\eta_s} \int_0^t \tau e^{G/\eta_s t} dt \right) \right] \qquad \ldots\ldots 4$$

where η = coefficient of shear viscosity,
γ_{os} = initial strain of the solid component
$\dot{\tau}$ = shearing traction rate
G_1 = shear modulus of the Maxwell component.

Carrying out differentiation in Equation 4, the Burger's equation can be written as:

$$\dot{\gamma} = \tau \frac{\eta + \eta_s}{\eta \quad \eta_s} + \dot{\tau}/G_1 - \frac{G}{\eta_s} e^{-G/\eta_s . t} \left(\gamma os + \frac{1}{\eta_s} \int \tau e^{G/\eta . t} dt \right) \qquad \ldots\ldots 5$$

where η_s = solid viscosity

Considering Equation 2, Jeffreys (1) has remarked that a substance follows the firmo-viscous law if $T_m = \infty$ and the elastico-viscous law if $T_k = o$. Further to this, Reiner (4) has said that the material will flow indefinitely with long, continuous stresses and that partial recovery on unloading will be gradual. In case of problems associated with simple elastic solids, the material behaviour could be determined by writing $G(1 + T_k \frac{d}{dt}) / (1 + \frac{1}{T_m (\frac{d}{dt})})$ for G, so long as squares of the displacements can be neglected.

An approximately simply elastic body has a large T_n and a small T_k and has G $[1 + T_k (d/dt) - 1/T_m (d/dt)]$ for G. The damping of surface waves resulting from earthquakes suggests that either $T_m = 750$ sec and $T_k = 0$ or $T_k = 0.004$ and $T_m = \infty$ (Reiner, (4)). In the rocky shell, approximately, T_m is greater than 3×10^8 sec, $T_k = 0.004$ sec, $G = 1.7 \times 10^{12}$ dynes/cm^2, and $\eta = 5 \times 10^{20}$ poises.

Rana (5) has indicated a value of the coefficient of solid viscosity of a Queenston limestone at about 5×10^{17} poises.

Terry and Morgans (8) have studied the rheological properties of coal, based on the Burger's model, using a sonic method. However, they have mostly been concerned with the variation of retardation time of elastic waves, when passed through coal specimens, with frequency. Their approach can be extended, with some modification, to determine the coefficient of equivalent viscosity of rocks by a sonic method.

If we assume that Burger's body closely approximates the rock behaviour, the attenuation of sound waves travelling through a sample would depend on the viscous losses associated with the opening and closing of the dashpot in the Kelvin component of the model. An attenuation constant is defined such that the amplitude of a sound wave falls to $\frac{1}{e}$th of its initial value after travelling a distance $\frac{1}{\alpha}$ in the material. The relationship between this coefficient of attenuation and the retardation time T_{kk}, associated with the dashpot in the Kelvin component of the model, has been shown (Terry, (7)) to be:

$$\frac{2\omega^2 T_{kk} \alpha}{c} - \left(\alpha^2 - \frac{\omega^2}{c^2} \right) - \rho \frac{\omega^2}{E_s} = 0 \qquad \ldots\ldots 6$$

where $\frac{\omega}{2\eta}$ = frequency

c = wave velocity

ρ = density of the material

and E_s = Young's modulus resulting from the combination of the similar moduli, arising out of the springs in the Maxwell and Kelvin components of the Burger's body.

E_s can be determined by the sonic method or mechanically.

For a vibrating rod of a material under test, if f_o is the resonance frequency and Δf is the difference between the two frequencies which correspond to a variation at half of the developed mechanical power at resonance, a mechanical quality factor Q can be defined as:

$$Q = f_o / \Delta f \qquad \ldots\ldots 7$$

Terry (7) has shown that:

$$1\alpha = \text{Sin } h^{-1} (\text{Sin } \frac{1\ f_o \pi}{cQ} \qquad \ldots\ldots 8$$

where 1 = length of rod.

Equation 7 indicates that a mechanical quality factor can be calculated if the resonance frequency and the damping factor of a sample are known. Then, Equation 8 can be used to evalnate the coefficient of attenuation α, if the length of the specimen and the velocity of propagation of sound waves are determined. Consequently, Equation 8 can be used to determine T_{kk} for a sample.

Now, following Kolsky (2), a coefficient of equivalent viscosity can be computed, using the relationship:

$$\eta_s = E_s \cdot T_{kk} \qquad \ldots\ldots 9$$

It should be obvious from what has been presented above, that the coefficient of equivalent viscosity refers to the internal friction of a material, which in turn, has been variously called as the "specific damping capacity", or the "specific loss".

Preparation and Description of Samples

Ten drill core samples were tested for this investigation. EX Cores (7/8-in. diam) were used and most samples were cut to a length of 12 in. Generally, a length to radius ratio of about 10:1 is considered satisfactory in sonic testing of rock samples, since the correction factor produces a percentage error less than 0.25 per cent, which can be neglected (U.S.B.M. R.I. 3891, 1946). This ratio, for the core samples used in this investigation, is 13.7:1 and the percentage error should, therefore, be less than 0.25 per cent.

The ten diamond drill cores from which the test samples were obtained, were selected at random from the discard pile of a producing mine.

The samples were classified into three groups based on their structural relationship. A geologist's report describes all these samples as belonging in a zone of hybrid norite or micronorite structurally related to a domed hanging-wall contact. The zone consists of noritic breccias; very fine grained noritic to granophysic rocks, usually with quartzo-feldspathic rags and granulated patches.

The samples can be roughly classified into three groups as shown in Table 1.

TABLE 1

Idealized Classification of Samples
Indicating Structural Relationship

Group	General Classification	Sample Nos.
I	Femic Norite, Hangingwall	1, 4, 5, 7, 8, 9
II	Norite Breccia, Contact Zone	2, 6, 10
III	Micronorite, Hanging-wall	3

A more detailed description of each one of the samples by number is given in the Appendix.

Experimental Equipment and Procedure

The main components of the apparatus are represented schematically in Figure 1. The equipment was designed in accordance with the details laid down by Obert, Windes and Duvall (3) and the general procedural and analytical details given by them are applicable. A brief description of the function of each one of the main components follows.

A beat-frequency oscillator is used, and produces a constant voltage signal that can be varied from 0 to 20,000 cps. It has a provision, using the damping factors of rocks, corresponding to a particular mode of vibration, which can be measured.

The power amplifier enhances the signal from the oscillator.

The cutting head (transmitter) changes the electrical signal to a mechanical vibration and transmits the vibration to the specimen.

The pick-up cartridge (receiver) needle is moved by the mechanical vibration of the specimen and a small electrical signal is produced in the cartridge. A variable reluctance cartridge is generally used, but the authors find that a ceramic cartridge produces a much larger signal.

The preamplifier is designed to amplify the pick-up signal and to filter out the low frequency noise that may have been transmitted.

The voltmeter indicates the magnitude of the pick-up signal. When resonance occurs, the signal is a maximum. If the peak is high enough above the background noise, the band width of the peak can be determined. This band width is determined when the frequency is moved in both directions off the resonance frequency and the voltmeter registers a drop of 3 decibels in each case.

The dual-wave oscilloscope used is useful in determining which resonant peak is the fundamental. The signals are taken from the beat - frequency oscillator and voltmeter outputs.

Figure 2 shows the sonic equipment as it looks when testing a sample. Figures 3 and 4 show the details of the pick-up end of the apparatus; one without and the other with the dual wave oscilloscope. Figure 5 shows the details of the transmitter end of the arrangement.

Generally, a drill core sample is balanced at its centre on a V-shaped stand. The vibrational energy is applied at one end of the sample and is picked up at the other end. An increment dial, provided on the oscillator, gives fine readings of $\pm$ 50 cps that can be taken at any frequency setting of the main dial. This increment dial is used only after a resonant peak is found.

For each sample, the resonant frequency, giving the best deflection of the voltmeter indicator needle, is read from the oscillator dial.

The bandwidth of the resonant peak, used to calculate Δf and hence the mechanical quality factor 'Q' is found by turning the increment dial off the resonance frequency position in either of the two directions until the voltmeter reading is 3 decibels less than the peak reading in each case. The sum of two readings on the increment dial gives the value of Δf.

The equipment can be used for measurements in each of the fundamental longitudinal and torsional modes. The measurements made during this investigation pertain only to the longitudinal mode.

96038—16½

TABLE 2
Results of Sonic Tests

Sample No.	1	ρ	f_1	Δf	Q	c $x10^5$	ω $x10^{-4}$	k	α $x10^{-4}$	E_α $x10^{11}$	E_s $x10^{11}$	T_{kk} secs $x10^{-3}$	η $x10^8$
1	29.92	2.81	7.4	120	61.6	4.43	4.65	.1050	8.52	5.54	1.38	5.31	7.34
2	30.65	2.80	9.0	55	163.6	5.52	5.65	.1023	3.13	8.51	2.13	11.12	23.7
3	30.65	3.12	8.8	110	80.0	5.41	5.525	.1023	6.39	9.04	2.26	5.82	13.15
4	30.48	2.92	8.4	97	86.6	5.13	5.275	.1030	5.96	7.66	1.92	6.56	12.6
5	30.73	2.90	7.9	100	79.0	4.85	4.96	.1021	6.51	6.86	1.72	1.37	10.9
6	30.65	2.85	9.4	28	335.7	5.76	5.90	.1023	1.524	9.40	2.35	22.80	53.6
7	30.65	2.84	8.2	89	92.1	5.03	5.15	.1023	5.58	7.16	1.79	7.13	12.8
8	30.73	2.91	8.7	87	100	5.34	5.46	.1021	5.11	8.39	2.10	7.25	15.2
9	30.65	2.87	8.5	97	87.6	5.22	5.34	.1023	5.84	7.77	1.94	6.58	12.75
10	30.73	2.82	9.2	46	200	5.59	5.775	.1021	2.55	9.05	2.26	13.90	31.4

LEGEND:

1 = length in cm;
ρ = density in gm/cc;
f_1 = resonance frequency in the longitudinal mode, kcps;
Δf = damping factor, cps;
Q = Mechanical quality factor, Equation 7
c = longitudinal velocity = $2lf_1$, cm/sec;
ω = $2\pi f_1$;
k = ω/c;
α = the coefficient of attenuation;
E_α = $c^2\rho$, gm/cm^2;
E_s = $E_\alpha/4$, gm/cm^2;
η = coefficient of equivalent viscosity, dyne sec/cm^2. (poises)

Results

Table 2 gives the results of sonic tests, performed on 10 samples, along with subsequent calculations leading to values of the coefficient of equivalent viscosity, η. All the results are recorded in c.g.s. units.

f_1 (which is equivalent to f_0 in Equation 7) and Δf were measured for each sample, from which Q's were calculated, using Equation 7. Velocities in the fundamental longitudinal mode were calculated using the relationship $c = 2lf_1$.

ω and k were calculated as shown at the end of Table 2. Equation 8 was then used to evaluate α's the coefficients of attenuation.

E_α was first calculated as shown in Table 2, and then in accordance with some implications of the work due to Terry and Morgans (8) E_s's were calculated as $E_\alpha/4$. T_{kk}'s were determined by using Equation 6. Finally, Equation 9 was used to determine η's.

Discussion

The results are of preliminary nature but compare reasonably well with those obtained by the first author (1963) concerning solid structural viscosity of Queenston limestone. The latter were in the 10^9 poises range. This agreement was not really desired since the structural viscosity determinations involved application of loads of the order of 1,500 psi and the present work is under no-load conditions. Moreover, different rock types are involved. This makes the agreement all the more undesirable. The only tangible explanation for this agreement can be derived from the fact that Queenston limestone is relatively young and has undergone no intensive penetrative deformation. This would account for the low structural viscosity of the limestone. If the coefficient of equivalent viscosity is determined for this limestone, it should fall in a range much lower than 10^8 poises range, encountered for the rocks used in this investigation.

It is hard to talk about the mechanism of internal friction from the above results. In general, however, it is known that two dissipative processes are involved, and are roughly the counterparts of viscosity losses and thermal conduction losses in the transmission of sound waves through solids. On a molecular scale, the explanation of viscous effects in solids is not well understood. This is because the types of microscopic processes resulting in the dissipation of mechanical energy into heat are not too well understood. It seems probable that the rock packing patterns play important part in dissipation of mechanical energy. The grain size and shape in a rock, the percentage composition of rock, the pore water, and the number of contact points between grains per unit length of a rock sample are some of the other factors bearing on dissipation of energy.

It appears from the work done by Terry and Morgans (8), by the first author (1963, 1965) and from the results presented in this paper that a suitable coefficient of solid viscosity can be experimentally determined. It goes without saying, however, that more work is required in this area before a standard method can be evolved for such determinations.

The question now is about the possibilities of the practical applications of a coefficient of solid viscosity. In structural engineering, generally, a plastic design is arrived at for the structures that are acted upon by constant, time-dependent loads. The plastic design involved takes into consideration the material behaviour within a range of loads of interest. However, the materials involved in the type of design under discussion, have been more thoroughly investigated than rocks. Compared to these materials, it will be difficult to establish similar plastic design parameters for rocks since they are not man-made materials. The known structural design criteria cannot, therefore, be applied to rational design involving rocks.

Rocks are known to behave as viscoelastic materials. The design parameters should, therefore, depend on viscous and elastic moduli. A complicated functional can be set up, which would combine the effects of shear modulus, Young's modulus of elasticity and the coefficient of solid viscosity. This functional could be a useful criterion in the design of time-dependent structures involving rocks, e.g., an underground mine opening with regard to its dimensions, a building foundation and a large earth dam. In view of the work done so far, it appears that incorporation of a coefficient of solid viscosity into structural design in rocks will be a worthwhile contribution since it will produce more realistic, and more functional structures.

Conclusions

The conclusions concerning the work presented in this paper can be briefly stated as follows:

1. A coefficient of equivalent viscosity of rocks can be determined by sonic means. The parameter is in fact the internal friction of rocks, the mechanism of which is not too well understood.

2. The rock viscosity, if determined realistically, can be a future criterion in structural design involving rocks and rock-like materials.

3. There is a need for a standard method for the determination of a coefficient of solid viscosity.

Acknowledgments

Most of this work was done by the authors as an undergraduate research project in the Department of Mining Engineering at Queen's University. The first author initiated the project during summer, 1966, with the help of some financial assistance from the Committee on Scientific Research of Queen's University. This assistance is gratefully acknowledged.

The authors are indebted to A. Jamison, a geologist, who provided the geological description of the samples.

Appendix

Description of Diamond Drill Samples for Sonic Tests

Sample No.	Description
1	Quartz diorite breccia, or brecciated dark norite, contains 50% norite fragments. The remainder is plagioclase - rich groundmass.
2	Plagioclase - rich material replacing possibly granulated, medium-grained norite breccia. One slip plane, contains minor sulphides and minor ultramafic fragments.
3	Fine to very fine grained, massive, ultramafic (peridotrite), peridotite associated with norite intrusion.
4	Brecciated ultramafic fragments in plagioclase - rich groundmass. Groundmass has igneous texture. 50% to 55% ultramafic fragments.
5	Brecciated ultramafic, fragments of ultramafic composition in plagioclase - rich groundmass. Fragments approximately 28%.
6	Brecciated ultramafic within plagioclase - rich groundmass approximately 35% to 40% ultramafic fragments.
7	Fine-grained, massive, ultramafic. Minor plagioclase intruded.
8	Medium-grained norite. Minor granophyre.

Sample No.	Description
9	Fine to medium-grained, brecciated norite in plagioclase - rich groundmass. Norite represents approximately 55% to 60% of the rock.
10	Plagioclase - rich material replacing granulated medium-grained norite. Minor sulphides; several stringers of very dense, mafic material.

References

(1) Jeffreys, H.
1929: The Earth, Cambridge, p. 128.

(2) Kolsky, H.
1963: Stress Waves Through Solids, Dover Publications Inc., New York, p. 120.

(3) Obert, L., Windes, S. L., Duvall, W.I.
1946: Standardized Tests for Determining the Physical Properties of Mine Rock, U.S. Bureau of Mines, R.I. 3891.

(4) Reiner, M.
1960: Deformation, Strain and Flow, 2nd Ed. H.K. Lewis & Co. Ltd., London.

(5) Rana, M.H.
1963: Experimental determination of viscosity of rocks, M.Sc. Thesis, Dept. of Mining Eng., Queen's Univ., Kingston, Ont.

(6) Rana, M.H.
1965: Experimental determination of viscosity of rocks, A paper presented at the SESA Meeting, Nov. 6-9, 1966, held in Pittsburgh, Pa.

(7) Terry, N.B.
1958: Fuel, London v. 37, p. 309.

(8) Terry, N.B. and Morgans, W.A.T.
1958: Studies of rheological behaviour of coal, mechanical properties of non-metallic brittle materials, Butterworths Scientific Publns., London, pp. 239-255.

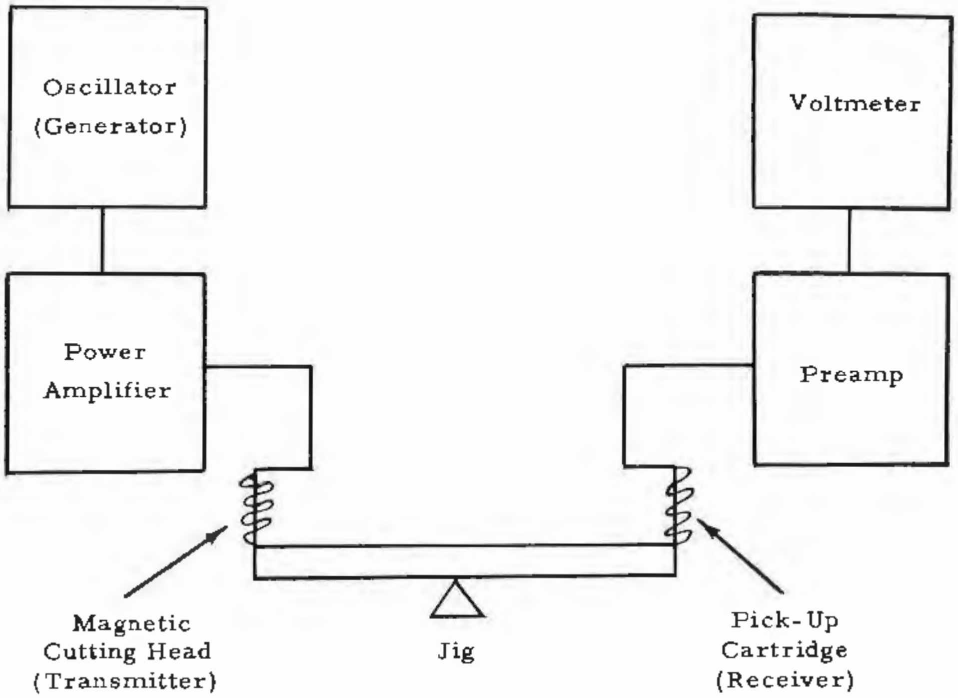

Figure 1. Schematic of the sonic equipment.

Figure 2. View of the sonic equipment testing a sample.

Geologists have simplified the study of joint patterns by using the equal area net, a sort of three-dimensional protractor, which permits the investigation of planar surfaces, evaluation of the angular relationship between them, and determination of the orientation of the lines of intersection between them.

The evaluation of a series of planar surfaces or joints by the equal area net is further simplified by the polar plotting technique in which any plane is represented on the equal area net by a point. This point on the net surface represents the point where a line perpendicular to the plane to be plotted penetrates the lower surface of the hemisphere from which the net is constructed. Polar plotting could be termed a reverse plotting technique because it produces mirror images on the net of the planar patterns to be studied.

Using this technique any number of planes plotted on the net are represented as points which can readily be contoured (Figure 1). The International Nickel Company's computer staff simplified the plotting by writing a Fortran program which plots the joints, evaluates the polar maxima, then obtains the orientations of the lines of intersection between any pair of maxima. The polar plots, the maxima, and the joint intersection lines are then printed out on an equal area projection by the machine.

In this study it was found that the normal contour method produced only from two to five maxima. These were considered inadequate because they did not make full use of the zonal distribution of points in the polar diagram (Figure 1). Furthermore, it was necessary to alter the conventional contouring method to adapt it for computer plotting on a 1132 printer. It was therefore decided to divide the plotting area on the printer into squares and to count the number of points falling in any one square. If this number exceeded a predetermined minimum then the square contained a maximum, whose location was then printed out by the printer (Figure 2).

Geologists refer the elements of the rock fabric, which includes the joint patterns in the rock, to three orthogonal axes a, b, and c, whose spatial distribution falls into any one of the four patterns shown in Figure 3. In rocks the fabric patterns are generally either monoclinic or triclinic.

It was decided to accept the geologic definitions which rule that:

1. the b-axis is the line of intersection between any two prominent planes and also the axis of rotation:

2. the a-b plane is the most prominent plane of the fabric.

It was found that these two definitions could be expressed statistically on the net, because the lines of intersection between any two joints, or joint maxima, derived from the polar diagram shown in Figure 1, intersect in a restricted area, and many more intersect in a belt or zone which contains most of the restricted area. In fact approximately 20 to 35 per cent of the total points describing lines of intersection in the diagram fall in the so-called restricted area, and between 40 and 55 per cent fall in the belt that contains the restricted area (Figure 4).

It was therefore decided to define the restricted area as the b-axis of the rock fabric, and the belt as the a-b plane.

In Figure 4 the b-axis and the a-b plane are rather obvious. However, in some joint intersection diagrams they are more difficult to determine, and the following procedure is used to define the b-axis (Figure 5):

1. The centre of the point scatter pattern is first determined by median distribution counts. With this point as centre a circle is drawn to surround 70 per cent of the points in the diagram (Figure 5).

2. The centre of the scatter pattern of points within this circle is redetermined. With this point as centre a second circle is drawn to surround 65 per cent of the points within the first circle.

This second circle is then taken to contain within it, all meaningful variations in orientation of the b-axis of the fabric examined, and the centre of the circle is taken to be the b-axis.

The belt which contains the greatest concentration of points and which also passes through the second circle is then taken to represent the a-b plane of the fabric.

As soon as it was found that recognizable fabric patterns could regularly be obtained in this way, it was decided to map a relatively undisturbed drift cutting through the hangingwall rocks and to examine the fabric patterns in the drift. The drift was divided into 20-ft-long units and all the joints in each unit were mapped and recorded separately. A total length of 600 ft was mapped in this manner and it was found that:

1. Prominent, weak, and small joints all belonged to the same family.

2. The preferred lines of intersection (b-axes) in successive units were similar but not necessarily the same.

3. Wherever shearing was noted in the drift the pattern of the b-axes in adjacent units was markedly different.

The mapping of an equivalent length of drift through the footwall rocks gave similar results. When the overall pattern in these two rock members was compared (Figure 6), it immediately became apparent that their fabric patterns were almost identical. It was therefore decided to treat the contact region between the hangingwall and footwall rocks as one structural domain, in spite of their difference in age and physical properties.

This observation was considered significant because:

1. Most of the ore in the Sudbury district occurs in the vicinity of the contact between these two rock types, the rocks of the Sudbury nickel irruptive and the footwall rocks.

2. It became apparent that it might be possible to evaluate the structure of the rock envelope surrounding the ore and thereby gain some knowledge of its manner of failure.

These two deductions invited further study because, from a rock mechanics point of view, they defined certain critical parameters in the relatively complex framework of the rock envelope surrounding the ore. Accordingly the rock envelope at one of the mines was studied by mapping all the available access headings to an orebody. On the level selected only two drifts, which flank the ore, were sufficiently free of timber to permit detailed mapping. These two drifts were again divided into 20-ft units and mapped as before.

Polar diagrams and b-axes were obtained for each unit. They were then plotted on a level plan showing the location of each unit. From the centre point of each unit the b-axes were projected upwards and then downwards onto plans representing the adjacent mining levels.

The upward projection of the b-axes produced a scatter pattern which was contoured. The emerging contour plan indicated that these b-axes tended to converge and produce an irregular shaped concentration (Figure 7A) which bore some resemblance to the outline of the ore on the same level (Figure 7B).

It was therefore decided to superimpose the contour plan on the trace of the ore outline. A remarkably close fit was obtained by an anticlockwise rotation of 40 degrees, as seen in Figure 8.

When the b-axes were projected downwards the contour plan of the b-axes distribution did not closely resemble the ore outline on the lower level (Figures 9A & B). However, a better fit was obtained when the contour plan of the b-axes was rotated 30 degrees anticlockwise with respect to the ore outline for the level (Figure 10).

The fact that both projections required an anticlockwise rotation is not yet fully understood, but the presence of a prominent wrench fault below this level may have something to do with it.

Thus far, this study has shown that the structural framework of the rock envelope surrounding an orebody bears a remarkable resemblance to the shape of the sulphide concentrations within the envelope and that in this case the resemblance is shown by the distribution of the b-axes orientations in the footwall members of the envelope.

Relationship of Structure to Failure Patterns

While studies relating the fabric pattern to the pattern of post-mining ground movement are still in a preliminary stage, two of the studies undertaken to date have been partially successful.

The first concerns a small orebody which was mapped and examined while still under development.

The orientation of the b-axis was determined in 50-ft-long units along two development drifts which penetrated the orebody on the level examined (Figure 11). The orientation of the b-axis varied from unit to unit but in general plunged between 70 and 85 degrees in a direction approximately parallel to the drift (Figure 11). The strike of the a-b plane, determined from all units, is oriented approximately 25 degrees west of the mean strike of the b-axes (Figure 11) and therefore is 75-80 degrees to the trend of the long axes of the proposed stope pattern, which was laid out parallel to the east-west co-ordinate grid. As this was not considered a significant discrepancy, the stope layout was not changed.

Subsequent mining of a modified blast hole stope exposed the pillar walls for a height of 60 ft and length of 150 ft.

This permitted a daily scrutiny of the pillar walls which on close examination were found to contain numerous steeply dipping and almost mutually perpendicular cracks. The most prominent of these strike obliquely to the pillar walls and almost perpendicular to the a-b plane determined from the joint study (Figure 12).

This is taken as reasonable evidence that pillar failure tends to occur both perpendicular and parallel to the a-b plane of the rock fabric.

In the second case an attempt was made to deduce the location and dimension of the eventual pattern of failure at one of the larger mines, in order to locate a new deep shaft as close to the ore as possible and yet outside the envelope of failure.

A broad yet detailed joint study on surface and on several underground levels was undertaken to determine the b-fabric axes on each level (Figure 13). The levels chosen were approximately 1,200 ft apart and the resultant b-axes for each level were projected to the surface from several points along the perimeter of the ore outlined on these levels.

The area at surface described by the projection of these b-axes was contoured to show pronounced concentrations (shaded areas), moderate concentrations (hatched area), and mild concentrations (areas delineated by dashed lines). The shaded and hatched areas were taken to represent areas prone to subsidence, and the dashed line was taken to delineate the outer limit of subsidence (Figure 14).

The shaded area shown in Figure 14 agrees fairly well with the shape of the area of surface subsidence resulting from the cave program, particularly as two blocks of low grade ore have not yet been undercut along the western boundary of the cave area.

An abandoned exploration drift on the 3,800 level, which penetrated the hangingwall for some considerable distance, permitted another comparison between the envelope of observed ground failure and the predicted area.

The cracks in the exploration drift were noted and taken to indicate the area of strongest post-mining ground failure (Figure 15); this figure shows the pronounced cracks noted in the drifts on this level and compares the area outlined by them with the area of predicted subsidence, as determined by the projection of b-axes from 5,400 level upwards (Figure 15A). Secondly, the b-axes on the 4,000, 4,200, and 4,400 levels were projected upwards to 3,800 level and compared with the pronounced cracks in the drift (Figure 15B). These two diagrams show fairly close agreement between predicted and observed data, especially when it is remembered that the area outlined in Figure 15A includes an as yet unmined shaft pillar west of the cracked ground. The dimension and shape of the projected area of failure from adjacent lower levels bears a much closer resemblance to the observed area of failure (Figure 15B).

Conclusion

Evidence has been presented which shows that the flaws in the rocks at the base and immediately below the Sudbury irruptive contact follow a pattern, and that this pattern is most apparent in the distribution of the lines of intersection between the flaws or joints themselves.

It has also demonstrated that along the outer margin of the Sudbury irruptive the distribution of the b-axes, defined by the lines of intersection between joint maxima, bears a marked resemblance to the distribution of copper-nickel concentrations.

Finally this study indicates that knowledge of the distribution of the b-axes and the a-b plane is also useful in predicting the eventual outline of post-mining failure.

Acknowledgments

The author wishes to extend his thanks to The International Nickel Company of Canada, Limited for permission to publish this paper. He also wishes to express his appreciation to other staff members for their assistance.

References

(1) Turner and Weiss.
1963: Structural Analysis of Metamorphic Tectonites. McGraw-Hill.

(2) Badgley.
1959: Structural Methods for the Exploration Geologist. Harper Brothers.

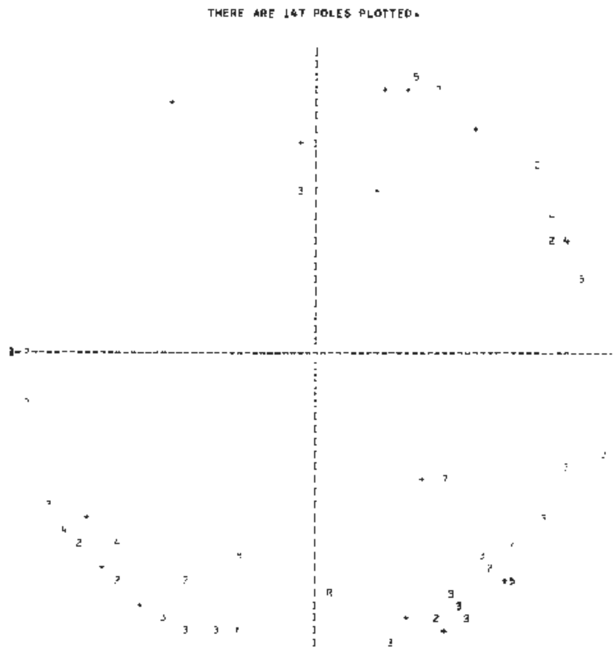

Figure 1. Polar plots of a number of joint planes on an equal area net (printed out by the computer).

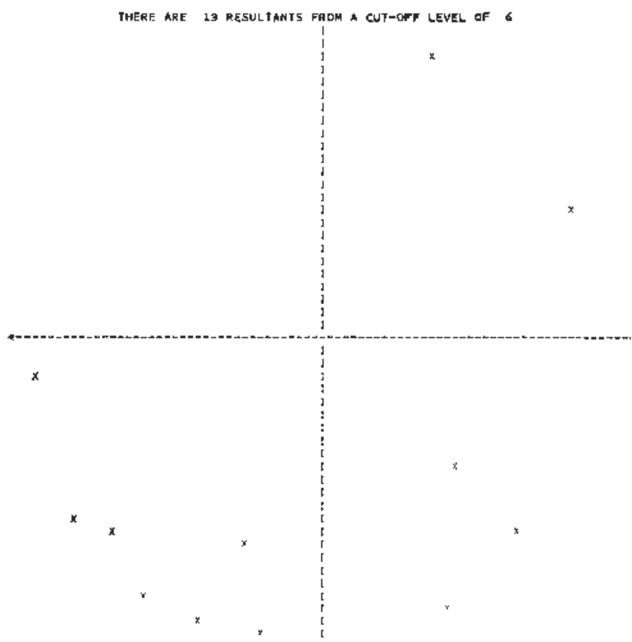

Figure 2. Distribution of maxima, derived from polar plots (Figure 1), using a computerized cut-off level of 6 poles per square.

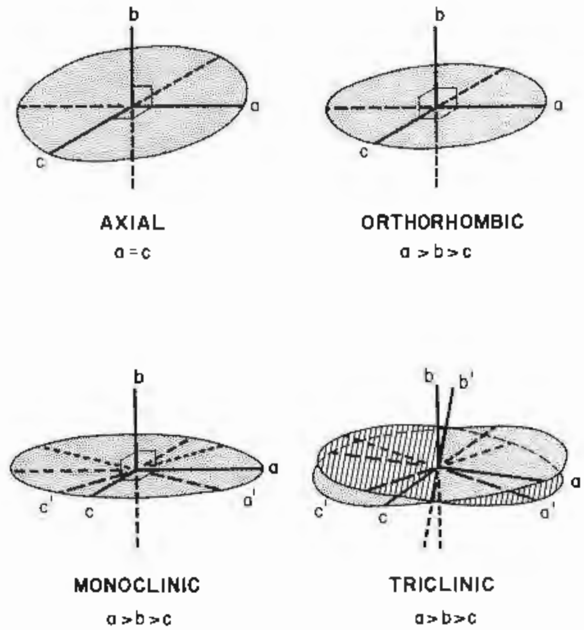

Figure 3. Symmetry of fabric patterns.

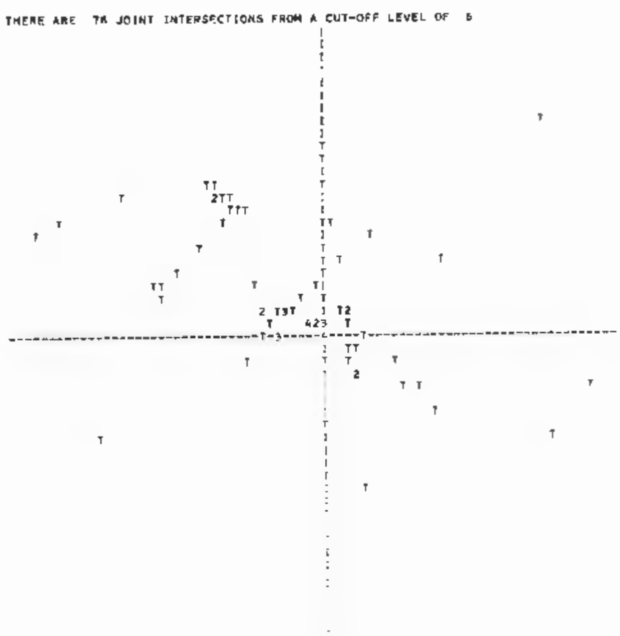

Figure 4. Print out showing plunges of the lines of intersection between any pair of joints.

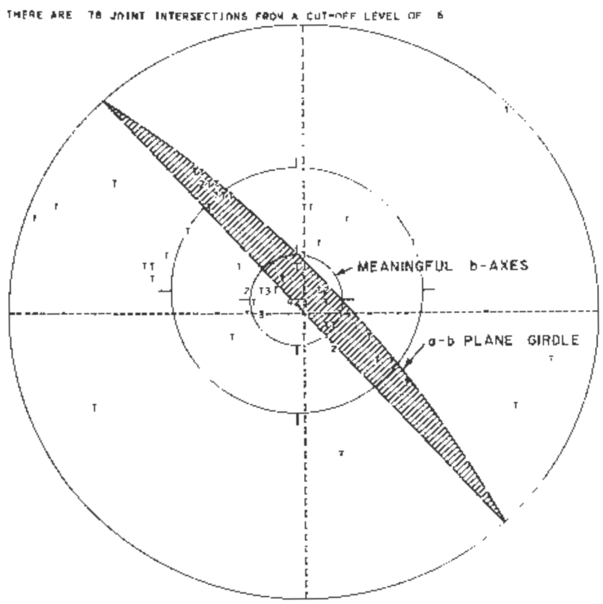

Figure 5. Evaluation of the print-out shown in Figure 4.

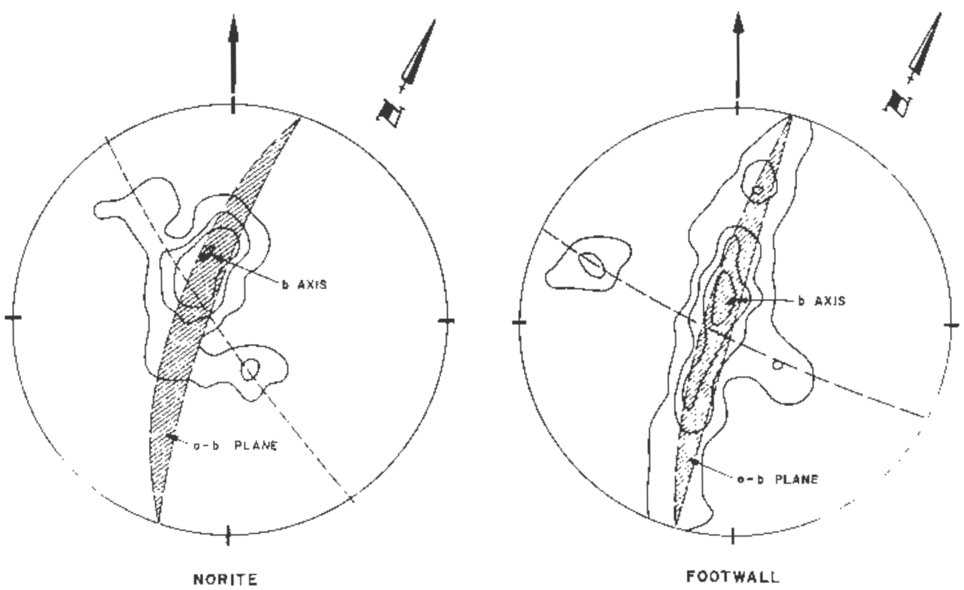

Figure 6. Contoured lines of intersection of joint planes in the norite and in the footwall succession.

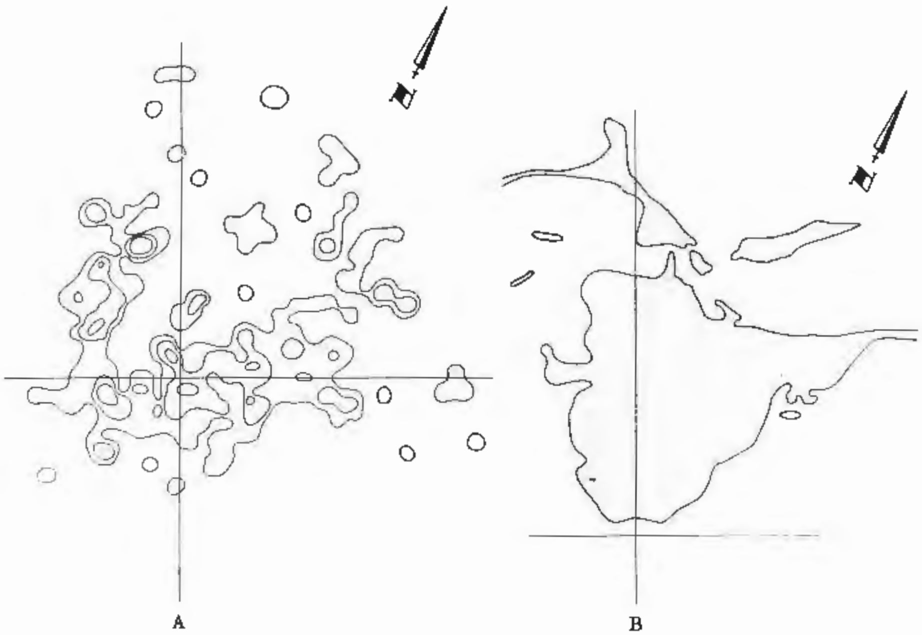

Figure 7. A - Contour plan of significant b-axes projected upwards to the 4,600 level.
B - The ore outline on this level.

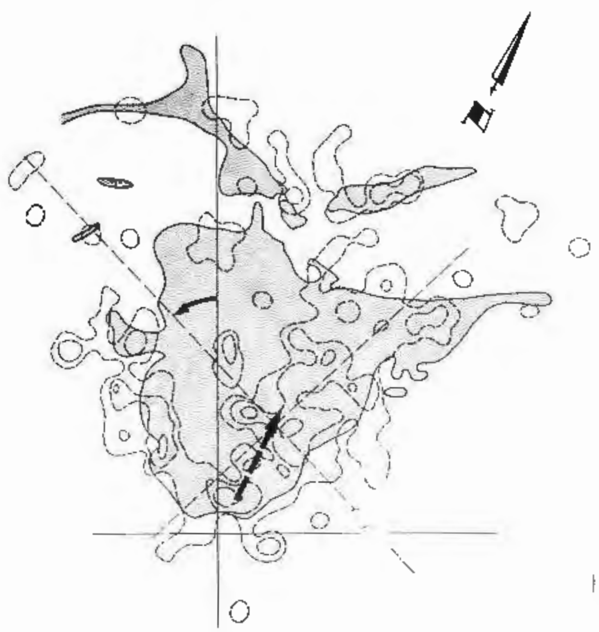

Figure 8. Contour plan of significant b-axes projected up to the 4,600 level as shown in Figure 7, when superimposed on the ore outline on this level by rotation and a lateral shift.

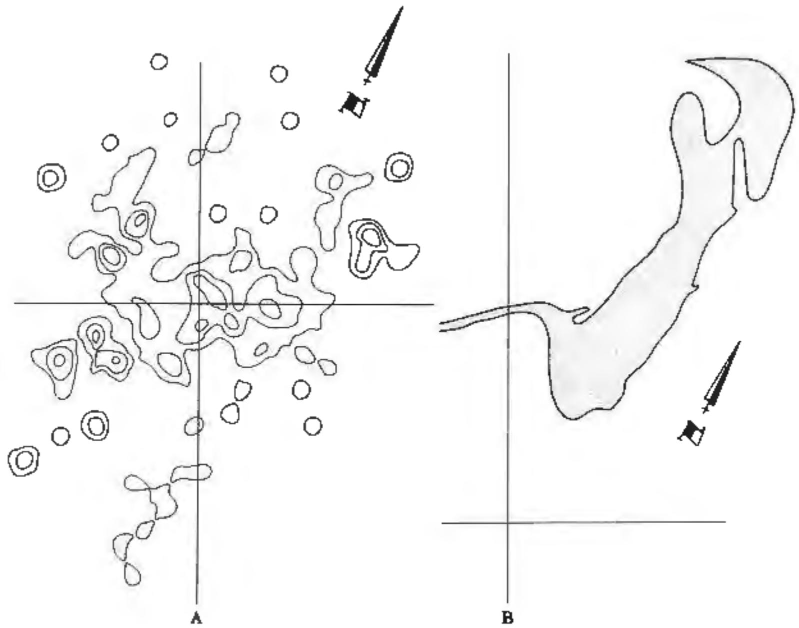

Figure 9. A – Contour plan of significant b-axes projected downwards to the 5,000 level.
B – The ore outline on this level.

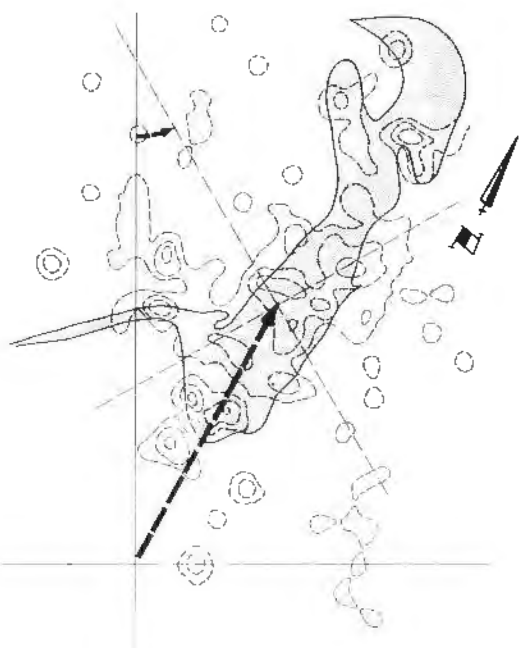

Figure 10. Contour plan of significant b-axes projected down to the 5,000 level, as shown in Figure 12, when superimposed on the ore outline on this level by rotation and a lateral shift.

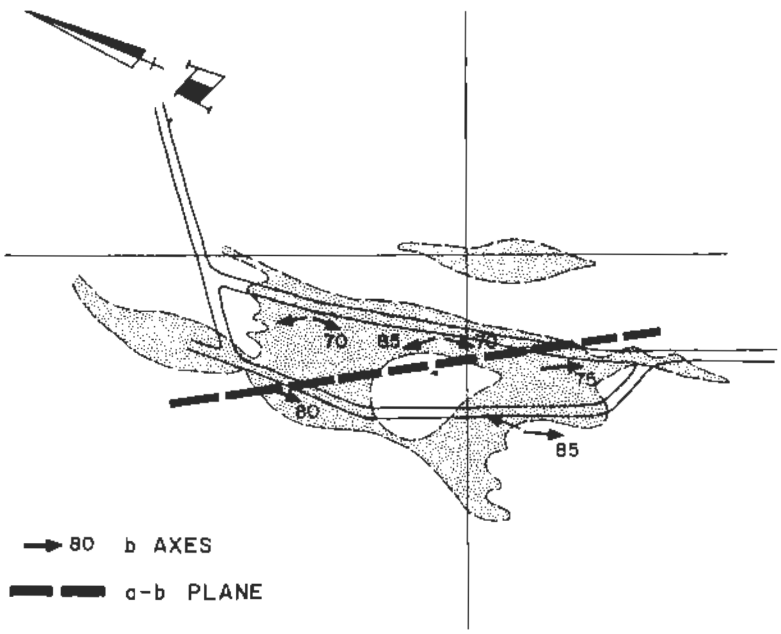

Figure 11. Orientation of the b-fabric axes and the a-b plane on 5,800 level (determined during the development stage).

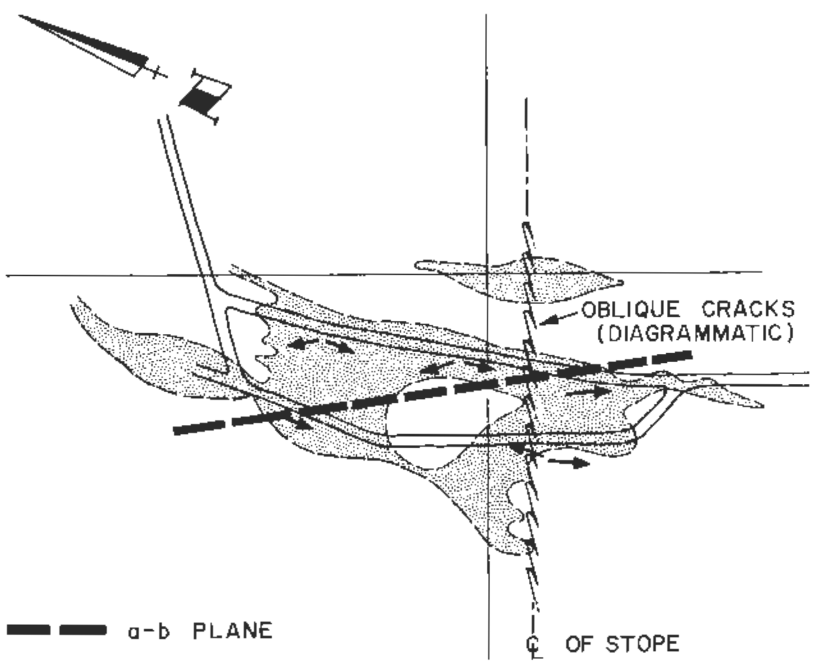

Figure 12. Planes of weakness, striking approximately perpendicular to the a-b plane, which developed in the pillar walls of the open stope.

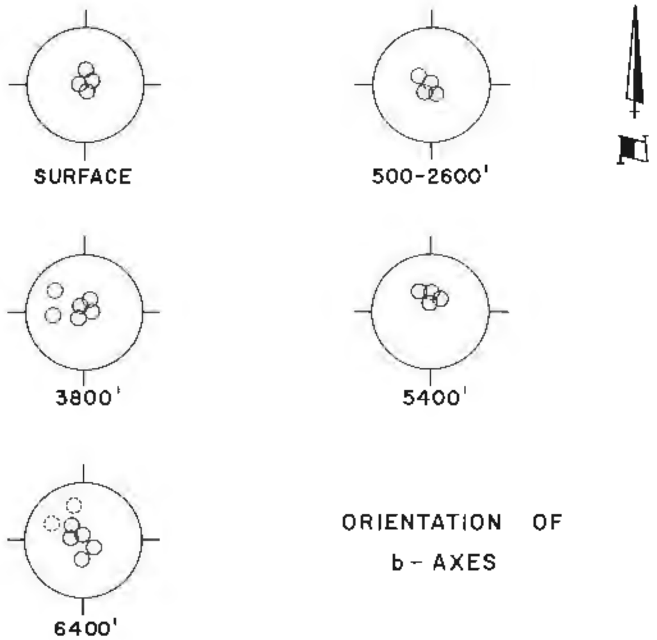

Figure 13. Orientations of b-fabric axes determined from joint studies on several underground levels.

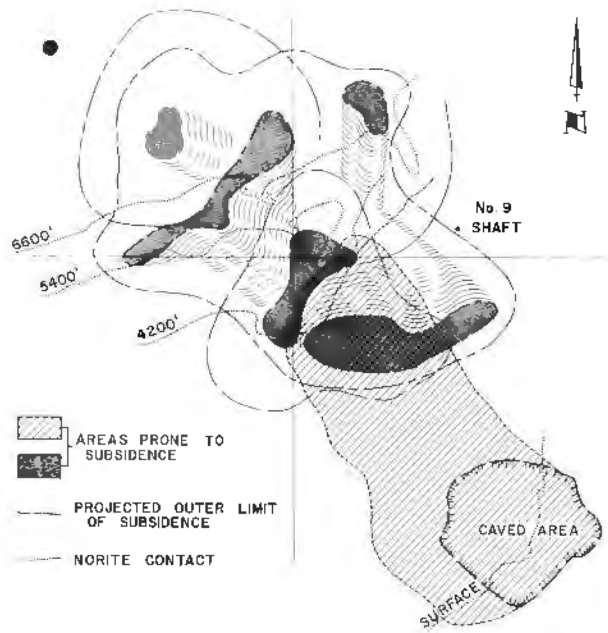

Figure 14. Surface plan showing location of 9 shaft in relation to envelopes of possible ground failure derived by projecting upwards the significant b-axes from several pre-selected levels.

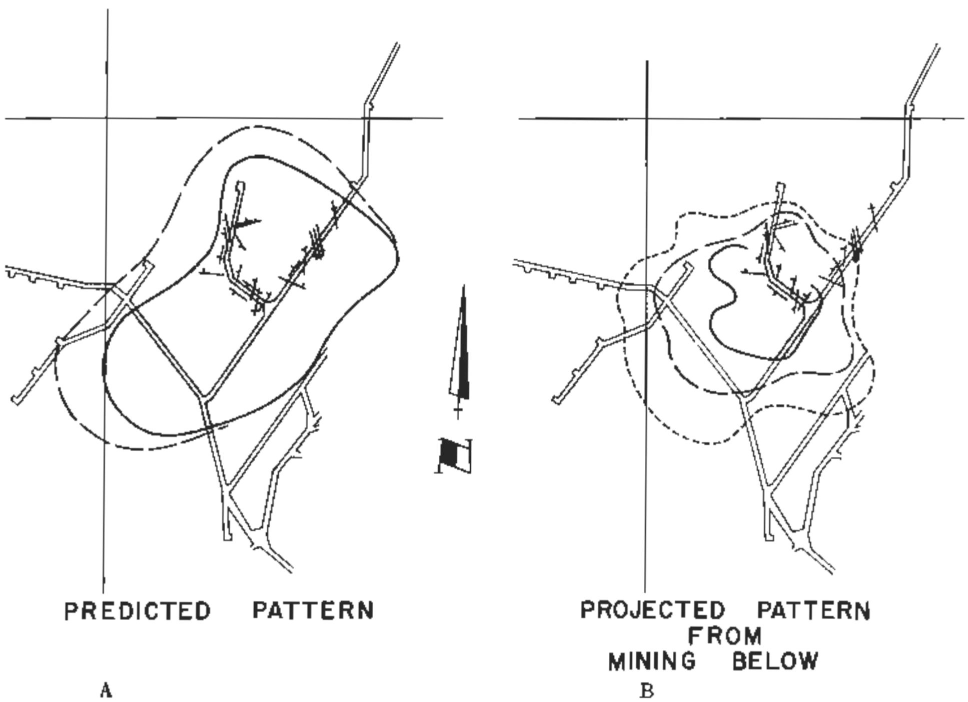

Figure 15. Subsidence cracks compared with predicted subsidence patterns.
A - Areas prone to subsidence determined by shaft study.
B - Areas prone to subsidence determined by projecting b-axes from several levels below this elevation.

MODIFYING MINE DESIGN FROM ROCK MECHANICS DATA

*J.D. Smith**

Abstract

The Fairport mine of the Morton Salt Company is considered to have good mining conditions and relatively stable rock formations in which to work. However, mining costs and safety conditions were being affected by significant amounts of rock movement, expressed by floor heaving, pillar rib failure, and roof spalling.

Mine management, recognizing these problems, authorized a rock mechanics program to provide data on rock movement so that the improved mine design would result in a reduction or elimination of these problems.

This paper describes the rock mechanics study conducted by C-I-M Consultants Limited in conjunction with the mine staff. It describes the means of accumulating data and presents summaries of the measurements obtained and how these were used to determine optimum face width and orientation, optimum pillar size and orientation, and rock movement control.

*Consulting Mining Engineer, 106 Holland Crescent, Kingston, Ontario.

The mine management has implemented several of the recommendations concerning mine design and the comparison of mining conditions, visual observations, and operational data are given between the older mining method and layout and the modified method and layout resulting from the study. Approximately one year after the completion of the study, a paper similar to this one was presented at the Second Symposium on Salt, held in Cleveland, May 3-5, 1965. The paper presented the initial results obtained from a test panel that had been oriented in the recommended directions. This paper includes an up-to-date assessment of the results obtained since May, 1965.

Introduction

The management of Morton Salt Company authorized C-I-M Consultants Limited to conduct a rock mechanics study to provide design criteria that could lead to the reduction or elimination of floor heaving, pillar spalling and roof deterioration at their Fairport mine. This study was conducted over a period of six months, starting in July of 1963. Approximately twenty man-days per month were spent on the project, half of which were used in field and travel time.

The Fairport mine is a salt producer recovering about 4,000 tons per day from a gently dipping bed of about 20 ft thickness. The ore zone is bounded above and below by Silurian shales, limestones and thinner salt beds. The regional dip is towards the south-east but locally there are rolls in the formations which change the dip over short distances. It appears that there has been little or no major tectonic movements in the region of the ore zone.

Mining was done by the room and pillar method laid out on a north-south and east-west grid. The rooms were approximately 40 ft wide and 17 ft high with pillars 100 ft x 100 ft. The rate of advance is approximately 10 ft every three weeks per room. In various sections of the mine, floor heaving, roof spalling and rib corner deterioration commenced shortly after the creation of a new face. The mining is planned to leave 2 to 3 ft of salt in the roof immediately below the shale contact. This means that a variable amount of salt is left on the floor but where local "pinches" occur in the salt bed both roof and floor shales are exposed.

Definition of Problem

The Fairport mine was and is currently being mined with a very acceptable tons-per-man-shift record and an excellent safety record. Mine operating personnel have evolved, during the life of the mine, techniques and mining procedures to cover most of the problems encountered by unexpected rock and salt movement. However, a continuous and significant number of man-shifts was being spent on scaling, clean-up and equipment maintenance caused by rock and salt movements expressed in floor heaving, roof spalling and pillar deterioration. The basic problem, from a mining standpoint, was how to reduce this maintenance cost to a minimum and hence improve efficiency and decrease mining costs.

The problem, as viewed by a rock mechanic, was to determine the inherent directional and strain magnitude characteristics of the formations affected by the mining operation, to utilize this knowledge in calculating design changes to reduce, eliminate or minimize the various movements causing failure, and to monitor the changes in design underground in order to evaluate their effectiveness.

Data Accumulation

Any study for the purpose of improving mine design by considering the inherent properties of the mine structure evolves first of all into a sampling problem. The statistical force vector and inherent strain magnitudes must be determined by analyzing the required number of oriented samples in the laboratory. Further, in situ measurement must also be done in a sufficient number of places to attain the required confidence in the result. The following sections explain how these data were obtained, why they were required and how they were used in mine design.

Inherent Directional Characteristics

One of the most important properties of the materials affected by mining is their inherent force field. This is the vectorial sum or resultants of all forces acting on the material. This property must be determined for each geologic material that will be affected by the mining operation as their behaviour and manner of movement is dependent upon this property.

Associated with the strain vecters acting in the various granular materials are curvilinear surfaces that possess higher orders of inherent energies than surrounding grains. These surfaces are called preferred shear planes.

The system of analysis used to determine the properties at the Fairport mine involved the instrumentation of many oriented pieces of salt and shale. Oriented samples were taken from the ore zone and the roof shale on a statistical basis so that the area of influence of each sample gave the required confidence on a minewide scale. Each oriented sample had a cube cut from it with a diamond saw, three mutually perpendicular planes were then instrumented with 2-in.-diam photoelastic strain gauges. As the time-dependent inherent energy stored in the grains and cement re-oriented and strained them in order to re-attain equilibrium, the photoelastic strain gauges recorded the directions and amount of movement. The vector components of the principal strains on each instrumented face were then combined using a stereonet to produce the force field vector (azimuth and dip). The preferred shear plane traces on each face also combined to produce the strike and dip of the various families of preferred shear. This work was also done using a stereonet.

Force Field. A total of 21 oriented samples were taken from the salt ore zone and 37 oriented core and hand samples from the roof shale. Two samples from the floor shale were also studied. The azimuth of the principal strains in the horizontal plane for the different materials is presented in Table 1.

G_1 is the major strain direction and G_2 is the minor strain direction. The azimuths are corrected for the local magnetic declination. It is apparent that there is little difference in force field direction in the different formations. The approximate force field dip is down towards the south-east at about 20°. The local variations in force field direction are best shown by a strain trajectory which is a plot of how the principal strains are propagated through a given plane and is a visual representation of how the rocks are strained directionally. The most useful representation for a bedded deposit with a slightly dipping force field is to show the strain trajectory in the horizontal plane. This has been done for the roof shale bed and is presented in Figure 1.

TABLE 1

Average Force Field Directions

Rock Type	No. of Samples	Principal Strain Directions in Horizontal Plane - Az.	
		G_1	G_2
Salt	21	133°	043°
Roof Shale	37	135°	045°
Floor Shale	2	137°	047°

The major and minor force field has been determined and defined by an azimuth and dip. The determination of the thrust direction or the placement of the arrowhead on the vector cannot be determined adequately from oriented samples. In situ measurement was used to determine this characteristic. Both north-south and east-west openings were instrumented around their peripheries with photoelastic gauges bonded to the surface as well as bolt tension meters placed on rock-bolts. The manner of load build-up on these instruments indicated that one wall of the openings was moving into the void at a faster rate than the other. This indicated that the thrust vector was thrusting downward at 20° on an azimuth of 135°.

Preferred Shear Planes. It is believed that these approximate planes of inherent weakness in a granular material are a function of the grain packing patterns, the type of "glue" cementing grains together and the tectonic forces that created its present configuration. These planes are very useful both in designing restraint and for drilling and blasting functions. These points will be discussed later. There are several families of preferred shear planes in both the roof shale and the salt bed. Table 2 shows the general agreement between these families.

From the table it is evident that families 1 and 2 have similar azimuth but opposite dips while families 3 and 4 have the same characteristic with their azimuths being approximately 90° from 1 and 2. An attempt was made to correlate the families of preferred shear planes with the local variation in salt bed thickness. It was found that in a "pinch" region of the salt bed that preferred shear plane families of 052° az. - 56° north-west dip and 142° az. - 48° north-east dip predominate while in "swells" and relatively undisturbed parts of the bed families of 052° az. - 56° north-west, 067° az. - 48° south-east and 188° az. - 42° south-west predominate.

TABLE 2

Preferred Shear Plane Families

Rock Type	Preferred Shear Planes - Az. and Dip			
	1	2	3	4
Roof Shale	153° - 22°N.E.	122° - 43°S.W.	050° - 30°N.W.	0° - 19°S.E.
Salt Bed (upper 2nd Salt)	142° - 48°N.E.	138° - 42°S.W.	052° - 56°N.W.	067° - 48°S.E.

Shear Strain and Strain Magnitudes. Only the time-dependent portion of the total elastic recoverable strain is recorded by the instruments on the oriented samples. These show the distribution of the time-dependent shear strain when viewed with the correct optical instrument. The graph presented in Figure 2 shows a typical relaxation rate for an oriented salt sample.

The shear strain pattern is useful in two ways. First it gives the traces of the preferred shear plane families on each instrumented face and secondly, it aids in calculating the multiplication factor for the force field due to mine geometry.

This "n" factor is an important part of the prestressed beam-column formula used to calculate room spans. Its determination involves the analysis of underground instrumentation as well as the relaxation rates from oriented samples. Disc rings (which consist of a 2-in.-diam photoelastic gauge bonded to the salt at each corner of the opening as well as in the centre of the roof) are installed in the two mining directions. The shear strain magnitudes from these instruments can be compared directly with the shear strains measured on the appropriate planes of the oriented samples provided the instruments in both cases are installed at the same time after creation of a new face and are read during the same time interval. Table 3 summarizes the shear strain readings from both sources. Resulte are presented for the horizontal plane as this plane is of greatest importance for span calculations in this type of deposit.

TABLE 3

Time-Dependent
Average Shear Strain Magnitudes

Plane of Measurement	Oriented Samples	Shear Strain - μ in/in Disc Rings			
		N - S Rings		E - W Rings	
		Disc C	Disc E	Disc C	Disc E
Horizontal Plane	120	813	783	323	1095

Figure 3 shows typical locations for individual discs used in this study.

It is evident that the force field thrust can cause rotational moments to act on an opening if it is incorrectly oriented. One would expect the angle at the corner of the opening at E for the north-south ring and at C for the east-west ring to be opening and to have decreasing strain. The reverse should be true for the opposite corners of the openings. The shear strain readings confirm this concept. For design purposes the least value of shear strain was used in each case to provide a safety factor. The high compression corners at C for the north-south ring and at E for the east-west ring are not used because these high shear strain values represent the sum of shear strain energy due to relaxation into the opening plus compression at the corners due to rotation of the opening. The values at the tension corners are conservative because relaxation into the openings is decreased by the tensional effect due to rotation.

The multiplication factors required were obtained by dividing the average inherent shear strain magnitude obtained from the oriented samples into the average shear strain values from disc E and disc C from the north-south and east-west rings respectively. The multiplication factor for openings of azimuth 135° is approximately 6 and for openings of azimuth 045° is 3. The major strain direction has the largest multiplication factor because it has the greatest inherent shear strain.

The magnitudes of the individnal strains, G_1 and G_2, were determined from the oriented samples. It must be understood that the values presented in the following table are a measure of the time-dependent elastically recoverable strains and hence are known to be conservative. The measured strains in the plastic are equal to the strains in the shale and can be converted into stresses for the shale by using the approximate physical constants. These measurements were done on the shale as the amount of prestress in this formation was required for structural design. The appropriate physical constants measured in the roof shale using the dynamic testing method developed by Obert, Windes and Duvall are $E = 12.88 \times 10^6$ psi and $\mu = 0.74$ for the 090° direction and $E = 11.40 \times 10^6$ psi and $\mu = 0.61$ for the 000° direction. All measurements were taken in the horizontal plane. The photoelastic theory applicable to this discussion can be found in Emery (1) and Roberts (3).

TABLE 4

Average Time-Dependent Strain Magnitudes and Calculated Stresses
Roof Shale Samples

	Measured Strain Measured - in/in		Calculated Principal Stresses - psi	
	G_1	G_2	G_1	G_2
Horizontal Plane	55	30	900	630

In calculating stresses from the measured strains the following should be considered:

1. The measured strains are a portion of the time-dependent re-orientation strains and should be extrapolated back to zero time for a newly created face.

2. The immediate elastic rebound component has been lost by the act of preparing the sample.

3. The material has different values of Young's modulus and Poisson's ratio in different directions.

4. Young's modulus varies with stress.

5. Strains in the plastic gauges are re-calculated in terms of stresses in the gauges. These are then multiplied by a suitable factor to determine approximate stresses in the rock.

These factors will be considered in the section on mine design to arrive at more accurate figures for the probable inherent stresses in the rock. Only 3. above has been used in the table.

Mine Design

The first phase of the study was spent in determining the characteristics of the granular material affected by the miuing operation. The knowledge of the rock movements was then used to modify the mine design and layout. The following sections explain how this was done and what the recommendations were.

Room and Pillar Orientation

To minimize rotational moments (Emery (2), p. 3), which can be one of the major reasons for rock failure, all mine openings and pillars should be oriented in one of the principal strain directions. Rooms and the long axis of the pillars should be aligned with the major strain direction and cross-cuts and the short axis of pillars should be aligned with the minor strain directions. In this type of deposit it is only practical to orient these in the horizontal plane.

The force field dip is small (about 20°) and so rotational moments are minimized and are resisted by the long axis of the pillars.

The oriented cores from the roof shale were taken primarily to provide the variation of the force field thrust on a mine-wide scale. The principal strain directions in the horizontal plane were plotted on a mine map, and strain trajectories were prepared from this. The strain trajectory shown in Figure 1 is a visual representation of how the roof shale is loaded. Since the roof shale movement, upon removal by mining, is what acts upon the pillars, the strain trajectory of the shale provides the room and pillar orientation directly.

The strain trajectory was determined from samples obtained from existing mine workings. To orient rooms and pillars at any location involved the extrapolation of the strain trajectory into the solid ahead of the mining face. On a statistical mine wide basis, the statistically optimum room and long axis direction of pillars is 135° azimuth and cross-cut direction is 045° azimuth.

In 1964 the mine staff decided to implement these recommendations by opening panels at the south-west and north-west corners of the mine. The panels were started approximately 3,400 ft apart. The north-west panel was advanced towards the north-west with cross-cut faces advancing in this direction. The south-west panel was advanced with room faces moving towards the south-west. To check on the variation of the principal strains as mining progressed in these panels, disc rings were installed at appropriate intervals. The data obtained from these instruments showed where and by how much the force field had turned from the average direction determined. They also measured the amount of variation in direction needed to increase the rotational moments to cause failure.

Room Span Calculation

Details of the beam-column theory used in this section to calculate safe room and cross-cut spans are to be found in Smith (4).

The beam-column is visualized as a flat slab of rock in the roof of an opening with effective depth equal to the rock-bolt lengths used or to the depth of some competent bed above the roof. The worst possible case would be to consider uniformly loaded, simply supported beams of one foot width, placed side by side and supported or loaded on the ends by the force field prestress. Using these conditions, a safety factor is immediately provided as the roof material is almost never simply supported. These conditions are illustrated in Figure 4.

σ m is the extreme fibre stress due to the uniform load of the beam and $\sigma \text{ m} = \pm \frac{Mc}{I}$ where $M = \frac{Wl^2}{8} \times 12$ in./lb and $\frac{I}{c} = \frac{bd^2}{6}$ where band d are in inches. The inherent force field, σ x, is multiplied by a factor n due to the geometry of the opening. Theoretically, n should be infinity at the corners but in actual practice the rock flows and readjusts to within its yield point. For stability and to reduce high horizontal shears in this beam, the span is adjusted such that the top and bottom extreme fibres are strained an equal amount. This is expressed by n $\sigma x - \sigma m = \sigma x + \sigma m$. The variables n and σx are measured from the materials and so this equation can be solved for σm. But

$$\sigma m = \pm \frac{Mc}{1} = \pm \frac{Wl^2}{8} \times 12 \times \frac{6}{bd^2}.$$

Solving this equation for ℓ one obtains:

$$\ell = \sqrt{\frac{m \times 8 \times bd^2}{W \times 12 \times 6}} \text{ ft.}$$

The effect of geometry was determined from disc rings installed on salt. It was considered safe to use these factors for the roof shale after comparing thc physical properties of salt and shale. The multiplication factor of n = 6 for openings of azimuth 135° and n = 3 openings of azimuth 045° will be used.

The roof shale is hard, competent and interbedded with thin salt stringers and beds. There is a good parting in the shale, about 4 ft above the shale-salt contact. When the skin of salt left on the roof gets too thin, bolts are used to tie it to the shale. The beam depth will be considered as 4 ft because this is the approximated shale bed thickness and if bolting is required 4 bolts should be used.

The sonic tests required the determination of the shale density. This was found to be 130 lb/cu ft and hence for a beam 1 ft wide and 4 ft deep this means a uniform load of 720 lb/ft of beam.

The measured field force σx was determined from oriented hand samples and hence reflects short time relaxation strain only. The variations of Young's modulus and Poisson's ratio under no load have been considered in calculating $\sigma 1$ = 900 psi and $\sigma 2$ = 630 psi from the measured strains. These strains should be extrapolated back to zero time in order to attain a more accurate time-dependent strain magnitude. An examination of the short time relaxation rates for the roof shale samples provided a multiplication factor of 1.25 for the time-dependent strains. An example of a relaxation graph is given in Figure 2. The immediate inherent elastic rebound of the shale was not measured by the photoelastic gauges due to the method of analysis. Overcoring techniques used on similar materials tested indicated that the elastic rebound was approximately 1/4 of the total inherent strain energy. The time-dependent strains should then be multiplied by a factor of 1.33 to obtain a more accurate figure. It is an established fact that Young's modulus increases with applied load. Since this figure was determined under a no load condition, a factor must be applied to compensate. Experience indicated that a reasonable figure for this type of material was a 1.33 increase in Young's modulus due to a load of the magnitude measured. Probable values $\sigma 1$ and σ_2 are 900 x 1.3 x 1.3 x 1.25 and 630 x 1.3 x 1.3 x 125 respectively. The values used in the following calcnlations are σ_1 = 1900 psi and σ_2 = 1330 psi.

Spans of rooms running in the 045° direction (supported by the major strain) are calculated as follows:

$$n = 6 \quad W = 720 \text{ lb/ft} \quad d = 48 \text{ in.} \quad b = 12 \text{ in.} \quad \sigma_1 = 1900 \text{ psi}$$

$$n \quad \sigma x \quad - \quad \sigma m = \sigma x + \sigma m$$

$$\sigma m = \frac{n \quad \sigma x - \sigma x}{2}$$

$$= \frac{8 \times 1900 - 1900}{2}$$

$$= 4750 \text{ psi}$$

$$\ell = \sqrt{\frac{\sigma m \times 8 \times bd^2}{W \times 12 \times 6}}$$

$$= \sqrt{\frac{4750 \times 8 \times 12 \times 48^2}{720 \times 12 \times 6}}$$

$$\ell = 142 \text{ ft.}$$

Similarly, the calculated span of the proposed cross-cuts running in an azimuth of 135° is calculated.

$$x \quad \sigma x - \sigma m = \sigma x + \sigma m$$

$$\sigma m = \frac{n \quad \sigma x - \sigma x}{2} = \frac{3 \times 1330 - 1330}{2} = 1330 \text{ psi}$$

$$\ell = \sqrt{\frac{1330 \times 8 \times 12 \times 48^2}{720 \times 12 \times 6}}$$

$$\ell = 75 \text{ ft.}$$

The measured spans of 142 and 75 ft are considered conservative. These spans are safe only if the rooms are driven in the principal strain directions. Because of the problem of maintaining a clean, unbroken back to aid in beam stability, it is imperative that the faces be advanced uniformly. In other words, the whole breast, after undercutting, should be drilled off and blasted at one time. The best sequence would be to drive the rooms ahead of the cross-cuts so that beam equilibrium could be established before the cross-cut mining disturbed the condition.

Pillar Size

The regional force field thrusts from the north-west to the south-east at about 20°. For maximum stability, the long axis of pillars should run in this direction to offset the overturning moment of the force field caused by the downward dip. The pillar should have sufficient mass so that it does not crush and also so that is does not punch into the roof or floor. These things are possible depending upon the pillar size and relative hardness and strengths of the roof, ore and floor materials. A physical examination of the mine showed that there was no pillar failure as such. The only evidence of failure was noted at pillar corners and this was attributed to rotation of the pillar caused by improper orientation. The size of the pillars in the older sections of the mine is 100 ft x 100 ft. The dimensions of the pillar should be in relation to the ratio of the principal strains. In this case, the ratio of the principal strains is 1.43 : 1. If the long axis of the pillars is 100 ft then the short axis should be 70 ft. It was felt that this would provide a pillar with sufficient mass in the correct direction to withstand the forces acting upon it. Recommended pillar sizes, provided they are oriented correctly, are 100 ft x 70 ft. Since this study, more sophisticated means of calculating pillar sizes have been developed. Using these methods, the above mentioned size is still considered safe.

General

Preferred shear planes can be utilized in determining the best direction of mining, fragmentation and ease of break as well as to aid in designing restraint in the form of rock-bolts. In this particular case there are two families of preferred shear planes roughly parallel to the proposed room and cross-cut direction. Because of this and their dips, good fragmentation should result in both directions. Whether the rooms are driven in an azimuth of 045° or in 225° should make no difference to the fragmentation and drilling rates. However, cross-cuts should be driven in an azimuth of 135° and not 315°. In this way, the force field thrust will be cut off and the drilling rates should improve. For optimum fragmentation, drill holes should be drilled perpendicular to preferred shear planes. In this way, explosive energy adds to the high inherent shears in a wedging action.

Consider restraint

These same preferred shear planes or planes of inherent weakness, if their attitudes in relation to mine openings produce a low angle, can be the source of shear failure in roof, floor and pillars. To prevent this, short high tensile steel rock-bolts should be placed in holes drilled perpendicular to the planes of preferred shear. These bolts should be placed in rows along the strike of these planes. For rooms, the azimuth of these rows should be about 060°. A compromise direction for the bolts would be to place them vertically to allow for all families of planes.

Summary of Recommendations

a. On a minewide basis the rooms should be driven in an 045° direction and cross-cuts driven in a 135° direction. These directions should be altered locally to conform to the strain trajectory variations.

b. The calculated safe mining width for rooms is 140 ft and for cross-cuts is 75 ft.

c. Salt pillars should be oriented with their long axis parallel to azimuth 135° and their size should not be smaller than 100 ft x 70 ft.

d. Rooms could be driven in 045° or in 225° direction without altering fragmentation, drilling rates and powder costs. Cross-cuts should be driven in 135° direction ouly. An improvement should be noted in drilling rate and powder cost.

e. Mining faces should be advanced uniformly and each round of advance should be blasted at one time. Rooms should be driven ahead of cross-cuts.

f. If rock-bolts are required they should be placed vertically in rows parallel to the azimuths of the preferred shear planes. Short bolts will be more effective than long bolts.

Results of Test Panel Mining

The mine management, treating this study as a research project decided to evaluate each major recommendation separately. During 1964 a test panel shown in Figure 5 was started from the south-west corner of the mine. This panel was laid out in the recommended directions of 135° and 045° azimuth but nothing further was changed. The following results show the effect of changing directions only.

During the first two months of mining this section the following changes were noted by underground supervision:

1. Slightly faster drilling rates.
2. Better fragmentation and lower powder factor.
3. Less bootleg and angle of faces more nearly vertical.
4. No floor heaving. This was the longest time an area had been open without some evidence of floor heaving.
5. Roof control and pillar slabbing reduced.
6. Both rooms and cross-cuts have squarer corners and the ribs are more uniform.
7. An average of 50 tons per round increase in break was noted.
8. The corners of the pillars still slabbed, but incidence and size of slabs reduced.

As mining advanced towards the west some floor heaving developed in several sections. These heaves had their axis parallel to the room and cross-cut directions and were not an approximate 45° angle as in the older mining method of north-south and east-west drives. The correct alignment of rooms and cross-cuts does not eliminate the forces causing such failure, it merely eliminates the moments acting on the roof and floor slabs. To eliminate floor heaving requires the use of wider spans and larger pillar combinations as well as correct directions.

Several mine openings were instrumented with bolt tension meters and disc rings to determine whether the openings were being driven in the optimum direction. The measurements indicate that statistically the panel is in the correct direction but locally some portions of openings are a little off. A significant thing is that the bolt tension meters are recording much higher readings in this new panel in the same relative period of time than instruments in the older parts of the mine. This indicates that the salt bed has increased inherent energy characteristics in this region. In the original mining directions, floor heaves are occurring 2 to 3 rounds back from the face.

The mine management, early in 1965, decided to plan for wider rooms and cross-cuts as well as larger pillars in an attempt to reduce the floor heaving problem. To provide some preliminary data, four rooms in the test panel were widened to 50 ft. The results were sufficiently encouraging for the mine staff to proceed with modifying the mine layout.

Modified Mining Method

In 1966, mine openings for the whole mining distance of 3,800 ft were re-oriented in the originally recommended directions of 135° and 045° for the cross-cuts and rooms respectively. To date, the mine faces have advanced towards the west by about 500 ft. The room spans have been varied between 50 and 55 ft in different locations and the cross-cuts have been varied in width between 40 and 45 ft. Depending on the geometrical problems found in turning existing openings into the recommended directions and to obtain some estimate of relative stability, the pillar sizes were varied between 80 ft x 130 ft to 90 ft x 120 ft.

In conjunction with the changes in mine design prompted by the rock mechanics study, the mine staff conducted tests to improve blasting efficiency and powder requirements. The following list of results therefore includes factors from both fields of research and summarizes briefly the results indicated up to December, 1966.

a. Better fragmentation and lower powder factor.

b. Less bootleg and angle of faces more nearly vertical.

c. Openings have squarer corners and more uniform ribs.

d. Pillar sloughing along the ribs has virtually been eliminated and pillar corners are more stable.

e. Overall decrease in maintenance and scaling costs.

f. Average increase in tons broken per round is 40-50 tons.

g. Some floor heaving and roof spalling still occurs which appears to be associated with "pinches" in the salt. The amount of salt left on the roof and floor is somewhat less than in other areas.

The mine staff plans to continue modifying the geometry in an attempt to further improve their efficiency and safety records. It is thought possible that if the present openings are in the optimum direction, the spans can be increased in a controlled manner in order to evaluate the effect on floor heaving and roof spalling.

In addition to the benefits obtained during the past three years, the mine staff feel that they have gained a better understanding of the materials with which they must work and as a result are in a better position to cope with any future problems.

Acknowledgments

The writer wishes to thank the Morton Salt Company for permission to use the data obtained from the rock mechanics study conducted at their Fairport mine. In particular, thanks are due to R. Ganong, Manager of the Fairport operation, for bringing the writer up-to-date on the changes made in mine design and on the results obtained.

References

(1) Emery, C.L.
1960: Photoelastic Coatings on Granular Materials. Institute of Physics, London, England.

(2) Emery, C.L.
1964: In situ measurements applied to mine design, Rock Mech. Symp., Missouri School of Mines, Rolla, Missouri, October.

(3) Roberts, A., Emery, C.L. and Chakravarty, P.K.
1961-62: Photoelastic Coating Technique Applied to Research in Rock Mech. Trans. Inst. Min. & Met., v. 71, part 10, pp. 583-596.

(4) Smith, J.D.
1963: The condition of stress surrounding a simulated mine opening. Proc. Rock Mech. Symp., Queen's Univ., Kingston, Ontario, December 6-7, p. 27.

(5) Smith, J.D.
1965: The use of rock mechanics in mine design at the Fairport mine, Morton Salt Company. 2nd Symp. on Salt, North. Ohio Geol. Soc., Cleveland, Ohio.

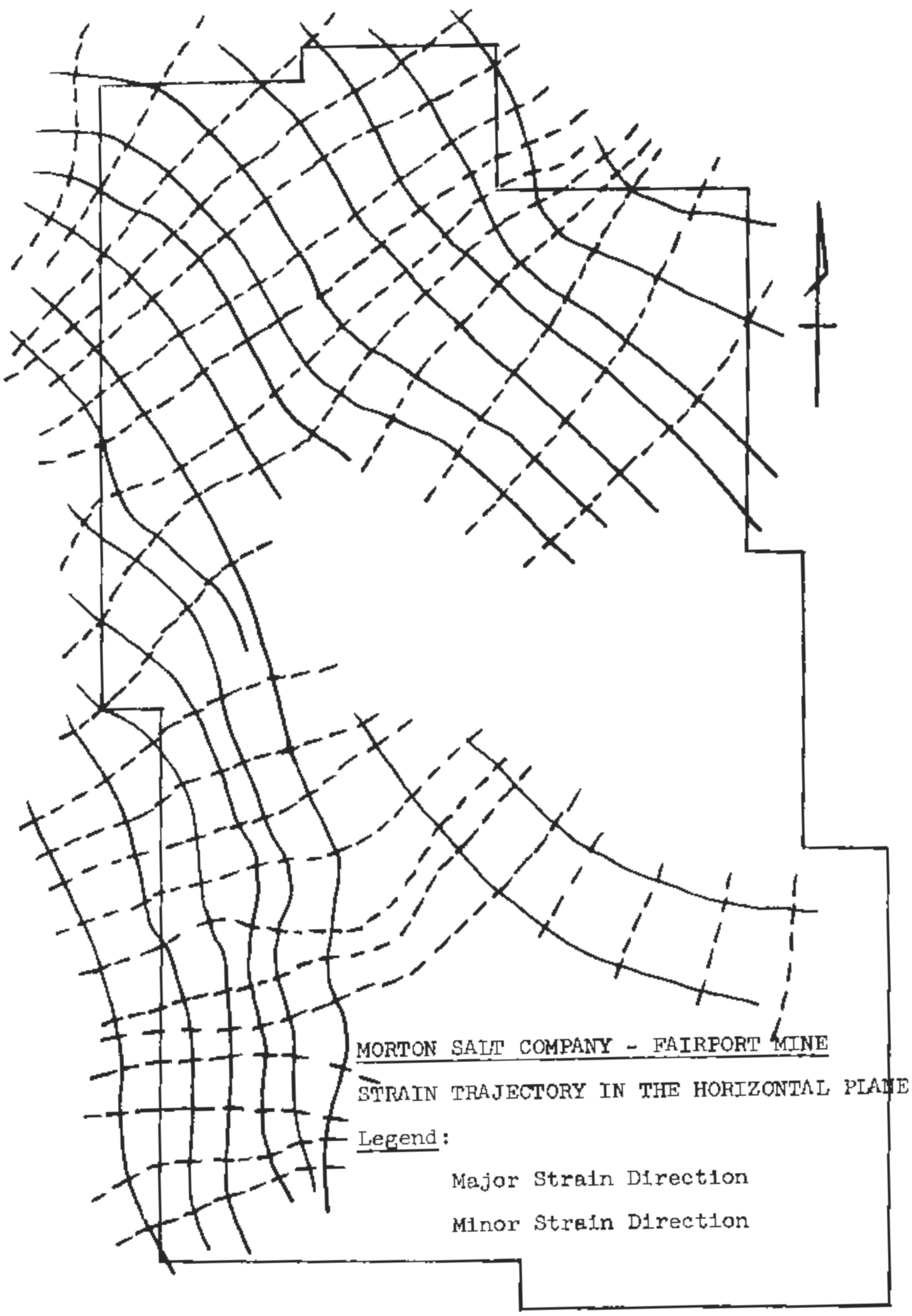
MORTON SALT COMPANY - FAIRPORT MINE
STRAIN TRAJECTORY IN THE HORIZONTAL PLANE
Legend:
Major Strain Direction
Minor Strain Direction

Figure 1

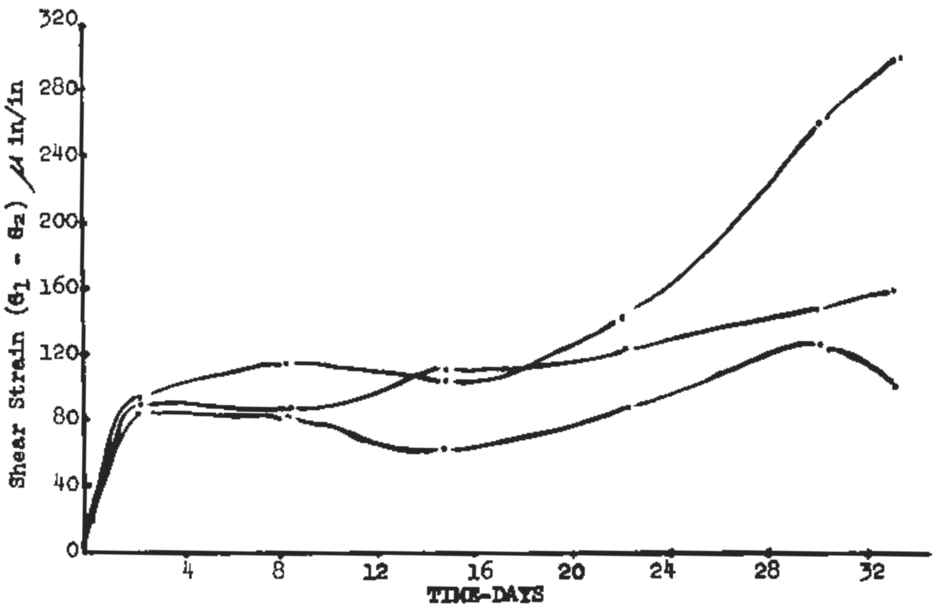

Figure 2. Typical relaxation rate - salt sample.

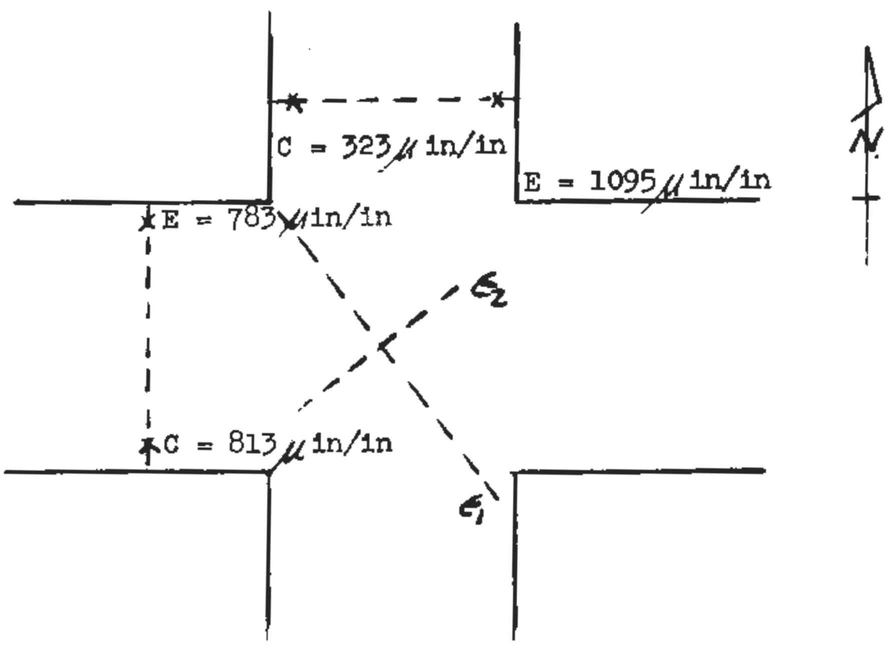

Figure 3. Typical instrument locations plan view of workings.

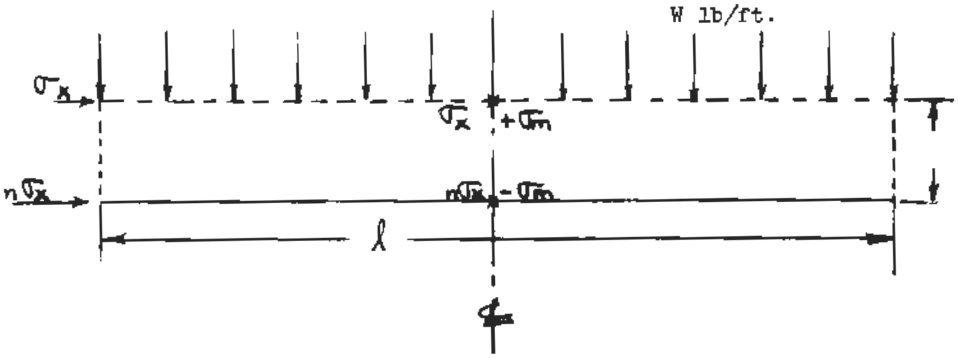

Figure 4. Uniformly loaded prestressed beam-column.

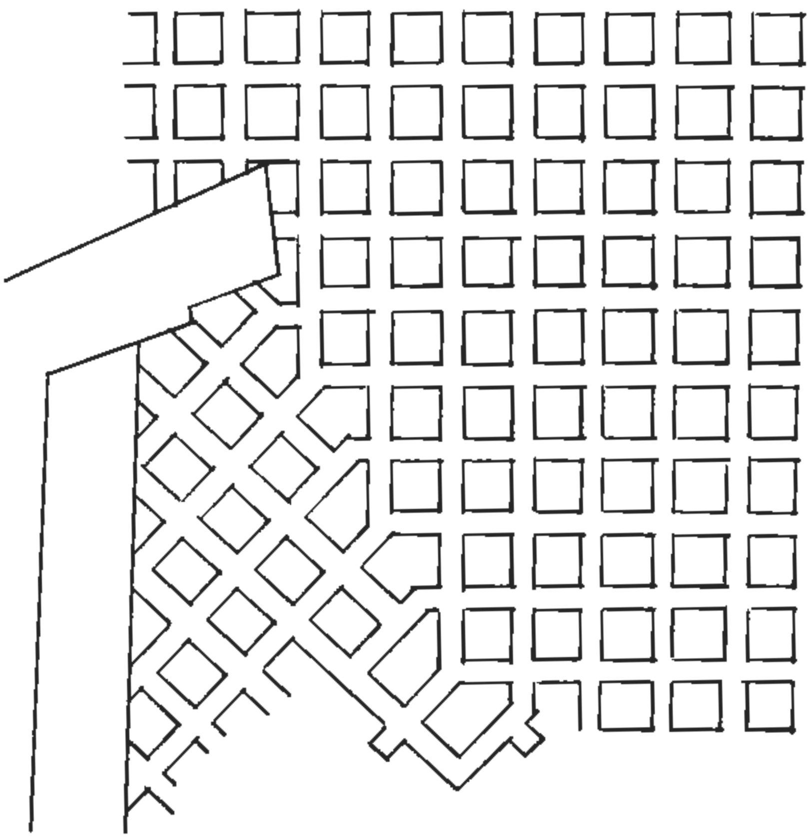

Figure 5. Test panel mining layout, Morton Salt Company, Fairport Mine.

DESIGN OF PARTIAL EXTRACTION SYSTEMS IN MINING

*K. Wardell**

Introduction

The variability of physical and geological conditions encountered in mining can impose unpredictable constraints on operational performance. Geological conditions are predetermined but the generation and distribution of rock movement and stress by mining extraction has considerable influence on such matters as the dimensions of mine openings and pillars, the optimum ratio of mineral extraction, the design and utilization of artificial supports, the maintenance of shafts and roadways in the mine, outbursts of rock and gas, mine subsidence and bumps. The primary aim of mine design is to control rock movement and stress as much as possible and thereby to maximize mine safety and operational efficiency.

The theoretical and practical studies in rock mechanics which have been made so far are, to some extent, fragmentary and imprecise. The former because their fundamental assumptions are almost impossible to verify satisfactorily, and the latter because they are usually so particular to a given set of circumstances that it is rarely possible, and may even be dangerous, to extrapolate from them.

The mining engineer, on whom the ultimate responsibility for mine safety and efficiency rests, has generally to use the broad qualitative rather than strictly quantitative conclusions which may be drawn from studies in rock mechanics and, in the present state of knowledge, to mix art or judgment liberally with science.

*Durnford, Lee & Wardell, Consulting Mining Engineers and Geologists, 32 Woodland Avenue, Wolstanton, Newcastle, Staffordshire, England.

96038—18½

The author has frequently been responsible for mine design and its implications, particularly in the mining of stratified deposits of coal, potash and iron-ore. This has led to a detailed consideration of partial extraction systems and to the development of a structural concept of mine design in which movement of the main strata is controlled by appropriate dimensional design of the areas of extraction and the pillars to be left.

Dimensions of Extraction Areas

In a broad sense, it may be said that the optimum dimensions of a mineral extraction area should be such that the main stresses generated by the extraction are directed away from it and imposed on solid boundaries or abutments. This postulates an arch or dome theory in most, if not all, mining conditions. That is to say, any given mine excavation should have critical maximum dimensions beyond which the main rock mass will no longer behave structurally and span the excavation but will fail in some way or another. It is necessary to enquire about the evidence for this.

Neither the movements nor the stresses within the main rock mass above an extraction area can be easily and certainly measured or predicted. It is, however, relatively simple to observe both the resultant transient and final effects of the whole complex of rock mass movement at the most accessible point, that is, at the surface. In fact, a number of research workers in rock mechanics have attempted to use measured surface subsidence over mine workings as a criterion against which to test the validity of their hypotheses. Berry (1), Salamon (2) and Litwinizsyn (3) are notable amongst these.

In European coal mining, for example, accurate field studies of surface subsidence caused by underground extraction have been carried out for more than fifty years and a mass of data has been accumulated. This shows conclusively that the maximum surface subsidence to be expected from an area of total mineral extraction is primarily a function of the width, length and depth of the area. This conclusion is illustrated in Figure 1 by observations made in British Coalfields over seams varying in gradient from 0 - 25°, in thickness from 2.25 ft to 18.0 ft and in depth from 102 ft to 2,628 ft.

It is apparent that, in these conditions, the maximum subsidence or surface deflection is very small when the width of an extraction area in relation to its depth is less than 0.3. The question can be considered in two dimensions only because in all the cases observed the length of working was greater than 1.5 x depth. These results strongly support the notion of an arch formation in the main strata.

The scatter of results at $W/D < 0.3$ is probably due, in part at any rate, to structural variations in the main rock mass from case to case, although the characteristics of coal measure rocks in Great Britain do not seem to vary widely as between one mine and another. It is also possible that the ration of subsidence to thickness of mineral extracted may not be a wholly valid parameter for very thick seams.

This criterion of an arch formation is strengthened by similar observations in quite different geological conditions and for other mineral deposits. Tincelin (4), for example, cites an extraction area, from an iron-ore mine in Lorraine, over which only marginal subsidence was observed although its width was 330 ft, its length greater than 1,000 ft and its depth 800 ft. Figure 2 shows the observed subsidence over a caved longwall extraction at a potash mine. The maximum observed subsidence was only 1.6 in. for an extraction area of 1,300 ft x 400 ft at a depth of 650 ft. The thickness of seam extracted was 8 ft and the W/D ration was 0.6 approximately. Thick, strong individual beds of rock were present in the overlying strata at both of these mines which may be supposed to have influenced the structural behaviour of the overlying rock mass.

The idea of a so-called 'pressure arch' has, of course, been prevalent in the thinking of coal mining engineers for several decades. In Britain, it was given approximate quantitative form (5) by the underground observations reproduced in Figure 3. It will be noted that relatively few of the results fall outside the range of W/D = 0.18 and W/D = 0.33.

In a crude and purely qualitative way the arch can be compared with the span formula for an encastred beam:

$$S = \sqrt{\frac{2fT}{w}} \qquad \ldots\ldots 1$$

where S is the width of unsupported span

f is the ultimate tensile stength of the beam

T is its thickness

and w is its specific weight.

This suggests that main parameters in the formation of an arch over mine workings might be the thickness and tensile strength not simply of individual beds of rock but of the composite rock mass. It goes without saying that tensile strength in this sense is virtually impossible to determine either theoretically or by measurement.

Denkhaus (6) has given a more sophisticated evaluation of the main dimensions and shape of an arch or dome over mine workings. He concludes that, in the case of a cohesive rock system (i.e., where the rocks do not separate or break away from the dome boundary), the maximum span will be:

$$S = \sqrt{\frac{2\,\sigma\,d}{w}} \qquad \ldots\ldots 2$$

where S is the maximum unsupported span

σ is the compressive strength of the unbroken rock

d is the depth of mining

and w is the specific weight of the rock.

In fact, it seems logical to use the tensile rather than the compressive strength of the rock in this analysis and to do so gives more comprehensible results. When this is done and if one substitutes d = T, expressions 1 and 2 are identical. For a non-cohesive rock system, the expression becomes

$$S = \sqrt{\frac{2.96\ \sigma\ d}{w}} \quad \ldots\ldots 3$$

This conception of an arch or dome and the use of surface subsidence as a guide to its limits, does not essentially contradict fundamental conceptions of elasticity, plasticity and rheology. It simple recognizes that, up to a certain limit, the rock mass tends to behave structurally. There may, of course, be exceptions if the extraction area is at very shallow depth, or if the overburden consists mainly of unconsolidated material.

Dimensions of Pillars

The literature concerning the laboratory testing of mineral rock samples is extensive. Without reflection on other workers in the field of laboratory testing, Dreyer (7) at Clausthal deserves special recognition. His work confirms and consolidates the bulk of the results from the compressive testing of prepared samples. Figure 4 illustrates his general results which may be summarized as follows:

a. The stress at failure of a laboratory test sample of a given mineral depends upon the ratio between the height and width of the sample (slenderness ratio).

b. For all the minerals tested and within the range of H/W ratios studied, the apparent strength of each mineral increased as the ration of H/W decreased.

c. For H/W ratios < 1.0 the apparent strength increased rapidly and it was impossible to induce failure in a test sample beyond a certain limit of H/W. That is to say, beyond this limit, samples were capable of sustaining very high stress indeed without failure in the accepted sense.

Similar tests have been carried out by the author and his colleagues on samples of slate, coal, iron-ore and herculite plaster. These results are also shown in Figure 4. They confirm Dreyer's general findings. All these tests were made at a uniform rate of loading.

One may suppose that the behaviour in c. above is a structural property of the mineral or rock as opposed to the mechanical properties of the mineral or rock substance. It seems a rational qualitative inference to utilize this structural concept in a mining situation, by the proposition that a single pillar of a given superficial area would sustain greater stress without failure than a larger number of smaller pillars with the same total area. On the other hand, it would be imprudent to import quantitative values from laboratory tests into the design of mine pillars without a substantial factor of safety. There appears, first of all, to be no wholly satisfactory way of calculating the amount or the direction of principal stress on mine pillars and secondly, there is a considerable scalar difference between laboratory specimens and pillars in the mine. The author has used laboratory tests of the form suggested by Dreyer but with a safety factor of at least 4. The hypothetical maximum pillar stress was calculated according to what Coates (8) has defined as the 'tributary area theory'.

This is certainly a crude method of assessment but the degree of extrapolation necessary from a controlled laboratory situation to the mine can hardly be recognized in any other way. So far, measurements of stress and deformation in mine pillars underground have not clarified the situation sufficiently to justify a more optimistic approach.

An Analysis of the Mechanics of Panel and Pillar Mining

The panel and pillar system of mining is illustrated in Figure 5. It has been used extensively in coal mining in Britain, France, Poland and the U.S.S.R.; in iron-ore mining in Lorraine and in potash mining in Alsace.

It is characterized, in all adequately designed cases, by a flat, shallow depression or subsidence at the surface. Details of ten examples are given in Table 1. Until recently, there was no rationalization of the mechanics of the system and design was largely based on 'rule of thumb'. That is to say, it was assumed that the widths of panels and intervening pillars should be of similar dimensions to give a nominal extraction ratio of about 0.5. The range of panel and pillar widths in Table 1 is from 0.08 x depth to 0.30 x depth.

In seeking possible interactions between the dimensional and structural parameters involved in this system, it is evident that these should proceed from or lead to some hypothesis about its mechanics.

At its simplest, in cross section, the system may be regarded as a series of arches supported by a series of abutments. If the abutments are capable of deformation, the deformation may be assumed to be a function of the stress imposed on them. The structural behaviour both of the rock mass and of the abutments will therefore be significant; the former will influence the widths of the arches and the latter the widths of the abutments.

Again, looking at the question quite simply, a first assumption is that the weight of the block W x L x D, as shown in Figure 5, is supported on the solid abutments. In the absence of any certain method of determining the distribution of this load, it is only possible, for the sake of comparison, to calculate the average stress imposed on the abutments.

It is necessary to assume that the width of the edge abutments is greater than half the width of the pillars. This gives an increasing average stress as the dimensions of the working area increase. There is support for this assumption from Jacobi (9) who reported measuring stress for a distance equal to

0.22 x depth into the solid abutment at a depth of 2,600 ft and from Tincelin (10) who reports a distance of 0.20 x depth at a depth of 800 ft.

Having calculated the average stress for the ten examples quoted by assuming a solid edge abutment in each case equal to 0.20 x depth, this was considered in relation to the observed maximum vertical deflection or subsidence at the surface as shown in Figure 6. The correlation was significant but examples 7 and 8 were discrepant.

If, however, average stress is a significant parameter, the behaviour of the abutments - and particularly the pillars, has to be considered. Apart from the mechanical properties of the material, the structural effect of pillar dimensions must be compared. It was therefore supposed that:

$$S\% = f(L_a,\ H/W)$$

The ten examples considered in this way are shown in Figure 7. The correlation is generally as good and leaves only example 8 still with a fairly wide discrepancy. Some other parameter or parameters were presumed to exist.

Structurally, the arches created by the extraction panels are of major importance and to a large extent, where the rocks above the extraction are non-cohesive, the volume of extraction will determine the height of breakdown into the extracted area. This, in turn, will determine the height of the arch and, as will be shown, the zone above and below the mineral extraction level which is highly stressed. It was further supposed therefore that:

$$S = f\ (PH)$$

$$\text{or } S\% = f\ (P)$$

and, combining this with the previous proposition, gives:

$$S\% = f(L_a, H/W, P)$$

The examples from Table 1 are shown on the basis of this hypothesis in Figure 8. The results are remarkably consistent with the view that each of the parameters has a dimensional and a structural significance.

Some Examples of Designed Panel and Pillar Workings

1. Figure 9 illustrates panel and pillar workings in a coal seam underlying part of the University of Nottingham (Example 5 in Table 1)(11). In this case panels and pillars were chosen largely on the customary basis of minimizing surface subsidence by utilizing panels having a low W/D ratio (i.e., W/D = 0.21) with pillars of similar dimensions to give a nominal extraction ratio of 0.50. Surface subsidence observations were supplemented by a variety of measurements and observations underground to try and throw some further light upon the mechanics of the system.

Measurements were made of convergence at the pillar edges and in the wall packs constructed in the extraction panels. The observed subsidence and convergence results are shown in cross-section in Figure 10 which also gives the significant dimensional details.

The immediate roof within the extraction panels caved freely behind the advancing longwall faces. The measured convergence was inferred to be the result of pressures imposed by the collapsed roof beds rather than by closure between the unbroken main roof and floor.

The convergence near the pillar edges - the continuous recorders were set 2 to 3 ft into the pillar sides - varied between 10 per cent and 25 per cent of the seam thickness (5.5 and 13.5 in.). Nevertheless, there was no material spalling at the pillar edges and no maintenance work was required in the access roadways at the edges of the extraction panels.

A heading was driven between Panels B and C and an attempt was made to measure its convergence. The results were largely inconclusive because it was clear that the movements were, in part at any rate, representative of purely local effects, created by the existence of the heading itself.

Stressmeters were also installed in boreholes drilled in the positions shown in Figure 9.

Of course, both the convergence and stressmeter results were incomplete since the apparatus could only be installed when the workings had reached appropriate positions. That is to say, some effects must have occurred before the measurements began.

The stressmeters were of the M.R.E. type (12) which are essentially strain gauges, monitored electrically, the strain changes being converted to equivalent stress values from calibration tests made in the laboratory. The results of the measurements in the two boreholes are shown in Figure 11.

One might draw two main conclusions from these results. In the first place it would appear that the increase in stress at the point nearest to the extraction panel occurred over a shorter period of time than at the point in the centre of the pillar. Secondly, that the stress increase was more than twice the value near the edge than at the pillar centre.

In the author's opinion such conclusions would be misleading. Fundamentally it was increasing or change in strain which was being observed. One could therefore expect that the difference in lateral constraint would be an important factor in the strains developed and would lead to both a higher strain rate and a higher total strain near the pillar edge.

Without a knowledge of the directions and relative magnitude of the principal stresses it is virtually impossible to correlate unidirectional strain measurements with applied stress. Unfortunately, there are still a number of unresolved practical and theoretical difficulties associated with the measurement or calculation of pillar stress.

2. The author has also designed similar panel and pillar workings in consultation with colleagues from Mines Domaniales de Potasse d'Alsace. The most important example concerns the mining of a seam of potash (Sylvinite) 7 ft in thickness at a depth of 1,500 - 1,680 ft. The cover to the surface consisted of interbedded shales, rock salt and anhydrite.

There was no observed data on which to judge either the optimum panel or pillar width and an experimental mine layout was set up with the observation of subsidence as the primary control, supplemented by stress and deformation measurements in the underground pillars and by laboratory tests on potash samples from the mine. The latter were conducted in collaboration with Potts (13) and McClain (14).

The primary objectives were the maximum rate of extraction consistent with good operating conditions, stability of the mine structure and access roadways and minimal surface subsidence.

The general layout is illustrated in Figure 12 and three phases may be distinguished. Initially, panels 108, 110, 112 and 114 were planned at widths of 130 ft (0.08 - 0.09 x depth) with intervening pillars of 250 - 300 ft. The panels were to be worked by room and pillar with the smaller pillars left intact. Panels 110 and 114 were begun first, followed later by panels 108 and 112.

When panels 108, 110 and 114 were virtually complete and panel 112 has advanced about 425 ft, the observed subsidence was virtually negligible. It was then decided to increase the width of panel 112 to 165 ft (0.10 x depth) and to extract the seam completely within this panel. The effect of this was marginally to increase the surface subsidence.

Further dimensional changes were therefore made in relation to panels 102, 106 and 104 as shown in Figure 12. in this second phase of mining, the panels were extracted in the sequence 106, 102 and 104. Figure 13 shows the finally observed surface subsidence.

The maximum panel width was that of 104 at 245 ft (0.18 x depth). The minimum pillar width was 102/104 at 165 ft (H/W ratio 1/24). The maximum hypothetical pillar stress was in the order of 3,500 psi. Again, a correlation calculation of the type

$$S\% = f(L_a, H/W, P)$$

was rather difficult to make because of the complete extraction area to the north-east, and the small left pillars in panels 108, 110, 112 and 114. An approximate calculation for the three adjoining total extraction panels - 102, 104 and 106 was made assuming an abutment support of 260 ft around this area of extraction. This result is also given in Figure 8.

Two conclusions were drawn from these data. The first, that the panel widths could be further increased without destroying the arch formation. The second, and rather less positive from a design point of view, that pillars with

H/W ratio of 1/24 were structurally stable under the stress imposed upon them in these circumstances.

These conclusions led to further changes in the dimensions of panels 116 and 118 to the west. At the moment, panel 116 has been extracted and panel 118 is in the position shown. The surface subsidence is not yet complete but broadly confirms the continuing structural stability of the system. The widening of the panel dimensions will be continued as the mining area extends until observations suggest that critical limits are being approached. Up to this time it seems that it will be possible to achieve an overall extraction rate of 65 - 70 per cent at this depth and still maintain stability and control.

3. The author has collaborated with colleagues from the Nord and Pas-de-Calais Coalfield in France, in the design of panel and pillar workings in a coal seam inclined at 25 - 40° (11) (15). The critical panel or arch dimensions were determined from the subsidence criterion for which there was ample observed evidence. This suggested a panel width of 0.25 x depth.

The coal was very friable but tests suggested a crushing strength of approximately 4,000 psi at a H/W ratio of 1/16. The calculated hypothetical maximum pillar stress at 70 per cent extraction and an average depth of 325 ft was approximately 1,000 psi, which gave a safety factor of 4. The general layout of the workings is shown in Figure 14. Between the two lower horizons, at an average depth of 620 ft, the H/W ratio of pillars was increased to 20 : 1 in order to maintain the factor of safety at the higher hypothetical maximum pillar stress.

The limiting conditions for the design were:

a. to achieve the maximum possible rate of extraction consistent with a maximum surface subsidence of 4 in.;

b. to maintain long term structural stability because of the existence of underlying workable coal seams; and

c. to provide the best possible operating conditions.

The seam had an average thickness of 3 ft 6 in. and the maximum allowable subsidence of 4 in. was only fractionally exceeded at a nominal extraction rate of 65 per cent. Working conditions were excellent and, in particular, no repair work was required in the level or slant roadways in the seam.

The inclination of the seam and the presence of surrounding areas of total extraction make difficult a correlation calculation of the type:

$$S\% = f(L_a, H/W, P)$$

An approximate calculation gives a predicted subsidence of 3.2 in. compared with an observed 4.0 in. This result is shown in Figure 15. If any inference can be drawn at all from this discrepancy, it would be that the situation might have been influenced by the different structural properties of this coal compared with the British examples in Table 1.

4. Figure 16 illustrates the extraction of a coal mine shaft pillar in the north of France by means of a modified panel and pillar system (15). The purpose in the case was to protect the shaft and surface installations to the greatest possible extent by controlling the movement of the main rock mass. The situation was not ideal because of the existence of previous extraction areas around the shaft pillar and the presence of faults which imposed limitations of the extraction boundaries. The final measured surface subsidence and vertical deformation of the shaft are given in Figure 17. The surface subsidence was broadly as predicted.

The example is of special interest because of the shaft measurements which appeared to indicate that:

a. There was little or no transient or final vertical deformation in the upper part of the shaft, that is, the main rock mass subsided more or less uniformly.

b. There was vertical compressive deformation in the shaft for a distance of about 390 ft (0.30 x depth) above and 190 ft (0.15 x depth) below the mined seam. This compressive deformation only reached measureable proportions when the two extraction areas had approached and were very close to the shaft.

c. The deformation was virtually static within a month or so of the completion of extraction. It was not possible to continue the observations after that time.

The uniformity of the surface subsidence and the absence of deformation in the upper part of the shaft would seem to confirm the general structural concept of the system developed from previous mine experiments and from observations. However, the compressive deformation in the lower part suggests that the abutment is not confined to the extracted horizon but includes the rocks for some distance above and below it. It would follow that the relative structural properties in compression of the rocks above and below the mineral pillars should also be brought into consideration. Further observations are required before this can be achieved.

An Analysis of the Mechanics of Room and Pillar Mining

Although it has long been believed that some surface subsidence would be caused by room and pillar mining, few observations are available from published literature. Certainly, no attempt seems to have been made to rationalize the subsidence process caused by such mining. Those details which the author has been able to find are assembled in Table 2. The examples are all from coal mines each of which showed the development of a shallow basin of subsidence with a peripheral extension beyond the actual extraction boundaries.

Examples 2 and 3 had the highest ratio of extraction and also the highest subsidence and a general examination of the data suggested a correlation between observed maximum subsidence and the hypothetical average pillar stress. The latter was again calculated from the weight of the overburden distributed over the area of the solid edge abutments plus the area of the left pillars as shown in Figure 18.

Total weight of overburden = D^3 (x + 0.4) (y + 0.4)

Area carrying load = D^2 xy (1 - R) + 0.4 (x + y + 0.4)

Average stress on pillars and abutments $= D \left[\dfrac{(x + 0.4)\ (y + 0.4)}{xy\ (1 - R) + 0.4\ (x + y + 0.4)} \right]$

Figure 19 shows the calculated variation in average stress for a working of length = 2.0 D, widths y = 0.2 D - 1.6 D and an extraction ratio of 0.5.

The other parameter which seemed likely to affect the maximum surface deflection was the pillar height to pillar width ratio. It was therefore postulated that:

$S\% = f\ (L_a,\ H/W)$

where S is the observed maximum subsidence

L_a is the average stress on pillars and abutments

H is the original height of the pillars or the worked seam thickness

and W is the width of the pillars.

Figure 20 shows the data given in Table 2 graphed according to this hypothesis. The correlation appears to be significant but the number of observations is insufficient to indicate its real strength.

In general, however, the results support the proposition that the average pillar stress is relatively small at low working width to depth ratios. That is to say, with the notion of an arch formation within which the pillars are not stressed to the maximum. Also, it emphasizes the importance of H/W ratio of the pillars and this is particularly clear from the comparison between examples 3 and 4.

Comparison Between Panel and Pillar and Room and Pillar Systems

Within the range of results studied, one is led to the conclusion that the panel and pillar system is inherently the more stable for the same conditions of stress and extraction ratio. Case No. 3 in Table 2 may be used as an example. The dimensions of the worked out area were 500 x 500 ft and the same ratio of extraction (0.69) would be produced by four panels of 105 ft (0.21 x depth) and three pillars of 55 ft (0.11 x depth) in width. For this system:

$$S\% = f\ (L_a, H/W, P)$$

$$= f\ (880 \times 0.146 \times 105)$$

$$= \underline{f\ (13{,}500)}$$

The value of S% from the graph in Figure 8 is only 15 per cent compared with the observed value of 34.8 per cent over the actual room and pillar workings.

The main problem of course in room and pillar mining is to determine the optimum pillar dimensions. This requires firstly an assessment of the maximum stress to which a pillar will be subjected in the mine and secondly an assessment of the capacity of the pillar to sustain stress. The risks attaching to extensive mining with the room and pillar system are emphasized by the disasters at Coalbrook in South Africa and Champagnoles in France. Even when loss of life has not been involved, mine operations have often been interrupted and areas have had to be abandoned with consequent economic loss. The problems of design for small pillars must obviously increase with working depth and increasing seam thickness and the room and pillar system is then only operable either at a relatively low rate of extraction or at a marginal factor of safety.

The panel and pillar system has, in the author's view, a much higher intrinsic factor of safety and also offers generally the possibility of higher extraction ratios. Moreover, it is probable that a combination of room and pillar working - within areas which were more generally supported by stabilizing pillars - could be used to considerable advantage both from the point of view of economic extraction and safe mine design.

Conclusions

The method given in this paper for analyzing and comparing partial extraction systems arises from a broad structural concept of mine design. The data available, although statistically limited, nevertheless underlime significant parameters which can and have been used in practical mine design.

Surface subsidence is relatively simple to measure compared with the measurement of stress and movement in the mine. Moreover, it appears that, by careful analysis of a sufficiently large number of results from a wide variety of physical and geological conditions, it is possible to isolate main parameters and to describe their probable interaction. Many measurements and observations underground are not susceptible to such analysis and, often enough, it is difficult to know exactly what is being measured. In the author's opinion the importance of surface subsidence as an analytical and practical tool in rock mechanics and mine design has not yet been sufficiently recognized.

It can be deduced from subsidence measurements and other supporting evidence that safe control of the movement of the main rock mass is possible with the panel and pillar system of mining. It is further suggested that extraction ratios up to 0.75 are possible without losing this control.

So far as room and pillar working is concerned, it can be envisaged that this could be used for extraction panels of planned dimensions separated by appropriately dimensioned barrier pillars. This might well serve to extend the range of application and the safety of small pillar mining.

References

(1) Berry, D.S.
1963-64: Ground movement considered as an elastic phenomenon. Trans.Inst.Min.Eng. no. 37, v. 123.

(2) Salamon, M.G.
An introductory mathematical analysis of the movements and stresses induced by mining in stratified rocks. v.9, Bull. no. 3 Series, Strata Control, Research no. 16, Univ. Newcastle-on-Tyne.

(3) Litwinizsyn, J.
1957: The theories and model research of movements of ground masses. Proc.Eur.Cong. on Ground Movement, Leeds.

(4) Tincelin, E.
1958: Conclusions de mesures de pression de terrain. Extrait de la thése Pressions et Déformations de Terrain dans les Mines de Fer de Lorraine.

(5) North of England Safety in Mines Research Committee
1948-49: Seventh progress report of an investigation into the causes of falls and accidents due to falls. The improvement of working conditions by the controlled transference of roof load. Trans. Inst. Min. Eng., v. 108.

(6) Denkhaus, H.G.
1964: Critical review of strata movement theories and their application to practical problems. J.South African Inst. of Min. and Met., v. 64, March.

(7) Dreyer, W.
1964: Die Bedeutung von Modellversuchen an Salzgestein für die Beurteilung gebirgsmechaniker Probleme imm Kalibergbau (Bergakademie Pt. 3)

(8) Coates, D.F.
1965: Pillar loading. Dept. of Energy, Mines and Resources, Ottawa. Research Reports 168, 170 and 180.

(9) Jacobi, O.
1956: The pressure on seam and goaf. Int. Strata Control Congress Essen.

(10) Tincelin, E. and Sinou, P.
1960: Collapse of areas worked by the small pillar method. Practical conclusions and an attempt to formulate laws for the phenomena observed. Int. Conf. on Strata Control, Paris.

(11) Wardell, K.
1965: Surface ground movements associated with the total and partial extraction of stratified mineral deposits. M.Sc., Thesis, Univ. Nottingham.

(12) Wilson, A.H.
1962: The measurement of rock stress. Coll. Guardian, v. 204, no. 5258, January.

(13) Potts, E.L.J.
1964: The influence of time dependent effects on the design of mine pillars. Int. Bur. of Rock Mech. 6th Internat. Meeting, November.

(14) McClain, W.C.
1964: A study of the strata movement in the partial extraction of potash. Ph.D. Thesis Univ. Newcastle-on-Tyne, December.

(15) Proust, A. and Grard, C.
1966: Utilisation, dans le Bassin du Nord et du Pas-de-Calais, des méthodes d'exploitation partielle. Revue de l'Industrie Minérale, September.

TABLE 1

MINE		D	P	W	H	S		R	L	n	$L \times \frac{H}{W}$	$L \times \frac{H}{W} \times P$
1 Handsworth		360	97	125	4.46	0.144	3.23	0.45	590	4	21.05	2040
2 Barbara	+	558	164	131	3.94	0.197	5.00	0.55	916	3	27.55	4520
3 Hucknall	o	576	145	145	4.50	0.208	4.63	0.50	861	3	26.72	3870
4 Glenochil	o	666	125	190	2.84	0.151	5.30	0.40	918	2	13.72	1715
5 Wollaton		725	150	145	4.50	0.292	6.48	0.50	1070	3	33.21	4980
6 Snibston	o	830	187	170	6.00	0.660	11.00	0.53	1205	5	42.53	7950
7 Wearmouth	o	1800	240	250	2.92	0.260	9.00	0.48	2450	3	28.62	6869
8 Easthouses	o	2020	545	550	5.92	0.940	15.90	0.50	3290	[illegible]	35.42	19300
9 Cadeby		2250	240	360	5.50	0.770	14.00	0.41	3210	5	48.95	11700
10 Bradford	o	2700	210	300	5.84	0.920	15.70	0.42	3680	5	71.64	15050

o Orchard

\+ By courtesy of Professor Knothe

D = depth (ft)
P = panel width (ft)
W = pillar width (ft)
H = seam thickness (ft)
S = subsidence (ft)
S% = subsidence as percentage of seam thickness
R = nominal rate of extraction
L = average load
n = number of panels

TABLE 2

Example	Source	D	H	W	H/W	S	R	L_a	S%	$L_a \times H/W$
1	N. Staffs	450/900	4.50	30	0.150	9	0.41	980	10.5	147
2	o	260	4.25	10	0.425	16	0.70	525	23.5	223
3	+	500	8.00	16 (approx)	0.500	24	0.69	880	34.8	440
4	Cannock	870	7.00	50	0.140	10	0.31	1050	9.6	147
5	o	330	4.25	44	0.097	16	0.46	470	2.0	46

o N.C.B. Production Department, Information Bulletin 61/231
\+ Herbert & Routledge, U.S. Department of Commerce, Bulletin 238

D = depth (ft)
H = seam thickness (ft)
W = pillar width (ft)
S = room width (ft)
R = nominal rate of extraction
L_a = average loading
S% = observed subsidence as percentage of seam thickness

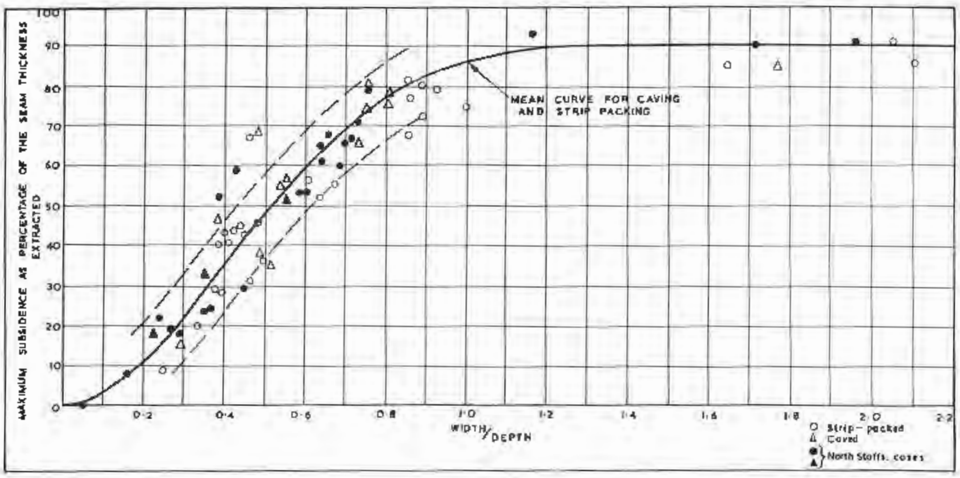

Figure 1. Subsidence at different widths and depths of extraction.

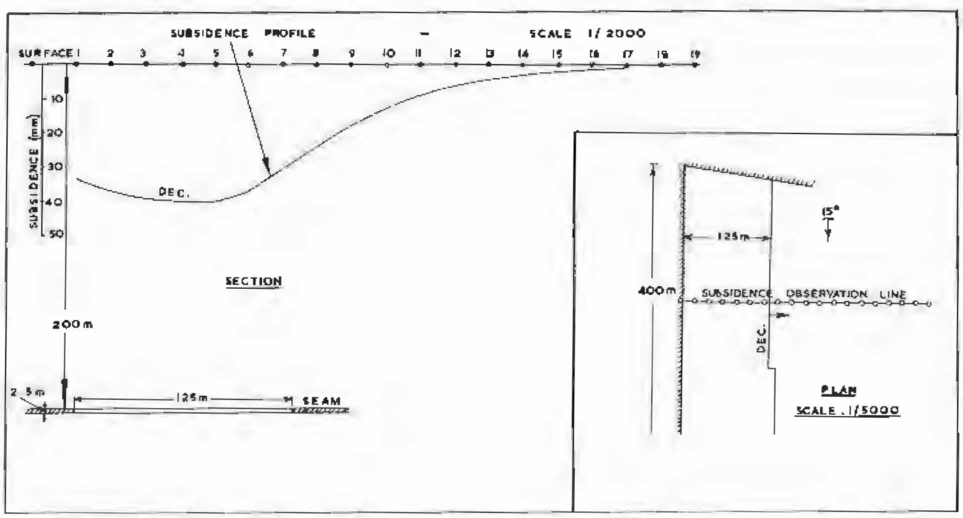

Figure 2. Subsidence observed over a longwall face at a potash mine in Spain.

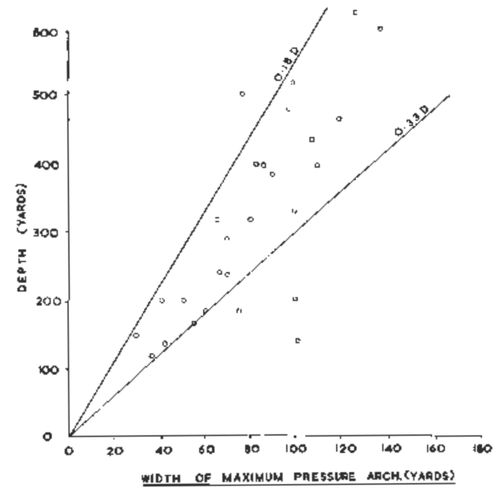

Figure 3. Diagram showing maximum width of pressure arch for different depths of working.

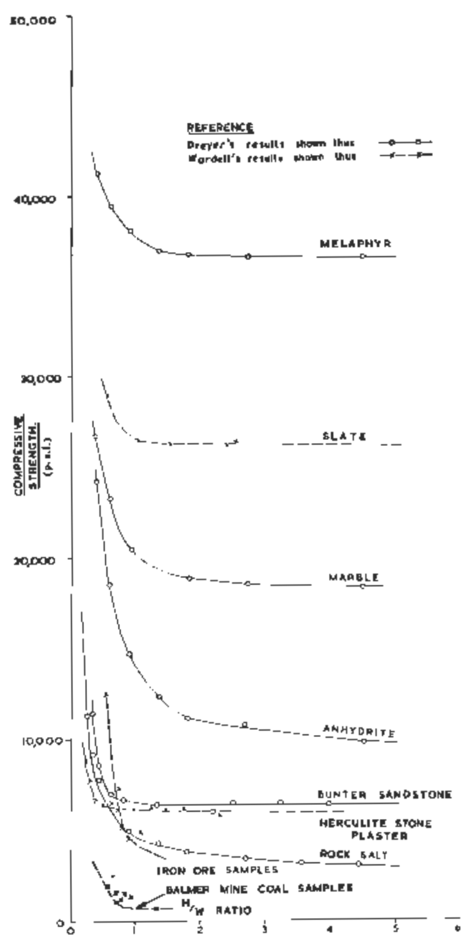

Figure 4. Graph showing variation in compressive strength in relation to slenderness ratio of various rock samples.

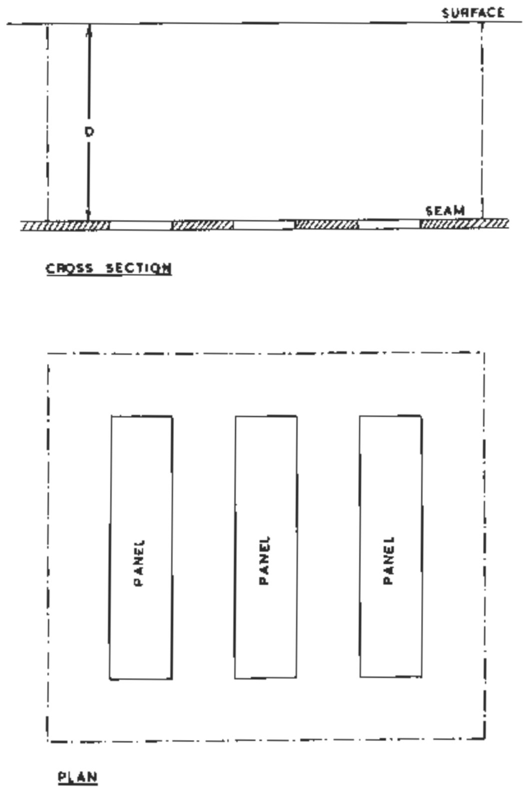

Figure 5. Diagram showing area considered in determination of average loading for panel and pillar mining system.

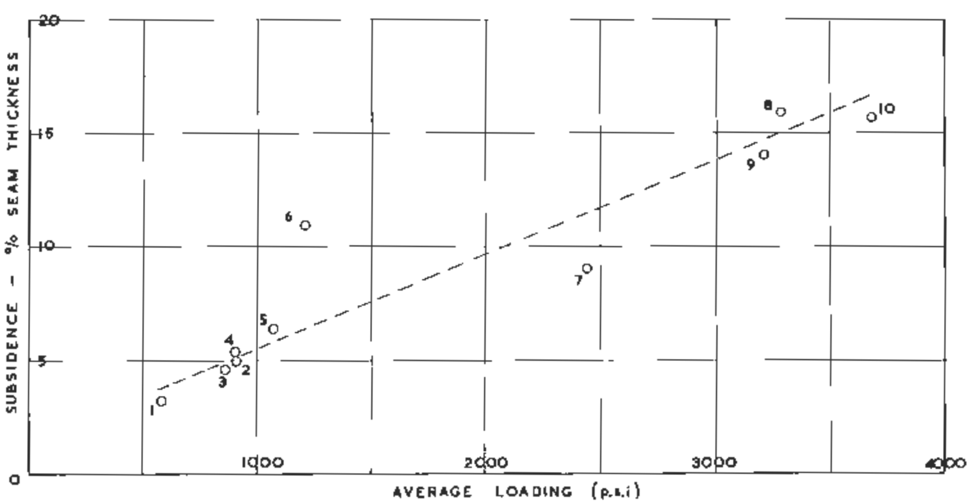

Figure 6. Graph showing correlation between observed subsidence and calculated average loading for examples of panel and pillar workings.

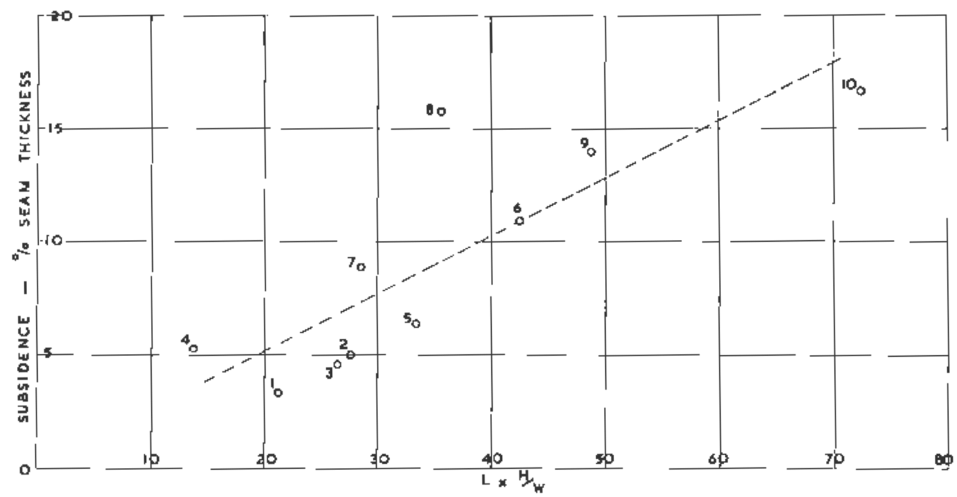

Figure 7. Graph showing correlation between observed subsidence and average loading multiplied by H/W ratio of pillars.

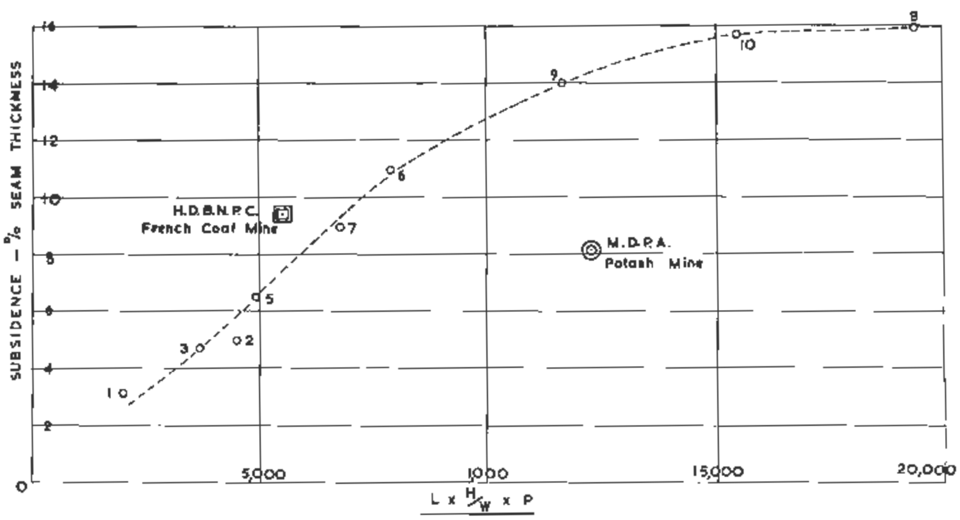

Figure 8. Graph showing relationship of observed maximum subsidence as a function of (L, H/W and P).

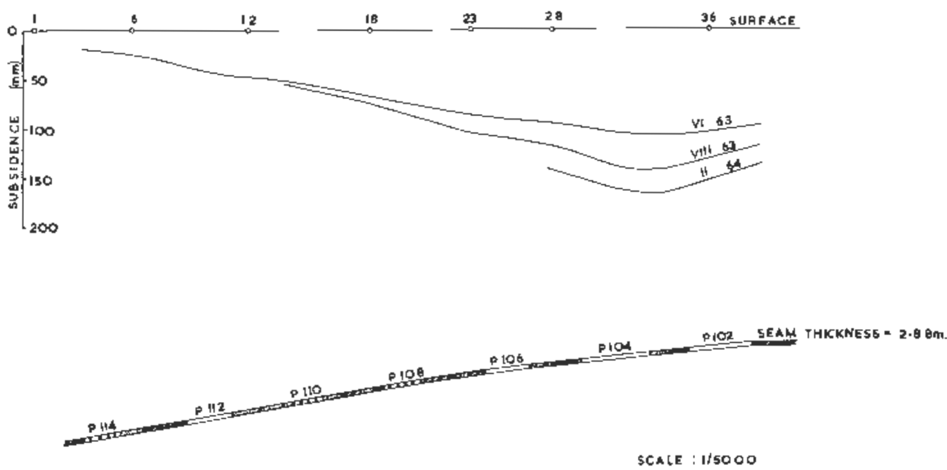

Figure 13. Cross-section through panel and workings at a potash mine in Alsace, France, showing observed surface subsidence.

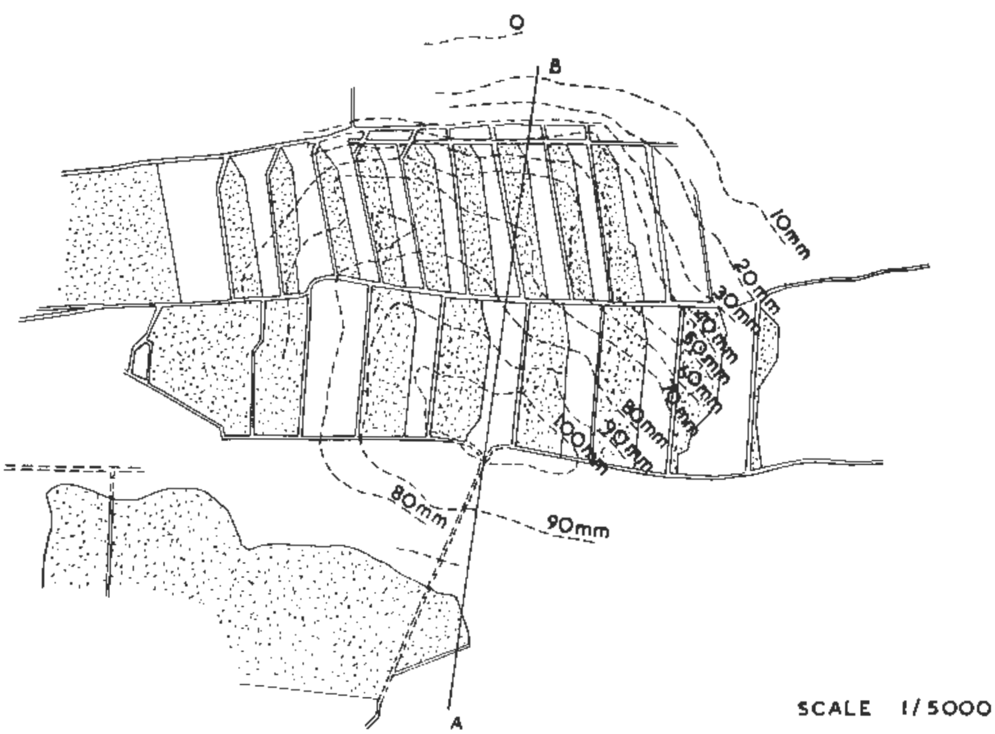

Figure 14. Plan of panel and pillar workings at a coal mine in the Nord and Pas-de-Calais Coalfield, France, showing observed contours of subsidence.

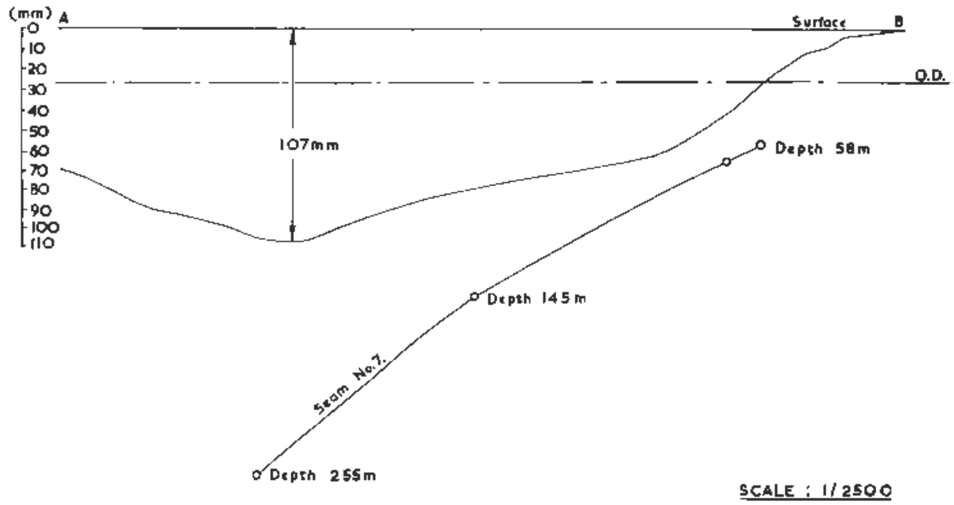

Figure 15. Vertical cross-section along line A-B Figure 14 showing observed subsidence over panel and pillar workings at a coal mine in the Nord and Pas-de-Calais Coalfield, France.

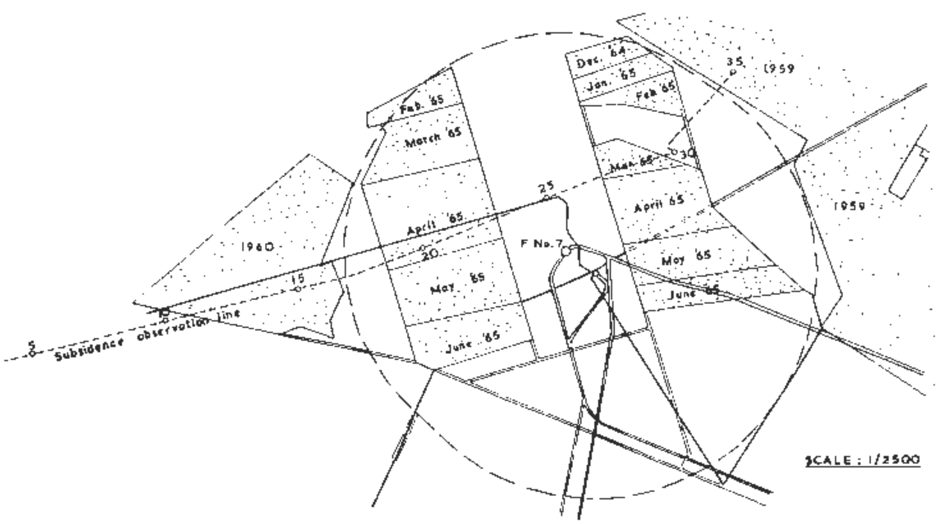

Figure 16. Plan of workings in shaft pillar at pit No. 7 H.D.N.B.C.

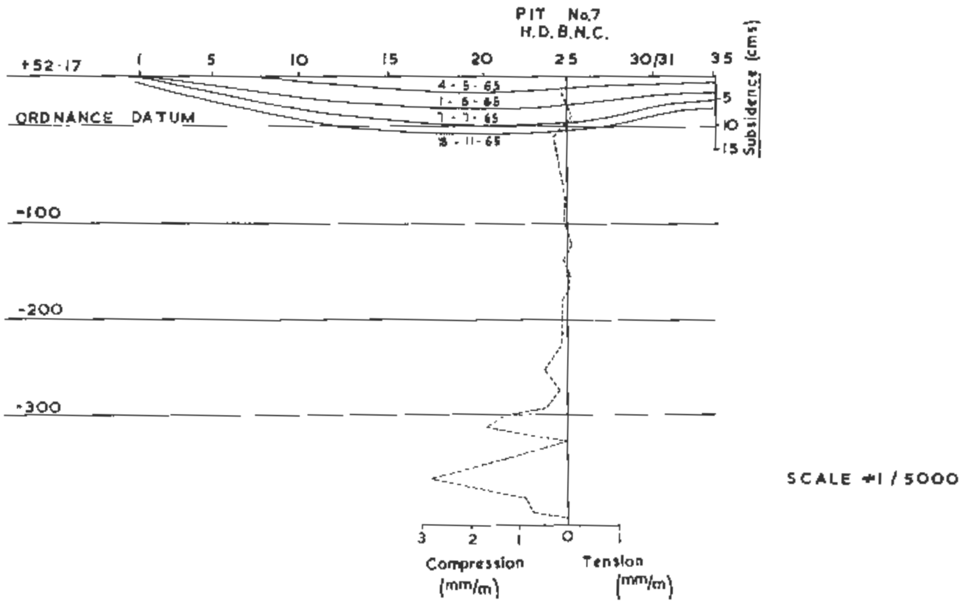

Figure 17. Surface subsidence and vertical deformation of shaft.

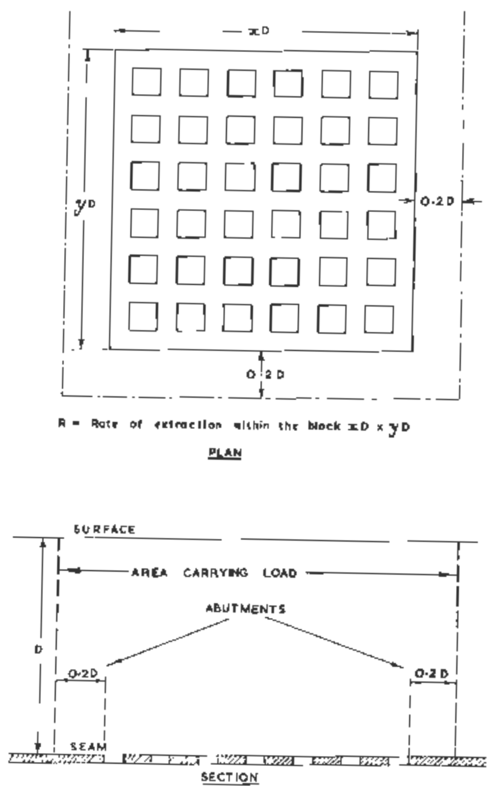

Figure 18. Diagram showing notation for average load calculations in room and pillar system.

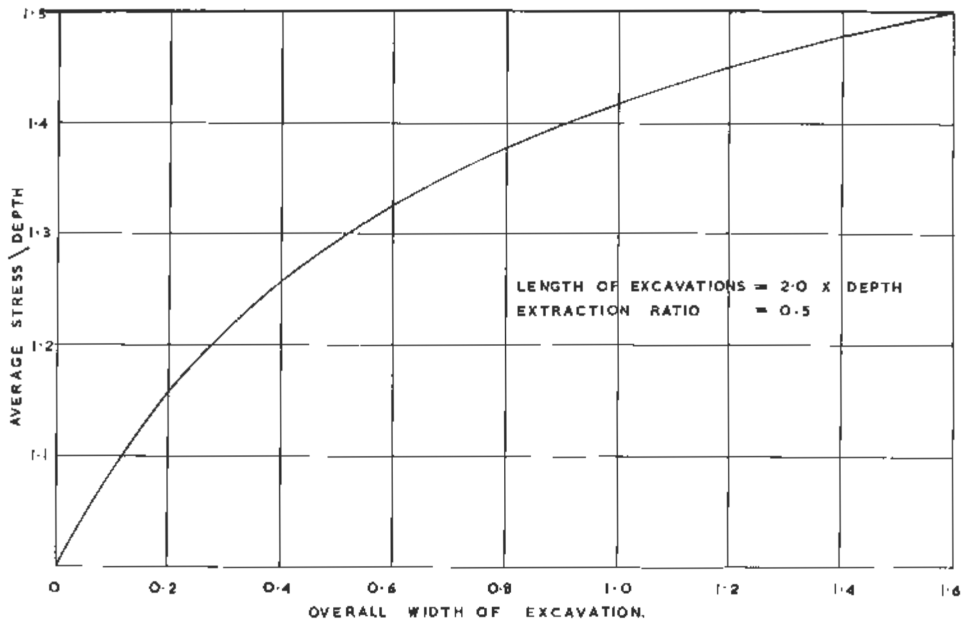

Figure 19. Graph showing relationship between average pillar stress and overall width of extraction for panel and pillar system or mining.

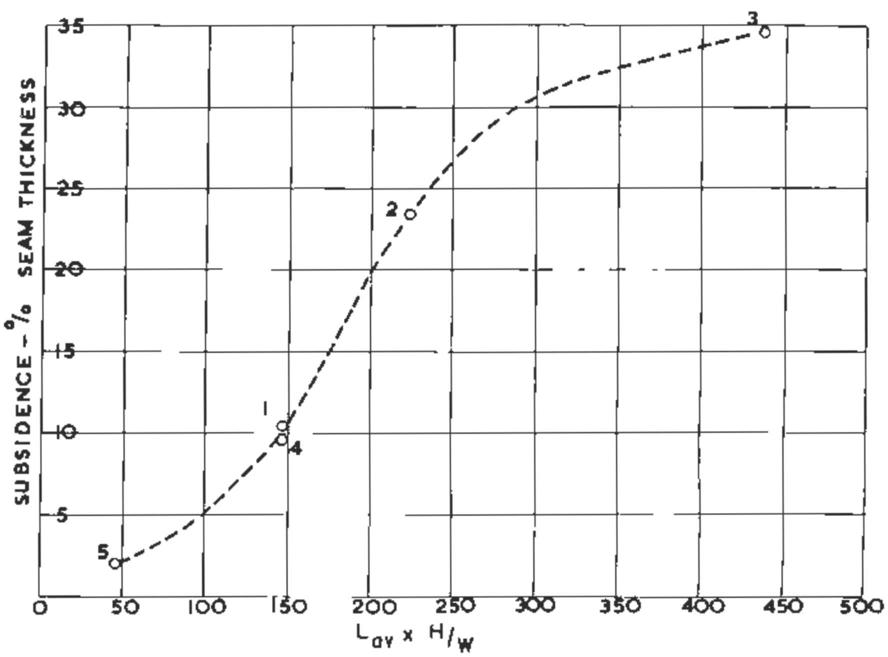

Figure 20A. Graph showing % subsidence against average load x H/W for room and pillar workings.

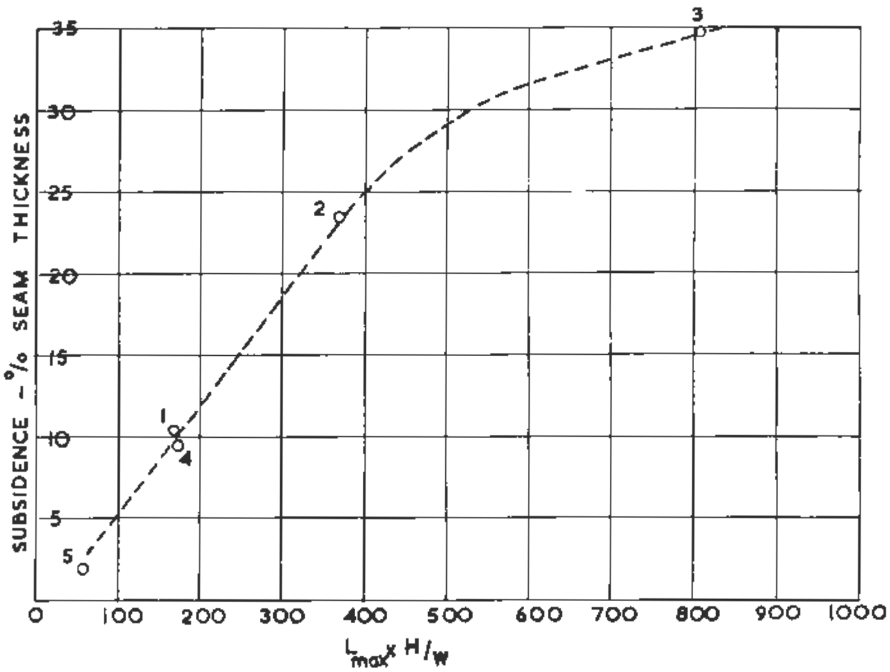

Figure 20B. Graph showing % subsidence against maximum load x H/W for room and pillar workings.